Electrochemical Society

NEW TECHNICAL DATA SHEETS AVAILABLE TO GLC ANODE CUSTOMERS

Recently issued data sheets prepared by our Technical Department contain important information about graphite anode properties.

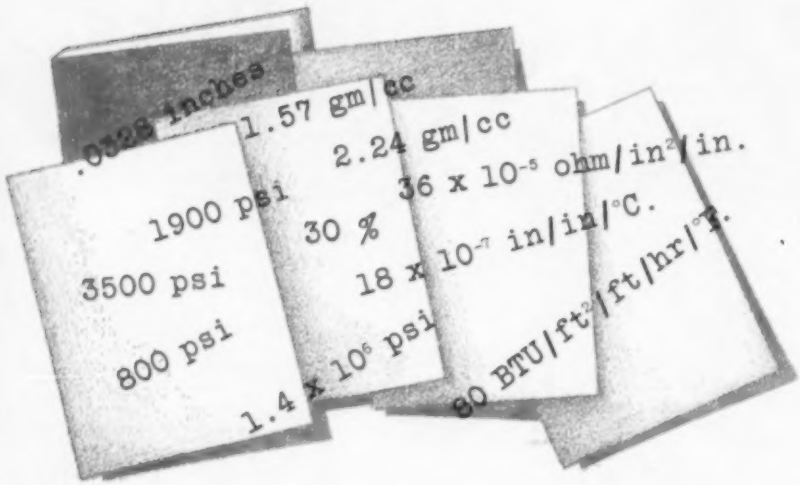

Among the typical physical properties detailed for anodes in various grades and sizes are maximum particle sizes... apparent and real density... porosity... resistivity... rupture... compressive and tensile strength... elasticity... thermal expansion and conductivity.

Typical chemical properties of the anode grades show percentages of ash, sulfur, silicon, iron, calcium, aluminum, vanadium sodium, titanium and other impurities.

Data on the surface finishing obtainable in various machining operations are also included.

We shall be happy to furnish a set of these technical data sheets, with our compliments, to anode users everywhere. Your request will be most welcome.

PRODUCTS ELECTRODE GLC DIVISION YOU CAN TRUST ®

GREAT LAKES CARBON CORPORATION

18 EAST 48TH STREET, NEW YORK 17, N. Y.

EDITORIAL STAFF

C. L. Faust, Chairman, Publication Committee

Cecil V. King, Editor

Norman Hackerman, Technical Editor

Ruth G. Sterns, Managing Editor

U. B. Thomas, News Editor

H. W. Salzberg, Book Review Editor

Natalie Michalski, Assistant Editor

DIVISIONAL EDITORS

W. C. Vosburgh, Battery

Milton Stern, Corrosion, I

R. T. Foley, Corrosion, II

T. D. Callinan, Electric Insulation

Seymour Senderoff, Electrodeposition

H. C. Froelich, Electronics, I

Ephraim Banks, Electronics, II

Ernest Peskell, Electronics—Semiconductors

Sherlock Swann, Jr., Electro-Organic, I

Stanley Wawzonek, Electro-Organic, II

John M. Blocher, Jr., Electrothermics and Metallurgy, I

A. U. Seybolt, Electrothermics and Metallurgy, II

N. J. Johnson, Industrial Electrolytic

C. W. Tobias, Theoretical Electrochemistry, I

A. J. deBethune, Theoretical Electrochemistry, II

ADVERTISING OFFICE

ECS

1860 Broadway, New York 23, N. Y.

ECS OFFICERS

R. A. Schaefer, President
The Bunting Brass and Bronze Co., Toledo, Ohio

Henry B. Linford, Vice-President
Columbia University, New York, N. Y.

F. L. LaQue, Vice-President
International Nickel Co., Inc., New York, N. Y.

W. J. Hamer, Vice-President
National Bureau of Standards, Washington, D. C.

Lyle I. Gilbertson, Treasurer
Air Reduction Co., Murray Hill, N. J.

I. E. Campbell, Secretary
National Steel Corp., Weirton, W. Va.

Robert K. Shannon, Executive Secretary
National Headquarters, The ECS, 1860 Broadway, New York 23, N. Y.

Manuscripts submitted to the Journal should be sent, in triplicate, to the Editorial Office at 1860 Broadway, New York 23, N. Y. They should conform to the Instructions to Authors, last published in the Sept. 1960 issue, pp. 229C-230C. Manuscripts so submitted become the property of The Electrochemical Society and may not be published elsewhere, in whole or in part, unless permission is requested of and granted by the Editor.

Inquiries re positive microfilm copies for volumes should be addressed to University Microfilms, Inc., 313 N. First St., Ann Arbor, Mich.

The Electrochemical Society does not maintain a supply of reprints of papers appearing in its Journal. A photoprint copy of any particular paper, however, may be obtained by corresponding directly with the Engineering Societies Library, 29 W. 39 St., New York 18, N. Y.

Journal of the Electrochemical Society

DECEMBER 1960 **VOL. 107 • NO. 12**

CONTENTS

Editorial

Our Future Electrochemists 264C

Technical Papers

Diffusion Theory of Polarization and Recuperation Applied to the Manganese Dioxide Electrode. *A. B. Scott* 941

Aluminum Reactions with Water Vapor, Dry Oxygen, Moist Oxygen, and Moist Hydrogen between 500° and 650°C. *P. E. Blackburn and E. A. Gulbransen* 944

Dissolution of Copper in Sulfuric Acid Solutions. *D. P. Gregory and A. C. Riddiford* 950

Microtopography of Oxide Films Formed on Tantalum. *R. E. Pawel, J. V. Cathcart, and J. J. Campbell* 956

The Difference Effect and the Chunk Effect. *G. A. Marsh and E. Schaschl.* 960

Flash Conductivity in Solution of Triphenylamine in n-Hexane. *H. Rüppel, U. Krog, and H. T. Witt* 966

Electrodeless Passage of Direct Current through an Electrolyte. *A. Brenner* 968

Formation of Phosphor Films by Evaporation. *L. R. Koller and H. D. Coghill* 973

Thermoelectric and Crystallographic Properties of Ag_2Se. *J. B. Conn and R. C. Taylor* 977

Separation of Sulfur, Selenium, and Tellurium from Arsenic. *J. M. Whelan, J. D. Struthers, and J. A. Ditzenberger* 982

Electrolytic Vanadium and Its Properties. *D. H. Baker, Jr., and J. D. Ramsdell* 985

On the Vacuum Sintering of Tungsten Ingots. *J. W. Pugh and L. H. Amra* 990

Liquidus Curves for Aluminum Cell Electrolyte, III. Systems Cryolite and Cryolite-Alumina with Aluminum Fluoride and Calcium Fluoride. *A. Fenerty and E. A. Hollingshead* 993

The Structure of Cryolite-Alumina Melts. *P. A. Foster, Jr., and W. B. Frank* 997

Technical Notes

On the Role of the Oxygen Concentration Cell in Crevice Corrosion and Pitting. *G. J. Schafer, J. R. Gabriel, and P. K. Foster* 1002

Electrodeposition of Pure Copper. *S. Barnartt* 1004

Some Observations on the System ZnS-AlP. *A. Addamiano* 1006

High-Temperature Base-Tab for Silicon. *L. Maissel* 1007

Copper Sulfide Creep on Porous Electroplate. *M. S. Frant* 1009

Brief Communication

Electronic Analysis of the Fe-Ni System. *S. Yamaguchi* 1011

Technical Feature

Plasma Thermionic Converters. *E. W. Salmi* 1013

Technical Review

Practical Neutron Activation Analysis for the Electronic Scientist. *J. P. Cali and J. R. Weiner* 1015

Discussion Section **1020-1026**

Current Affairs **268C-278C**

Published monthly by The Electrochemical Society, Inc., from Manchester, N. H., **Executive Offices, Editorial Office** and **Circulation Dept.,** and **Advertising Office** at 1860 Broadway, New York 23, N. Y., combining the JOURNAL and TRANSACTIONS OF THE ELECTROCHEMICAL SOCIETY. Statements and opinions given in articles and papers in the JOURNAL OF THE ELECTROCHEMICAL SOCIETY are those of the contributors, and The Electrochemical Society assumes no responsibility for them. Nondeductible subscription to members $5.00; subscription to nonmembers $10.00. Single copies $1.25 to members, $1.75 to nonmembers.

Copyright 1960 by The Electrochemical Society, Inc.

Entered as second-class matter at the Post Office at Manchester, N. H., under the act of August 24, 1912.

SARGENT-SLOMIN ANALYZERS
are standard equipment in prominent laboratories

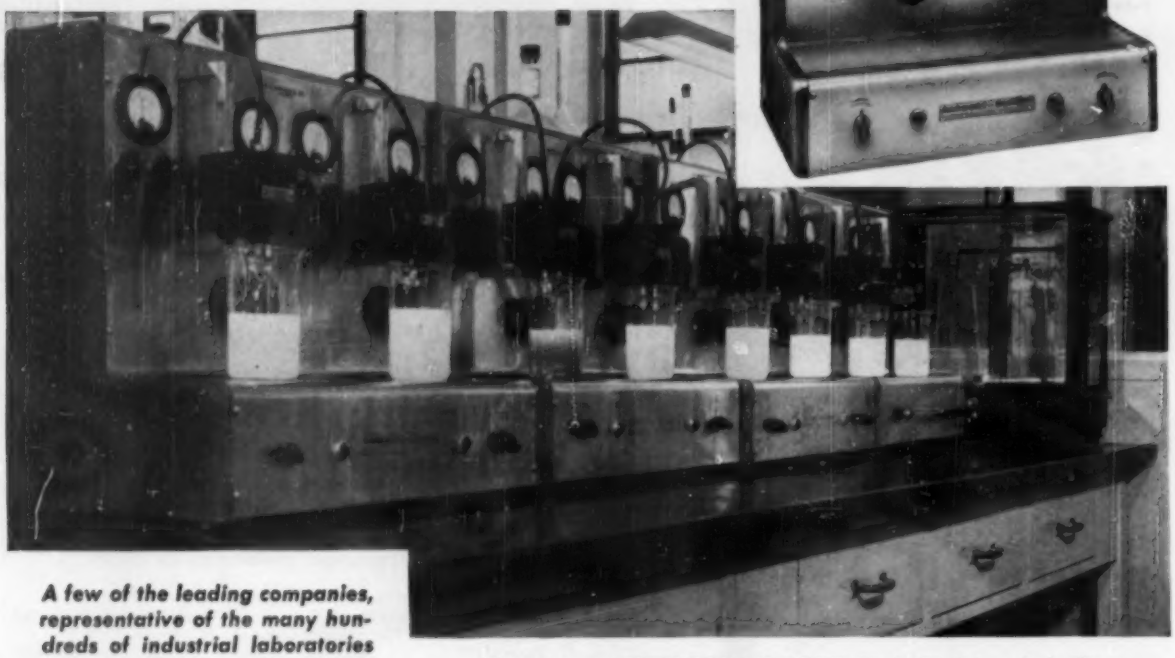

Photo Courtesy INTERNATIONAL HARVESTER COMPANY, Melrose Park, Illinois

A few of the leading companies, representative of the many hundreds of industrial laboratories using the Sargent - Slomin and Heavy Duty Analyzers for control analyses . . .

AMPCO METAL, Inc.
ANDERSON LABORATORIES
CALERA MINING COMPANY
EUREKA WILLIAMS COMPANY
THE FEDERAL METAL CO.
FORD MOTOR COMPANY
THE GLIDDEN COMPANY—Chemical, Metal and Pigment Division
HOT POINT CO.
HOWARD FOUNDRY COMPANY
INTERNATIONAL HARVESTER COMPANY
KENNAMETAL Inc.
McQUAY - NORRIS MANUFACTURING CO.
NATIONAL LEAD COMPANY, Fredericktown, Missouri
PIASECKI HELICOPTER CORPORATION
REVERE COPPER & BRASS INCORPORATED
THE RIVER SMELTING & REFINING COMPANY
SILAS MASON COMPANY
THE STUDEBAKER CORPORATION
THOMPSON PRODUCTS, INC.

Sargent-Slomin Electrolytic Analyzers are recommended for such electro analytical determinations as: Copper in—ores, brass, iron, aluminum and its alloys, magnesium and its alloys, bronze, white metals, silver solders, nickel and zinc die castings. Lead in—brass, aluminum and its alloys, bronze, zinc and zinc die castings. Assay of electrolytical copper, nickel and other metals.

Sargent analyzers are completely line operated, employing self-contained rectifying and filter circuits. Deposition voltage is adjusted by means of autotransformers, with meters indicating volts and amperes and controls on the panel. An easily replaceable fuse guards against circuit overload. Maximum D.C. current capacity is 5 to 15 amperes; maximum D.C. voltage available, 10 volts.

Sargent-Slomin Analyzers stir through a rotating chuck operated from a capacitor type induction motor, having a fixed speed of 550 r.p.m. with 60 cycle A.C. current or 460 r.p.m. with 50 cycle A.C. current. Motors are sealed against corrosive fumes and are mounted on cast metal brackets, sliding on ½" square stainless steel rods, permitting vertical adjustment of electrode position over a distance of 4". Pre-lubricated ball-bearings support the rotating shaft. All analyzers accommodate electrodes having shaft diameters no greater than 0.059 inch. Stainless steel spring tension chucks permit quick, easy insertion of electrodes and maintain proper electrical contact. Special Sargent high efficiency electrodes are available for these analyzers. Illustrated above is one model of the five types of Sargent-Slomin and Heavy Duty Analyzers.

S-29465 ELECTROLYTIC ANALYZER—Motor stirred, Two Position, 5 Ampere. With two adjustable heaters, pilot lights and control knobs. For operation from 115 volt, 50 or 60 cycle A.C. circuits.....**$390.00**

SARGENT *SCIENTIFIC LABORATORY INSTRUMENTS • APPARATUS • SUPPLIES • CHEMICALS*

E. H. SARGENT & CO., 4647 W. FOSTER, CHICAGO 30, ILLINOIS
DETROIT 4, MICH. • DALLAS 35, TEXAS • BIRMINGHAM 4, ALA. • SPRINGFIELD, N. J.

any way you measure
ANODE PERFORMANCE

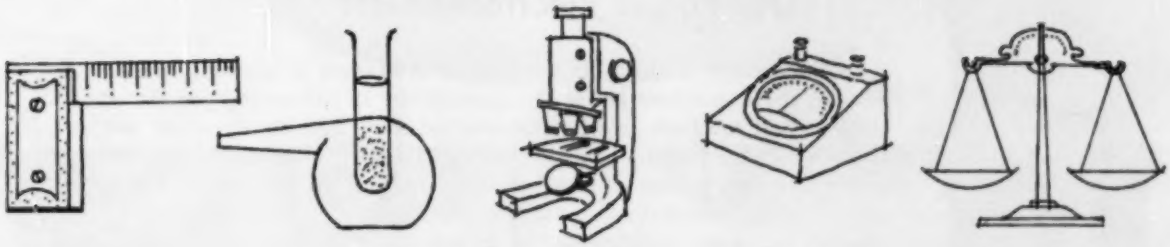

Structural and Dimensional Uniformity? | Chemical Stability of Treatments? | Uniform Texture? | Cell Voltage? | Pounds Consumed per ton of Chlorine Produced?

STACKPOLE
GraphAnode® ANODES
prove second to none for
Economical Chlorine Production

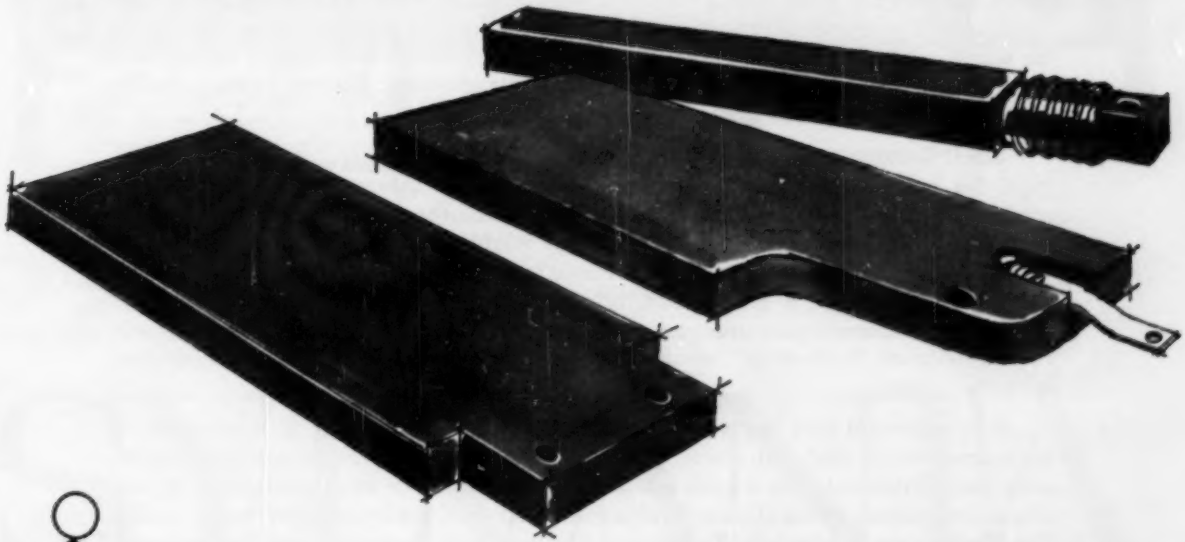

STACKPOLE CARBON COMPANY,
St. Marys, Pa.

CATHODIC PROTECTION ANODES • FLUXING & DE-GASSING TUBES • SALT BATH RECTIFICATION RODS • ROCKET NOZZLES • RISER RODS • GRAPHITE BEARINGS & SEAL RINGS • ELECTRODES & HEATING ELEMENTS • WELDING CARBONS • VOLTAGE REGULATOR DISCS • "CERAMAGNET"® CERAMIC MAGNETS • ELECTRICAL CONTACTS • BRUSHES FOR ALL ROTATING ELECTRICAL EQUIPMENT • AND MANY OTHER CARBON, GRAPHITE AND ELECTRONIC COMPONENTS.

263C

Editorial

Our Future Electrochemists

OUR Society naturally is very much interested in growing, not so much for the sake of mere numbers as for the opportunity of promoting the use of electrochemical ideas and methods in research and industry. Not nearly all of our members can be called "pure electrochemists," but all have some compelling interest in the field, and find some phase of the Society's activities useful to them. Every student of chemistry learns a certain amount of electrochemical theory and practice in his college courses, but many decide that the formal study of electrochemistry is something of use only to the expert, to be avoided by the average chemist like other abstruse and difficult topics (thermodynamics?).

It is important to stress the values of electrochemical study at the level of our future scientists, namely the college students, both graduate and undergraduate. Our Society has had very little success in making a direct approach to students. If all graduate students in chemistry were asked to name several internationally known chemical societies, how many would mention ours? Is there any way to make our name more familiar in the Graduate Departments?

Several years ago, a Prize Essay Contest was instituted by the Corrosion Division. It was dropped after a few trials showed that it did not arouse any wide-spread enthusiasm or even attention; only half a dozen essays were submitted each year. (To be sure, if 1000 essays had been entered, the Committee would have squawked very loudly). This year the Contest has been revived on a smaller scale, with more intense effort to stimulate interest in a smaller number of schools. We await the results of this new approach with interest.

A student round table at the Houston Meeting met with fayorable response: some 35 students and faculty members attended from various colleges up to 200 miles away. They heard brief talks by Society officers and Divisional representatives, then had an opportunity to meet with Society members individually. The program should be worth repeating at future meetings; the very personal knowledge of several students in each of a few cities that an active Electrochemical Society exists is worth more than a great deal of impersonal advertising.

Local Sections have had only limited success in attracting students to their meetings. No matter how well advertised, no matter how interesting the speaker, few students will go to a $3.50 dinner meeting, nor will they go to a lecture held in a restaurant after the dinner. Local Sections might do better to secure cooperation with the various colleges, having dinner nearby if they wish, then meeting for a well-announced lecture in a college auditorium or classroom. At this point, the topic of the lecture assumes importance; an excellent discourse on the subject "Developments in Molybdenum Technology" would hardly help to secure future hearty cooperation with the college.

It is important that the well-trained student realize the value of those parts of his courses which deal with electrochemistry, even though he has no complete course with that formal title. He should also realize that before or after graduation he can join a professional group of considerable industrial and academic importance, called The Electrochemical Society. To this end the Society will have to make close personal contact with each chemistry department, its faculty, and students, so that its name becomes familiar as that of a society with something of value to offer.

—CVK

NEW SYLVANIA CR-407 PHOSPHOR

to brighten the face of TV

Sylvania CR-407 phosphor, a totally new phosphor, offers outstanding characteristics in adherence, contamination and ion burn resistance, and brightness that promise to put a new glitter in your TV picture tube quality.

One long-sought-after characteristic, superior adherence during the rewetting cycle, has been developed into this new phosphor. Sylvania CR-407 phosphor offers up to 20% better adherence than any phosphor now commercially available.

Another reason: Sylvania CR-407 phosphor provides greater contamination resistance than phosphors available in production quantities.

Advances like these are common at Sylvania. The Chemical & Metallurgical Division is fully equipped to provide extensive engineering research in a wide variety of technological areas. We are continually seeking new and better materials to help you make a better, more stable and salable product. For additional information on Sylvania CR-407 phosphor, write Chemical & Metallurgical Division, Sylvania Electric Products Inc., Towanda, Pennsylvania.

SYLVANIA

Subsidiary of **GENERAL TELEPHONE & ELECTRONICS**

265C

ANACONDA "PLUS-4"

phosphorized copper anodes

in a new form

CURVED ANODES

for plating cylinders faster and more uniformly

To make anode surfaces parallel the rotogravure cylinder being plated, and to fit the curve of the current-carrying slings, Anaconda "Plus-4" phosphorized copper anodes are now extruded to precisely curved shapes.

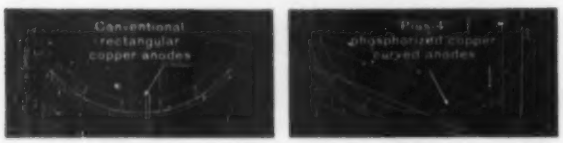

This design offers possible cost savings and improved cylinder quality.

It is reported that very uniform deposits are obtained from these specially shaped anodes, thus helping to cut finishing costs. The solution of the anode is also more uniform, thereby reducing the scrap.

For more information, write: Anaconda American Brass Company, Waterbury 20, Conn. In Canada: Anaconda American Brass Ltd., New Toronto, Ont.

NO EXTRA DIE COST
Simply specify inside radius of anode.

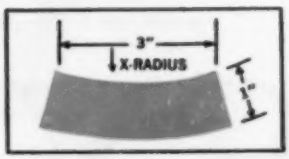

"Plus-4"® phosphorized copper anodes

ANACONDA®

Anaconda American Brass Company

Diffusion Theory of Polarization and Recuperation Applied to the Manganese Dioxide Electrode

Allen B. Scott

Union Carbide Consumer Products Company, Parma, Ohio and

Department of Chemistry, Oregon State College, Corvallis, Oregon

ABSTRACT

The behavior of MnO_2 electrodes during and following cathodic discharge is accounted for on the basis of diffusion of the reduction product into the solid electrode. A solution of the diffusion equation predicts the general form of the discharge and recuperation curve satisfactorily. A method for determining the electrode surface area and diffusion coefficient is given and results of some preliminary experiments outlined.

Polarization and recuperation processes in oxide electrodes have received much attention in recent years, particularly those in manganese dioxide primary cell cathodes. Vosburgh (1) recently reviewed current theories of the MnO_2 electrode and has given a comprehensive bibliography. Of the mechanisms proposed, that which appears to have been originally advanced by Coleman (2) seems to have the greatest body of experimental and logical support, at least in the case of discharge at moderate current density in electrolytes having pH in the middle range. Coleman proposed that polarization and recuperation resulted from the accumulation of lower (hydrous) oxide on the surface and its subsequent diffusion into the solid MnO_2 and suggested that the diffusing entities were protons and electrons. He applied Fick's law to the process in order to find a relation between drain and capacity of actual electrodes; his development was complicated by allowance for the transport of the lower oxide by the electric field as well as by ordinary diffusion, although he recognized that only the latter might actually occur. Simple calculations given later show that transport by the field is insignificant. Easily available solutions for the diffusion equation, applied to a simplified model of the electrode, lead to equations for both polarization and recuperation well in accord with experiment.

Kozawa (3) reduced MnO_2 with a known amount of Mn^{++} ion and concluded that the lower oxide produced remained primarily on the surface, and that diffusion of the lower oxide into the MnO_2 was not of importance. However, his calculations were based on surface area measured by the BET method with nitrogen, and it is probable, as is shown later, that the surface presented to the electrolyte was smaller than the BET area by 5 to 10 times. In such a circumstance, the lower oxide comprised perhaps as much as the equivalent of 20 layers, and the samples were already in late stages of recuperation when potentials were measured.

The MnO_2 electrode is very nearly reversible to H^+ ion, its potential decreasing by about 0.06 v with a unit increase of pH. The primary electrochemical reaction for the electrode operated at moderate current densities is thus

$$MnO_2 + H^+ + e = MnOOH \qquad [1]$$

Mn^{++} is found in the electrolyte (4, 5) during discharge (except during early stages at pH > 7.5) but is undoubtedly produced by secondary chemical reactions. For example ΔF at 25°C for the consecutive reactions

$$MnOOH + H_2O = Mn^{+++} + 3OH^-$$
$$2Mn^{+++} + H_2O = Mn^{++} + MnO_2 + 4H^+$$

is −26.0 kcal at pH = 7 and Mn^{++} activity = 0.01, according to approximate data given by Latimer (6). Alternatively MnOOH may decompose in the solid state, $\Delta F°$ for the reaction

$$2MnOOH = Mn(OH)_2 + MnO_2$$

being estimated (6) at −10 kcal. $Mn(OH)_2$ would dissolve readily at pH = 7. Thus there appears to be no necessity to assume the reduction to divalent manganese as a primary step except perhaps at high current density or excessively low pH.

A complete theory of polarization and recuperation would have to take cognizance of a great variety of secondary reactions[1] as well as the role of carbon; for the present, it seems that more will be gained by restricting consideration to the process [1], polarization and recuperation occurring by the mechanism of Coleman.

Diffusion Theory of Polarization and Recuperation

The bobbin of a dry cell is a complicated electrochemical system, and for our purposes it will be preferable to simplify the arrangement of components to the following:

Carbon/Black/MnO_2/Solution

Conduction is entirely electronic in the carbon and the black, and almost entirely electronic in MnO_2, since MnO_2 has a conductivity between 0.1 and 0.01

[1] A theory of the effect of the removal of Mn^{++} from the electrode during discharge in acid electrolytes on polarization and recuperation has been developed by Yoshizawa and Vosburgh, (7).

ohm^{-1} cm^{-1} at room temperature (8) which certainly cannot arise from ionic migration. The electrochemical reaction, therefore, takes place at the MnO_2-solution interface. The field in the MnO_2 is very low; for example, at a current density of 1 ma cm^{-2}, taking the MnO_2 conductivity to be 0.01 ohm^{-1} cm^{-1}, the field is only 0.1 v cm^{-1}. This result shows that any migration of ions which occurs within the MnO_2 must take place as the result of chemical potential gradients rather than electric potential gradients. By comparison, if we assume unit activity coefficient, a change in mole fraction of MnOOH from 0.5 at the surface to 0.1 at a point 1 μ inside the surface of MnO_2 undergoing cathodic reduction results in a mean chemical potential gradient of 4 x 10^7 joule mole^{-1} cm^{-1}, which would exert the same effect as an electric field of 420 v cm^{-1}.

During discharge the following processes occur. Protons are transferred from solvent molecules to oxide ions on the MnO_2 surface under the influence of the negative potential of the cathode. At the same time, electrons are stably trapped on neighboring Mn^{+4} ions, reducing them to Mn^{+3}. The dilution of MnO_2 with MnOOH in the form of a solid solution reduces the MnO_2 activity and thus the electrode potential decreases as the reaction proceeds. Johnson and Vosburgh (9) studied the potential of electrodes made of mixtures of MnO_2 and MnOOH which were presumably allowed to come to equilibrium, 50 days being allowed for interdiffusion of the two solids, and found that the emf could be represented by

$$E = E^\circ + 0.073 \ln \frac{\text{mole \% } MnO_2}{\text{mole \% MnOOH}} \qquad [2]$$

at 25°C. The difference between the factor 0.073 and the theoretical value 0.059 is ascribed to the use of mole per cents rather than activities. E° varies with pH; the average at pH = 7.5 was found to be 0.416 v with respect to saturated calomel.

Recuperation consists of the diffusion of protons and electrons toward the interior under the driving force of the chemical potential gradient.

A quantitative theory for the polarization and recuperation can be obtained readily by the use of the foregoing model. Consider the MnO_2 to consist of a semi-infinite solid, bounded by the plane $x = 0$. The region $x < 0$ is occupied by solution. During discharge at constant current density, F_0 equivalents of MnOOH are produced per unit area per unit time. The diffusion problem can be solved by analogy to a problem in heat transfer, namely, the case of linear heat flow in a semi-infinite solid, initially at zero temperature, with a constant flux of heat across the boundary surface. Equations of interest in the present application, after throwing into a form suitable for mass transfer, are the following (10).

At $x = 0$, that is, on the surface of the MnO_2, the concentration of MnOOH as a function of time is

$$C = \frac{2F_0}{(D\pi)^{1/2}} \{t^{1/2} - (t-T)^{1/2}\} \qquad [3]$$

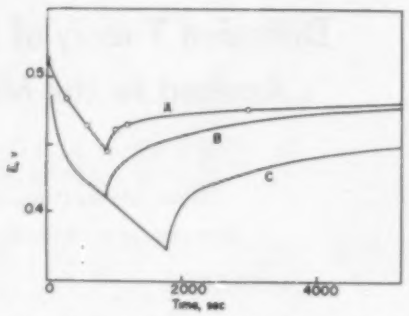

Fig. 1. Discharge and recuperation curves for the MnO_2 electrode. B, C, calculated; A, experimental (Ferrell and Vosburgh).

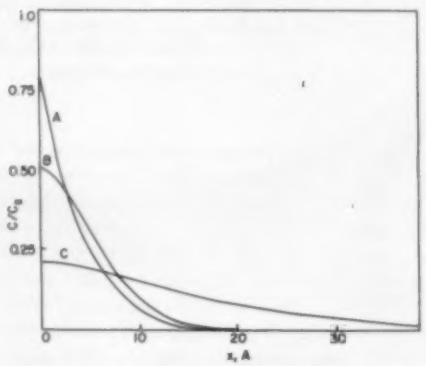

Fig. 2. Variation of MnOOH concentration with distance from surface. A, 1800 sec, discharged stopped; B, 2200 sec; C, 8200 sec.

and within the solid the concentration of MnOOH as a function of x, the distance from the surface, at any time t is

$$C = \frac{2F_0}{D^{1/2}} \left[t^{1/2} \left(\text{ierfc} \frac{x}{2(Dt)^{1/2}} \right) - (t-T)^{1/2} \left(\text{ierfc} \frac{x}{2D^{1/2}(t-T)^{1/2}} \right) \right] \qquad [4]$$

Here D is the diffusion coefficient for protons, accompanied by electrons, in the solid (assumed constant for the present), t is the time following start of the discharge, and T is the time at which the discharge stops and recuperation begins.[2] For $t<T$ the terms involving $t - T$ are to be taken as zero.

Using discharge and recovery curves such as those of Ferrell and Vosburgh (11) as a guide, the following values of the constants were arbitrarily assigned:

$F_0 = 1 \times 10^{-10}$ eq cm^{-2} sec^{-1} ($i = 9.5 \times 10^{-6}$ amp cm^{-2})

$D = 1.2 \times 10^{-10}$ cm^2 sec^{-1}

The concentration of MnOOH when pure, computed from the density, is 5.47×10^{-3} eq cm^{-3}. That of MnO_2 is 5.70×10^{-3} eq. cm^{-3}. The concentration of MnO_2 is given approximately by

$$C_{MnO_2} = 5.47 \times 10^{-3} - C_{MnOOH} \text{ eq cm}^{-3}$$

With these values and Eq. [2], [3], and [4], the curves of Fig. 1 and 2 were computed for discharge at pH = 7.5.

Figure 1 shows the variation in E with time for a discharge at current density 9.5×10^{-6} amp cm^{-2}, the

[2] ierfc (y) is defined by

$$\text{ierfc}(y) = \pi^{-1/2} \exp(-y^2) - 2y\pi^{-1/2} \int_y^\infty \exp(-z^2)\, dz.$$

discharge being discontinued at $T = 900$ sec and at $T = 1800$ sec. Recuperation occurs very rapidly on first stopping the discharge, but the rate of recuperation declines with time. Figure 2 shows the calculated distribution, as a function of the distance from the surface, of the MnOOH produced. Curve A represents the situation at the time of discontinuance of the discharge, curve B, 400 sec later, and curve C, 6400 sec later. It is evident that the surface was nearly saturated at 1800 sec, C_s indicating the concentration corresponding to pure MnOOH. In fact, from [3] it may be calculated that the surface would have been saturated after 2800 sec of continuous discharge.

Curve A of Fig. 2 shows clearly why the initial part of the recuperation is very rapid. The concentration gradient at the surface is extremely high during discharge; after the discharge stops the steep gradient at the surface is rapidly leveled (curve B), after which the potential rises much more slowly.

In Fig. 1 is also shown typical data of Ferrell and Vosburgh (11) for the discharge of an electrolytically deposited MnO_2 electrode at pH near 7.5, to be compared with the form of the calculated curve. The ordinates are not particularly significant, as the initial potential of MnO_2 is quite variable and further the choice of E° in Eq. [2] is somewhat arbitrary. Diffusion in the solid is seen to be adequate to account for the chief aspects of the discharge and recuperation.

It is to be noted that the slope of the calculated curve is greater than that of the observed curve after an extended period of recovery. This is almost certainly the result of assuming the solid to be semi-infinite. In the actual material composed of small, highly irregular particles, there will be many regions where advancing diffusion fronts will overlap, thus retarding diffusion.

There are two additional assumptions in the theory which require comment. First, it has been assumed that D is independent of C. It would appear, however, that D should be proportional to the concentration of unoccupied sites for protons, *i.e.*, proportional to C_{MnO_2}, and thus its variability would make itself felt wherever the concentration of MnOOH becomes large.

Second, the solid is not a continuous medium, and consequently the surface, instead of being a geometrical plane, is a region of finite thickness, namely about half the unit cell edge[3] (there being two MnO_2 formulas per cell). When $D = 0$ the rate of increase of concentration in the surface layer during discharge is not infinite, as given by Eq. [3], but is $F_s/1$ where 1 is the thickness of the surface layer. As D and t increase, the effects of the discontinuous structure diminish, and the surface concentration, instead of increasing linearly with time, becomes proportional to $t^{1/2}$.

If E is plotted against time for a constant-current discharge, the time required to saturate the surface with MnOOH, indicated by t_s, is located approxi-

[3] There is no unique way to compute the thickness of the surface layer of MnO_2, as this depends on the crystal plane assumed to lie parallel to the surface; further, the value would depend to some extent on the fraction of MnO_2 reduced to MnOOH.

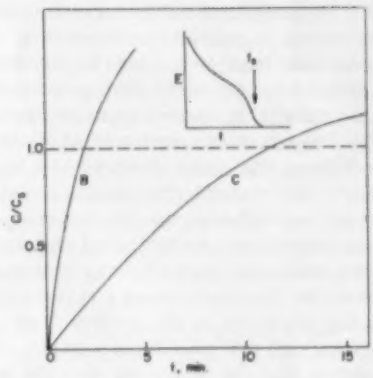

Fig. 3. Growth of MnOOH concentration at surface. A, location of t_s, the saturation time; B, t_s = 1.8 min; C, t_s = 11 min.

mately at the second inflection (inset, Fig. 3). If the discharge is very rapid,

$$C_s = \frac{F_s}{1} t_s \qquad [5]$$

In case the surface area of the oxide is unknown, F_s may be determined in this manner, and from it, by use of the known current, the surface area may be found. Having the surface area, the oxide may be discharged at a lower rate, for which Eq. [3] may be expected to hold and

$$C_s = \frac{2F_s}{(D\pi)^{1/2}} t_s^{1/2} \qquad [6]$$

This provides a method for the measurement of D.

Experimental

To illustrate the application of the theory, some simple experiments were carried out. Using a modification of the Utilization Test (12) discharge tests were performed on electrolytic MnO_2 of surface area 63.9 m^2/g, determined by the BET method. Figure 4 shows the results of three such experiments. In an even layer against the face of a large graphite electrode, 0.706 g of MnO_2 was pressed. The electrode was made the cathode at a current of 200 ma, with an electrolyte of NH_4Cl and NH_3 at pH = 7.0 and a zinc anode. The potential of the cathode with respect to a saturated calomel electrode was measured by

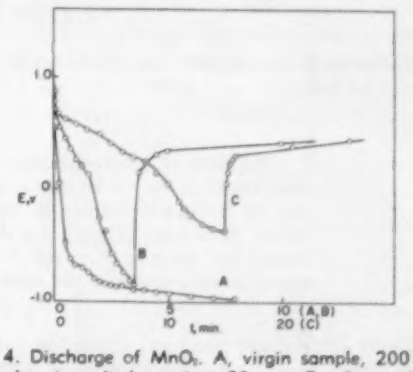

Fig. 4. Discharge of MnO_2. A, virgin sample, 200 ma; B, after recharging, discharged at 50 ma; C, after recharging, discharged at 10 ma.

means of a vacuum-tube voltmeter. An inflection at 1.8 min is barely discernible in curve A.

The oxide was then recharged, by making it the anode at 200 ma for 4 min, at 100 ma for 6 min, and allowing it to stand on open circuit until the voltage was steady. Upon cathodic discharge at 50 ma (curve B), the inflection was again observed at 1.8 min, but it was more pronounced. The polarization in the early part of the discharge was much diminished. At 3.5 min the current was discontinued and the recuperation was observed. Curve C was obtained, after again recharging the oxide, using a current of 10 ma.

Taking the thickness of the surface layer as one-half the mean unit cell edge for $\beta-MnO_2$, or 1.94Å, and assuming [5] to apply to the 50 ma discharge, $F_o = 9.8 \times 10^{-15}$ eq cm^{-2} sec^{-1}, and the effective surface area is 5.4 m^2 or 7.7 m^2/g. This is only about 12% of the surface area measured by the BET method. As previously mentioned, this result has an important bearing on the experiments of Kozawa. D from [6] is 2.7×10^{-17} cm^2 sec^{-1}. This should be taken as a rough approximation only, on the basis of these preliminary experiments.

The effects of diffusion are apparent at 10 ma, where t_s is greater than 5 times t_s for the 50 ma discharge. A schematic plot of concentration at $x = 0$ *vs.* t is given in Fig. 3 for experiments B and C. It would assist in verifying the diffusion theory if further simple experiments of this kind were carried out to establish if $F_s t_s^{1/2}$ were constant at higher values of $t_s^{1/2}$. The value of D could then be established.

The potential at t_s is not clearly defined. Equation [2] predicts a sigmoid discharge curve, E going to $-\infty$ at t_s; however, at $t > t_s$, E would be governed by a second relation involving MnOOH and $Mn(OH)_2$. Practically, E at t_s should be about that reported by Kozawa (3) for the Mn_2O_3 electrode, or 0.23 v with respect to the saturated calomel electrode. The observations reported here indicate that a large part of the polarization during the 200 ma discharge of the virgin MnO_2 was activation polarization. At the lower current densities, after recharging the oxide, E at t_s was still about 0.2 v less than that of the Mn_2O_3 electrode. Whether there is activation polarization under these conditions may be decided by means of an oscillographic method; however, previous results (1) make this appear unlikely. In any case, the choice of t_s is probably not much affected by the magnitude of E.

Acknowledgment

It is a pleasure to acknowledge the valuable contributions of G. E. Evans and J. A. Krumhansl who suggested the application of the physics of solids to the electrode process, of N. C. Cahoon and M. P. Korver who made available the utilization test equipment and provided much useful information concerning the theory of discharge and recuperation, and of D. R. Allenson and A. W. Smith with whom beneficial discussions were held.

Manuscript received April 5, 1960.

Any discussion of this paper will appear in a Discussion Section to be published in the June 1961 JOURNAL.

REFERENCES

1. W. C. Vosburgh, *This Journal*, **106**, 839 (1959).
2. J. J. Coleman, *Trans. Electrochem. Soc.*, **90**, 545 (1946).
3. A. Kozawa, *This Journal*, **106**, 79 (1959).
4. N. C. Cahoon, *ibid.*, **99**, 343 (1952).
5. A. M. Chreitzberg, D. K. Allenson, and W. C. Vosburgh, *ibid.*, **102**, 557 (1955).
6. W. M. Latimer, "Oxidation Potentials," Prentice-Hall, New York (1952).
7. S. Yoshizawa and W. C. Vosburgh, *This Journal*, **104**, 339 (1957).
8. R. Glickman and C. K. Morehouse, *ibid.*, **103**, 149 (1956).
9. R. S. Johnson and W. C. Vosburgh, *ibid.*, **100**, 471 (1953).
10. H. S. Carslaw and J. C. Jaeger, "Conduction of Heat in Solids," p. 56, Oxford (1947).
11. D. T. Ferrell and W. C. Vosburgh, *This Journal*, **98**, 334 (1951).
12. N. C. Cahoon, *ibid.*, **99**, 343 (1952).

Aluminum Reactions with Water Vapor, Dry Oxygen, Moist Oxygen, and Moist Hydrogen between 500° and 625°C

P. E. Blackburn and E. A. Gulbransen

Chemistry Department, Research Laboratory, Westinghouse Electric Corporation, Pittsburgh, Pennsylvania

ABSTRACT

The rate of reaction between water vapor and aluminum is greater than that between the metal and oxygen. Mixtures of water vapor with either oxygen or hydrogen react with the metal at the same rate as does water vapor alone. Hydrogen blisters are formed in the metal in the presence of water vapor, but none is observed when water is absent. Blister formation in water vapor is not detected if the metal is first reacted with HCl solution.

Relatively little study has been given the reaction between water vapor and pure aluminum, although considerable research has been done on aluminum oxidation in air, oxygen, and liquid water. Oxidation of the metal in oxygen within the temperature range 350°-550°C was measured by Gulbransen and

Wysong (1). They found a parabolic rate from 350° to 475°C and a linear oxidation rate above this temperature region. Smeltzer (2) has measured oxygen reaction rates of metallographically polished and annealed aluminum between 400° and 600°C. He fitted his data to two parabolic rate constants which apply to thin and thick films. The oxide film was observed to grow very slowly above a weight gain of 35 to 40 $\mu g/cm^2$.

The barrier oxide thickness of films formed on aluminum in dry and moist atmospheres from room temperature to 600°C has been measured by Hunter and Fowle (3). Their method consisted of measuring the voltage necessary to produce normal leakage through the oxide film. The barrier oxide formed between 25° and 500°C was found to be amorphous, while a thicker crystalline film was discovered above 475°C. The thickness of each type of barrier oxide is a linear function of the temperature. For crystalline forms the thickness reaches 205Å at 600°, and for amorphous films it is 55Å at 500°. The oxide layer in excess of the barrier film is porous.

Plumb (4) has measured the specific surface area of aluminum with various surface preparations. The procedure required determining the thickness of a known amount of oxide deposited anodically on aluminum. The specific area relative to the apparent area decreased with oxide thickness. Surface roughness of 25 for rough abrasion, 6 for metallographic polish, 2 for chemical polish, and 2.5 for as-rolled samples were observed at oxide thicknesses of about 30Å.

Draley and Ruther (5) studied the reactions of both commercial 2 S aluminum and the pure metal with liquid and gaseous water. They have observed the presence of blisters in specimens oxidized in liquid water. Although these blisters usually contained corrosion products, some were found to be gas filled. Samples exposed to liquid water for two weeks at 290°C were completely destroyed. A cycle of decomposition resulted from water filling the blisters succeeded by further attack producing more blisters. Draley and Ruther have postulated a mechanism for blister formation. Briefly, protons from the reacting water diffuse through the oxide film to the metal, balancing the charge of aluminum cations moving to the gas-oxide interface. The protons are then reduced to hydrogen atoms, some of which diffuse into the metal where they combine in rifts and cavities to form hydrogen molecules. The molecular hydrogen pressure expands the soft metal, forming blisters. Vacuum fusion analyses of oxidized samples showed that the gas filling the blisters was hydrogen. It is proposed that impurities with low hydrogen overvoltage potentials catalyze the combination of hydrogen atoms within the metal. Alloys containing additions of such elements were found to resist water attack. It is suggested that these added materials catalyze formation of hydrogen molecules at the oxide metal interface. Hydrogen molecules cannot diffuse into the metal, since only atomic hydrogen is believed to diffuse.

Carlson (6) has found that intergranular attack of aluminum at 100°C is considerably less in hydrochloric acid than in distilled water.

Coriou, *et al.* (7) found that pure aluminum was severely corroded in liquid water above 200°C. Blisters formed in the pure aluminum resulted in an appreciable expansion of the metal. Practically all of the blisters were formed in grain boundaries since there was little change in the volume of aluminum single crystals.

The present research was proposed to study the reaction of aluminum in water vapor and in mixtures of water vapor with hydrogen or oxygen.

Experimental Procedure

Apparatus.—The apparatus used for this study consisted of a vacuum system made of Pyrex tubing and metal Alpert (8, 9) valves. The apparatus was evacuated with two-stage oil diffusion pumps separated from the "clean" system by crackers. A Bayard-Alpert (10) gauge and a mercury manometer, separated from the system by a null manometer, were used to measure pressures within the apparatus. Samples were heated inside a mullite furnace tube, which was sealed directly to the Pyrex system.

A Kanthal resistance furnace which heated the mullite tube was held to within ± 0.5°C by a L & N controller. Bake out ovens enclosed the system, permitting degassing or maintenance of temperature above the condensation point of water wapor.

An all-quartz microbalance was constructed of small rods. Sensitivity was increased by using a girder type beam which weighed less than half a gram. Fine quartz filaments, sealed directly to the beam and quartz frame, were employed in vertical suspension at the fulcrum and at each end of the beam. This balance had a sensitivity of 321 $\mu g/cm$ where the position of the beam could be read with a traveling microscope to ±0.0005 cm.

Gases.—Either spectroscopically pure oxygen obtained from Linde Air or tank hydrogen diffused through a palladium tube was admitted to a mixing bulb from which it could be added to the system as a

Table I. Spectrographic analysis of aluminum

Treatment	Cu	Fe	Mg	Mn	Si	Al
	parts per million					
Chemically polished	10	20	20	10	10	balance
Chemically polished and vacuum annealed	20	<10	20	10	10	balance
H_2O (blisters)	20	10	15	10	10	balance
H_2O and O_2 (blisters)	20	15	15	10	10	balance
H_2O and H_2 (blisters)	<20	<10	<10	<10	<10	balance
1M HCl-H_2O (no blisters)	20	10	10	10	10	balance

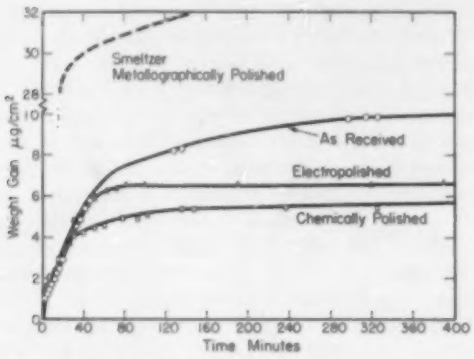

Fig. 1. Oxidation of vacuum annealed aluminum in 0.1 atm of oxygen at 600°C.

single component gas or mixed with water vapor. Water vapor was generated from a bulb of degassed distilled water.

Samples.—Two types of very pure rolled aluminum were kindly furnished by the Kingston Laboratories of Aluminium Limited. Table I compares spectrographic analyses of polished and annealed materials with those of reacted samples.

The effects of three types of surface treatment on oxidation behavior are compared in Fig. 1. The greater apparent oxide thicknesses formed on the "as-received" and on Smeltzer's metallographically polished sample are attributed to greater surface roughness for these samples (see Results and Discussion).

The electrochemical polish was carried out in a solution consisting of one part perchloric acid and 5 parts methanol at 10°C and 25 v. The chemical polishing solution was 6% nitric acid and 94% phosphoric acid, used at a temperature of 95°C. The sample was washed in 55°C distilled water. Oxidation behavior of the two specimens appeared to be similar. All of the remaining experiments were made with chemically polished samples.

Procedure.—The procedure consisted of suspending a polished specimen in the furnace tube from one end of the balance beam. After evacuating and degassing the system, the specimen was degassed and annealed at 600°C for one hour. The pressure in the system varied between 10^{-5} and 10^{-6} during the degassing treatment. The samples lost an average of 1 μg of gas per cm² during the annealing process. The furnace was adjusted to the desired temperature, gases were admitted from the mixing bulb, and the change in weight with time was observed.

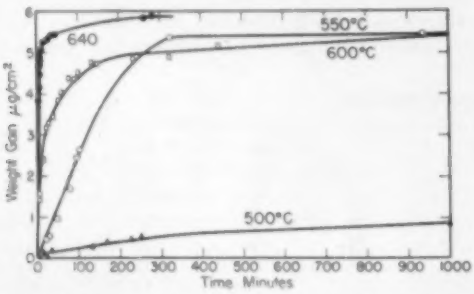

Fig. 2. Oxidation of aluminum in 0.1 atm O_2 between 500° and 640°C.

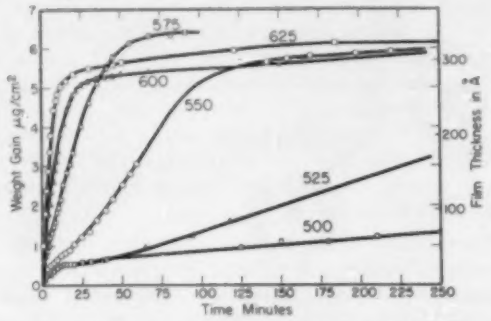

Fig. 3. Oxidation of aluminum in 0.1 atm water vapor

Results

Kinetics.—Figure 2 shows the weight gain *vs.* time curves obtained for samples oxidized in 0.1 atm of oxygen at 500, 550, 600, and 640°C. For the latter three temperatures the reaction consists of a relatively fast oxidation rate up to a weight of 5 to 6 μg/cm², where the rate becomes very slow. The 500° measurement was considerably slower than the higher temperature experiments. In these cases, as in the remainder of the kinetic studies, the data failed to conform to any of the theoretical curves, *i.e.*, linear, parabolic, cubic, logarithmic, or inverse logarithmic.

The oxidation of aluminum in 0.1 atm of water vapor for samples reacted at 25° intervals from 500° to 625°C is shown in Fig. 3. Here the extent of rapid oxidation is again between 5 and 6 μg/cm². No significance is attached to the apparently greater oxide thickness on the 575°C measurement. It is believed to be due to a larger surface roughness as a result of pitting during chemical polishing. After 24 hr the 500° measurement reached 6.0 μg/cm² while the 525° measurement was at 7.1 μg/cm². Assuming smooth surface and formation of Al_2O_3, the oxide depth is 53Å for each microgram of oxygen reacting per square centimeter. Film thicknesses based on these assumptions are given in Fig. 3. The slower rate then begins at about 300Å. However, Plumb has shown that chemically polished aluminum has a surface roughness of between 1.5 and 2.0, so the onset of the lower oxidation rate is actually between 170 and 220Å when the room temperature film of 20Å is added. Hunter and Fowle indicate that crystalline barrier films for aluminum oxide vary between 170 and 205Å over this temperature range. It is apparent that rapid oxidation ceases once the barrier oxide layer has formed. The lower rate is thus due to growth of a porous oxide over the barrier oxide. This mechanism applies to both oxygen and water vapor corrosion. The difference between this data and Smeltzer's may be attributed to a difference in surface roughness. According to Plumb the surface roughness of abraded samples may vary between 6 and 25, depending on the method and grit size used. Smeltzer's values for the extent of aluminum oxidation would fall in line

with a barrier oxide thickness of 200Å if average surface roughnesses of 8 to 10 are used for his specimens.

Apart from the extent of oxidation described above, other features of the kinetic curves are less readily explained. Between 575° and 625°C the rapid rate from 1 to 5 $\mu g/cm^2$ appears to be almost linear, whereas between 500° and 550°C there is an upward curvature. The latter effect is characteristically observed in nucleation and growth controlled reactions. The rate over the first 0.5 to 1 $\mu g/cm^2$ is seen to be much more rapid than the subsequent weight gain. In this region the amorphous barrier layer described by Hunter and Fowle may be formed. These authors observed that the amorphous layer grows much faster than the crystalline film.

Samples oxidized in oxygen and water vapor gave identical electron diffraction patterns, indicating that the reaction in water vapor above 500°C results in a nonhydrated oxide film. This is consistent with the thermodynamics of alumina hydrates, compounds which are unstable at these temperatures.

Blister formation.—All of the 10-mil samples oxidized in water vapor developed blisters within the metal large enough to form easily visible mounds on the surface. Blisters were formed either on grain boundaries or along lines parallel to the rolling direction. A photomicrograph of the surface of a sample oxidized in water vapor at 600°C clearly shows swellings on the grain boundaries (Fig. 4).

Fig. 4. Surface of aluminum oxidized in 0.1 atm water vapor at 600°C. Magnification 25X before reduction for publication.

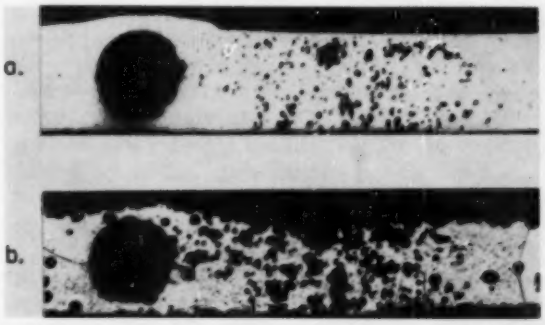

Fig. 5. Aluminum reacted in water vapor at 600°C: a, metallographic polish; b, etched in 10% HF. Magnification 100X before reduction for publication.

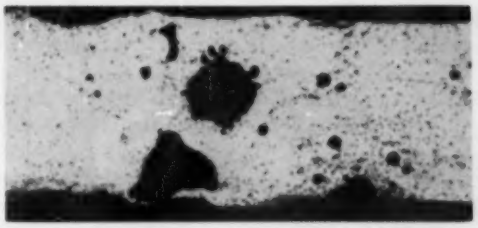

Fig. 6. Aluminum reacted in water vapor at 600°C, etched in 10% HF. Magnification 200X before reduction for publication.

No blisters formed on any of the samples oxidized in oxygen. Cross sections of water vapor samples (Fig. 5) show that, in addition to large blisters which swell the metal, there are many small cavities. Cross sections of as-received British specimens revealed the presence of small cavities and occasionally some large ones. It was observed that large cavities in water vapor reacted samples could be classified into two categories: (*a*) smooth walled blisters which swelled the metal, and (*b*) nondeforming cavities with walls constructed of a series of many small pits (Fig. 6). Since as-received specimens had both small cavities and the second type of large cavity, it was not possible to tell whether blisters appearing in the reacted specimens were already there or were increased by the reaction. The large smooth walled cavities resulted from the water vapor reaction since they were found only after samples had been oxidized in water vapor.

Although small blisters appear in as-received specimens, their presence in reacted samples occurs to a much greater extent. It would seem that small blisters, as well as large cavities, may form during the reaction.

The total hydrogen content of samples after reaction in water vapor (Table II) is less than 0.6% of the total weight gain, while the hydrogen content of water is 11% by weight. Thus, if the presence of hydrogen is due to reaction with water, only a small fraction of the available hydrogen enters the sample. Since the blister formation appears to be limited to impurity sites, either in grain boundaries

Table II. Gas analysis of aluminum vacuum fused at 700°C

Treatment	H_2	H_2O	CO and N_2	CH_4
	Moles/g of Al x 10^6			
As-received	1.13±0.08	0.011	0.025	0.025
Chemically polished	0.72±0.15	0.008	0.006	0.004
Annealed for 1 hr at 600°C	0.47±0.07	0.011	0.019	0.006
Oxidized in oxygen	0.40	0.011	0.038	0.013
Oxidized in water vapor	1.08±0.68	0.031	0.029	0.010
As-received*	1.21±0.25	—	0.027	0.063
Oxidized in moist air (blisters)*	1.26	—	0.043	0.035
Treated in HCl and oxidized in moist air (no blisters)*	0.35	—	0.036	0.017
Solubility at 600°C in 1 atm hydrogen	0.014			

* 40-mil French sheet; all others, 10-mil British sheet.

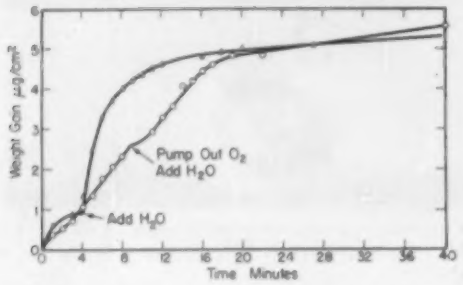

Fig. 7. Effect of oxide film on aluminum reaction at 600°C. △, sample A, very few blisters visible on surface; ○, sample B, one blister visible on surface.

or at inclusions, this low yield of hydrogen is not surprising.

The effect of an oxygen formed oxide layer on the water vapor reaction is shown in Fig. 7. Two samples were oxidized in oxygen; sample A for 3 min followed by addition of water vapor, sample B for 9 min followed by removal of oxygen and addition of water vapor. For the first case the reaction rate was sharply accelerated with addition of water vapor. In both cases the extent of oxidation was the same as in either water vapor or oxygen alone. The oxygen formed oxide layer appears to suppress formation of blisters which swell the metal, since there were very few in sample A and only one in sample B. There are two possible explanations for this finding. First, hydrogen may diffuse less readily through an oxygen formed film. Second, hydrogen pickup, which occurs simultaneously with formation of the oxide layer, is decreased in an amount proportional to the thickness of the oxygen formed film. The latter interpretation is derived from the fact that the total oxide thickness is the same whether it is formed in oxygen or in water vapor.

Before water vapor was added to these two specimens, 0.9 μg of oxygen per cm² reacted with sample A, and 2.5 μg of oxygen per cm² was taken up by sample B. If hydrogen pickup is proportional to the amount of oxide formed during the water vapor reaction, the second explanation implies that blisters would not be formed from hydrogen evolved from a μg/cm² oxygen pickup. Another water vapor sample was reacted until the weight gain reached 3.4 μg/cm². This specimen was covered with blisters somewhat smaller than those on samples oxidized

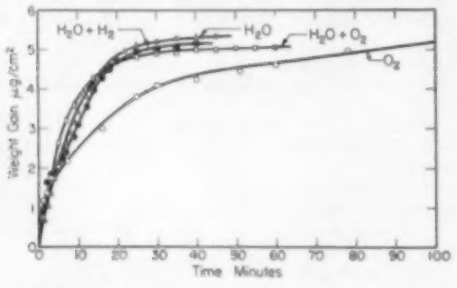

Fig. 8. Effect of corrosive atmosphere on aluminum oxidation rate at 600°C.

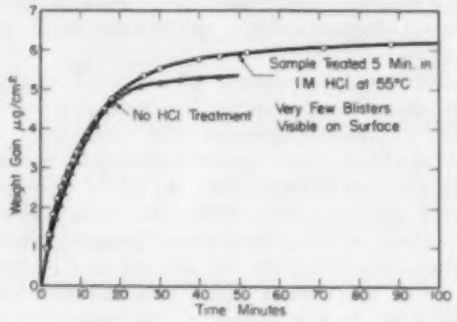
Sample Treated 5 Min. in 1M HCl at 55°C
No HCl Treatment
Very Few Blisters Visible on Surface
Weight Gain μg/cm²
Time Minutes

Fig. 9. Effect of treatment in HCl solution on aluminum water vapor reaction at 600°C.

to 5.5–6.0 μg/cm². Thus, the chief inhibitor of blister formation appears to be the resistance to hydrogen diffusion offered by oxygen formed oxide films.

The addition of oxygen or hydrogen to water before reacting it with aluminum made no apparent change in either reaction kinetics or blister formation. This is consistent with earlier observations (1) that the aluminum oxidation rate is independent of oxygen pressure. Here the oxygen partial pressure was varied between 10^{-1} and 10^{-8} atm. The rate of reaction in water vapor or in mixtures of water vapor with hydrogen or oxygen was about twice that in oxygen alone. Figure 8 presents reaction rates for samples oxidized at 600°C by the various treatments.

The suppression of intergranular attack by HCl additions to water, observed by Carlsen, was tested here. Samples were treated with HCl solutions at 55°C, washed in distilled water, annealed in vacuum, and reacted with water vapor. The kinetics of the reaction (Fig. 9) were the same as for samples without the HCl treatment, but no blisters were observed.

Table II shows the effect of HCl treatment on hydrogen content of French aluminum oxidized in moist air at 600°C. The hydrogen content of samples treated in HCl before reaction with water vapor is lower than any of the other samples tested. This is further evidence, although of a negative character, that the blisters are filled with hydrogen.

The role played by HCl in the suppression of blisters is not clearly understood from the available information. If impurities in the metal are important

Table III. Vaporization and solubility of chlorides

	Boiling point, (11) °C at 1 atm	Boiling point, (11) °C at 10^{-4} atm	Solubility, (12) g/100 g soln at 50°C
$AlCl_3$	447	142	32
Al_2Cl_6	180	77	—
$CuCl_2$	—	—	45
Cu_2Cl_2	1595	423	(1.5)
$FeCl_3$	1025	(512)	42
Fe_2Cl_6	319	172	76
$MgCl_2$	1418	677	37
$MnCl_2$	1190	562	50
$MnCl_3$	(627)	(262)	*
$SiCl_4$	57	—	*
Si_2Cl_6	139	—	*

* Unstable.

in the mechanism of blister growth, then treatment in HCl solution may result in removal of some of the impurities. This could occur either by solution of their chlorides during preparation or by vaporization of the chlorides during the degassing and annealing at 600°C. Table I gives results of spectroscopic analysis of samples following various reactions. The boiling points of the chlorides at 10^{-4} atm (10) and solubility of the chlorides in water (11) are found in Table III. There appears to be very little difference in the level of impurities in various samples. All the chlorides are water soluble, and iron, silicon, and aluminum chlorides have extremely high vapor pressures at the annealing and reaction temperature. Copper, magnesium, and manganese chlorides evaporate at a lower rate.

It is also possible that HCl suppresses blister formation by reacting with aluminum to form a chemisorbed layer of $AlCl_3$. Such a barrier may inhibit the diffusion of hydrogen.

Discussion

Since the as-received material held a considerable amount of hydrogen, the cause of the blisters is difficult to uncover. From Table II, however, it may be seen that a very low hydrogen content is found in chemically polished and vacuum annealed samples. The amount of hydrogen does not change with reaction in oxygen, whereas water vapor reaction significantly increases the hydrogen content. The rather wide scatter in these values is a function of sample size. Each specimen weighed about 0.3 g, and thus liberated only a few tenths of a microgram of gas for vacuum fusion analysis.

The data from this study are in general agreement with Draley and Ruther's experimental results. It may be noted that these earlier authors did not locate the blister with reference to grain boundaries. It is believed that their specimens came of material of much smaller grain size, making the relationship between grain boundaries and blisters obscure. Although these results appear to substantiate the Draley and Ruther theory, further work is necessary to clearly establish mechanism of blister formation.

Grace and Seybolt (13) studied the selective oxidation of aluminum in an iron-aluminum alloy between 700° and 900°C in hydrogen-water vapor mixtures. Since their study was on an alloy, their results are not applicable to our work on pure aluminum. In spite of this, there are some points which are worth mentioning. First, Grace and Seybolt made no correction for surface roughness, which could have been from 2 to 10. Second, they assume an initial weight gain of 2 to 3 $\mu g/cm^2$ (uncorrected surface area) during the first 15 min. In our work almost all of the oxide formed during the first 15 min at temperatures above 600°, i.e., about 3.5 $\mu g/cm^2$ (area corrected for surface roughness). Third, Grace and Seybolt determined an oxygen pressure dependence by varying the water pressure in a constant pressure of hydrogen. This dependence was near the 1/7 power of water vapor-hydrogen ratio where H_2O/H_2 was varied by three orders of magnitude. In this study the oxygen pressure was varied by a factor of 10^{20} with no apparent change in the rate of aluminum oxidation. The suggestion may be made that the pressure dependence observed by Grace and Seybolt is due to the water vapor pressure and not to the H_2O/H_2 ratio.

The Grace and Seybolt study gives a much lower rate of reaction than that which one would find by extrapolation of this data to their temperature range. They also found parabolic oxidation which was not found here (with the possible exception of the initial 50Å film). In view of these differences it would appear that the selective oxidation of the iron-aluminum alloy cannot be treated as if it were aluminum alone oxidizing at a higher temperature.

Thermodynamic calculations were made for the 600°C reaction,

$$H_2O = H_2 + 1/2\ O_2 \qquad [1]$$

The minimum partial pressure of oxygen in water and hydrogen and the lowest partial pressure of hydrogen in water and oxygen may be computed for reaction [1]. The mixed gases each contained 0.1 atm of water with an equal amount of hydrogen or oxygen.

Although the thermodynamic oxygen pressure was varied from 10^{-1} to $10^{-20.0}$ atm and the thermodynamic hydrogen pressure was varied from $10^{-19.5}$ to 10^{-1} atm, there was no apparent change in either the kinetics of the oxide growth or the formation of hydrogen blisters.

These calculations indicate that the reaction rate is independent of oxygen partial pressure. Vacancy diffusion is therefore excluded as a rate-controlling mechanism both by the failure of the curves to obey the parabolic rate law and by the absence of pressure sensitivity.

Conclusions

Aluminum reacts rapidly with water vapor above 500°C to form a crystalline oxide layer about 200Å thick. The rate of reaction beyond this oxide thickness is extremely low. The mechanism of reaction is rather complex, involving the formation of a thin amorphous barrier layer which crystallizes and thickens. Inasmuch as the kinetic curves fail to fit theoretical curves it is not possible to determine the method of oxide formation. Hydrogen and oxygen additions to the water vapor appeared to have no effect on the kinetics.

Hydrogen-filled blisters formed in the metal along rolling lines and between grain boundaries when water vapor was present in the gas phase. Hydrogen or oxygen added to the water vapor had no effect on blister formation.

Acknowledgment

The authors are grateful to Professor Duval for his helpful suggestions, to W. M. Hickam for developing a microgas fusion analysis for use here, and to J. Senko for the spectroscopic analysis.

Manuscript received Dec. 21, 1959. This paper was prepared for delivery before the Ottawa Meeting, Sept. 28-Oct. 2, 1958. This study was supported by the U.S.A.E.C. under subcontract to Bettis Plant.

Any discussion of this paper will appear in a Discussion Section to be published in the June 1961 JOURNAL.

REFERENCES

1. E. A. Gulbransen and W. S. Wysong, *Phys. Coll. Chem.*, **51**, 1087 (1947).
2. W. W. Smeltzer, *This Journal*, **103**, 209 (1956).
3. M. S. Hunter and P. Fowle, *ibid.*, **103**, 482 (1956).
4. R. C. Plumb, *ibid.*, **105**, 502 (1958).
5. J. E. Draley and W. E. Ruther, "Experiments in Corrosion Mechanism: Aluminum at High Temperatures," ANL-5658, Apr. 1957; also J. E. Draley and W. E Ruther, *This Journal*, **104**, 329 (1957).
6. K. M. Carlsen, *ibid.*, **104**, 147 (1957).
7. H. Coriou, L. Grall, J. Hure, D. Lelong, and J. Herenguel, *Rev. Met.*, **53**, 775 (1956).
8. D. Alpert, *Rev. Sci. Instr.*, **22**, 536 (1951).
9. D. Alpert, C. G. Matland, and A. O. McCoubrey, *ibid.*, **22**, 370 (1951).
10. R. T. Bayard and D. Alpert, *ibid.*, **21**, 571 (1950).
11. L. L. Quill, "The Chemistry and Metallurgy of Miscellaneous Materials, Thermodynamics," pp. 196-207, McGraw-Hill Book Co., New York.
12. A. Seidell, "Solubilities of Inorganic and Metal Organic Compounds," D. Van Nostrand Co., Inc., New York (1940).
13. R. E. Grace and A. U. Seybolt, *This Journal*, **105**, 582 (1958).

Dissolution of Copper in Sulfuric Acid Solutions

D. P. Gregory[1] and A. C. Riddiford

Department of Chemistry, The University of Southampton, United Kingdom

ABSTRACT

When copper disks rotate in sulfuric acid solutions, the observed rate of dissolution is first order with respect to the concentration of dichromate ion used as a depolarizer. By studying the effect of temperature and stirring speed at high and low acid concentrations, the process is shown to be determined completely by the rate of transport of dichromate ion to the reacting surface. This has been confirmed by studying the effect of different surface preparations, by measuring the rate of reaction of brass and amalgamated copper with these solutions, and by comparing the observed values with the theoretical rates. The effect of blocking off progressively larger areas of the working surface is reported.

From a number of studies of the dissolution of copper in acid solutions containing a suitable depolarizer (1-12), it appears that in some cases the surface process is so slow that the observed rate is a measure of the dissolution process occurring at the interface, whereas in others the observed rate is determined partly or wholly by a transport process. It is difficult to draw any general conclusions concerning the conditions under which one might expect to be able to study the surface process itself inasmuch as some of the investigations were purely qualitative in nature, and most of the others were confined to very narrow ranges of experimental conditions; but the results as a whole do suggest that the extent to which transport processes obscure the surface reaction is governed by the pH of the solution and by the concentration and nature of the species used as a depolarizer.

Published results leave little doubt that varying the type of depolarizer used may have a very marked effect on the character of the dissolution process. In the case of molecular oxygen, for example, the recent, detailed study of the dissolution of polycrystalline copper in sulfuric acid solutions (12) has shown that the observed rate is free from any measure of transport control. At the other extreme, the work of King and his co-workers (5, 6, 8) and of Buben and Frank-Kamenetskii (9) makes it fairly certain that the rate of dissolution in acid solutions of ferric salts is controlled entirely by the rate of transport of ferric ion to the interface under the chosen experimental conditions. Intermediate between these extremes are cases where the observed rate is controlled jointly by both the surface process and a transport process, *e.g.*, the dissolution of copper cylinders in an acetate buffer containing *p*-benzoquinone (10).

Much less is known concerning the effect of varying the concentrations of acid and depolarizer. Van Name and Hill (2) studied the dissolution of a number of metals in sulfuric acid solutions containing either ferric alum or the dichromate ion as depolarizer, and in hydrochloric acid solutions containing ferric chloride. In each case, they studied the effect of varying the concentration of acid and concluded that, whereas the observed rate is purely transport controlled at high concentrations, there is a general tendency for the surface process to begin to affect the over-all rate as the concentration of acid is diminished. The work of Lu and Graydon (12) provides the only other study of the effect of pH on the rate of dissolution of copper. In this case, as mentioned above, sulfuric acid solutions containing molecular oxygen were used, and the observed rate is a measure of the dissolution process at the copper/solution interface. Varying the concentration of acid has very little effect on the rate as long as the acid is present in excess; above pH 1, however, the rate declines rapidly as the concentration

[1] Present address: "Shell" Research Ltd., Thornton Research Centre, Chester, U. K.

is decreased, probably as a result of film formation on the surface of the copper.

This investigation provides the only detailed information available concerning the effects of varying the concentration of the depolarizer and the temperature. The study of these effects demonstrated the absence of any measure of transport control and thus enabled Lu and Graydon to suggest a possible mechanism for the dissolution process when oxygen is used as a depolarizer. For this reason, however, it throws little light on the general problem of deciding the conditions under which one might expect to be able to study the surface process, and it therefore seemed desirable to make a detailed study of the effect of a different depolarizer on the rate of dissolution of copper in sulfuric acid solutions.

The dichromate ion was chosen since it appeared possible that the observed rate might be controlled jointly by the surface process and by one of the transport processes at low acid concentrations. From the results of Van Name and Hill (2), the observed rate is purely transport controlled at sulfuric acid concentrations of 0.25M and above, whereas King and Weidenhammer (5) have indicated that the rate of dissolution of copper in 0.1M acetic acid solutions may be controlled by a slow surface process when the concentration of dichromate ion is less than 0.1M. The present study has been made using the rotating disk system, and particular attention has been paid to experimental conditions for which the rates of the transport processes may be calculated (13, 14).

Experimental

The main features of the apparatus have been described elsewhere (14). Disks were cut from ANALAR grade copper foil (*ca.* 0.15 mm thick) and were fixed to a brass former with black wax as shown in Fig. 1. The brass former fitted closely over the end of the stirring shaft and was held in place by a locking pin. The exposed brass of the former and the upper surface of the disk were protected from attack by a coating of black wax applied in hot benzene solution. This was shown to be impervious to acid dichromate solutions. Mounting the disks in this way was found to be more satisfactory than the previous method whereby disks were cut from thick foil and mounted on metal or perspex studs (14). In addition to minimizing edge effects, a fresh disk could be used for each run, easing the task of securing a reproducible surface for processes which may not be entirely transport controlled.

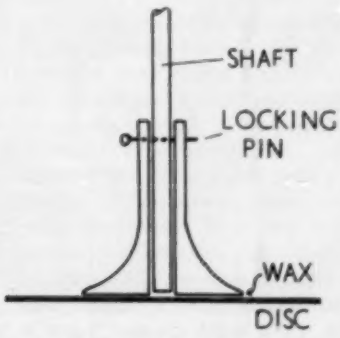

Fig. 1. Method of mounting disk

Experimental solutions were warmed to the thermostat temperature and degassed before being transferred to the reaction vessel. In the vessel, a stream of nitrogen ($O_2 < 0.05\%$) was bubbled through the solution for at least 5 min to maintain it free from atmospheric oxygen. During this period, the disk was mounted on the stirring shaft and, with the motor running, a beaker containing a solution identical with that in the reaction vessel was brought up to immerse the disk. All bubbles were removed from the under surface, and the copper was subjected to a preliminary etch for 5 min ±5 sec in an attempt to secure a reproducible surface. On removal of the beaker, the motion of the disk threw off most of the adhering liquid. The disk then was immersed in the reaction vessel, the underside of the disk was inspected to ensure that no bubbles had been trapped, and the nitrogen delivery tube was raised above the surface of the solution to maintain a slight positive pressure of nitrogen within the vessel.

Samples were withdrawn at 5-min intervals, run into excess ferrous ammonium sulfate solution, and back-titrated with standard dichromate solution. At the end of the run, the disk was removed from the solution, washed, stripped from the former, and its mean diameter measured using vernier calipers. The unit rate constant, k_1, was evaluated graphically from the first order expression (14): $k_1 t = (2.303 \Sigma V . \Delta\log c)/A$, where t is the time in min, A is the apparent area of the underside of the disk, and $\Delta\log c$ denotes the difference in the logarithm of the concentration of dichromate, c, at the beginning and end of an interval during which the volume is V.

The following were chosen as standard conditions: a disk rotating at 146 rpm in a solution 1.0M in sulfuric acid and 3.0×10^{-5}M in potassium dichromate, at 25°. In most cases, runs were performed at least in duplicate for each set of experimental conditions, and standard runs were conducted at frequent intervals as a check. In general, the rate constants for any set of conditions seldom differed by more than 3%, and frequently agreed to within 1%. Figure 2 exemplifies the good first order plots obtained.

The diffusion coefficient of dichromate ion under various conditions and the kinematic viscosity of

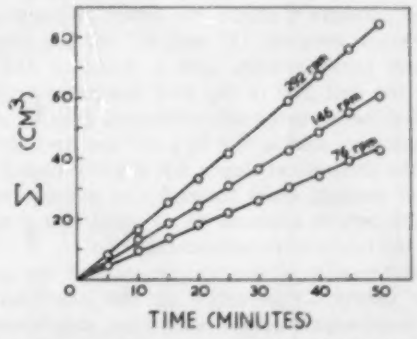

Fig. 2. Representative first order plots, 1.0M H_2SO_4, 3.0×10^{-5}M $K_2Cr_2O_7$, 25°.

Table I. Rate constants in 1.0M H_2SO_4
(146 rpm; 25°)

Initial conc. dichromate, M	k_1, cm min^{-1}	Mean k_1, cm min^{-1}
7.5×10^{-4}	0.137, 0.139, 0.137	0.138
1.5×10^{-3}	0.136, 0.136	0.136
3.0×10^{-3}	0.131, 0.128, 0.133, 0.132	0.131
6.0×10^{-3}	0.126, 0.124	0.125
1.2×10^{-2}	0.130, 0.137	0.134
1.5×10^{-2}	0.131, 0.130	0.131
1.8×10^{-2}	0.131	0.131
3.0×10^{-2}	0.132, 0.130, 0.129, 0.131 0.132	0.131

the solutions were determined by methods described elsewhere (14).

Results and Discussion

Solutions 1.0M in sulfuric acid.—When the ratio of the concentration of sulfuric acid to that of the dichromate ion is high, the rate of dissolution of copper is first order with respect to the concentration of dichromate ion. This is shown both by the linearity of the kinetic plots, examples of which are shown in Fig. 2, and by the fact that variation of the initial concentration of dichromate ion over a wide range is without significant effect upon the observed rate constant (Table I).

The extent to which the observed rate is governed by the transport of a solute species to the surface may be determined by comparing k_1, the observed unit rate constant, with k_t, the unit rate constant computed from the extended Levich theory (14). On this theory,

$$k_t = (0.554 D^{2/3} \nu^{-1/6} \omega^{1/2}) / [0.8934 + 0.316 (D/\nu)^{0.33}] \text{ cm sec}^{-1} \quad [1]$$

where D (cm^2 sec^{-1}) is the diffusion coefficient of the solute species, ν (cm^2 sec^{-1}) is the kinematic viscosity of the solution, and ω (rad. sec^{-1}) is the angular velocity of the disk.

Application of this equation to the experimental results shows that for solutions 1.0M in H_2SO_4 the observed rate is determined by the transport of dichromate to the copper surface. Thus, Fig. 3 shows the effect of varying the rate of stirring over the range 73-292 rpm for a solution 3.0×10^{-3}M in dichromate ion at 25°. The full line is the slope computed from Eq. [1] using the directly determined values $D_m = 9.07 \times 10^{-6}$ cm^2 sec^{-1} and $\nu_m = 1.01 \times 10^{-2}$ cm^2 sec^{-1}. Figure 4 shows the effect of varying the temperature between 15° and 45° for the same dichromate concentration, and a speed of 146 rpm. Again, the full line is the plot computed from the extended theory using the additional data $D_m = 1.39 \times 10^{-5}$ cm^2 sec^{-1} and $\nu_m = 6.83 \times 10^{-3}$ cm^2 sec^{-1}. In both cases, the theoretical slopes are slightly higher than the best straight lines through the points, but the deviation, which amounts to no more than 2%, lies within the limits of experimental error.

In confirmation of this conclusion that the surface process exerts no influence on the observed rate under these experimental conditions, supplementary experiments under the standard conditions showed that amalgamated copper disks (mean $k_1 = 0.133$ cm min^{-1}) and brass disks (mean $k_1 = 0.130$ cm min^{-1}) dissolve at the same rate as copper (mean $k_1 = 0.131$ cm min^{-1}).

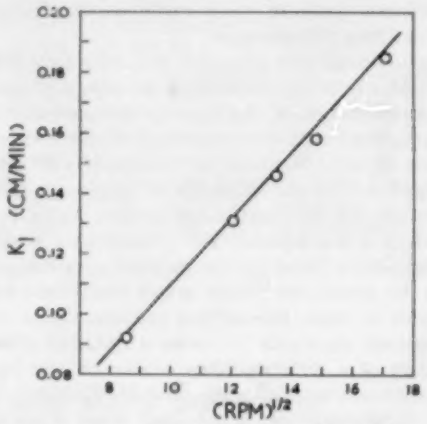

Fig. 3. Effect of stirring, 1.0M H_2SO_4, 3.0×10^{-3}M $K_2Cr_2O_7$, 25°.

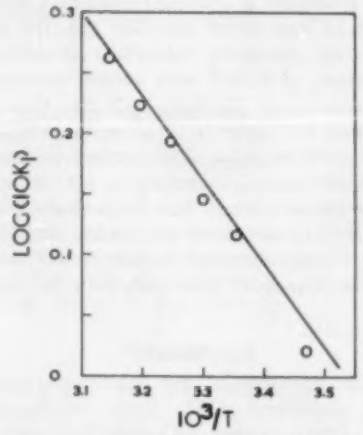

Fig. 4. Temperature coefficient, 1.0M H_2SO_4, 3.0×10^{-3}M $K_2Cr_2O_7$, 146 rpm.

Interesting results were obtained when the dependence of the observed rate on the method of preparation of the copper surface was studied. It has been suggested (13, 15) that roughening the surface should be without effect on the rate of transport controlled processes provided that the degree of roughening is not so large that the critical Reynolds number for the onset of turbulence is exceeded, whereas the rate of processes controlled by the surface reaction should increase. To test this suggestion, copper disks were coated cathodically with a spongy copper deposit and others were cut from a sheet of copper which had been ground with 100 grade carborundum powder. Under standard conditions, rather poor reproducibility was obtained for runs using the plated disks, probably because of the difficulty experienced in coating the upper surface and edges of the disk with black wax. The plated surface was so porous that the wax tended to be absorbed and to run over onto the lower working surface. Nevertheless, the observed rate constants ($k_1 = 0.128$, 0.132, 0.136 cm min^{-1}) are in fair agreement with the standard value. In the case of the

ground surfaces, however, the first order plots showed a high initial rate, which decreased with time and finally settled down to the standard rate.

A change from a high initial rate to a lower rate is sometimes due to a shift from transport control toward control by the surface process. In the present case, however, the lower (standard) rate is in excellent agreement with the theoretical value computed from Eq. [1], so that another explanation must be sought. It is possible that the irregularities produced on the surface by the carborundum treatment set up a small degree of local turbulence with a corresponding increase in the initial rate. Bircumshaw and Riddiford (15) reported a marked increase in the rate of dissolution of zinc in iodine solutions when jewellers rouge, used as a polishing agent, was embedded in the metal surface. Again, there was no question of control by the surface process. King (16) has reviewed other studies in which enhanced transport controlled rates have been found for roughened or etched surfaces.

In the present system, a similar effect was noted when small gas bubbles were inadvertently trapped on the underside of the disk. As in the case of bubbles trapped under zinc disks rotating in iodine solutions (14), the observed rates were higher than the standard value. Examination of the disks after withdrawal from the reaction vessel showed markings following the fluid flow lines at the surface of the disk (13) and resembling the tracks made by drops of liquid on a rotating disk (17). Microscopic examination of the marking caused by one such bubble, or surface obstruction, is shown in Fig. 5. It will be seen that a trough has been etched around the protected part of the copper surface, penetrating the 0.15 mm thick disk in one place, and along a "tail" following the flow line. The trough is very much larger than the surface obstruction and, if due to local turbulence, is certain to increase the observed rate.

The initial concentration of acid.—The effect of varying the initial concentration of acid over the range 0.01-1.53M was studied at 146 rpm and 25°

Fig. 5. Enlargement of marking caused by surface obstruction. Magnification 30X before reduction for publication.

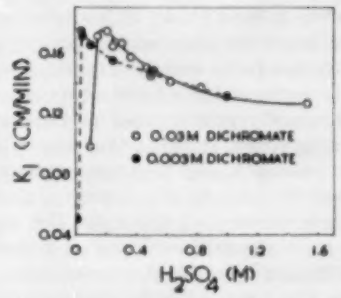

Fig. 6. Dependence on concentration of acid, 25°, 146 rpm

for both low (3×10^{-3}M) and high (3×10^{-2}M) dichromate concentrations. The mean values of k_1 are shown in Fig. 6, and it will be seen that the concentration of dichromate ion is without effect provided that the acid concentration is greater than *ca.* 0.5M.

At very low acid concentrations, there is a marked decrease in the rate. The first order kinetic plots were no longer linear, and the rate constants were estimated from the initial slopes. Acid-soluble films were formed on the disks, suggesting acid "starvation" under these conditions. From the stoichiometry of the over-all reaction, the acid, expressed as moles H_2SO_4, is consumed at a rate seven times faster than the rate at which dichromate ion is reduced. Dissolution in any solution for which the initial acid/dichromate ratio is less than 7 will be hindered eventually by a shortage of acid; on the other hand, if the initial ratio is greater than 7, this trouble will not be experienced. In the present case, an initial ratio of 7 corresponds to 0.2M H_2SO_4 for the high, and 0.02M H_2SO_4 for the low dichromate concentrations. The actual breakdowns occur in these regions (see Fig. 6). No further study of this region was made, since more interest attached to the reason for the divergence of the curves at moderate acid concentrations.

When the initial acid concentration is 0.25M, the divergence is very marked, although there can be no question of a deficiency of acid in the sense dis-

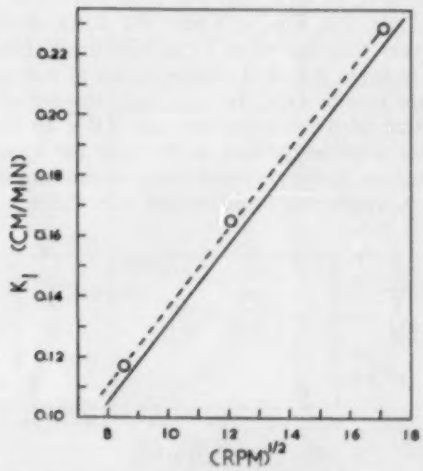

Fig. 7. Effect of stirring, 0.25M H_2SO_4, 3.0×10^{-3}M $K_2Cr_2O_7$, 25°.

cussed above. A brief study of the effect of stirring speed was made for this acid concentration using 3×10^{-5}M dichromate, and the results are shown in Fig. 7. The mean value of the observed rate constant is accurately proportional to the square root of the stirring speed, showing that under these conditions the process is also transport controlled. Consideration of Eq. [1] shows, however, that another factor is now influencing the rate. The determined values for the diffusion coefficient of dichromate ion at 3.0×10^{-2}M and 3.0×10^{-4}M, respectively, are identical within the limits of experimental error ($D_m = 1.16 \times 10^{-6}$ cm^2 sec^{-1}) for this acid concentration and lead to theoretical values for k_T at 146 rpm of, respectively, 0.158 and 0.157 cm min^{-1}. This is in good agreement with the observed value (0.155 cm min^{-1}) for the lower dichromate concentration. The observed value for the higher dichromate concentration (0.165 cm min^{-1}) is distinctly higher than the theoretical value, as indeed are the observed values at other stirring speeds. The full line in Fig. 7 indicates the theoretical slope computed from Eq. [1].

Since Eq. [1] predicts the maximum rate at which dichromate ions can be transported to the surface by the combined effect of diffusion and convection, it must be assumed that, at 3.0×10^{-5}M dichromate concentration, the transport process has been speeded up in some way; a shift toward control by the surface process would be marked by a decrease in the observed rate.

In general, ions may be transported to a surface in three ways, by diffusion, convection, and by migration under the influence of an electrical potential gradient (18). At high acid concentrations, when the relative concentration of dichromate ion is small, ionic migration will be negligible, and Eq. [1] will be applicable. If there is insufficient acid or foreign ions to suppress ionic migration through the electrical double layer, however, the rate of transport of dichromate ion will be increased. To check this explanation and to eliminate the effect, a series of runs were conducted using solutions to which sodium sulfate had been added.

Effect of adding sodium sulfate.—The initial concentration of sulfuric acid was varied over the range 0.1 to 1.0M. For runs in which the initial acid concentration was less than 1.0M, sodium sulfate was added to bring the total concentration of sulfate and bisulfate ions to 1.0M. In each case, the initial concentration of dichromate ion was 3.0×10^{-5}M, and the runs were performed at 25° and 146 rpm. The mean values of the observed rate constant are shown in Fig. 8, which may be compared with Fig. 6.

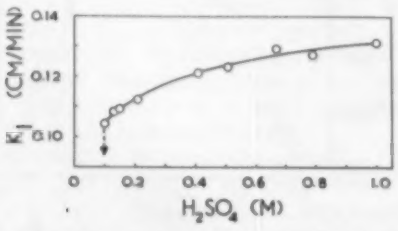

Fig. 8. Dependence of rate on concentration of acid, with added Na_2SO_4, $3.0\ 10^{-5}$M $K_2Cr_2O_7$, 25°, 146 rpm.

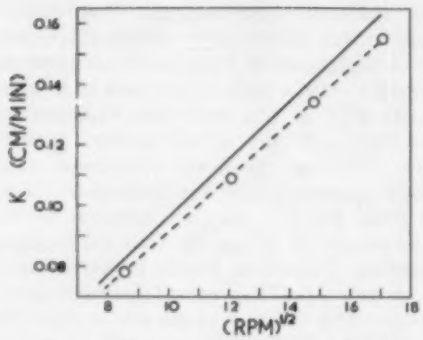

Fig. 9. Effect of stirring, 0.15 H_2SO_4, 0.85M Na_2SO_4, 3.0×10^{-5}M $K_2Cr_2O_7$, 25°.

The marked fall-off at very low acid concentrations is still observed, but the general trend now has altered. The observed rate constant now decreases with decreasing acid concentration due to the marked increase in the kinematic viscosity of the solution.

It is of particular interest to note that the value for a solution 0.21M in sulfuric acid and 0.79M in sodium sulfate ($k_1 = 0.112$ cm min^{-1}) is the same as that found for runs under the same conditions except that the initial concentration of dichromate was 3.0×10^{-4}M, *i.e.*, the divergence apparent in Fig. 6 has been eliminated by the added electrolyte. The observed value is, however, distinctly lower than that predicted by Eq. [1].

Since the addition of sodium sulfate increases the viscosity of the solution, the rate of the transport process is retarded, so that a shift toward surface control may be ruled out. The reason for the discrepancy between the observed and computed values may be traced to the fact that Eq. [1] is limited to the case of electrolyte solutions containing not more than three ion species.[2] In the absence of sodium sulfate, and with sufficiently high acid/dichromate ratios, it has been shown that the present system approximates closely to the theory. The presence of a large excess of sodium sulfate, however, introduces another ion species, and the theory is inapplicable.

In order to study the characteristics of this case, tests for transport control were applied to a solution 0.15M in sulfuric acid, 0.85M in sodium sulfate, and 3.0×10^{-5}M in dichromate.[3] The effect of varying the stirring speed at 25° is shown in Fig. 9, in which the full line is the slope computed from Eq. [1] using the determined values $D_m = 7.71 \times 10^{-6}$ cm^2 sec^{-1}, $\nu_m = 1.19 \times 10^{-2}$ cm^2 sec^{-1}. It is seen to be distinctly higher than the experimental slope. The effect of varying the temperature at 146 rpm is shown in Fig. 10. From the slope, the apparent energy of activation is 3.4 kcal mole^{-1}, in good agreement with

[2] For this case, the problem of calculating the concentration profile through the transport boundary layer can be separated from the problem of determining the variation of the electrical potential through the double layer (19). When more than three ion species are present, however, this separation is not possible, and the path to a complete solution of the transport equations is barred by formidable mathematical difficulties. Nevertheless, the dependence of k_T on D, ν and ω is dimensionally of similar form to Eq. (1), but the number of proportionality must be determined by experiment (13).

[3] In the presence of added sodium sulfate, acid starvation is not detected until the acid/dichromate ratio is reduced to 7/2. The sodium sulfate decreases the rate both by increasing the viscosity of the solution and by eliminating ionic migration through the double layer. At this lower rate, for 0.15M H_2SO_4, acid exhaustion is not approached over the time intervals studied.

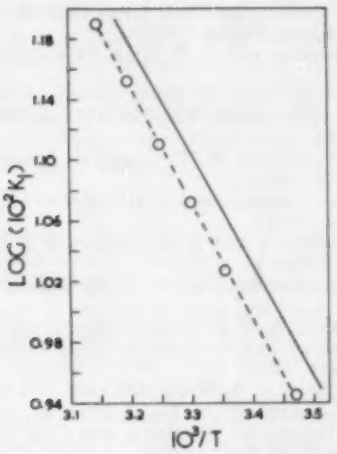

Fig. 10. Temperature coefficient, 0.15M H_2SO_4, 0.85M Na_2SO_4, 3.0×10^{-5}M $K_2Cr_2O_7$, 146 rpm.

the value found from Fig. 4. Again, the full line is the plot computed from Eq. [1] using the additional values $D_{as} = 1.20 \times 10^{-5}$ cm^2 sec^{-1}, $\nu_{as} = 7.96 \times 10^{-3}$ cm^2 sec^{-1}.

Figures 9 and 10 suggest that, for these conditions

$$k_T = \text{const. } D^{2/3} \nu^{-1/6} \omega^{1/2} \text{ cm sec}^{-1} \qquad [2]$$

where the constant is less than the value given by Eq. [1]. On dimensional grounds, the only effect of increasing the number of ion species beyond three should be a change in the number of proportionality. In this case, the mean value for the constant in Eq. [2] is found to be 0.562, *ca.* 7% lower than the value 0.605 predicted by Eq. [1].

That the process is indeed transport controlled under these conditions was checked by studying the effect of deliberately roughening the surface. For solutions 3.0×10^{-5}M in dichromate at 146 rpm and 25°, grinding the surface with carborundum gave a mean value for k_1 of 0.105 cm min^{-1} compared with the value 0.109 cm min^{-1} obtained with the standard surface. It is of interest to note that these runs with roughened surfaces gave linear first order plots without the initially high rates found in the absence of added sodium sulfate. Presumably, the high viscosity of the sodium sulfate solutions diminishes the local turbulence.

Edge effects.—For the dissolution of zinc disks rotating in aqueous iodine solutions (14), the observed rate constants at low stirring speeds were found to be higher than those predicted by Eq. [1]. It was pointed out that this could be explained equally well either by the assumption that the thickness of the disks gave rise to edge effects, or by assuming a contribution to the observed rate by natural convection.

In the present investigation, this effect is not observed, as will be seen from Fig. 3, 7, and 9, k_1 being accurately proportional to the square root of the stirring speed over the same range as that studied with the zinc disks. The very much thinner disks used in this investigation make it fairly certain that the earlier observations were in fact due to edge effects. Experiments with rotating disk cathodes have confirmed this view.

Blocking off the working surface.—It has been reported that the use of inert Perspex center studs is without effect on the observed rate of dissolution of zinc disks rotating in iodine solutions, although the exposed area of the stud amounted to *ca.* 4% of the working surface of the disk (14). Since the copper/dichromate reaction has been shown to be transport controlled under standard conditions, a similar effect should be found for this system. Progressive enlargement of an inert patch at the center should be without effect on the observed rate up to a certain point. Beyond this point, the exposed copper will be unable to cope with all the dichromate supplied by normal and radial transport, and this will result in a decrease in the observed rate. This decrease will become more marked as the blocked area is increased.

In general, the temperature coefficient of a surface process is larger than the temperature coefficient of the transport process (20). The effect of increasing the temperature will be a relative increase in the rate at which the exposed copper can cope with the dichromate supplied, and the breakdown point should then occur at a larger value of the blocked area.

To test these views, black wax was used to block off circular patches at the center of the copper disks, care being taken to ensure that the blocked off circles were concentric with the disks. Runs were carried out at 25° and 45° under otherwise standard conditions, and the mean values for k_1, computed per unit area of the *total* surface of the underside of the disk, are shown in Fig. 11. It will be seen that at 25° there is no significant effect on k_1 until the area blocked off exceeds *ca.* 10% of the total area; above this value there is a marked decrease. At 45°, the breakdown occurs at a higher value, *ca.* 15%.

Further study of this effect is desirable, but it would be better to use an inert electrode for the purpose since, when the disk is attacked, a step is formed at the edge of the blocked area which may promote a measure of local turbulence.

Acknowledgment

The authors thank Professor Cecil V. King for providing them with a manuscript copy of his review article in advance of publication, and they are grateful to the Department of Scientific and Industrial Research for an award to D. P. G.

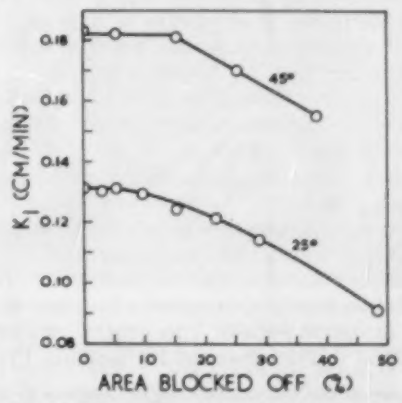

Fig. 11. Effect of blocking off working surface

Manuscript received May 27, 1960; revised manuscript received Aug. 22, 1960. This paper was prepared for delivery before the Houston Meeting, Oct. 9-13, 1960.

Any discussion of this paper will appear in a Discussion Section to be published in the June 1961 JOURNAL.

REFERENCES

1. V. H. Veley, *J. Soc. Chem. Ind.*, **8**, 858 (1889); *Phil. Trans.*, **182A**, 279 (1891).
2. R. G. Van Name and D. U. Hill, *Am. J. Sci.*, (4) **42**, 301 (1916).
3. R. Glauner and R. Glocker, *Z. Metallkunde*, **20**, 144 (1928); *Z. Krist.*, **80**, 377 (1931); R. Glauner, *Z. physik. Chem.*, **142A**, 67 (1929).
4. E. S. Hedges, *J. Chem. Soc.*, **1930**, 561.
5. C. V. King and L. Weidenhammer, *J. Am. Chem. Soc.*, **58**, 602 (1936).
6. C. V. King and P. L. Howard, *Ind. Eng. Chem.*, **29**, 75 (1937)
7. A. T. Gwathmey and A. F. Benton, *Trans. Electrochem. Soc.*, **77**, 211 (1940).
8. C. V. King and L. Appleton, *ibid.*, **77**, 219 (1940).
9. N. Ya. Buben and D. A Frank-Kamenetskii, *Zhur. Fiz. Khim.*, **20**, 225 (1946).
10. M. Hochberg and C. V. King, *This Journal*, **97**, 191 (1950).
11. T. G. Owe Berg, *Z. anorg. u. allgem. Chem.*, **265**, 332 (1951); **266**, 118, 130 (1951); **269**, 210, 218 (1952).
12. B. C.-Y. Lu and W. F. Graydon, *Canad. J. Chem.*, **32**, 153 (1954).
13. L. L. Bircumshaw and A. C. Riddiford, *Quart. Rev.*, **6**, 157 (1952).
14. D. P. Gregory and A. C. Riddiford, *J. Chem. Soc.*, **1956**, 3756.
15 L. L. Bircumshaw and A. C. Riddiford, *ibid.*, **1951**, 598.
16. C. V. King, Review entitled "Dissolution of Metals," presented at a symposium of The Electrochemical Society, 1959.
17. B. E. Dixon, A. A. W. Russell, and J. E. L. Swallow, *Brit. J. Appl. Phys.*, **3**, 115 (1952).
18 C. W. Tobias, M. Eisenberg, and C. R. Wilke, *This Journal*, **99**, 359C (1952).
19. V. Levich, *Acta physicochim. U.R.S.S.*, **17**, 257 (1942).
20. A. C. Riddiford, *J. Phys. Chem.*, **56**, 745 (1952).

Microtopography of Oxide Films Formed on Tantalum

R. E. Pawel, J. V. Cathcart, and J. J. Campbell

Metallurgy Division, Oak Ridge National Laboratory,[1] Oak Ridge, Tennessee

ABSTRACT

Optical and electron microscopy were used to characterize the surface of tantalum specimens oxidized at temperatures ranging from 300° to 700°C. At the lower temperatures, the initial stages of oxidation were shown to consist of an aggregation of oxide platelets visible on the surface as crystallographically dependent, acicular structures extending from the grain boundaries. At higher temperatures, nodular growths were observed whose nucleation was not a grain-boundary phenomenon. Continued oxidation at temperatures of 500°C and above produced blistering and cracking of the oxide layer. The oxide platelets were shown to have grown during oxidation and not during cooling from the reaction temperature. At higher temperatures, both platelets and nodules served as preferred sites for blister and crack formation in the oxide and thus played an important role in the transition from the protective to the nonprotective stage of oxidation of tantalum.

Previous work (1, 2) has shown that the gaseous oxidation of tantalum takes place in a nonuniform fashion, characterized at least in the initial stages by the formation in the metal of discrete platelets of oxide resembling a typical Widmanstätten structure. The tendency for tantalum to react in such a heterogeneous manner illustrates the need for consideration of oxide morphology in any interpretation of the oxidation mechanism.

Oxidation rate measurements of Cathcart, *et al.* (1) have shown that the oxide film formed on tantalum in pure oxygen at atmospheric pressure is initially protective but becomes nonprotective as the oxidation proceeds beyond a critical point. The rate of oxidation finally approaches a constant value for longer oxidation periods. This general rate behavior is identical to that observed for niobium (3). Electron optical observations on oxidized specimens of both metals show that the onset of the nonprotective portion of the rate curves may be correlated to the formation of small blister-like cracks on the surface of the oxide. Presumably, these cracks permit easy access of oxygen to the reaction zone, resulting in the marked increase in oxidation rate.

While remarkable similarities exist in the oxidation rate curves for niobium and tantalum and in the physical and chemical properties of the two metals and their oxides, there are significant differences in the morphology of the oxide films formed on these metals, especially in the early stages of oxidation. The oxidation of niobium in the protective region is characterized by the formation of a reasonably uniform oxide film and the development of a normal sequence of interference colors as the oxide thickens. However, the initial stages of tantalum oxidation show the aforementioned platelet struc-

[1] Operated for the U. S. Atomic Energy Commission by the Union Carbide Corporation.

ture, and well-defined interference colors are not observed. It is of interest to observe that other gas-tantalum reactions, notably those with sulfur (4) and nitrogen (5), also produce a platelet structure.

In the present investigation, an effort has been made to characterize the morphology of the early stages of tantalum oxidation.

Specimen Preparation

Tantalum specimens (nominal analysis: 99.71% Ta-0.15% Nb-0.03% Fe-0.03% C-0.05% W) were cut from 0.5 mm sheet in the form of coupons, 1 x 2 cm. In most of the work reported here, the specimens were preannealed in vacuum for 1 hr at 1200°C; some specimens were strain annealed for longer periods at 1200° and 1300°C to produce a larger grain size. The specimens were mechanically polished through 0.3-μ levigated alumina and finally electropolished in a 90% H_2SO_4-10% HF solution. The specimens were then placed in quartz reaction tubes and annealed at a pressure of approximately 2×10^{-4} mm Hg at the reaction temperature for approximately 16 hr prior to oxidation. This method of specimen preparation yielded surfaces which appeared smooth in the light microscope, and which, upon oxidation, gave consistently reproducible results. Except as noted, all oxidations were performed in dry oxygen at atmospheric pressure.

The surface topography of the oxidized tantalum specimens was examined by both optical and electron microscopy. Both direct and indirect carbon replicas were used for electron microscopy, the indirect method (preshadowed carbon replica of a stripped parlodion intermediate) being used exclusively with the heavier oxide films. Each method yielded essentially identical results on a given specimen.

Mode of Platelet Formation

The resemblance of the platelet structure to the patterns observed in many precipitation systems suggested the possibility that the platelets were formed during cooling from the reaction temperature rather than during oxidation. This possibility was investigated using "hot" direct replication and hot-stage optical microscopy.

In a hot replication experiment, the specimen was oxidized in air at 400°C on a small hot plate in the vacuum evaporator. After oxidation, the system was evacuated and, with the specimen still at 400°C, a direct carbon replica, preshadowed rather heavily with gold or palladium, was made of the surface. After cooling, this replica was removed and the specimen re-replicated in the normal fashion. Electron micrography showed that essentially the same structure existed before and after cooling from the reaction temperature. The presence of shadows in the hot replica was regarded as conclusive evidence that the platelets were present at the reaction temperature.

The results of the hot-stage microscope studies served to confirm that the platelets formed during oxidation. Although the magnification and resolution of the microscope were not sufficient to permit observation of fine details, the general progress of the air oxidation at 400°C could be followed. First, a gradual darkening of several grains in the specimen was seen as platelets became visible in other lighter grains. Many platelets were observed to grow after nucleation at grain boundaries. As oxidation continued, the platelets frequently developed small feather-like subplatelets. No detectable changes in topography occurred as the specimens were cooled to room temperature in vacuum.

It should be indicated that the specimens used in this phase of the study were all oxidized in air and that the temperature control was poorer than with the standard apparatus; however, the morphology of these specimens compared favorably with that of the more carefully oxidized samples.

Oxide Morphology

The first stages of tantalum oxidation were studied over the temperature range 300°-700°C. Particular attention was paid to the initial growth behavior and its possible influence on the onset of blistering or rupturing of the oxide film. It has been suggested that the large oxide-metal volume ratios and the predominance of anion diffusion in the oxides lead to the generation of significant stresses in the oxide films formed on niobium and tantalum (1, 3). The phenomenon of highly localized crack formation in the oxide films can then be interpreted as resulting from the severe, localized deformation of the existing oxide by the forces exerted when fresh oxide is formed in a partially restricted region such as a cavity at the oxide-metal interface. The geometry associated with an oxide platelet is such that it is reasonable to expect that directional stresses would develop at such a site and lead ultimately to the formation of a crack or a blister in the oxide film. Thus, the manner in which platelet growth occurs may influence the oxidation kinetics markedly.

Only the very initial stages of oxide formation occurred on specimens oxidized at 300°C for times varying up to 95 hr. In the electron microscope, the oxide appeared as fine needles originating in the grain boundaries and extending into the grains along definite crystallographic directions as shown in Fig.

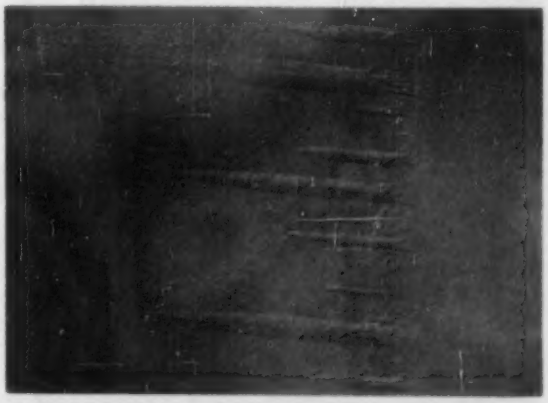

Fig. 1. Typical grain-boundary platelet growth on tantalum oxidized at low temperature. Note "bubble raft" background texture. Annealed 1 hr at 1200°C; oxidized 95 hr at 300°C; indirect replica. REF: J. V. Cathcart, R. Bakish, and D. R. Norton, This Journal, in press. Magnification 16,800X before reduction for publication.

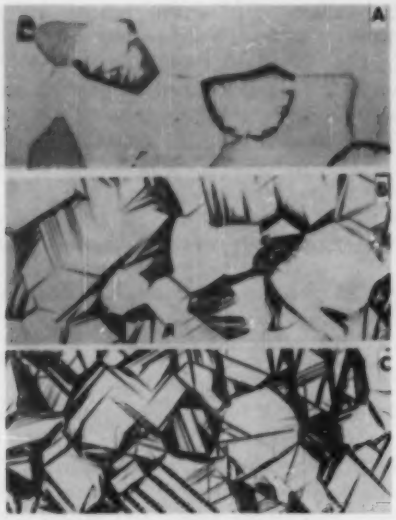

Fig. 2. Early stages of oxidation on coarse grain size tantalum at 500°C. Annealed 16 hr at 1200°C; oxidized (a) 15 min, (b) 30 min, and (c) 1 hr at 500°C. Magnification 500X before reduction for publication.

1. The "bubble-raft" structure discernible in Fig. 1 was found to be present on electropolished surfaces prior to oxidation and occurred as a result of electropolishing. Use of this fine-structure as a marker has been reported by one of us (1). At 400° and 500°C, the growth process was similar although the rate of oxidation was much greater. Prolonged oxidation at 500°C resulted in the formation of blister-like cracks in the oxide. Optical micrographs of tantalum specimens after oxidation at 500°C in the pre-blister range are shown in Fig. 2. The importance of grain-boundary nucleation in the oxidation process and the course of the subsequent growth of the platelets are illustrated.

Glancing-angle x-ray diffraction patterns obtained from specimens oxidized for times up to 8 hr at 500°C indicated that Ta_2O_5 was the major oxide formed under these conditions. After 15 min of oxidation, only a few extremely faint lines, other than the metal lines, were observed. After 1 hr of oxidation, corresponding to the time required to develop the platelet structure shown in Fig. 2c, the pentoxide lines were quite evident. The intensity of these lines increased during growth of the platelets. Very weak lines in the diffraction pattern could not be attributed with certainty to any known lower oxide of tantalum.

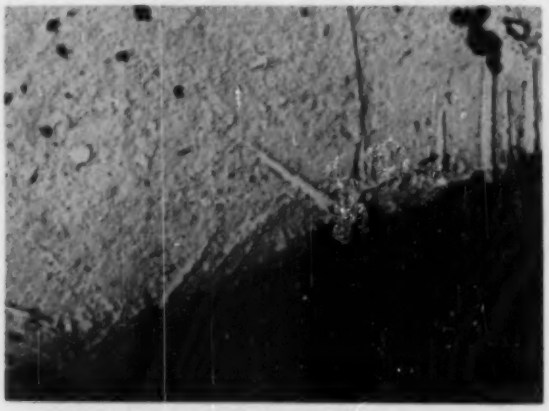

Fig. 4. Cross section of oxidized tantalum specimen showing growth of platelets into the metal. Annealed 1 hr at 1200°C; oxidized 6 hr at 500°C; indirect replica. Magnification 6900X before reduction for publication.

As oxidation continued at 500°C, randomly distributed blisters and cracks appeared on the surface, as shown in Fig. 3. Although the platelet structure in this micrograph is rather obscure, the size, shape, and position of the blisters do not seem to coincide with the traces of the platelets on the surface of the specimen. An electron micrograph of a cross section of a tantalum specimen oxidized at 500°C is presented in Fig. 4. The edge of the specimen is distorted; however, the platelets are seen to have grown into the metal to an appreciable depth. The largest platelets extend approximately 5 μ into the metal.

At 600°C a change in the basic oxide morphology was observed. On some grains, nodular oxide growths were interspersed with platelets. In some instances, the nodular growths showed crystallographic character and even the tendency to develop in the manner of a platelet. These characteristics are

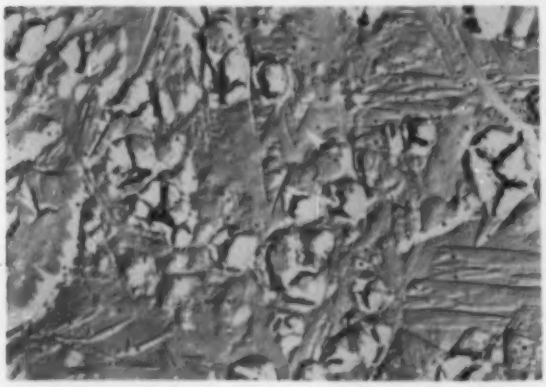

Fig. 3. Blister-like cracks observed on oxidized tantalum surface after prolonged oxidation. Annealed 1 hr at 1200°C; oxidized 7 hr at 500°C; indirect replica. Magnification 9600X before reduction for publication.

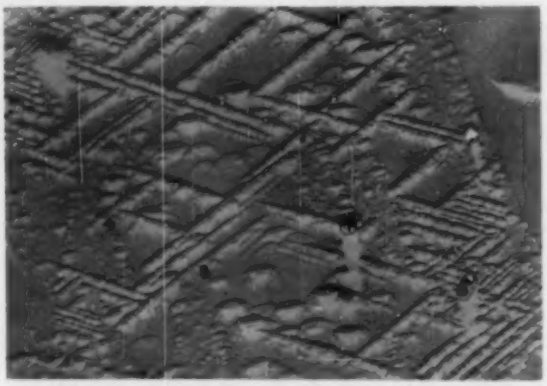

Fig. 5. Platelets and nodules formed on single grain on oxidation at 600°C. Annealed 1 hr at 1200°C; oxidized 1 min at 600°C; direct replica. Magnification 6900X before reduction for publication.

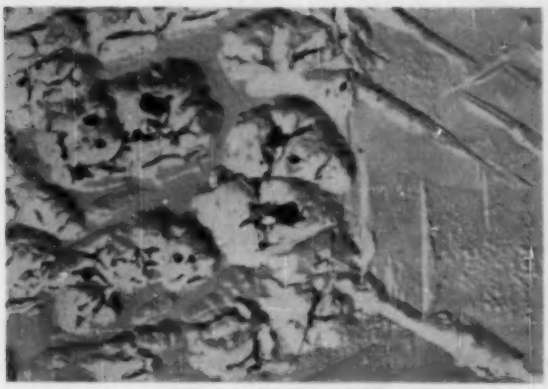

Fig. 6. Blister-like cracks appearing in grain after prolonged oxidation at 600°C. Annealed 1 hr at 1200°C; oxidized 15 min at 600°C; indirect replica. Magnification 6900X before reduction for publication.

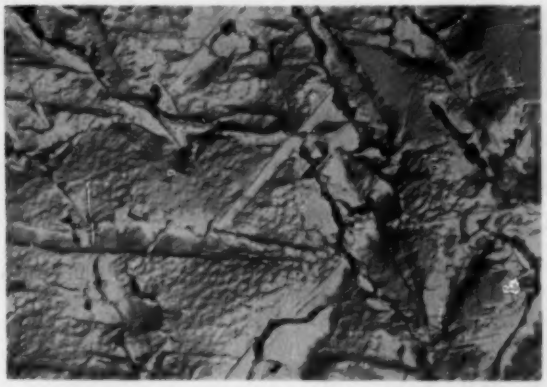

Fig. 7. Elongated cracks appearing along platelets after prolonged oxidation at 600°C. Annealed 1 hr at 1200°C; oxidized 15 min at 600°C; indirect replica. Magnification 6900X before reduction for publication.

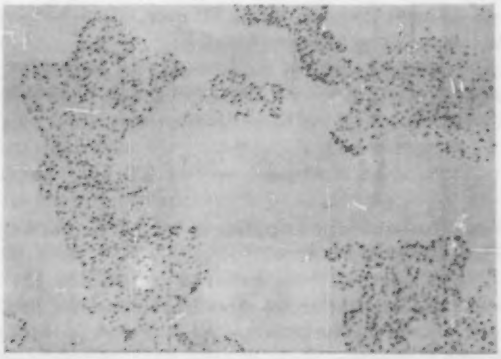

Fig. 8. Low magnification of nodular growths on tantalum surface oxidized at 700°C. Annealed 16 hr at 1200°C; oxidized 6-10 sec at 700°C. Magnification 500X before reduction for publication.

illustrated in Fig. 5. On the basis of longer (15 min) oxidation experiments at 600°C, nodular growths were found to be preferred sites for blister formation. Certain grains, originally exhibiting dense nodular formations, became blistered and oxidized much more heavily than adjacent grains where the oxide was present predominantly in platelet-type structures. Moreover, at this temperature, there appeared to be a more definite relation between the platelet growths and crack formation. In former platelet areas of these specimens, the fissures were elongated and closely followed the traces of the platelets. Even during earlier stages of oxidation at this temperature, blisters tended to form at intersections of platelets. Figures 6 and 7 are examples of crack formation in the two types of areas. Figure 6 also illustrates the extreme difference in oxidation behavior from grain to grain which was observed in these specimens.

Fig. 9. Nodular growths on tantalum surface oxidized at 700°C. Annealed 16 hr at 1200°C; oxidized 6-10 sec at 700°C; indirect replica. Magnification 9600X before reduction for publication.

At 700°C the nodular growth was even more pronounced, and the first stages of oxidation consisted almost entirely of nodular-type attack. Figures 8 and 9 are typical optical and electron micrographs of these features.

Conclusions

The results of this investigation serve to illustrate the complex behavior of the initial stages of gaseous oxidation on tantalum surfaces. While the mechanism for platelet formation is not yet known, the fact that they contribute importantly to the oxidation process, at least at higher temperatures, has been demonstrated. On the basis of the results obtained, the following conclusions appear justified:

1. Oxide platelet formation on tantalum occurred at the temperature of oxidation and involved a highly directional growth process. At any one time during oxidation a wide spectrum of platelet sizes existed. X-ray data indicated Ta_2O_5 as the predominant oxide.

2. At lower temperature, the nucleation of platelets occurred primarily at grain boundaries, but at 600°C and higher, nodular growths were observed whose nucleation did not involve a grain-boundary process.

3. At lower temperatures, no direct correlation was observed between the platelet structures and blister formation in the oxide. At higher temperatures, both nodules and platelets served as preferred sites for blisters and elongated cracks.

4. Tantalum, especially at the higher temperatures, exhibited a pronounced dependence of first-stage oxidation rate on crystallographic orientation.

Acknowledgment

The authors wish to thank W. O. Harms of the University of Tennessee for his aid in the preparation of this paper. The assistance of W. H. Bridges and H. R. Tinch of the Metallography Group of this laboratory is also gratefully acknowledged.

Manuscript received May 9, 1960. This paper was prepared for delivery before the Houston Meeting, Oct. 9-13, 1960.

Any discussion of this paper will appear in a Discussion Section to be published in the June 1961 JOURNAL.

REFERENCES

1. J. V. Cathcart, R. Bakish, and D. R. Norton, *This Journal*, **107**, 668 (1960).
2. R. Bakish, *ibid.*, **105**, 71 (1958).
3. J. V. Cathcart, J. J. Campbell, and G. P. Smith, *ibid.*, **105**, 442 (1958).
4. J. V. Cathcart and J. B. Wagner, Unpublished research.
5. R. Bakish, *This Journal*, **105**, 574 (1958).

The Difference Effect and the Chunk Effect

G. A. Marsh and E. Schaschl

Research Center, The Pure Oil Company, Crystal Lake, Illinois

ABSTRACT

The negative difference effect in the case of steel can be explained in terms of corrosion by removal of blocks or "chunks" of metal containing perhaps only a few atoms. The "chunk effect" also explains the observed fact that, under conditions of high corrosion rate, minimum protective current can be much less than the calculated corrosion current. It is suggested that the chunk effect and anodic polarization occur on the same piece of metal. Either the positive or the negative difference effect may be observed depending on the corrodent.

Positive Difference Effect

The positive difference effect has been considered one of the supporting pillars of the electrochemical theory of aqueous corrosion. This effect was first recognized and named by Thiel and Eckell (1), who worked with aluminum dissolving in sodium hydroxide solution.

Thiel and Eckell reasoned that, when a metal is made an anode in an electrolytic cell, its rate of corrosion should be the sum of (*a*) local action as observed in the absence of external current, and (*b*) the corrosion rate equivalent to the applied current (utilizing the electrochemical equivalent of the metal in question). In actual tests with aluminum, however, they found the observed corrosion rate to be *less* than the sum of the components (*a*) and (*b*). To state their observation quantitatively, let I_o equal the freely corroding rate,[1] I_a equal the observed corrosion rate occurring on application of I_a, and I_c equal the externally applied current.

From Faraday's law I_c, when positive (anodic), results in an equivalent corrosion rate. To rephrase Thiel and Eckell's discovery, they expected to find

$$I_o + I_c - I_a = 0 \qquad [1]$$

Actually, they found

$$I_o + I_c - I_a = \Delta \qquad [2]$$

Δ was a positive number which they called the "difference effect." (Later they found that Δ could be negative in some cases; this discovery led to the use of the terms "positive" and "negative" difference effect.) Furthermore, Δ was linear over a certain range of I_c, so

$$\Delta = KI_c \qquad [3]$$

Since I_a and I_c are expressed as current densities, Eq. [2] and [3] can be combined:

$$I_a = I_o + I_c\,(1 - K) \qquad [4]$$

K is a slope; if it has a value of $+1$, the applied current will have no effect on measured corrosion rate. Where the positive difference effect has been observed, K lies between 0 and 1.

For small values of I_c, linearity of the curve I_a *vs.* I_c is often obtained, permitting one to obtain K from easily measured quantities:

$$K = \frac{I_o - I_{a1}}{I_{c1}} + 1 \qquad [5]$$

where the subscript 1 applies to one particular value of applied current.

The constant K was believed by Müller (2) to have fundamental significance regarding the mechanism of the anodic process. As K is independent of applied current, it must depend only on the system of metal/solution being studied.

Straumanis (3, 4) has explained the positive difference effect in terms of anodic polarization. According to his view, the positive difference effect is pronounced if there is interference with the delivery of electrons to the local cathode, or if there is interference with dissipation of ions into the corrosive agent. We believe that the latter effect is the more likely one. So with increasing anodic current, whether originating in local cells or externally applied, there is increasing anodic polarization which

[1] Corrosion rates in this paper are stated in terms of the equivalent current densities. Applied currents are also stated as current densities.

decreases the driving force for local action and gives rise to the observed positive difference effect.

The positive difference effect is *observed* only upon application of anodic current, but the phenomenon responsible for it takes place at zero applied current as well as at applied anodic currents. That anodic polarization occurs in freely corroding metals (*e.g.*, steel) is apparent from the fact that the current required for cathodic protection of a specimen showing the positive difference effect is greater than the corrosion current of the freely corroding metal. If there were no anodic polarization, the protective current would necessarily equal the corrosion current.

Negative Difference Effect

Müller (2) and Kroenig and Uspenskaja (5) found that the difference effect was negative for some metal-corrodent combinations. They and others (4, 6, 7) explained this as the result of disruption of a surface film. According to this theory, application of positive current to a specimen gradually breaks down its shielding film, thus exposing more metallic surface to attack by the corrodent and thus increasing local action. In some cases these investigators observed flaking of films in systems in which the negative difference effect was found.

Relationship between Cathodic Protection and Positive and Negative Difference Effects

In local action, assuming the local anodes do not polarize, the anodic current (i.e., I_a) is equal to the current of the local cathodes. External cathodic current can be substituted for the local cathodic current. The current I_p required for cathodic protection is then identical to I_a. Thus I_p is a measure of the actual electronic current given up in the anodic process.

Anodic polarization, always present to some extent, requires I_p to be greater than I_a. Actual I_p/I_a ratios for numerous cases reported in the literature average about 1.2, indicating that for common cases such as soil corrosion there is almost but not quite complete cathodic control. Since I_p/I_a ratios above unity indicate some degree of anodic polarization, if one applied anodic current to a specimen which displayed an I_p/I_a ratio of 1.2 one should expect the positive difference effect to be evident.

For many cases the I_p/I_a ratio turns out to be far *less* than unity (8). These cases are found (for steel) in highly corrosive solutions, *viz.*, low pH or high dissolved oxygen concentration with a high degree of agitation. Under these same conditions of pH and dissolved oxygen, the negative difference effect is observed upon application of anodic current.

The low I_p/I_a ratio is not explained readily by the film-breakdown theory of the negative difference effect. The negative difference effect by definition drops to zero as applied anodic current becomes zero; Δ is not defined for negative values of I_a.

To explain the facts observed upon application of negative current, i.e., cathodic protection, it is not enough for the potential of cathodic areas to be changed (in proportion to the current) to the open-circuit potential of the anodes. If such a proportional change occurred, I_p/I_a would remain at or slightly greater than unity. In order for the I_p/I_a data to be explained in terms of films, the potential of cathodic areas must change much faster than the applied current. The area or the efficiency of the cathodes must be affected by negative current. Or, alternatively, the application of negative current must result in the growth of a film over the anodic areas. But the system is under essentially cathodic control; variations in anodic area should have little effect on the cathodic reaction. Also, application of negative current would not be expected to stabilize an anodic film on steel. Indeed, the negative current should cause the reduction of films such as oxides that we normally associate with steel.

Under violently corrosive conditions where films are least likely to be present the negative difference effect is very pronounced. Under conditions of partial aeration, low velocity, neutral pH, where such films should be more stable on steel, the negative difference effect is *less* pronounced; under static conditions most favorable to film stability (*e.g.*, soil corrosion), the negative difference effect is absent altogether. Thus, the facts do not support the film breakdown theory of the negative difference effect in the case of steel. (This in no way suggests that the film breakdown theory may be invalid for other metals.)

Dissolution by "Chunks"

External current just sufficient for cathodic protection merely takes the place of local cathodic current, which in turn is essentially equal to the local anodic current. A low I_p/I_a ratio indicates that much more metal is being dissolved under freely corroding conditions than can be accounted for by local anodic current. To explain the low I_p/I_a ratio found when steel corrodes at high rates, the authors suggested that corrosion of steel under these conditions might proceed with the removal of "chunks" of iron containing several atoms (8). Dissolution by chunks would also explain the negative difference effect.

Relatively little work has been done on the difference effect in steel. So far particles of free iron have not been observed, perhaps because they are of only atomic dimensions. But dissolution by chunks has been observed in other metals.

Straumanis (9) points out that Al displays the negative difference effect when dissolving anodically in KCl-HCl solution. He writes: "The self-dissolution of the Al . . . increases with [application of anodic current]. After interruption of the current, H_2 evolution decreases and a cloud of white dust appears . . . . Very small hydrogen-evolving particles can be seen floating in the electrolyte, which evidently were separated from the Al together with the scale." Straumanis does not say what the particles might be, but we believe they are most likely tiny fragments of aluminum released from the parent metal by undermining.

Roald and Streicher (10) actually found "blocks" of aluminum of the order of 0.005 mm in length when certain Al alloys were dissolved in HCl. Similarly, Hoey and Cohen (11) and Higgins (12) found free Mg metal particles in the corrosion products

when Mg was dissolved anodically in NaCl solutions. Hoey and Cohen suggested that "local corrosion and/or undermining of metallic magnesium at the anode are appreciable and may, in fact, account for the observed low anodic current efficiencies of magnesium." Vermilyea (13) dissolved silver anodically and found "anode slime" composed of minute particles of metallic silver. If corrosion rate and applied current data had been taken by these workers, they would necessarily have observed the negative difference effect.

Generalized picture of corrosion rate as a function of applied current.—It has been mentioned above that the film disruption theory is inadequate to explain the low I_p/I_c ratio encountered with steel in high corrosion rate conditions, and that dissolution by chunks explains not only this but also the negative difference effect. If corrosion occurs by chunks in anodic dissolution, would it not occur in the same manner during free corrosion? To explain the low I_p/I_c effect one must assume that it does. Then

$$I_c = I_s + I_a + I_b \qquad [6]$$

where the applied current I_p results in corrosion in strict accordance with the Faraday equivalent, the rate I_s is the true local action rate, and the rate I_b is due to corrosion by chunks, *i.e.*, the "chunk effect" rate. If I_s is zero, $I_a = I_c$; the observed corrosion rate equals the freely corroding rate. Under this condition

$$I_c = I_{aa} + I_{ab} \qquad [7]$$

In this case I_{aa} and I_{ab} are the particular local action and chunk effect rates occurring together which are measured as the freely corroding rate.

For corrosion under cathodic control, the protective current

$$I_p = I_{aa} \qquad [8]$$

because the current consumption of the local cathodes is completely satisfied by the external current, so that no local action is possible. Since I_s is zero when current I_p is applied, (by definition of I_p) it follows from Eq. [7] that I_b must be zero also when I_p is applied. Therefore the chunk effect varies with applied current. The variation is believed to be more or less linear with applied current, inasmuch as I_a *vs.* I_p curves for steel are essentially linear.

Figure 1 depicts theoretical relationships between the observed corrosion rate and applied current for several types of conditions. The 45° line DBM represents the theoretical Faraday equivalence for corrosion under cathodic control. The line AB represents cathodic protection of a common corrosion system under partial anodic control (the ratio of currents AJ/DJ for steel in typical soils appears to be about 1.2). Since anodic polarization is involved, line BL (representing the extension of line AB) depicts the metal corroding with a positive difference effect, namely, the distance ML. The freely corroding rate in each case is I_c.

The line EB represents cathodic protection in cases where the ratio I_p/I_c is much less than unity. (As analyzed above, partial anodic control explains why I_p/I_c can be greater than unity, while the chunk effect explains why this ratio can be less than unity.) Ideally, I_p equals the true local action I_{aa}. The corrosion rate I_{ab} due to chunk effect is

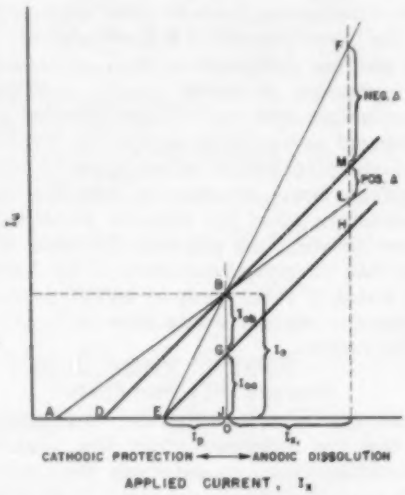

Fig. 1. Generalized corrosion rate—applied current relationships. Point B is the freely corroding rate in each case. Points E, D, and A are minimum protective currents. Points F, M, and L are observed corrosion rates with a given anodic current I_{a1}. The particular curve followed is dependent on the corrodent and the metal.

$$I_{ab} = I_c - I_p \qquad [9]$$

From Eq. [9] the chunk effect rate can be computed from the freely corroding rate and the minimum protective current. However, the freely corroding rate is merely one arbitrary point on the corrosion rate *vs.* applied current curve. If this curve is extended, (EBF on Fig. 1), a region is entered where the measured corrosion rate is greater than the Faraday equivalent rate. The true local action on application of anodic current is represented by point H; the observed corrosion rate is represented by point F. The distance FM is, by Thiel and Eckell's definition, the negative difference effect. The part of the corrosion rate occurring by chunk effect is represented by the distance FH.

Figure 1 illustrates that the chunk effect may be a fundamental property of a corroding system, while the negative difference effect is one of several possible manifestations of this property. If the chunk effect occurs, it does so even at zero applied current; that is, it occurs while the metal is freely corroding. The negative difference effect on the other hand by definition is nonexistent at zero applied current.

In Fig. 1 the curve EBF, corrosion rate *vs.* applied current, is represented as a straight line. It is recognized that none of the curves other than the Faraday equivalent is necessarily an exact straight line over the whole range of I_a. In the case of steel, however, I_a appears to be quite linear both with negative and positive values of I_a, at least up to I_p values equal to I_c. If corrosion rate varies linearly with applied current, the part of the freely corroding rate that is due to local action, I_{aa}, can be readily obtained:

$$I_{aa} = \frac{I_c I_{a1}}{I_{a1} - I_c} \qquad [10]$$

where I_{s1} is the observed corrosion rate when a current I_{s1} is applied to the corroding specimen. I_{s0} is also numerically equal to the current I_p required for cathodic protection.

This leads to a calculation of chunk effect ratio, C, which is the fraction of the freely corroding rate that is due to chunk effect:

$$C = \frac{I_{s0}}{I_o} = 1 - \frac{I_{s1}}{I_{s1} - I_o} \qquad [11]$$

The chunk effect ratio can also be computed by combining Eq. [9] and [11]:

$$C = \frac{I_o - I_p}{I_o} \qquad [12]$$

The difference effect can be determined experimentally as:

$$I_o + I_{s1} - I_{s1} = \Delta \qquad [13]$$

and since I_{s1} is larger than the sum of $I_{s1} + I_o$, the difference effect Δ is negative. From the Thiel and Eckell slope K (Eq. [5]) it is seen that K and the chunk effect ratio C are related:

$$C = \frac{-K I_{s1}}{I_{s1} - I_o} \qquad [14]$$

Up to this point the cases of corrosion with anodic polarization (positive difference effect) and corrosion with chunk effect have been considered as occurring separately. In a general case anodic polarization and the chunk effect occur simultaneously on the same piece of metal. If the decrease in local action rate exactly equals the rate at which the chunks are leaving the metal, there will be no measurable departure from the Faraday equivalence (line DBM of Fig. 1). Ordinarily, the two effects would not be equal: either the positive difference effect or the chunk effect is predominant and is observed depending on the nature of the corrodent.

Experimental

Demonstration of the negative difference effect in the case of steel.—The negative difference effect was observed as an incidental effect in experiments with dissolved oxygen concentration cells. From the standpoint of studying concentration cells the mode of generation of cell current is important; but here we are concerned with cell current merely as an externally applied current, I_p. This applied current could just as well have been obtained by using an external cathode and current source. A suitable apparatus is shown schematically in Fig. 2. The solutions used contained NaCl at various concentrations, with known dissolved oxygen concentrations between 0 and 6.5 ppm. The pH of the solutions was adjusted with NaOH or HCl at frequent intervals. The electrodes were electrical resistance probes (14) of SAE 1010 mild steel, unannealed. They were etched prior to use by immersion for 10 sec in 6*N* HCl containing 1% ferric chloride. Following this, the probes were washed in water and acetone, dried, and stored temporarily in a desiccator until used.

In such a dissolved oxygen concentration cell, the cell current depends mainly on the degree of aeration and agitation in each zone. By suitable choice of conditions the current density on the anode could be made as high as 170 μa/cm^2 (160 ma/ft^2). To compute the difference effect in such experiments one had only to obtain the freely corroding rate I_o of the unconnected probe in the anodic compartment of the cell, add the cell current I_p, and subtract the corrosion rate I_o of the anodic connected probe. Corrosion rates were obtained with the probes *in situ* by means of a corrosion meter (14). The difference effect using this method is measurable in terms of loss of metal rather than in terms of the generation of hydrogen as in most previous experiments.

As a further refinement, one could interrupt the cell current at any point and apply cathodic protection in small increments while continuously measuring the corrosion rate, thereby obtaining the minimum current needed for cathodic protection. Using steel probes initially 25 μ thick (0.001 in.) one could measure thickness changes of the order of 0.05 μ (0.2 μ in.) by means of the changes in electrical resistance.

The results with neutral solutions show a trend in the direction of negative difference effect, the effect becoming quite pronounced at low pH (Fig. 3). It is significant that some of the runs of Fig. 3

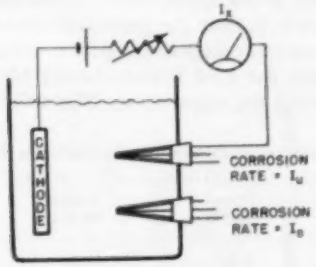

Fig. 2. Apparatus for studying corrosion rate—applied current relationships. Electrical resistance corrosion probes were used to determine the corrosion rates. The polarity of the battery could be reversed to permit study of cathodic protection.

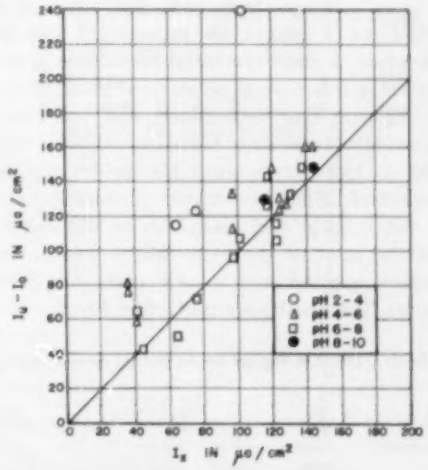

Fig. 3. Effect of pH on difference effect of steel, various NaCl solutions. Each point represents a separate run. By Thiel and Eckell's definition, points lying above the 45° line of equivalence indicate a negative difference effect; points lying below the line indicate a positive difference effect.

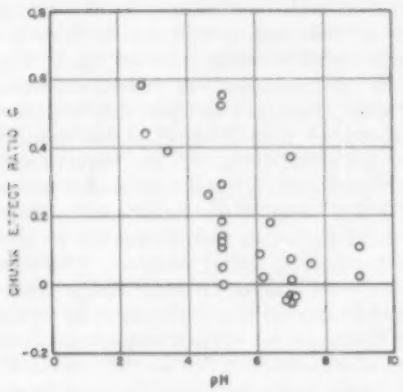

Fig. 4. Variation of chunk effect with pH. Data used in plotting Fig. 3 were replotted in terms of chunk effect ratio C calculated from Eq. [11]. Note the pronounced increase in C at low pH.

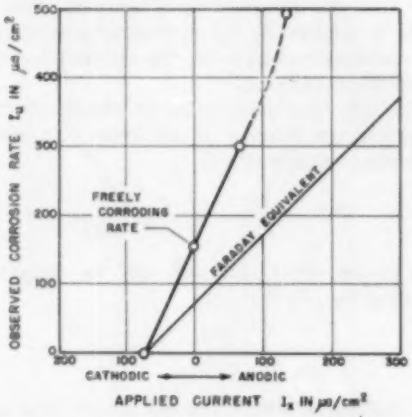

Fig. 5. Chunk effect of steel dissolving in dilute HCl, pH 2. Based on the Faraday equivalent of the cathodic protection current, about half the freely corroding rate is attributable to corrosion by more than one atom at a time.

were made in oxygen-free solutions. Thus while oxygen appears to be necessary in order to obtain the negative difference effect in, say, magnesium (5), there is no such restriction in the case of steel.

In Fig. 4, the data of Fig. 3 were replotted in terms of the fraction of the freely corroding rate due to chunk effect (C) as a function of pH. It is seen that at low pH values C may be greater than 0.5, indicating that over half of the corrosion rate is attributable to the chunk effect mechanism. This result is in general agreement with I_p/I_a data tabulated in ref. (8).

In Figs. 3 and 4 each point represents a single run with a cell of certain composition; I_a is the cell current, and $I_a - I_p$ is the difference in two measured corrosion rates. At low values of I_a, the quantities I_a and I_p are not very different, so that scatter of the data is inevitable. With a given set of conditions the cell currents were reproducible within a few microamperes; the corrosion rates in the low range were reproducible within about 2 $\mu a/cm^2$.

To illustrate the improvement in the quality of data when a single specimen was used to obtain several I_a *vs.* I_p points, an experiment was carried out in which a steel electrical resistance probe was immersed in an aqueous solution of pH 2. The freely corroding rate was determined and was converted into equivalent current; then cathodic current was applied in increments until the protective current was reached. Next the freely corroding rate was again determined and found to be the same as it was at the start of the experiment. Anodic current was again applied and a new corrosion rate was measured. The results are plotted in Fig. 5.

Based on the freely corroding rate (equivalent to 153 $\mu a/cm^2$) and the protective current (75 $\mu a/cm^2$) the chunk effect ratio C for the system of Fig. 5 was about 0.5. The measured corrosion rate was linear with applied current up to a high anodic current.

After the probe of Fig. 5 had been made anodic for a period long enough to obtain the corrosion rate, the anodic current was turned off and the protective current was again determined. This current (82 $\mu a/cm^2$) was still essentially the same as before the anodic treatment, indicating that the local action current had not been affected by the treatment. The freely corroding rate increased slightly when measured before and after the treatment.

This phenomenon occurs consistently when steel is made highly anodic at low pH: I_a increases after each treatment while I_p remains constant. Disruption of a shielding film would explain the increase in I_a but not the constancy of I_p. If more area is exposed for local action, more protective current should be required. These facts indicate that the chunk effect increases as corrosion proceeds, if the corrosion rate is very high.

Table I lists data obtained with a smooth mild steel probe immersed in dilute HCl of pH 2. Both I_a and I_p were obtained at intervals after applying anodic current. The local action current as reflected by I_p remained practically constant. "Blank" probes, not subjected to anodic current, maintained constant values of I_a and I_p over the period of the experiment; the values were reproducible within about 3 μa per cm^2. However the I_a of the anodically treated probe doubled during the experiment. The difference effect

Table I. Effect of applied anodic current on minimum protective current and on freely corroding rate—steel corroding in HCl, pH 2

Elapsed time, hr	I_{a_1}, $\mu a/cm^2$	I_{p_1}, $\mu a/cm^2$	I_{a_2}, $\mu a/cm^2$	I_{p_2}, $\mu a/cm^2$	C from Eq. [12]	C from Eq. [11]	K
0	153	—	—	75	0.44	—	—
1	—	73	307	—	—	0.48	—0.7
2	—	151	527	—	—	0.53	—1.1
3	230	—	—	82	0.64	—	—
4	—	43	484	—	—	0.81	—4.2
5	291	—	—	87	0.70	—	—

slope K decreased from −0.7 to −4.2, but K could be calculated only for the periods of time in which anodic current was being applied. The chunk effect ratio C, calculated from either Eq. [11] or [12], showed a gradual increase, with a reasonably good fit of values obtained by the two methods.

From this type of experiment, K appears to be of little value in depicting the mechanism of corrosion. If K in the example above is some measure of the disruption of a shielding film, one must ask why I_p does not vary with K. The chunk effect hypothesis on the other hand might aid in the study of mechanism. The gradual increase in C indicates that, as corrosion proceeds under conditions of high corrosion rate, a greater per cent of the freely corroding rate takes place by removal of more than one atom at a time. As I_p is essentially constant, this is not likely due to an increase in cathodic surface area, but rather to the geometric pattern by which the lattice dissolves.

Summary

Theories of film shielding of anodic areas do not explain adequately the negative difference effect and the relationship between minimum protective current and freely corroding rate in the case of steel. These effects can be explained by supposing that under certain conditions corrosion proceeds partly through removal of chunks of metal containing perhaps only a few atoms. This is believed to occur over the whole range of applied currents from cathodic protection to high anodic currents. The chunk effect is most pronounced (in steel) under conditions which yield high corrosion rates. In experiments at pH 2, for example, about 50% of the observed corrosion rate could be attributed to the chunk effect mechanism.

It is suggested that the chunk effect and anodic polarization occur on the same piece of corroding metal. Thus either the positive or the negative difference effect may be observed, depending on the corrodent.

Manuscript received Feb. 5, 1960; revised manuscript received Sept. 9, 1960. This paper was prepared for delivery before the Houston Meeting, Oct. 9-13, 1960.

Any discussion of this paper will appear in a Discussion Section to be published in the June 1961 JOURNAL.

REFERENCES

1. A. Thiel and J. Eckell, *Korrosion u. Metallschutz*, **4**, 121 (1928); **4**, 145 (1928).
2. W. J. Müller, *Trans. Electrochem. Soc.*, **76**, 167 (1939).
3. M. E. Straumanis, *Korrosion u. Metallschutz*, **14**, 67 (1938).
4. M. E. Straumanis and Y. N. Wang, *This Journal*, **102**, 304 (1955).
5. W. O. Kroenig and V. N. Uspenskaja, *Korrosion u. Metallschutz*, **11**, 10 (1935).
6. N. D. Tomashoff, "Corrosion of Metals with Oxygen Depolarization," book condensed and translated in *Light Metals*, **11**, 505 (1948).
7. M. A. Streicher, "Pittsburgh International Conference on Surface Reactions," p. 105, Corrosion Publishing Co. (1948).
8. E. Schaschl and G. A. Marsh, *Corrosion*, **13**, 243t (1957)
9. M. E. Straumanis, *This Journal*, **105**, 284 (1958).
10. B. Roald and M. A. Streicher, *ibid.*, **97**, 283 (1950).
11. G. R. Hoey and M. Cohen, *ibid.*, **105**, 245 (1958).
12. W E. Higgins, *ibid.*, **105**, 757 (1958).
13. D. A. Vermilyea, *ibid.*, **105**, 547 (1958).
14. G. A. Marsh and E. Schaschl, *Oil and Gas J.*, **54**, No. 29, 135 (1955).

Symbols Used

- Δ — Thiel and Eckell's difference effect.
- K — Thiel and Eckell's slope constant.
- I_a — Applied current density.
- I_o — Observed corrosion rate expressed as equivalent current density.
- I_c — Freely corroding rate expressed as equivalent current density.
- I_p — Minimum protective current density.
- I_c — Local action current density.
- I_b — Chunk effect corrosion rate expressed as equivalent current density.
- I_{co} — Local action current density under the condition of zero applied current.
- I_{bo} — Chunk effect corrosion rate at zero applied current.
- C — Chunk effect ratio.

Correction

In the September 1960 issue of the JOURNAL on page 768 of the paper by K. B. Oldham "Theory of Faradaic Distortion" the term "C +" was omitted from Eq. [6]. Equation [6] should read

$$C(0,t) = C + \sum_{j=0}^{\infty} \mu_j \cos j\omega t + \sum_{j=1}^{\infty} \lambda_j \sin j\omega t \qquad [6]$$

Flash Conductivity in Solution of Triphenylamine in n-Hexane

H. Rüppel, U. Krog, and H. T. Witt

Physikalisch-chemisches Institut der Philipps-Universität, Marburg/Lahn, Germany

ABSTRACT

A method is described for detecting short-lived charged primary products (ions, electrons) produced in photochemical reactions. The photochemical reaction is initiated by a light flash in an electric field of approximately 1000 v/cm. Photochemical changes produced in the solution are measured by a current impulse which occurs between the electrodes. The method is applicable for organic solutions which have a very small conductivity in the dark. Solvents such as hexane, benzene, and toluene may be used. The method was applied to detect light-produced short-lived radical ions of triphenylamine and similar substances in n-hexane. The electrical detection of flash conductivity in the case of triphenylamine was examined optically by measuring the transient absorption band of the photoproduct by flash photometry.

Ultraviolet radiation of a wave length $\lambda > 200$ mμ generally causes no additional conductivity in liquid organic media. That is to say, organic liquids either have no absorption bands in this spectral range (*e.g.*, hexane) or only such absorption bands as lead to excited electron states and not to the splitting off of an electron (*e.g.*, benzene). When there are ionization bands the radical ions produced in the liquid generally have a very short lifetime. Therefore the stationary amount of charge carriers produced by steady light is so small that an additional conductivity cannot be detected readily.

Conditions may be more favorable if, instead of steady light, the light of an electronic flash is used. Flash light is about 1000 times more intense than steady light, and, if ionization bands exist, it may be expected that flash light will give rise to a brief but measurable conductivity in the organic liquid. This conductivity phenomenon has been designated by us as "flash conductivity" (1).

Detection of flash conductivity was first attempted in the system triphenylamine in liquid n-hexane. According to Lewis and Lipkin (2) it is probable that there is an ionization of triphenylamine by u.v. with $\lambda > 200$ mμ. On irradiating a solid solution of triphenylamine at 90°K by u.v. light, Lewis discovered a new absorption band at 660 mμ. Comparing this with the known absorption spectrum of the radical ion of triparatolylamine, he assumed that he had produced a triphenylamine positive ion. Furthermore, according to the electron gas model of Kuhn (3) one could even expect the triphenylamine to have an absorption band in the visible spectral range. There had been, however, no direct electrical proof for the ionization ion in the solid solution. In the *liquid* solution the triphenylamine radical ion had not been detected either electrically or optically.

For the detection of the triphenylamine positive ion in liquid solution it had to be demonstrated that flash excitation of the triphenylamine solution gives rise to: (*a*) a brief additional conductivity, and (*b*) a transient absorption band in the visible red.

Methods of Measurement

A schematic drawing of the arrangement for measuring flash conductivity is shown in the upper part of Fig. 1. The triphenylamine solution was placed between the electrodes of a quartz cell. The electric field was approximately 1000 v/cm. If charge carriers are produced by the flash, they will move in the electric field during their lifetime, inducing a current impulse on the electrodes. The current impulse can be amplified by the pulse amplifier (PA) and indicated on the oscilloscope (CRO).

The current impulse comes about as follows. Every charge carrier produced by the flash moves in the electric field E with a velocity $u = v \cdot E$, where v is the mobility of the charge carrier. During its lifetime τ, the charge carrier travels a distance $s = v \cdot E \cdot \tau$. By this means a definite charge q is induced on the electrodes,

$$q = e \cdot s/d = e \cdot (v \cdot E \cdot \tau)/d \qquad [1]$$

where e is the electrical charge of the particle and d the distance between the electrodes.

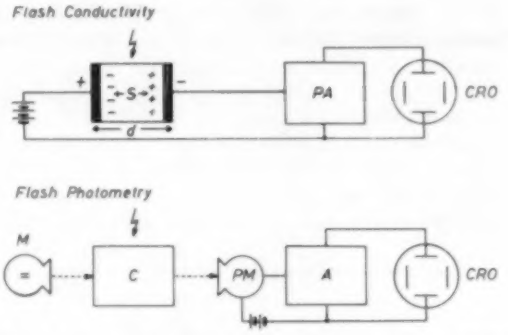

Fig. 1. Upper part: schematic drawing of the electrical arrangement (flash conductivity), d—distance between the electrodes, s—distance the charge carrier travels in the electric field during its lifetime, PA—pulse amplifier, CRO—cathode-ray oscilloscope; lower part: schematic drawing of the optical arrangement (flash photometry); M—measuring light source, C—quartz cell, PM—photomultiplier, A—amplifier.

If the production of ions per flash results in a total charge Q_o, then the current impulse at the amplifier input is given by the expression

$$Q = Q_o \cdot (v_+ + v_-) \cdot E \cdot \tau / d \qquad [2]$$

where v_+ is the mobility of the positive and v_- that of the negative charge carrier. This simple equation is valid if $(v_+ + v_-) \cdot E \cdot \tau << d$ (1).

The lower limit of measurement is fixed by the noise of the preamplifier tube. In the present case the noise level corresponded to a charge of approximately 5000 electrons. Substituting this value for Q and the known values for E, d, and v (4) one obtains a given lower limiting value of the product $Q_o \cdot \tau$, $(Q_o \cdot \tau)_{lim} \sim 5 \cdot 10^{-8}$ e·sec, which is just within the limit of measurement. Thus, the flash conductivity method is very sensitive. Assuming an ion lifetime of 10^{-4} sec, a concentration of about 10^{-10} mole/l [1] can be detected, or, in the other extreme, at a given ion concentration of 10^{-5} mole/l, ions with a lifetime of 10^{-10} sec can be detected.

In the lower part of Fig. 1 a schematic drawing of the optical arrangement for flash photometry is shown, the principle of which was reported by Norrish and Porter (5) and by Davidson and co-workers (6). A beam of monochromatic measuring light (M) passes through the quartz cell (C) and falls onto a photomultiplier (PM). If the flash produces photochemical changes in the solution which give rise to a new absorption band, the photomultiplier will detect a change in the intensity of the measuring light. The corresponding current variation in the photomultiplier output can be amplified (A) and indicated on the oscilloscope (CRO). The lower limit of measurement is fixed by the noise of the photomultiplier cathode. The theoretical value of the resolution limit is practically reached by our arrangement (7). At a signal risetime of $\sim 10^{-5}$ sec an absorption change of 0.1% is detectable.

Results

Electrical measurements.—Excitation of the triphenylamine solution in n-hexane with unfiltered flash light produced the expected current impulses. The current impulses rise linearly with the electric stress E, indicating that the lifetime of the ion is small enough to satisfy the condition for Eq. [2], or, in this case, $\tau << 1$ sec. In order to determine which of the absorption bands of the triphenylamine (see Fig. 3, solid curve) gives rise to ionization, the light of the flash was filtered. Measurements indicated that ionization accompanies absorption only in the u.v. absorption with $\lambda < 250$ mμ. Other parameters such as concentration of triphenylamine, oxygen content of the solution, etc., were also varied. The results of these measurements confirmed expectations (1).

Flash conductivity could also be detected in n-hexane solutions of diphenylamine, tetramethylparaphenylendiamine, and both types of chlorophyll. (Under equal experimental conditions the electrical signal in the case of chlorophyll is about three times larger than with triphenylamine. The order of magnitude of the current impulse is $Q \sim 10^{-10}$ amp sec.) On the other hand, exciting a solution of benzene in n-hexane with u.v. light of the spectral range $\lambda > 200$ mμ produced, as had been expected, no electrical signal (see above).

[1] The volume of the quartz cell was approximately 0.1 l.

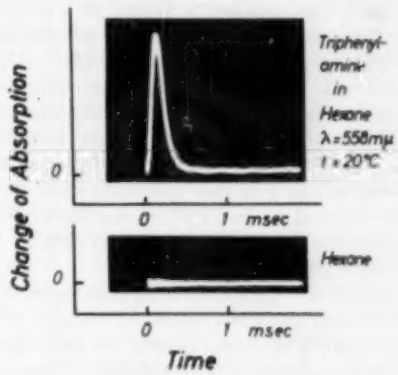

Fig. 2. Change of absorption vs. time as received on the oscilloscope. Upper part: increase of absorption was produced by irradiating triphenylamine in n-hexane with the intensive light of an electronic flash. Concentration of triphenylamine: $3 \cdot 10^{-5}$ mole/l. Wavelength of the measuring light, 558 mμ ($\Delta\lambda = 17$mμ); temperature, 20°C; electrical energy of the flash discharge, 240 j; length of the quartz cell, 10 cm. The maximum of the absorption change corresponds to a decrease of transmission of approximately 6%. Lifetime of the photoproduct (triphenylamine positive ion) $\tau < 10^{-4}$ sec. Lower part: Response of the optical arrangement on flash light excitation of pure n-hexane.

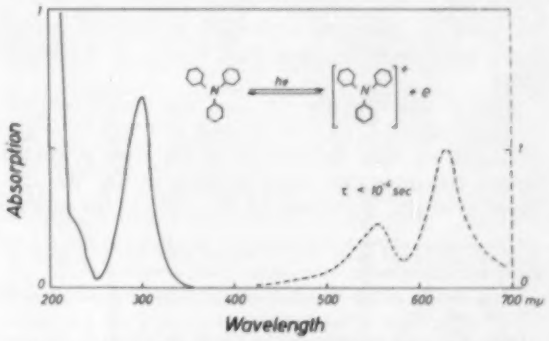

Fig. 3. Absorption vs. wave length. Solid line: normal absorption spectrum of triphenylamine in n-hexane; dashed line: transient absorption spectrum received by flash photometric measurements on illuminating triphenylamine in n-hexane by intensive flash light. (Preliminary measurements; position and relative heights of maxima may be submitted to some change.) Temperature: 20°C. Electrical energy of the flash discharge, 240 j; flash duration, approximately $2 \cdot 10^{-4}$ sec; lifetime of the photoproduct (triphenylamine positive ion) $\tau < 10^{-4}$ sec. (Both absorption spectra are plotted in arbitrary units.)

Optical measurements.—In addition to the electrical detection of charged photoproducts in the triphenylamine solution, there was also a brief appearance of a new absorption band. This may be due to the triphenylamine positive ion. The optical signal measured at a wave length of 558 mμ is shown in the upper part of Fig. 2. It was received on the oscilloscope when the intensive flash light excited the triphenylamine solution. The time course of the optical signal corresponds approximately to that of the flash light emission, indicating that the lifetime of the transient photoproduct is shorter than 10^{-4} sec. The entire transient absorption spectrum could be

traced from measurements taken at various wave lengths. The main peak of the new absorption band lies in the spectral range around 650 mμ[2](Fig. 3, dashed curve). According to the experimental work of Lewis (2) as well as to the calculations of Kuhn (3) based on the electron gas model, there is good evidence for the triphenylamine radical ion to show an absorption band in this spectral range. Thus, the transient absorption band observed on exciting the triphenylamine solution may be ascribed to the triphenylamine positive ion.

Experimental.—The measurements have been described in their essential features without regard to experimental difficulties. Owing to its high sensitivity, the apparatus is very subject to interference, most of which is caused by the intensive flash discharge. Measurements are disturbed by the electromagnetic field and by the sound and any random light of the flash. The latter causes electrode effects in the cell or false light signals on the photomultiplier. Nearly all of these troubles may, however, be handled appropriately.[3]

Conclusions

The method of using flash conductivity may be extended to quantitative measurements, i.e., it may be used to measure ionization potentials, which have, until recently, been little known in the liquid state.

Finally, there is one circumstance which remains to be discussed. In a system such as triphenylamine in liquid or rigid solution it is not clearly known where the separated electron stays during its lifetime.[4] It might, therefore, be desirable to investigate systems with a definite electron acceptor present. There are donor-acceptor systems in which an electron transfer takes place from the photo-excited electron state:

$$A^* + B \rightarrow A^+ + B^- \rightarrow A + B$$

[This scheme has been used to explain the quenching of fluorescence of certain organic compounds (9)]. Owing to the high sensitivity it should be possible to detect such an electron transfer electrically in the apparatus described above. Reactions of this kind are the subject of our current investigation.

[2] Independent of the flash photometric measurements (Fig. 1) the transient absorption curve (Fig. 3, dashed line) was measured recently by us also using the method of flash spectroscopy (5).

[3] More details of the experimental technique are described in ref. (1) and (7).

[4] Tentative ideas are discussed by Lewis (2), Linschitz (8), and especially by LeBlanc (4) (see also paper by O. H. LeBlanc, Jr., presented at the Philadelphia Meeting of the Society, May 6, 1959.

Acknowledgment

The authors wish to thank Miss Rilla Spangler, West Chester, Pa., and Mr. Günter Eckel, Marburg/Lahn, for helpful suggestions regarding the textual revision of this manuscript. Grateful appreciation for research support is expressed to the Research Corporation, New York, and the Deutsche Forschungsgemeinschaft, Bad Godesberg.

Manuscript received March 1, 1960. This paper was prepared for delivery before the Philadelphia Meeting, May 3-7, 1959.

Any discussion of this paper will appear in a Discussion Section to be published in the June 1961 JOURNAL.

REFERENCES

1. H. Rüppel and H. T. Witt, *Z. physik. Chem. N. F.*, **15**, 321 (1958).
2. G. N. Lewis and D. Lipkin, *J. Am. Chem. Soc.*, **64**, 2801 (1943).
3. H. Kuhn, *Chimia*, **9**, 237 (1955).
4. O. H. LeBlanc, Jr., *Insulation*, **5**, 6, 26 (1959).
5. R. G. W. Norrish and G. Porter, *Nature*, **164**, 658 (1949).
6. N. Davidson, R. Marshall, A. E. Larsh, and T. Carrington, *J. Chem. Phys.*, **19**, 1311 (1951).
7. H. T. Witt, R. Moraw, and A. Müller, *Z. physik. Chem. N. F.*, **20**, 193 (1959).
8. H. Linschitz, M. G. Berry, and D. Schweitzer, *J. Am. Chem. Soc.*, **76**, 5833 (1954).
9. Th. Förster, "Fluoreszenz organischer Verbindungen," p. 221 ff, Vandenhoeck & Ruprecht, Göttingen (1951).

Electrodeless Passage of Direct Current through an Electrolyte

Abner Brenner

National Bureau of Standards, Washington, D. C.

ABSTRACT

An experimental setup is described for directly observing the electrical migration of a dye in a conducting system without electrodes. Direct current was produced in a continuous circuit of electrolyte, which included the dye solution, by means of a transformer and a mechanical commutator.

The passage of direct current between electrodes immersed in a conducting solution produces two phenomena: chemical reactions at the electrodes and mass transport of the solute. If one looks at this process phenomenologically, one is tempted to ask naively whether the mass transport would occur if current were passed through the solution in such a way that no electrode reactions occurred. To perform this experiment it would be necessary to produce direct current in an electrolyte without using electrodes.

On the basis of the currently accepted theories of the structure of electrolytes, it seems obvious that electrical migration[1] would occur even in the ab-

[1] Ionic or electrical migration is considered to be the flux of dissolved matter, in accordance with Faraday's law, through an electrolyte as a result of the flow of current.

sence of electrolysis. The ions in solution, being charged particles, would move in the electric field that is applied across the solution. However, the possibility could be envisioned that in the absence of electrolysis the positive and negative ions consort together as dipoles and the current then could be carried by a flow of electrons or holes as in a semiconductor or metal. As an example, the conduction of electricity through the solution of an alkali metal in ammonia is supposed to occur by a flow of electrons.

Even though current theory predicts that electrical migration would occur in the absence of electrolysis, the auther considered that direct observation of the predicted phenomena would make an interesting experiment. An additional element of interest was provided in designing the apparatus for producing direct current in the electrolyte without using electrodes.

In looking into the literature of the electrodeless passage of current through an electrolyte, the author found the subject was a rather old one. It had been the center of lively discussion and controversy 60 years ago and then had been forgotten. The author learned of the early literature somewhat by accident. In the course of preparing the J. W. Richards Memorial Lecture, the author learned that both Richards, the first president of The Electrochemical Society, and Carl Hering, the fourth president of the Society, published papers on the subject. Richards (1, 2) believed that conduction through an electrolyte occurred by the same mechanism as "metallic conduction" and that electrical migration was a secondary phenomenon which resulted from the chemical changes that occurred at the electrodes. According to his view, in the absence of electrolysis there should be no electrical migration.

Richards also attempted to show that current could be passed through an electrolyte without causing chemical changes. His experiment, which involved zinc electrodes immersed in solid zinc chloride, was unsatisfactory, because the current used was so small that evidence of electrolysis could not be detected. It was severely criticized.

Hering was of the opinion that the electrodeless passage of current through a solution would not produce any phenomena radically different from those obtained with the passage of current introduced through electrodes. He did not actually do any experimental work on the problem, but he described (3, 4) various types of unipolar devices that would achieve the electrodeless flow of current.

Marvin (5) constructed a unipolar device which, however, did not yield sufficient current for experimental purposes. By introducing two copper electrodes into the circuit he was able to obtain a deflection of a galvanometer. His other experiments involved the use of alternating current. Both he and others (6) have shown that an alternating magnetic field can induce an alternating current in a continuous tube of electrolyte. The presence of the current in the electrolyte was demonstrated by its magnetic field or by its heat effect. The electrodeless measurement of the conductivity of electrolytes by making a tube of electrolyte one element of a transformer is now in routine use (7). Experiments with induced alternating currents give no direct information on transport of material in the absence of electrodes.

The major part of the effort in this investigation was expended on the construction of apparatus and the development of a method for detecting electrical migration produced by small currents of the order of microamperes. The objective of the investigation was to set up an experiment which would permit one to observe, qualitatively, electrical migration in the absence of electrolysis. However, a comparison between the effects of the induced direct current and a current introduced by electrodes put the experiments on a semiquantitative basis.

Apparatus

Electrical and mechanical.—The apparatus consisted of three parts: a transformer, a commutator, and an electrolyte system. The apparatus is shown diagrammatically in Fig. 1 and 3 and a photograph is shown in Fig. 4.

The transformer core was originally part of the control equipment on an electric furnace and had large secondary windings that carried several hundred amperes. All windings were removed and the core was wound with a primary consisting of several hundred turns of No. 12 copper wire and a secondary consisting of a rubber tube, about 4 cm inside diameter and 8 meters long, filled with a saturated ammonium nitrate solution. This salt solution was chosen because it is a fairly good conductor and is not very corrosive.

The method of producing the direct current in the electrolyte circuit was periodically to reverse a direct current passing through the primary coil of the transformer. This ordinarily would produce an alternating current in the tube of electrolyte, but by breaking the circuit in the latter at the proper time the reversal of current was prevented. The appara-

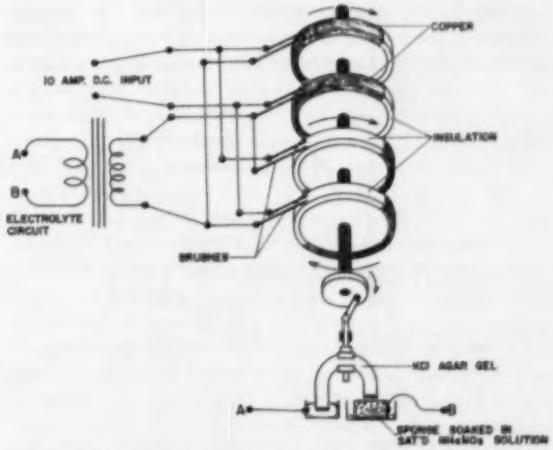

Fig. 1. Diagram of commutator. U-tube at bottom of figure closes electrolyte circuit by being brought into contact with a sponge saturated with ammonium nitrate solution. The U-tube moves vertically up and down in synchronization with the rotation of the commutator wheels. The current through the primary is reversed when the junctions between the copper and insulating parts of the wheels pass under the four pairs of brushes.

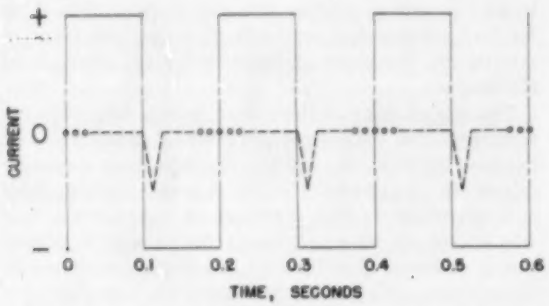

Fig. 2. Schematic representation of the currents in the primary winding of the transformer and in the secondary winding comprising the tube of electrolyte. ————, Current through primary; — — — current through secondary; o o o o, open circuit in secondary.

tus corresponds to a mechanical half-wave rectifier. The principle of operation is made clear with the aid of Fig. 1 and 2. The commutator consisted of four wheels with half of the periphery of each covered with copper and the other half with insulation. Two adjacent copper brushes contacted each wheel. When the junctions between the copper and the insulating segments passed the four pairs of brushes, the current through the primary coil was reversed.

The circuit in the electrolyte was made and broken by a U-tube containing potassium chloride solution in agar-agar gel. The tube was given a vertical reciprocating motion by a crank attached to the same shaft as the commutator wheels. The U-tube (see Fig. 4) was closed at both ends with porous glass diaphragms which served to retain the agar-agar gel during operation of the device. When the U-tube was in its lowest position, it pressed against a sponge saturated with ammonium nitrate solution and thereby completed the electrolyte circuit shown diagrammatically in Fig. 3.

The commutator operated in three steps: Step 1. The electrolyte circuit is closed by the U-tube (connected to the crank) pressing against the sponge. Figure 1 shows the arrangement of components just prior to closing the circuit for step 1. The closing or

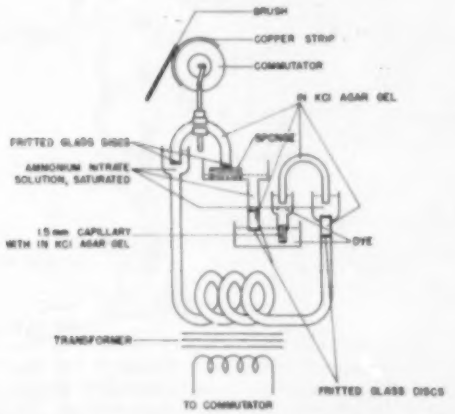

Fig. 3. Diagram of electrolyte circuit. A direct current is produced in the circuit by means of cyclically reversing the current though the primary of the transformer and interrupting the current in the secondary by means of the vertically actuated U-tube.

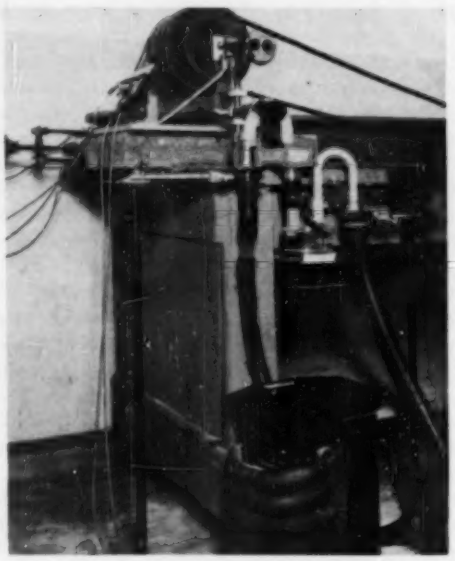

Fig. 4. Photograph of the apparatus

opening of the electrolyte circuit does not produce a flow of current through the electrolyte. Step 2. The junctions on the wheels pass under the brushes and cause the current to reverse through the primary. This change of magnetic flux induces a current in the electrolyte circuit. Step 3. The U-tube is raised from the sponge, which motion breaks the electrolyte circuit. Shortly thereafter the junctions on the wheels again pass under the brushes, causing the current through the primary to reverse to its original direction. Since the electrolyte circuit was broken previously, this produces no current in it. The positions of the brushes and the U-tube are now again as shown in Fig. 1 and the cycle is ready for a repetition.

The commutator was operated at about 300 rpm. The current in the primary was about 10 amp. The current in the electrolyte was measured roughly by intercalculating a microameter and two cadmium electrodes immersed in cadmium chloride solution into the electrolyte circuit. The latter consisted of the tube of ammonium nitrate solution, the dye solutions, and the 1.0M potassium chloride solution in the capillary. The current flowed in pulses having a peak value of 300 μ amp. The voltage was about 0.5 v.

The success of the transformer device depended largely on the use of the U-tube and sponge to break the electrolyte circuit. At first, various types of revolving and reciprocating stopcocks were used to break the circuit. However, they were unsuccessful for two reasons. The film of solution that formed around the plug prevented the circuit from being broken efficiently and the plugs galled and caused the cocks to leak. The use of Teflon plugs did not solve the problem. Another important factor in the operation of the apparatus was the reversing of the current through the primary instead of merely breaking the circuit. Reversing the primary current increased the current in the electrolyte circuit about fivefold.

Apparatus for observing ionic migration.—Since only small currents were generated in the electrolyte, a sensitive method of observing electrical migration was necessary. The moving boundary method was found to be unsuitable. The method adopted was to observe the movement of a dye, erythrosine B, (the di-sodium salt of tetraiodofluorescein) into a capillary containing a gel.

The size of the capillary was important. Preliminary experiments had shown that in a capillary about 0.5 mm in diameter, the migration caused by a current of 25 μamp in 15 min was readily detected. With still smaller capillaries, probably the migration effects of even smaller currents can be detected. However, the minimum size of the capillary that could be used in the experiment was limited by the small voltage that was available, and the gain in sensitivity was offset by the reduction in current due to the high electrical resistance of the solution in the capillary. On the other hand, a large capillary decreased the sensitivity of the experiment because of increased amount of dye diffusing into the capillary. This could be greater than that carried in by electrical migration. The optimum inside diameter of the capillary was 1.5 mm. The capillary was filled with an agar gel containing about 2% agar-agar and 1.0*N* in potassium chloride. A more dilute solution of potassium chloride would have been preferable, since it would carry less current at the junction with the dye solution. However, the resistance of a 0.1*N* solution of potassium chloride in the capillary was too high.

The use of the capillary filled with agar gel also involved a mechanical problem, because the thread of gel readily became detached from the capillary wall and occasionally even slipped out of the tube. To obviate this difficulty the capillary surface was roughened with glass powder in the following manner. A drop of mineral oil was allowed to flow through the capillary and wet the surface. Then glass powder was drawn through the tube by connecting one end to a vacuum line and placing the other end near a small quantity of powder. Finally, the capillary was heated several hours at 600°C to cause the glass powder to fuse to the wall. Capillaries about 20 cm long were prepared and pieces about 2 cm long which were used in the experiments were cut off with a diamond wheel.

The capillary was connected to the funnel shaped piece of glass shown in Fig. 4 by a rubber stopper or tube. The entire current in the electrolyte circuit passed through the capillary.

Procedure

The experiments themselves were simple and required little time. A 0.01M solution of erythrosine was poured into that vessel to which the capillary was attached, and the lower end of the capillary protruding from the end of the vessel was immersed in a beaker of the dye solution. In this manner both ends of the capillary were in contact with the dye. In Fig. 4 the dye solution has been omitted. The circuit between the beaker of dye solution and the solution in the electrolyte coil was completed with another U-tube filled with potassium chloride-agar gel.

Since during the experiment dye diffused into the capillary tube, it was necessary to make a control experiment to correct for it. This was done by immersing another piece of capillary in the dye solution for the same length of time as the duration of the experiment. No current flowed through the control capillary.

Induced current was passed through the system for 30 min, which time was adequate to produce appreciable migration of dye into the main capillary. Both the main and the control capillaries were removed from the dye solution and rinsed. The ends containing the dye were cut off and placed in small test tubes containing 7 ml of water, and the gel was dissolved by heating. The concentration of dye in the solution was measured with a spectrophotometer, and the content of dye in the capillary was calculated.

Since the color of the dye is due to the anion, during current flow it migrated into one end of the main capillary and away from the other end. However, diffusion caused some dye to enter the latter end, but the amount was only about one-third that in the control capillary. The content of the dye in the control capillaries was reproducible within the limits of the measurement of the dye concentration.

Three types of experiments were made. These are listed in Table I. Experiments 1 and 2 dealt with electrical migration in the absence of electrodes. Experiments 3 and 4 involved the use of electrodes and permitted a comparison with the electrical migration of experiments 1 and 2. Experiment 5 was made with induced direct current, but cadmium electrodes were placed in series with the electrolyte circuit.

Table I. Summary of experiments

Comparison of the electrical migration of erythrosine B with and without conventional electrodes. Dye solution, 0.01M. Solution in capillary was 1.0M potassium chloride and contained about 2% of agar. Diameter of capillary, 1.5 mm. Thirty minute run at about 300 rpm. Peak current, 300 μamp.

	Description of experiment	Migration of dye,* mole × 10^{-6}
1.	Electrodeless	6.0
2.	Electrodeless. Direction of current opposite to that of No. 1	6.7
3.	Current, 150 μamp, from an external source introduced by electrodes	6.0
4.	Current, 90 μamp, from an external source introduced by electrodes	3.4
5.	Induced direct current as in No. 1 and No. 2, except that Cd electrodes were placed in the electrolyte circuit	2.8
6.	Control. Diffusion of dye into capillary without current	1.4

* All electrical migration experiments were corrected by subtracting 1.4 × 10^{-6} moles of dye as determined by control experiment No. 6.

Results

The data in the table show that the electrical migration of the dye was roughly about the same in the presence or absence of electrodes. This was of the order of 6 x 10^{-6} moles. The current was not

measured during the electrodeless experiments so that a qualitative comparison with experiments 3 and 4 was not possible. However, the currents in the latter experiments were of about the same order of magnitude, since the peak value of the induced current was about 300 μamp.

Comparison of experiments 3 and 4 shows that the electrical migration into the capillary was approximately proportional to the current, so that the capillary method is valid as a comparative method of studying electrical migration.

To make certain that no geometrical or extraneous effects were involved in the electrodeless experiments, the currents in experiments 1 and 2 were made to flow in opposite directions. In one experiment the dye migrated into the upper end of the capillary and in the other into the lower end.

The amount of migration obtained in experiment 5 with cadmium electrodes in the circuit was less than in experiments 1 and 2. This indicates that the current during this experiment must have been less than that in 1 and 2. This could have been caused by the resistance of the additional electrolyte in the circuit (the cadmium chloride solution) and a microameter or by variations in the performance of the equipment.

The amount of electrical migration of the dye in all of these experiments indicated that it was carrying only about one-thirtieth of the current. This is understandable, since the dye, which was only 0.01M, was migrating into a capillary containing 1M potassium chloride. Hence, at the juncture of the two solutions, the major portion of the current must have been carried by the potassium chloride solution.

Since the induced direct current produced normal electrical migration, it was of interest to determine whether it also produced normal electrolysis. The induced direct current was passed through a copper wire and a platinum wire, serving as anode and cathode, respectively, immersed in a copper sulfate solution. A copper deposit was obtained in an amount roughly corresponding to the current that passed.

Summary

An apparatus was devised for producing a direct current in an electrolyte without the use of electrodes. With this apparatus it was possible to observe the electrical migration[9] of a dye in a capillary.

Acknowledgment

The author acknowledges the patient and skillful assistance of O. V. Hurst in constructing the mechanical and electrical parts of the induced current apparatus and the assistance of J. L. Sligh in performing the experiments involving the passage of current through the gas phase.

Manuscript received June 13, 1960; revised manuscript received Aug. 9, 1960. This paper was prepared for delivery before the Columbus Meeting, October 18-20, 1959.

[9] It has been suggested that the movement of the dye, instead of being due to ionic migration, might be caused by electroosmosis of water through the capillary. This possibility cannot be completely discounted, but it is unlikely, since the movement of water in solutions as strong as the one in the capillary (1.0M) is considered to be due to ion hydration and not to electroosmosis.

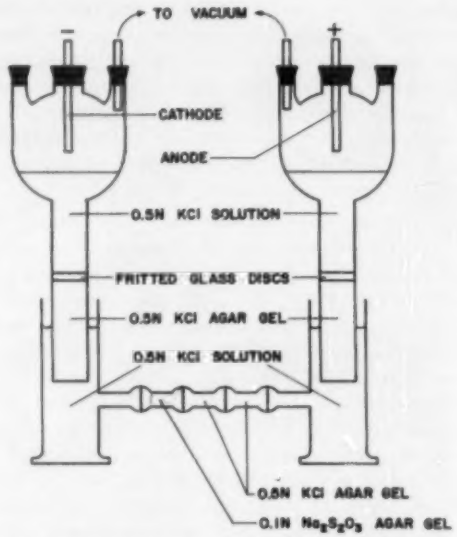

Fig. 5. Diagram of the circuit used for studying the migration of thiosulfate ion in a system provided with a gaseous discharge.

Any discussion of this paper will appear in a Discussion Section to be published in the June 1961 JOURNAL.

REFERENCES

1. J. W. Richards. *Trans. Am. Electrochem. Soc.*, **6**, 152 (1904).
2. J. W. Richards, *ibid.*, **19**, 119 (1911).
3 Carl Hering, *Trans. Am. Inst. Elec. Eng.*, **19**, 309 (1902).
4. Carl Hering, *Trans. Am. Electrochem. Soc.*, **13**, 273 (1908).
5. A. B. Marvin, *ibid.*, **3**, 347 (1903).
6. A. N. M. Hopkins, Discussion, *ibid.*, **3**, 356 (1903); B. Experiment Über Elektrolytische Leitung ohne Elektroden Hs. Behn-Eschenburg, *Z. Elecktrochem.*, **5**, 402 (1899).
7. A. Electrodeless Conductivity System, Industrial Instruments Inc. U.S. Pat. 2,542,057; B. Miroslav Salamon and Peter Svitok, *Chem. Prumysl*, **6**, 10 (1956); C. Raymond Calvert, J. A. Cornelius, V. S. Griffiths, and D. Irwin Stock, *J. Phys. Chem.* **62**, 47 (1958).
8. Alfons Klemenc, *Chimia*, **6**, 177 (1952).

APPENDIX

Electrical Migration in an Electrolyte in Contact Only with a Gas

Another method of passing current through an electrolyte without immersing electrodes in the liquid is to pass the current through the gaseous space above the liquid. The experimental arrangement for this is shown in Fig. 5. It is well known that the chemical effects at the solution-gas interface are several times greater than the amount predicted by Faraday's law (8). Hence, it was of interest to determine whether the electrical migration in the electrolyte was normal or greater than normal.

Metallic electrodes were suspended several centimeters above the surface of the electrolyte which was contained in a closed vessel, and the system was pumped down to a pressure of about 1 cm. A discharge through the gas phase was obtained with a few hundred volts. The current was set at 0.1 amp, although larger currents could have been obtained. The current passed from the metallic electrodes through the gas and the electrolyte which was contained in tubes. To prevent the electrolyte from being forced into the evacuated chambers, a KCl-agar gel was placed in the circuit in contact with a fritted glass partition.

The migration of ions in the electrolyte was investigated by using a gel containing sodium thiosulfate. The migration of the thiosulfate across a boundary into a KCl-agar gel was determined by titration with a standard iodine solution. The amount of thiosulfate that migrated in the system with the gas discharge was compared with that which migrated in a conventional system provided with metallic electrodes. The amounts were the same within the experimental precision which was about 5%.

Formation of Phosphor Films by Evaporation

L. R. Koller and H. D. Coghill

Research Laboratory, General Electric Company, Schenectady, New York

ABSTRACT

Three processes for making ZnS phosphor films are described. One process for ZnS activated with Cu, Ag, or Mn involves evaporation of powder phosphor onto a room-temperature substrate followed by heat treatment of the film in an H_2S + HCl atmosphere. A process for ZnS:Mn alone involves the single step of evaporating the phosphor onto a substrate held between 250° and 400°C. The third process involves evaporating the phosphor in a single step onto a heated substrate in a uniformly heated enclosure such as the "Hot Wall Bell Jar." A fourth process used for silicate, phosphate, and borate phosphors involves a reaction during the course of evaporation between ZnF_2 and a heated substrate.

Thin continuous films of phosphors a few microns thick are useful for practical applications as well as for investigation of cathodo, photo, and electroluminescent phenomena. One method of preparing such films is by evaporation *in vacuo*. The technology of forming phosphor films by evaporation is relatively new. DeBoer (1) patented a process for evaporating ZnS and $CaWO_4$ x-ray intensifying screens in 1934 although it is questionable whether his films would be considered luminescent by present standards. Williams (2) prepared a number of different kinds of phosphor films by evaporation in 1947. He found that efficient films of manganese-activated zinc fluoride could be evaporated but that zinc sulfide, zinc sulfoselenide, and zinc cadmium sulfide films failed to show appreciable luminescent efficiency. More recently Koller (3), and Feldman (4) described methods for making sulfide and fluoride phosphor films. Feldman also described methods for making oxygen containing phosphors. Rychlewski (5) patented methods for forming films of ZnS as well as some oxygen containing phosphors. All three of these methods involve heat treatment at some stage of the process. Studer and Cusano (6) have formed films of a variety of ZnS:Se phosphors by a different but related procedure, namely, vapor reaction.

Although ZnS and some other host lattice materials may be readily evaporated *in vacuo* and condensed again in the form of thin transparent films, these films are not necessarily luminescent (with the possible exception of ZnF_2). The formation of a phosphor film imposes the additional requirement that the film be crystalline and contain activator and coactivator materials in suitable lattice sites and concentration.

Since the vapor pressures of the various constituents of a phosphor differ widely, the condensate (*i.e.* the film) will not have the same composition as the phosphor material evaporated. Furthermore the composition of the condensate will change during the course of the deposition as the phosphor composition changes due to this fractional distillation. These effects result in a gradation of composition throughout the depth of the film.

The composition of the film is also affected by the difference in accommodation coefficients of the phosphor components. Not every molecule which arrives at the substrate surface remains there. Many are reflected from the surface and condense on the relatively cold wall of the bell jar. The composition of the film will depend on the relative accommodation coefficients of the phosphor constituents which in turn are functions of the temperature of the substrate. Accordingly, the composition of a film will depend in a rather complex way on the nature of the material being evaporated, the length of time during which the evaporation has been in progress and the temperature of the evaporator and the substrate.

From these considerations it can be seen that the optimum conditions for forming films of any given phosphor will depend on the nature of the phosphor and that no one method will be satisfactory for all phosphors.

The procedures for forming phosphor films may be broadly classified as follows.

Two-step processes: (*a*) simultaneous evaporation of host lattice and activator materials and condensation on room-temperature substrate followed by heat treatment; (*b*) sequential evaporation of host lattice and activator materials (order immaterial), both condensed on room-temperature substrate followed by heat treatment.

One-step processes: simultaneous evaporation of host lattice and activator onto heated substrate.

Reaction processes: phosphor formed in one step by reaction of a compound with a heated substrate.

Apparatus

All of the two-step processes and some of the one-step processes were carried out in a vacuum system with an 18 in. bell jar exhausted by a 6 in. oil diffusion pump. The system had no cold trap. During the course of an evaporation the pressure maintained was about 10^{-4} mm.

A number of different types of evaporators made of tungsten wires and tungsten foil were used. The most versatile and useful was a foil boat formed by folding a strip of 0.001 in. tungsten foil lengthwise and clamping the ends. A boat ⅜ in. high 1¾ in. long is heated to a temperature of 1673°K by a current of 60 amp with a drop of about 3.2 v. Tungsten was the most satisfactory material for evaporating sulfide phosphors and did not react significantly with them. It also had less copper impurity present than either platinum or molybdenum. Platinum was used for evaporating fluoride phosphors.

The heater for the substrate consisted of a bank of four 500-w tubular quartz infrared lamps mounted on a reflector and placed a few inches above the substrate.

Most of the materials evaporated were in the form of crystalline powders. In order to keep these from jumping out of the boat and sputtering, they were compressed into pellets by means of a small hydraulic press. These compact pellets could be evaporated at the rate of about 0.05 g/min with very little sputtering.

Preparation of Surface

Most of the films were deposited on 2 in. diameter Pyrex disks. The glass was cleaned with a mild abrasive, rinsed in distilled water, and air dried. Other cleaning methods appeared to give equally satisfactory results.

Evaporation

After the preliminary heating of the substrate, films were formed by evaporating the phosphor at rates of about 0.05 g/min with the source 3-6 in. from the substrate. Films were usually deposited to a thickness of about 2μ. The film growth could be monitored by observation of the interference color.

The effect of the vapor pressures of the constituents on the composition is illustrated by the analysis of ZnS:Mn films formed by evaporating a ZnS:Mn phosphor having an Mn content of 0.1%. By means of a slide changer, films were collected during the first, second, and third minutes of evaporation. The Mn/Zn ratios in these films were 0.003, 0.007, 0.011, respectively, compared with 0.001 for the original material. Thus the Mn/Zn ratio in the film was greater than that of the source material and increased progressively during the course of the evaporation. A number of analyses of other ZnS:Mn films showed a Mn/Zn ratio of as much as ten times that of the original film. Thus in addition to a variation in activator concentration with film thickness, ZnS:Mn films tend to have an over-all higher Mn content than the source material.

The effect of the accommodation coefficient on film composition is illustrated by some experiments on evaporation of a ZnCdS phosphor onto substrates at various temperatures. The same evaporation procedure was followed in successive runs. The substrate temperature is given in the first column of Table I. In these experiments the substrate temperature was not constant but increased during the course of the evaporation due to the heating effect of the evaporator. The second column gives the cadmium to zinc ratio. The source material had a cadmium to zinc ratio of 9/1. Table I shows the marked decrease in the Cd/Zn ratio with increasing substrate temperature. The maximum at the low temperature end of the range was not investigated further.

Table I.

Substrate temp, °C	Cadmium to zinc ratio
190-250	6.4/1
250-280	8.1/1
280-330	4.2/1
330-370	2.2/1
430	2.1/1

Two-step process for zinc sulfide phosphors activated with Ag, Cu, *and* Mn.—Evaporation of sulfide phosphors and condensation on a glass substrate at or near room temperature results in clear transparent films. The presence or absence of activator has relatively little effect on film formation. The films formed in this way, however, are not luminescent. Electron diffraction shows them to be amorphous. In order to convert these films to phosphors they must be crystallized by heat treatment. This is accomplished by heating them in an atmosphere of H_2S + 10% HCl at about 650°C for ½ hr. This treatment converts them from the nonluminescent amorphous state to the luminescent crystalline state. Electron diffraction shows that after this heat treatment the films are hexagonal and microcrystalline with the crystal size of the order of 1000Å. After this treatment, the films have a matte surface. They become quite transparent if polished.

The HCl vapor is necessary in order to introduce Cl coactivator into the lattice simultaneously with the recrystallization as it is probable that Cl coactivator is lost during the evaporation process. A higher concentration of HCl than 25% results in excessive attack on the film while less than 2% is not effective. The H_2S flow is regulated at about 2 ft³/hr. The optimum time of heating is about ½ hr. Shorter times result in significantly less efficient films while heating up to several hours does not result in any further improvement. No activation is obtained below 550° or above 750°C. The lower limit is probably determined by the rate of diffusion of activator and coactivator. The upper limit is probably determined by the retention of chlorine by the phosphor which Goldberg and Kremheller (7) found to be a maximum at 650°C.

Attempts to introduce Cl by evaporation of AgCl or $ZnCl_2$ simultaneously with the ZnS were not successful.

Attempts were made to use Al as a coactivator for ZnS:Ag by evaporating Al onto the surface of the film and then heat treating *in vacuo* or dry nitrogen. Amounts of Al less than 1% of the weight of the film were ineffective. Larger amounts resulted in moder-

ate bluish-green luminescence. The films remained clear, transparent, and colorless although similar films without the Al subjected to the same heat treatment developed a matte etched surface.

Indium and gallium coactivators only resulted in weak orange luminescence when added to ZnS:Ag.

The method of introduction of the activator is relatively unimportant. It may be introduced simultaneously with the deposition of the ZnS by evaporating a standard powder phosphor. It may be mixed with the ZnS, or it may be evaporated from a separate boat in the form of a salt or the pure metal either simultaneously with, prior to or after the ZnS evaporation. The over-all activator phosphor ratio must be correct however; hence the evaporation conditions must be determined empirically.

The temperature of the substrate on which the phosphor is deposited is crucial. Films deposited *in vacuo* on a substrate at a temperature above about 100°C are crystalline but they are nonluminescent (with the exception of ZnS:Mn) and do not become luminescent when heat treated (at 650°C) in H_2S + 10% HCl. A possible explanation is that in the crystallized material diffusion of chlorine at this temperature takes place mainly along the grain boundaries, and not through the body of the crystals. Heat treatment (below 650°C) is only effective in activating sulfide films provided they are initially in the amorphous condition corresponding to deposition at substrate temperatures below 100°C.

This two-step procedure has proved to be effective for making photo and cathodoluminescent Zn and Cd sulfide films with Ag, Cu, and Mn activators having brightnesses 1/5 to 1/10 of the corresponding phosphors.

One-step process for Mn *activated* ZnS.—Manganese activated ZnS differs from the Cu and Ag activated Zn sulfides in that it can be formed by a one-step process. This consists of evaporating the phosphor material and depositing it on a substrate in the range from 250° to 400°C. This results, without any further treatment, in a cathodo and weakly photoluminescent film. The reason for this difference in behavior between the Mn and the Ag and Cu activated phosphors is that the luminescence is the result of electron transitions between levels in the Mn center while in the other phosphors the transition is from the conduction band to the center. The latter process requires a higher degree of perfection of the host lattice than is obtained by crystallization at 250°C. At higher substrate temperatures the chlorine coactivator is lost as pointed out in the previous section.

One-step process for ZnS *phosphors—"Hot Wall Bell Jar."*—The ideal condition for forming phosphor films is to deposit them on a substrate at a temperature high enough so that the incident molecules will have sufficient mobility to form an ordered structure. With sulfide phosphors evaporated in an ordinary bell jar the substrate temperature is limited to not much above 300°C. This is because of the re-evaporation or reflection from the heated substrate. At 400°C this is so great that only very thin films are formed while at 600°C no deposition takes place at all. This is in spite of the fact that at 600°C the rate of evaporation of ZnS is only of the order of 10^{-11} g/cm²/sec. In order to form films on surfaces at elevated temperatures it is necessary to carry out the evaporation in a vessel whose walls are uniformly at the substrate temperature. In any ordinary bell jar system the walls and the base are usually at a substantially lower temperature than the substrate and so act as a sink for ZnS.

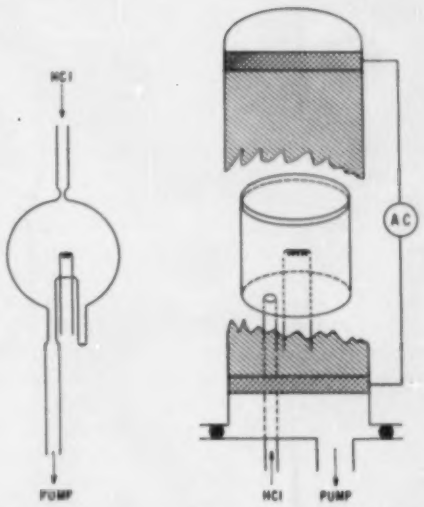

Fig. 1a. Bulb for evaporation on heated wall; Fig. 1b. Hot wall bell jar.

This difficulty can be avoided by depositing the film on the wall of a uniformly heated spherical bulb with an evaporator at the center. This arrangement is shown in Fig. 1. The evaporator consists of a helical tungsten filament in which is placed a pellet of the phosphor. The bulb is pumped continuously and is in an oven to maintain a uniform wall temperature. A small flow of HCl is maintained through the bulb to make up for the loss of coactivator during the evaporation of the phosphor. The loss of host lattice material or activator through the connection to the pump is negligible, but the chlorine is more volatile and it is necessary to introduce some to make up for the losses. The HCl flow required is about 10,000 μl/g of phosphor evaporated.

To the extent that the bulb walls are at uniform temperature there is no tendency for the different phosphor components other than the coactivator to separate out, and the composition of the deposit will be the same as the material evaporated. The relatively high temperature of the walls during deposition insures diffusion of the activator uniformly throughout the film.

By this procedure Cu, Ag, and Mn activated ZnS phosphor films were made by evaporation of commercial powder phosphors. A number of sulfoselenide phosphor films have also been prepared in the same way. The films show both cathodo and photoluminescence when deposited at 650°C. As the deposition temperature is lowered, both of these decrease in efficiency but the effect on the photoluminescence is more marked. At 500°C the latter is negligible while the cathodoluminescence is still fairly efficient. Below this temperature the cathodoluminescence also falls off rapidly.

The phosphors prepared in this way show approximately the same emission and excitation spectra as the corresponding powder phosphors. Their brightness is 1/5 to 1/10 of that of the powders under the same excitation. The decay rate of the luminescence is usually higher for the films than for the corresponding powders.

While this procedure is very effective in forming films, the samples on curved bulb walls are unsuitable for many applications. Accordingly a system was devised for depositing the films on flat 2 in. diameter Pyrex disks. This system is shown schematically in Fig. 1b. It consists essentially of a small quartz chamber closed at the top and bottom by glass disks which seat against ground shoulders. The upper disk is the sample to be coated, the lower one is perforated for evaporator filament leads and HCl inlet tube. This chamber is essentially a demountable bulb. It is placed in a small quartz bell jar. The bell jar is coated on the outside with a conducting tin oxide coating having a resistance of about 30Ω between the silver paste ring electrodes. By passing a current through this coating the walls may be heated rapidly and uniformly to as much as 700°C. The bell jar is sealed by an "O" ring. The base plate is water cooled and an additional metal ring on top of the bell jar flange is also water cooled to protect the "O" ring.

Various cathodo, photo, and electroluminescent sulfoselenide phosphors have been made with this apparatus.

Reaction process for forming oxygen containing phosphors.—A number of oxygen containing phosphors may be formed by reaction of a vaporized substance with a heated substrate in a single step. One of these is Zn_2SiO_4:Mn. This is formed by reaction of ZnF_2:Mn with a heated substrate consisting of a high silica content glass such as fused quartz, Vycor, Pyrex, or Corning No. 1710. The glass substrate is maintained at a temperature in the 550°-650° range while ZnF_2:Mn is evaporated from a platinum evaporator filament. The ZnF_2 reacts with the SiO_2 of the glass according to the reaction

$$2ZnF_2 + 2SiO_2 \rightarrow Zn_2SiO_4 + SiF_4$$

The SiF_4 is volatile and is pumped out of the system leaving a layer of Zn_2SiO_4 well bonded to the glass. As the evaporation continues, the willemite becomes covered with a layer of ZnF_2. Thus the deposit consists of two layers; the Zn_2SiO_4 next to the glass and on top of this layer of ZnF_2. The ZnF_2 can be readily dissolved in NH_4OH leaving the insoluble film of willemite. The two-layer system of a yellow phosphor on top of green phosphor may also be used as a penetron (8, 9). This reaction method of forming willemite permits the formation on Pyrex or other high silica glasses at temperatures several hundred degrees below those required when the phosphor is formed by the two-step process.

Rottgardt (10) has described a related method of forming silicate phosphors by evaporating a fluoride onto a silicate base and subsequently carrying out the reaction by heat treatment in air.

An analogous process may be used to form a zinc borate phosphor. In this case a borate glass is used as the substrate and ZnF_2 again is evaporated. Since good borate glasses with sufficiently high melting points are not available this process is carried out with a borate glass glaze on the surface of No. 7052 FN glass. The resultant phosphor is a red cathodoluminescent zinc borate with an overlying layer of ZnF_2:Mn. The latter may be dissolved off in NH_4OH without damage to the zinc borate.

An analogous process can also be used with phosphate glasses. These, however, are low melting and unsatisfactory for many purposes. An alternative process is possible here. This is to first evaporate a layer of ZnF_2:Mn onto a Pyrex substrate at, say, 300°C, which is low enough to avoid reaction with the glass but high enough to insure good adhesion. The temperature is then raised to 550°C and a pellet of P_2O_5 is evaporated. This reacts with the ZnF_2 to form $Zn_3(PO_4)_2$:Mn.

Summary

A considerable number of zinc cadmium sulfoselenide phosphor films can be made by vacuum evaporation of commercial powder phosphors. Luminescent films of zinc sulfide activated with Cu, Ag, or Mn may be formed by deposition at room temperature followed by heat treatment in a suitable atmosphere. The same phosphors may be formed in a single step by evaporation onto a heated substrate in the "Hot Wall Bell Jar."

Manganese activated ZnS may also be formed in a single step by deposition on a substrate between 250° and 400°C.

Zinc silicate, phosphate, and borate may be formed in a single step by reaction of zinc fluoride with a heated substrate.

Manuscript received June 15, 1960; revised manuscript received July 20, 1960. This paper was prepared for delivery before the Chicago Meeting, May 1-5, 1960.

Any discussion of this paper will appear in a Discussion Section to be published in the June 1961 JOURNAL.

REFERENCES

1. J. H. deBoer and C. J. Dipple, U. S. Pat. 1,954,691, April 10, 1934.
2. F. E. Williams, *J. Opt. Soc. Am.*, **37**, 302 (1947).
3. L. R. Koller, Electrochem. Soc., Spring Meeting (1957).
4. C. Feldman and M. O'Hara, *J. Opt. Soc. Am.*, **47**, 300 (1957); C. Feldman and M. O'Hara, *ibid.*, **48**, 816 (1958); C. Feldman, *J. Soc. Motion Picture & Tel. Eng.*, **67**, 455 (1958).
5. T. Rychlewski, U.S. Pat. 2,898,225, Aug. 4, 1959; T. Rychlewski, U.S. Pat. 2,903,378, Sept. 8, 1959.
6. F. J. Studer and D. A. Cusano, *J. Opt. Soc. Am.*, **45**, 493 (1955).
7. P. Goldberg, D. J. Bracco, and A. Kremheller, *This Journal*, **102**, 79C (1955).
8. L. R. Koller and H. D. Coghill, *J. Appl. Phys.*, **29**, 1064 (1958).
9. C. Feldman, *J. Opt. Soc. Am.*, **47**, 790 (1957).
10. J. Rottgardt, U.S. Pat. 2,876,129, March 3, 1959.

Thermoelectric and Crystallographic Properties of Ag_2Se

J. B. Conn and R. C. Taylor

Research Laboratories, Merck Sharp and Dohme, Rahway, New Jersey

ABSTRACT

Silver selenide has been prepared by fusion techniques and found to be a good thermoelectric material. The Seebeck coefficient, resistivity, and thermal conductivity have been measured as a function of temperature. The effect of doping with 30 different elements and compounds at different doping concentrations has been studied. The inter-relationships between the thermoelectric properties have been examined and are discussed. The crystal lattice of silver selenide has been determined, and the subcell and superstructure are elucidated.

During the past few years, this laboratory has been engaged in a study of thermoelectric materials. In the course of these investigations, the excellent properties of silver selenide were discovered. A thorough examination of the material was made, including crystallographic studies, temperature dependence of its thermoelectric properties, and effect of alloying and doping on these properties.

The semiconducting properties of silver selenide have been put to use in thermopiles by Schwarz (1). His n-type material was a silver sulfide-silver selenide alloy with a figure of merit of 0.9×10^{-6} deg^{-1}. The corresponding p-type material was an alloy of silver, copper, tellurium, and selenium with a figure of merit of 1.0×10^{-6} deg^{-1}. Resistivity and Hall effect of silver selenide have been studied by Mooser and Pearson (2) and by Busch and Junod (3). The energy gap and room-temperature electron mobility were also determined by Busch and Junod to be 0.075 ev and 2000 cm^2/v-sec, respectively. They found the material to show metallic behavior above the transition temperature of 133°C. They observed no measurable ionic conductivity. Miyatani (4) measured the properties of silver selenide via the emf of the galvanic cell Ag/AgI/Ag_2Se/Pt and at 130°C determined the electron mobility to be 810 cm^2/v sec and the effective electron mass to be 0.11 m. Junod (5) recently published an extensive investigation of the crystallographic and semiconducting properties of silver selenide, silver sulfide, and copper selenide, including conductivity, Hall effect, Seebeck coefficient, and other properties.

Materials

Starting materials were sufficiently pure so that further purification was not considered necessary. Selenium was obtained in 99.999+% purity from American Smelting and Refining Company. Silver of 99.99+% purity from American Smelting and Refining and of 99.9999% purity from Consolidated Mining and Smelting Company of Canada, Ltd. was used. Doping materials were of a similar high purity.

Preparation.—All samples were prepared in 12 mm 1D quartz tubes which had been carbon-coated prior to introduction of the materials. Carbon-coating was accomplished by pyrolysis of acetone vapor (using nitrogen as a carrier gas) on the inside surface of the quartz tube at about 900°C. Carbon-coating had the reducing properties which are found so advantageous in graphite crucibles and so prevented reaction of oxides with the quartz. At the same time the undesirable absorption of selenium vapor into graphite was eliminated by substitution of the thin carbon coating. The materials were then introduced into the quartz tube in the desired composition, the tube evacuated to about 10^{-4} mm and sealed. The tube was kept at 1050°-1100°C for 16 hr followed by a 3-hr cooling period in the furnace, or a 24-hr drop time through a temperature gradient. No difference in properties was found between ingots prepared by the two different methods, nor were we able to produce more than slightly oriented ingots because of the phase change at 133°C. Ingots weighed about 40 g. After removal from the quartz tubes, the ingots were machined for measurement. Samples were found to be homogeneous, with clean, but slightly pitted surfaces. Except in the few cases where the quartz tubes cracked in cooling (and this was invariably found to be due to insufficient carbon coating) the ingots were free of surface oxidation. In most cases the ingots were malleable and easily machined. A few of the samples which had been doped with excess sulfur, selenium, tellurium, or silver iodide were found to be brittle; apparently the high vapor pressure of these doping agents produces internal cracks in the ingot. Many of the ingots were annealed at 125°C for 48 hr with no apparent effect.

Measurements

The samples were cut to approximately ¾ in. long and faced off on a lathe. Two rings were machined into the surface of the sample and into these rings platinum wires were tightly wound to act as the probe for a-c resistivity measurements. The sample was then placed between two resistance wire wound graphite heaters, and pressure for thermal and electrical contact was applied to the unit by a vise type jig. A temperature gradient of 5°-15° was maintained across the length of the sample by

power supplied from a d-c source to the resistance heaters. At thermal equilibrium ΔT was determined from two thermocouples placed through the center of each heater and in contact with the sample. The thermal emf was measured from the copper leads of each thermocouple. Measurements were made with a L&N type K-3 potentiometer. The measurement temperature was taken as the average between hot and cold ends of the sample.

Resistivity as a function of temperature was determined by means of current contacts made to the sample through the graphite heaters; the potential drop was measured across the platinum probes.

Thermal conductivity data were obtained by placing the sample between a copper sink in contact with an ice-water reservoir and a resistance heater; ΔT was measured with thermocouples placed in the sink and heater about 1 mm from the sample contact. The heat lost by conduction through the sample to the cold sink was balanced by the input to the heater, the temperature of which was kept within 1°C of ambient. K is calculated from the resistance and the current required to keep the heater at ambient.

Crystallographic Investigations

An extensive study of the structure of low-silver selenide was published by Boettcher, *et al.* (6). The unit cell was described as tetragonal, a = 7.06Å, c = 4.98Å, the axial ratio changing with temperature. The lattice was deduced as essentially selenium packing, with silver atoms occupying random sites in the interstices.

Numerous samples of cast silver selenide have been subjected to x-ray diffraction study during the course of this work, and the patterns were sensibly the same, save for crystal ordering. However, far too many reflections were present to be accounted for on the basis of Boettcher's tetragonal axes. On the other hand, an assignment was arrived at on the basis of a 4-molecule orthorhombic unit cell, a = 4.344Å, b = 7.111Å, c = 7.790Å; this reproduced nearly all of the observed reflections exactly, the exceptions being occasional split lines, one member of which could not be incorporated unless all axes were doubled. This suggested the existence of a superstructure, but its nature remained in doubt until completion of the experiment described below.

It was decided to attempt direct preparation of crystalline low-silver selenide by wet process at room temperature, involving reaction of a water-soluble silver salt with a soluble selenide. Since the silver chalcogenides are soluble in alkali cyanide solutions, it was anticipated that interaction of potassium silver cyanide with potassium selenide would provide a crystallization medium for silver selenide. Accordingly, a concentrated solution of silver(I) oxide in potassium cyanide, having composition $K_2Ag(CN)_3$, was added gradually to a freshly prepared strongly alkaline solution of the stoichiometric amount of potassium selenide under stirring and nitrogen atmosphere. The precipitate produced at first was black and finely divided, but when about half of the silver cyanide reagent had been added, a rapid transformation set in, with conversion to a gray, coarse, and very bulky solid. After completion of the metathesis, the product was collected, washed, and dried *in vacuo*.

Under the microscope the particles were seen to consist of globular rosettes of lustrous minute prisms; the x-ray diffraction pattern was essentially that of all other low-silver selenide samples but was exceptionally bright, and showed a wealth of detail not previously observed. The analytical data were surprising and at first sight very disappointing: the Ag/Se ratio was 2.28, a large divergence from the stoichiometric. It was noticed however, that this ratio is 16/7 within the accuracy of the microanalytical determination.

For $Ag_{16}Se_7$, F. W. 2278.8,	Calc.	Found
	Ag 75.75	76.1
	Se 24.25	24.4
	100.00	100.5

The x-ray diffraction data were then worked up (Norelco Wide-Range Diffractometer, CuKα radiation). The spacings fit an orthorhombic unit cell, a = 8.630Å, b = 14.13Å, c = 15.50Å, and containing $4Ag_{16}Se_7$. The calculated density is 8.00; observed pyknometrically, 7.96. The subcell contains $4Ag_2Se$; the superstructure is derived from it by a systematic vacancy at every eighth selenium lattice site. The formation of this defect phase is all the more striking when it is recalled, as stated above, that it began to crystallize in the presence of a large excess of selenide ion.

Inspection of the phase diagram for the system Ag-Se, as published by Hansen (7), shows that a homogeneous phase of composition $Ag_{16}Se_7$ cannot be attained from a melt, since a liquid miscibility-gap intervenes. Indeed, when the powder was melted in sealed quartz under vacuum, the resulting ingot was coated with silver. Evidently, when high-silver selenide, which is stoichiometric, is cooled through the transition, it can only approximate the structure of the true low-temperature phase.

The question concerning the tetragonal phase described by Boettcher becomes even more puzzling in view of the recent publication of Junod (5) who states that his x-ray diffraction data were in complete agreement with Boettcher. The present authors have had opportunity to discuss this matter with members of the research staffs of other organizations, who also have studied low-silver selenide; they found as we did, that the system is not tetragonal. In fact, one group arrived independently at an orthorhombic axial assignment in close agreement with our own data for the subcell. It can only be surmised that if the tetragonal phase does exist, it must be a metastable transitional form.

Thermoelectric Properties

Stoichiometric silver selenide.—Silver selenide is a semiconducting material with orthorhombic symmetry at room temperature. At 133°C it undergoes a transition to a cubic lattice. The melting point is 897°C. According to the phase diagram (7), the range of miscibility in the liquid state of excess silver or selenium in silver selenide extends from 32 to 44.5 at. % selenium. Beyond these limits a layered ingot results on cooling from the melt.

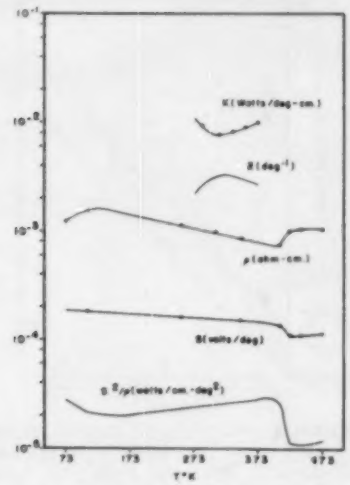

Fig. 1. Variation of thermoelectric properties of stoichiometric silver selenide with temperature.

The variation of the thermoelectric properties of silver selenide with temperature is shown in Fig. 1. The Seebeck coefficient shows a linear decrease from −167° to 120°C, then falls sharply at the transition temperature of 133°C, followed by a slow rise to 220°C. The data of Junod (5) show an increase in Seebeck coefficient to about 0°C followed by a decrease to the transition point, then a sharp break at the transition point. While our studies indicate a decrease in Seebeck coefficient of only about 40 μv/°C through the transition point, those of Junod show a decrease of about 80 μv/°C.

Silver selenide exhibits typical nondegenerate semiconductor behavior in its resistivity, which decreases with increasing temperature from −180°C to the transition point. Here a sudden increase in resistivity occurs followed by a slow rise. Thus the cubic high-temperature form exhibits the behavior of a metal or degenerate semiconductor, as reported by Junod. His data, while being in substantial agreement with ours, show a decrease in resistivity through the transition point, this being followed by a slow increase.

Table I. Room temperature properties of Ag_2Se

R(cm³/coulomb)	μ(cm²/v-sec)	n(cm⁻³)
2.2	2050	2.8×10^{18}
S(μv/°C)	ρ(ohm-cm)	k(watts/deg-cm)
−150	10.2×10^{-4}	0.009

The thermal conductivity curve shows a minimum at room temperature. An increase occurs as the temperature increases due to the presence of transport processes other than those associated solely with electrons or phonons, such as ambipolar diffusion. The increase as temperature decreases is a result of reduced phonon-phonon interactions. A maximum figure of merit, in excess of 3.0×10^{-3} deg^{-1} occurs at about 40°C.

A summary of the room temperature properties of stoichiometric silver selenide are shown in Table I. These values are found to be in close agreement with those of Junod.

Effect of doping.—The thermoelectric properties are listed in Table II. With the exception of Cu, AgI, and the group IIB elements, doping agents had very little effect on Ag_2Se. In many cases, the thermoelectric properties are identical for a particular element at the doping levels of both 0.1 and 0.5 mole %, indicating that Ag_2Se is saturated with respect to that element at <0.1 mole %. This low solubility of most foreign materials in Ag_2Se is a prime factor in its insensitivity to doping. It is obviously impossible to p-dope silver selenide, a phenomenon which has been observed in other cases such as ZnSb (8).

The reproducibility of Seebeck coefficient for duplicate ingots, with very few exceptions, has been excellent. Reproducibility of resistivities was not

Table II. Properties of doped Ag_2Se

	S, μv/°C	ρ, × 10⁴ ohm-cm	K, watts/deg-cm	Z, × 10³ deg⁻¹		S, μv/°C	ρ, × 10⁴ ohm-cm	K, watts/deg-cm	Z, × 10³ deg⁻¹
Stoich	−150	10.2	0.0092	2.4	0.1 Ga	−118	4.9	0.0119	2.4
0.5 Cu	−52	2.2	0.0254	0.5	0.5 Ga	−113	4.7	0.0125	2.2
0.5 Ag	−122	6.2	0.0113	2.1	0.1 In	−114	5.4	0.0121	2.0
0.1 Au	−151	10.5	0.0094	2.3	0.5 In	−118	5.1	0.0129	2.1
0.5 Au	−139	8.5	0.0101	2.2	0.1 Tl	−151	13.0	—	—
0.1 S	−153	13.5	0.0090	1.9	0.1 Zn	−123	6.6	0.0099	2.3
0.5 S	−142	8.9	0.0100	2.3	0.5 Zn	−124	6.3	0.0124	2.0
0.5 Se	−151	9.8	0.0089	2.6	0.1 Cd	−98	4.6	0.0152	1.4
0.5 Te	−152	12.0	0.0093	2.1	0.5 Cd	−73	3.2	0.0167	1.0
0.1 Ge	−118	6.6	0.0115	1.8	0.1 Hg	−66	2.7	0.0226	0.7
0.5 Ge	−125	6.5	0.0108	2.2	0.5 Hg	−35	2.5	—	—
0.1 Sn	−150	12.0	0.0091	2.1	0.1 Fe	−110	4.8	0.0122	2.1
0.5 Sn	−120	5.3	0.0115	2.4	0.1 Co	−119	5.8	0.0108	2.3
0.1 Pb	−120	5.9	0.0109	2.2	0.1 Pd	−151	9.7	0.0094	2.5
0.5 Pb	−121	5.8	0.0125	2.0	0.1 V	−117	5.5	0.0119	2.1
0.1 P	−136	7.6	0.0104	2.3	0.1 Cr	−149	9.4	0.0091	2.6
0.1 As	−152	10.6	0.0104	2.1	0.1 Mn	−104	4.6	—	—
0.5 As	−124	5.6	0.0114	2.4	0.1 Re	−145	10.6	0.0094	2.1
0.5 Sb	−114	5.5	0.0121	2.0	0.5 Li	−127	6.0	0.0104	2.6
0.1 Bi	−119	6.2	0.0105	2.2	0.1 AgI	−60	3.1	—	—
0.5 Bi	−122	5.9	0.0117	2.2	0.5 AgI	−23	1.8	0.0552	0.05
0.1 Al	−147	9.0	—	—	0.01 $MoSe_2$	−149	10.1	0.0097	2.3
					0.03 $MoSe_2$	−149	9.4	0.0098	2.4

quite as good, especially in the case of stoichiometric Ag_2Se, where Seebeck coefficient for six samples is within the limit of -146 to -153 $\mu v/°C$ while ρ covers a range of 7.7 to 13.3 ohm-cm.

The effects of the various doping agents can be considered from the viewpoint of the periodic groups of elements. Only the effect on one parameter need be discussed, since the value of one determines the values of the others, as will be seen in the following sections.

Elements of groups IB and IIB are the only ones to show a large effect on the thermoelectric properties. In group IB, the order of effect is Cu > Ag > Au. In group IIB, the order is reversed, being Hg > Cd > Zn. The order in the group IIB elements parallels the energy gaps of the selenides of these elements, as shown in Table III.

In both cases metallic behavior is approached as one goes from Zn to Cd to Hg. The energy gap of Ag_2Se is 0.075 ev (3). The compound Au_2Se does not form. The energy gap of Cu_2Se is not known but is most likely lower than that of Ag_2Se, since the Seebeck coefficient and resistivity of Cu_2Se are lower than those of Ag_2Se. Thus in the group IB elements, metallic behavior would be approached in the order Au-Ag-Cu, as shown in Table IV. The implication of the reverse trends in the two groups in their doping action on Ag_2Se is that the elements form their normal bond patterns rather than entering in simple isomorphous replacement.

Group VIA has no effect whatsoever, the Seebeck coefficient remaining in the range of -150 $\mu v/°C$ at both doping levels for S, Se, and Te. If, as mentioned previously, elements form their normal selenide bonds, this would explain the lack of effect of the VIA elements. Groups IIIA (Al, Ga, In, Tl), IVA (Ge,Sn,Pb), and VA (P,As,Sb,Bi) all behave similarly, lowering the Seebeck coefficient to the range of -120 $\mu v/°C$ at 0.5 mole %. Apparently all but Sn and As saturate Ag_2Se at less than 0.1 mole %, accounting for the leveling of Seebeck coefficient at -120. The transition elements displayed widely divergent effects on the properties, no trends being obvious.

As shown in Fig. 3 and 4, the samples mainly fall into two groups, one with a Seebeck range of 115-125 $\mu v/°C$ and the second with a range of 145-155 $\mu v/°C$. The average figure of merit of 18 materials in the 145-155 range is 2.4×10^{-3} deg^{-1}, with six of the samples exceeding 2.5×10^{-3} deg^{-1}. The average Z in the 115-125 range, for 19 alloys is 2.2×10^{-3} deg^{-1}, with only one exceeding 2.5×10^{-3} deg^{-1}.

Table III

Element	S of Ag_2Se at 0.5 mole % doping level	Energy gap of selenide, ev
Hg	−35	HgSe = 0.16
Cd	−80	CdSe = 1.74
Zn	−126	ZnSe = 2.58

Table IV

Element	S of Ag_2Se at 0.5 mole % doping level	Energy gap of selenide, ev
Cu	−51	$Cu_2Se < 0.075$
Ag	−122	$Ag_2Se = 0.075$
Au	−139	Au_2Se —

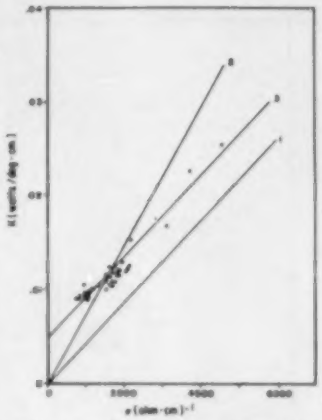

Fig. 2. Electrical conductivity vs. thermal conductivity for stoichiometric and doped samples of silver selenide at room temperature. Curve 1, Wiedeman Franz law, nondegenerate semiconductor, $Kel\rho = 4.35 \times 10^{-8}$ v^2/deg. Curve 2, Wiedeman Franz law, metals, $Kel\rho = 7.35 \times 10^{-8}$ v^2/deg. Curve 3, silver selenide.

Relationship between K and σ.—The relationship between thermal and electrical conductivity at room temperature is shown in Fig. 2. Line 1 represents the Weidemann-Franz ratio for nondegenerate semiconductors ($<2.5 \times 10^{19}$ carriers cm^{-3}), where $Kel/\sigma = 4.35 \times 10^{-8}$ V^2/deg. Line 2 is the Wiedemann-Franz ratio for metals (or degenerate semiconductors) where $Kel/\sigma = 7.35 \times 10^{-8}$ V^2/deg. Line 3 is that for the experimentally determined values for Ag_2Se, stoichiometric and doped, where K is the sum Kel + Kph. It is seen that a straight line relationship exists between K and σ for silver selenide which parallels the Wiedemann-Franz law for nondegenerate semiconductors. Since Ag_2Se is then a nondegenerate semiconductor, the ratio $Kel/\sigma = 4.35 \times 10^{-8}$ V^2/deg must hold. Extrapolation of the data to $\sigma = 0$ yields a Kph value of 0.0046 watts/deg-cm. By reducing the thermal conductivity values of the silver selenide samples 0.0046 watt/deg cm, it is found that the line for Ag_2Se and that for nondegenerate semiconductors coincide. The average product $Kel\rho$ for all samples is 4.37×10^{-8} V^2/deg, as necessitated by the Wiedemann-Franz law. Any deviation from line 3 for any silver selenide samples can be attributed theoretically to some degree of structure doping, which would then alter the lattice contribution, Kph, from its value of 0.0046 watt/deg-cm. Deviation of the product $Kel\rho$ from 4.35×10^{-8} V^2/deg is then a measure of the crystal disorder, except at very high conductivities where the materials become degenerate.

Relationship between S and σ.—The relationship existing between Seebeck coefficient and electrical conductivity is shown in Fig. 3. A large scattering exists at the high conductivity end of the line. As doping agents inject a higher concentration of carriers, electrical conductivity increases and Seebeck coefficient decreases. The values of $S^2\sigma$ remain within the region of $2\text{-}3 \times 10^{-3}$ watts/cm-deg^2, for materials with Seebeck coefficients between -90

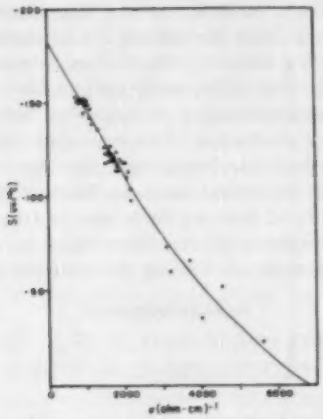

Fig. 3. Electrical conductivity vs. Seebeck coefficient for stoichiometric and doped silver selenide at room temperature.

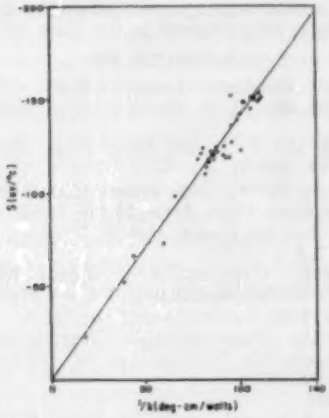

Fig. 4. Thermal resistivity vs. Seebeck coefficient for stoichiometric and doped samples of silver selenide at room temperature.

and −150 μv/°C. The highest values of $S^2\sigma$ are found in the Seebeck coefficient range of −120 μv/°C; however, their Z values are lower than those in the −150 μv/°C range due to higher thermal conductivity.

Relationship between S and K.—The product of Seebeck coefficient and thermal conductivity is remarkably constant at 1.4, resulting in a straight line passing through the origin when Seebeck coefficient is plotted against thermal resistivity, as shown in Fig. 4. The constancy of this product suggests a considerable phonon drag term in the Seebeck coefficient, the product being (Sel + Sph) (Kel + Kph). If no phonon term were present for S, the product would not be expected to be constant any more than it would be for ρ (Kph + Kel), since one term would be entirely electronic, and the other both electronic and phonon. Thus the product Sel σ is probably constant as is Kel ρ. However, the problem of determining Sel presents far more difficulty than does Kel since only a certain proportion of the phonon activity contributing to K will contribute to S. A wavelength requirement for phonons must be met before they will contribute to S. This requirement is that only phonons which have wave lengths not less than the electron wave length will contribute to S.

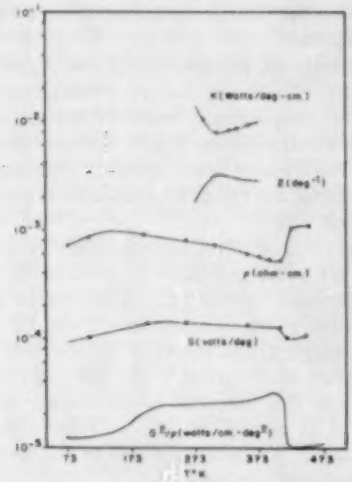

Fig. 5. Variation of thermoelectric properties with temperature of silver selenide doped with 0.1 mole % P.

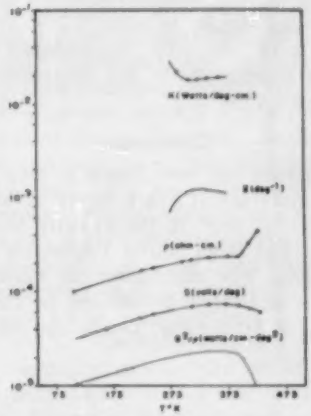

Fig. 6. Variation of thermoelectric properties with temperature of silver selenide doped with 0.1 mole % Hg.

Phonons satisfying this requirement possess a much longer free path length than the bulk of the phonons, and these phonons possess the most marked directional properties along the temperature gradient (9). Therefore the effect of dragging of electrons by such phonons is particularly large. The number of phonons possessing these long wave lengths is probably extremely dependent on crystal perfection. Normally a phonon wave length ranges from one to a few atomic distances, while electronic wave lengths may easily exceed 10 atomic distances.

Effect of temperature on doped Ag_2Se.—The temperature dependence of Seebeck coefficient, resistivity, and thermal conductivity of silver selenide doped with 0.1 mole % phosphorus and 0.1 mole % mercury was investigated. The results are shown in Fig. 5 and 6. The Seebeck coefficient for phosphorus-doped Ag_2Se increases fairly rapidly with temperature to a maximum at about −40°C and then falls slowly to the transition temperature where a sharp drop occurs, followed by a rise to 175°C. In the mercury-doped sample, the Seebeck coefficient increases with temperature to a maximum at 95°C, followed by a decrease at the transition point which is more

gradual than for the stoichiometric or phosphorus-doped samples.

In its resistivity, phosphorus-doped Ag_2Se behaves in a fashion similar to the stoichiometric material except that degenerate conduction exists below −120°C. Mercury-doped Ag_2Se, on the other hand, acts as a degenerate semiconductor throughout the entire temperature range as would be expected from its low resistivity.

The variation of thermal conductivity and figure of merit with temperature is similar to that for Ag_2Se. Thermal conductivity minima in all cases occur at about room temperature. It can be seen that the high-temperature increase in thermal conductivity is much more gradual for the mercury-doped sample. Since this material is degenerate, ambipolar diffusion, if it occurs at all, will have much less effect at higher temperatures due to the larger number of excess carriers present.

Stoichiometric and mercury-doped silver selenide alike display a maximum figure of merit at about 40°C. However, the maximum figure of merit for mercury-doped Ag_2Se is only 1.2×10^{-3} deg^{-1} as against 3.3×10^{-3} deg^{-1} for the undoped compound. Phosphorus doping shifts the maximum to about 30°C and is 3.2×10^{-3} deg^{-1}.

Conclusions

Silver selenide has been found to be a good thermoelectric material. It has a figure of merit of the order of 3×10^{-3} deg^{-1} in the vicinity of room temperature. It has been found impossible to p-dope silver selenide. The stoichiometric material shows the best thermoelectric properties, no improvement being obtained by doping. The compound is nondegenerate from −167°C to the transition point of 133°C, after which its behavior is metallic. Doping was found to occur by formation of normal bond patterns. Kph for silver selenide is 0.0046 watt/°cm, and it is believed that a phonon drag term exists in the Seebeck coefficient. The material becomes degenerate if doped with mercury. The favorable combination of electrical and thermal conductivities characteristic of low-Ag_2Se is ascribed to the existence of a crystal superstructure based on an orthorhombic defect phase having composition $Ag_{10}Se_7$.

Acknowledgments

The authors wish to thank Dr. G. V. Downing and associates for measurements of the thermoelectric parameters.

Manuscript received May 9, 1960. This paper was prepared for delivery before the Houston Meeting, Oct. 9-13, 1960.

Any discussion of this paper will appear in a Discussion Section to be published in the June 1961 JOURNAL.

REFERENCES

1. E. Schwarz, *Research* (London), **5**, 407 (1952).
2. E. Mooser and W. B. Pearson, *Phys. Rev.*, **101**, 492 (1956).
3. G. Busch and P. Junod, *Helv. Phys. Acta.*, **30**, No. 6, 420 (1957).
4. S. Miyatani, *J. Phys. Soc. Japan*, **13**, 317 (1958).
5. P. Junod, *Helv. Phys. Acta.*, **32**, 567 (1959).
6. A. Boettcher, G. Haase, and H. Treupel, *Z. Angew. Phys.*, **7**, 478 (1955).
7. M. Hansen, "Constitution of Binary Alloys," 2nd Ed., pp. 49-51, McGraw-Hill Book Co., Inc., New York (1958).
8. A. F. Ioffe, "Semiconductor Thermoelements and Thermoelectric Cooling," p. 63, Infosearch Ltd., London (1957).
9. *Ibid.* p. 33.

Separation of Sulfur, Selenium, and Tellurium from Arsenic

J. M. Whelan, J. D. Struthers, and J. A. Ditzenberger

Bell Telephone Laboratories, Incorporated, Murray Hill, New Jersey

ABSTRACT

Three methods have been investigated for separating trace amounts of sulfur present in high-purity arsenic. These are: (*a*) vacuum sublimation, (*b*) sublimation in a hydrogen stream, and (*c*) distillation of arsenic from an arsenic-lead solution. The last method is somewhat more effective than the second. The first was unsatisfactory. The lead process yielded arsenic containing the following atom fractions of sulfur, selenium, and tellurium; 1×10^{-6}, $\leq 2.7 \times 10^{-6}$, and $\leq 2 \times 10^{-6}$, respectively. Concentrations of these impurities were measured with the aid of radiotracer techniques.

Arsenic of high purity is required for the preparation of the semiconductors InAs and GaAs. The atom fractions of sulfur and selenium in available "semiconductor grade" arsenic are in the range 0.2 to 5×10^{-4}. These impurities are donors in the above semiconductors which cannot be removed readily by zone refining because of their unfavorable distribution coefficients (1-5). The donor concentrations, $\sim 2 \times 10^{16}$ cm^{-3}, in better samples of InAs and GaAs can be attributed to the residual amounts of sulfur and selenium in the arsenic.

A number of methods have been proposed to reduce further the concentration of sulfur in arsenic. These are: (*a*) vacuum sublimation (6), (*b*) sublimation in H_2 (5, 7), (*c*) condensation into Pb followed by distillation (7), (*d*) repeated oxidation and reduction with carbon (8), and (*e*) H_2 reduction of redistilled $AsCl_3$ (9). These methods have been

evaluated primarily by differences in the carrier concentrations and mobilities of InAs samples made from the initial and purified As. This evaluation is subject to a number of uncertainties such as the purity of the indium and contamination associated with the InAs preparation. However, the Pb condensation-distillation proposed by Harman, Stambaugh, and Goering was somewhat more promising than the others. An atom fraction of sulfur in the arsenic equal to 9×10^{-7} would account for the net donor concentration in their InAs. Compensation or other donor impurities would either raise or lower this estimate.

We re-examined the vacuum sublimation, H_2 sublimation, and Pb condensation-distillation methods for their relative efficiencies for reducing the sulfur content in arsenic. As will be described, we found the Pb condensation-distillation to be more effective than the others. Quantitative results are given later to indicate the residual concentrations of sulfur, selenium, and tellurium in arsenic purified by this method. Concentrations of the above impurities were measured by radiotracer techniques. By the use of radioactive tracers it is possible to determine concentrations of sulfur, selenium, and tellurium which are lower by several orders of magnitude than can be determined by chemical, spectrographic, or spectrophotometric methods. Sulfur[35] was obtained as BaS in $Ba(OH)_2$ solution and converted to As_2S_3 for arsenic doping. Radioactive Se and Te were used directly after irradiation at the Brookhaven reactor in a flux of 8×12^{12} neutrons/cm^2/sec for 31 days. Beta counting was used for the powdered arsenic samples containing sulfur and tellurium. Gamma counting was used for those samples containing selenium.

The three methods used for separating trace amounts of sulfur from arsenic are based on the relative vapor pressures of arsenic and the sulfur species. At low concentrations, ~ 1 ppm, sulfur is probably present in arsenic as a solute, As_2S_3. The relative difference in vapor pressure of this sulfide and arsenic (1.0 and 0.4 atm, respectively, at 565°C) is probably too small for the degree of separation desired under ideal conditions by a single sublimation. Sublimation in hydrogen favors the reduction of the sulfide in the vapor phase to $H_2S(g)$ and $As_4(g)$. Arsenic is condensed in the exhaust hydrogen stream. It is desirable to use a high ratio of H_2 to As_4 partial pressures to shift the equilibrium to the right for the reaction: $As_2S_3(g) + 2H_2(g) = \frac{1}{2} As_4(g) + 2H_2S(g)$. The third method consists of dissolving arsenic in lead followed by distillation from the resulting solution. Many metals form stable sulfides with low vapor pressures. Lead was a particularly good choice because it does not form arsenides. This facilitates the arsenic recovery by distillation.

Experimental

The first series of experiments were intended to determine the relative effectiveness of the three processes for separating small amounts of sulfur from arsenic. Arsenic, containing an estimated sulfur concentration of 1–10 ppm, was mixed with an amount of radioactive sulfur equivalent to 2 ppm of the arsenic. This mixture was sublimed twice to mix the tracer sulfur with that originally present. The arsenic was condensed as a rod during the second sublimation. The end and center sections were analyzed to determine their relative sulfur concentrations. Absolute concentrations were not obtained because of the uncertainty of the sulfur concentration originally present in the arsenic. Intermediate sections of the arsenic rod were used for the separation experiments described below. The initial sulfur concentrations of these sections were taken as averages of the appropriate end and center sections. One section of the above rod was sublimed in a sealed quartz tube 50 cm long which had been previously evacuated. This tube was heated uniformly to 600°C and then one end cooled to 350°C. The resulting temperature gradient was maintained for 58 hr. Arsenic condensed in the cold end to form a rod 22 cm long. The rod was then divided into five approximately equal sections. The first and last section corresponded to the coldest and hottest sections of the rod, respectively. Sulfur concentrations of the five sections are listed in the first column of Table I. The initial sulfur atom fraction is 1.6 α where α is a constant having a value between the limits 10^{-6} to 10^{-4}. As previously mentioned, the uncertainty in the value of α arises from the uncertainty in the sulfur concentration of the arsenic before doping with tracer sulfur. After sublimation, the first and last sections to condense had atom fractions of sulfur equal to 2.7 α and 1.0 α, respectively. The small difference between these concentrations illustrates the limitations of simple vacuum sublimation for separating trace amounts of sulfur from arsenic.

A second arsenic sample in which the sulfur atom fraction was 1.4 α was sublimed in a hydrogen stream at 450°C. The hydrogen at 1 atm was first passed through a charcoal trap at 78°K and then over the arsenic at 450°C at a rate of approximately 400 cc/min. From the time required to sublime the arsenic, we estimated the ratio of H_2 to As_4 pressures to be between 100 and 200 to 1. The atom fraction of sulfur in the arsenic collected in the exhaust stream was 0.004 α, a substantial reduction from 1.4 α in the starting material.

The sulfur atom fraction in the arsenic used for the Pb-condensation-distillation experiment was 2.0 α. This arsenic was condensed into lead at 550°C contained in a sealed tube. The weight ratio of arsenic to lead was 1:2. It was then distilled from the solution at 535° and condensed into a cooler region

Table I. Relative effectiveness of vacuum sublimation, H_2 sublimation, and Pb condensation-distillation for separating trace amounts of sulfur from arsenic

	Vacuum sublimation	Sublimation in H_2	Pb condensation and distillation
Initial atom fraction of S in As	1.6 α	1.4 α	2.0 α
Final atom fraction of S in As	1st fraction 2.7 α 2nd fraction 1.6 α 3rd fraction 1.4 α 4th fraction 1.5 α 5th fraction 1.0 α	0.044 α	<0.001 α

$10^{-6} > \alpha > 10^{-4}$

of the tube. The atom fraction of the sulfur in the recovered arsenic was equal to or less than the detection limit, 0.001 α. These results are summarized in Table I.

The lead condensation-distillation was somewhat more effective than sublimation in hydrogen for removing small amounts of sulfur from arsenic. The latter method would not be expected to be as good for separating small amounts of selenium and tellurium from arsenic because of the lower stability of H_2Se and H_2Te. Lead selenide and telluride are stable. They were expected to have low vapor pressures when diluted with a large excess of lead at temperatures in the range of 600°-700°C. The experiments described below illustrate the effectiveness of the lead method for separating trace amounts of sulfur, selenium, and tellurium from arsenic. The example for sulfur differs from the previous one in that isotopic dilution effects were greatly reduced.

The arsenic used in these experiments was supplied by American Smelting and Refining Co. Estimated atom fractions of sulfur, selenium, and tellurium in the arsenic are $\sim 2 \times 10^{-6}$, $\sim 10^{-7}$, and $< 10^{-7}$, respectively. Those for sulfur and selenium were furnished by the supplier and that for tellurium was based on the failure to detect it by mass spectrographic means (10). Dilution errors associated with tracer techniques were minimized by first doping the arsenic with the large amount of the appropriate tracer impurity in comparison to that originally present. An amount of radioactive sulfur as As_2S_3 equivalent to 500 times the sulfur originally present was sealed in an evacuated quartz tube with the first arsenic sample. This was sublimed and condensed six times from one end of the tube to the other at approximately 600°C to insure adequate mixing. The sample was then crushed and resublimed to form a rod. After discarding the ends of this rod, the remainder was divided into five sections. The end and center sections were analyzed for their sulfur content. Averages of these were used to estimate the concentration of the two remaining pieces prior to purification by distillation from lead. The minimum and maximum atom fractions of sulfur were 1.1 and 3.9×10^{-6}. These figures combined with those in Table I show that sublimation is a satisfactory method for reducing the atom fraction of sulfur in impure arsenic to $\sim 10^{-6}$.

Radioactive elemental selenium was mixed with another arsenic sample in the same manner as that described above for mixing arsenic and As_2S_3. The minimum and maximum limits for the atom fraction of selenium in this sample were 1.0 and 1.7×10^{-4}. The large amount of selenium in the final arsenic suggests that simple sublimation is relatively ineffective for separating even moderate amounts of selenium from arsenic.

Tellurium doped arsenic was prepared by subliming twice a mixture equivalent to an atom fraction of radioactive tellurium of 10^{-6}. The tellurium atom fraction in the center portion of the final arsenic prior to the purification was between 1.3 and 2.4×10^{-7}.

Each of the arsenic samples prepared for purification was sealed in an evacuated quartz tube with twice its weight of high-purity lead and placed in a vertical tubular furnace. The bottom of the tube containing the lead was maintained at 600°C and the upper portion between 600° and 650°C. The arsenic dissolved in the lead overnight. Following this, the thermal gradient of the furnace was readjusted to give a uniform temperature of 600°C. Arsenic was distilled from the solution by gradually withdrawing the tube from the furnace and allowing the arsenic to condense in the upper colder section. This section containing the arsenic was sealed off and an additional amount of arsenic was distilled and condensed after increasing the temperature of the lead solution to 700°C. The arsenic fractions distilled from the lead at 600° and 700°C were analyzed for sulfur, selenium, and tellurium. Atom fractions of sulfur, selenium, and tellurium in the arsenic distilled from the lead solution of 600°C were 1.1×10^{-6}, $\leq 2.7 \times 10^{-6}$ and $\leq 2 \times 10^{-6}$, respectively. The major errors in concentrations of sulfur, selenium, and tellurium found in the purified arsenic result from errors in the preparation of the comparison standards and from the statistical fluctuations inherent in counting data. It is estimated that the analytical data are accurate to within ±25%. The average arsenic yield was 65% when distilled from the solution at 600° and 84% at 700°C. However, the atom fractions of sulfur and selenium in the fractions distilled from the solution of 700°C were substantially higher, 6.6×10^{-6} and 7.4×10^{-7}, respectively. No change was observed in the tellurium concentration of the condensate even when the temperature of the lead solution was raised to 760°C. These results are summarized in Table II. The weights of the initial doped arsenic samples varied between 1.5 and 5 g. Increasing the amount of arsenic to 250 g and maintaining the 1:2 weight ratio of arsenic to lead has raised the average yield distilled from the lead solution of 600°C to 85%.

Discussion

Lead has a vapor pressure of $\sim 10^{-6}$ mm at 600°C. Therefore, one expects to find a small concentration

Table II. Effectiveness of Pb condensation and distillation for separating sulfur, selenium, and tellurium from arsenic

	Sulfur	Selenium	Tellurium
Initial atom fraction	1.1 to 3.9×10^{-6}	1.0 to 1.7×10^{-4}	1.3 to 2.4×10^{-7}
Atom fraction in As distilled from Pb bath at 600°C	1.1×10^{-6}	$\leq 2.7 \times 10^{-6}$	$\leq 2 \times 10^{-6}$
Atom fraction in As distilled from Pb at 700°C	6.6×10^{-6}	7.4×10^{-7}	$\leq 2 \times 10^{-6}$

of lead in the arsenic after separation of sulfur, selenium, and tellurium. Before using the arsenic to prepare GaAs, it is resublimed twice. The lead concentration after this is ~ 1 ppm. Concentrations of 1 ppm of lead in arsenic are not nearly as serious as similar concentrations of sulfur and selenium, because the lead can be readily removed from GaAs by zone refining. Its distribution coefficient is < 0.02 (4).

The results in Table II indicate that even lower concentrations of sulfur and selenium in arsenic could be obtained by distilling the arsenic from the lead solution at a lower temperature. The only disadvantage to using a lower temperature is the reduction in arsenic yield due to a lower arsenic vapor pressure. Distillation below 550°C would require a more dilute solution of arsenic in lead in accordance with the As-Pb phase diagram. This would further reduce the arsenic yield.

Assuming arsenic is the only source of sulfur, selenium, and tellurium in GaAs or InAs, the equivalent concentrations in these compounds to those in Table II would be 2×10^{18}, $\leq 6 \times 10^{14}$, and $\leq 4 \times 10^{14}$ atoms cm^{-3}, respectively. Weisberg and Rosi noted a difference in the electrical properties of InAs made from arsenic distilled from lead when the lead arsenic solution was first equilibrated at 600° and 750°C prior to distillation from the solution at 600°C (5). The InAs made from arsenic equilibrated at the higher temperature had a net donor concentration of 1.4×10^{16} whereas arsenic equilibrated at 600°C yielded InAs with a net donor concentration of 2.7×10^{16} cm^{-3}. These differences are not likely to be due to differences in the sulfur and selenium concentrations in the two arsenic samples in light of the data in Table II.

Conclusion

Simple sublimation is not a satisfactory method for separating trace amounts of sulfur from arsenic. Sublimation in hydrogen is somewhat less effective than distillation of arsenic from a lead-arsenic solution. The latter method has been used to reduce the atom fractions of sulfur selenium and tellurium in arsenic to 1×10^{-9}, $\leq 2.7 \times 10^{-6}$, and $\leq 2 \times 10^{-6}$, respectively.

Manuscript received May 17, 1960; revised manuscript received Aug. 22, 1960. This paper was prepared for delivery before the Columbus Meeting, Oct. 18-22, 1959.

Any discussion of this paper will appear in a Discussion Section to be published in the June 1961 JOURNAL.

REFERENCES

1. E. Schillmann, Z. *Naturforsch.*, **11a**, 463 (1956).
2. T. C. Harman, H. L. Goering, and A. C. Beer, *Phys. Rev.*, **104**, 1562 (1959).
3. R. Gremmelmairer, Z. *Naturforsch.*, **11a**, 511 (1956).
4. H. C. Gatos, Editor, "Properties of Elemental and Compound Semiconductors," p. 141, Interscience Publishers, New York (1960).
5. *Ibid.*, p. 25.
6. J. Richards, see R. Barrie, F. A. Cunnell, J. T. Edmond, and I. M. Ross, *Physica*, **20**, 1087 (1954).
7. T. C. Harman, E. P. Stambaugh, and H. L. Goering, Paper delivered at Electrochemical Soc. Meeting, Cleveland (1956).
8. D. P. Enright, Naval Ordnance Laboratory Report 6024 (1958).
9. R. H. Harada and A. J. Strauss, *J. Appl. Phys.*, **30**, 121 (1959).
10. A. J. Ahearn, Bell Telephone Laboratories, Private communication.

Electrolytic Vanadium and Its Properties

D. H. Baker, Jr.,[1] and J. D. Ramsdell

U. S. Bureau of Mines, Boulder City, Nevada and Reno, Nevada, respectively

ABSTRACT

The fused salt electrorefining technique has been applied successfully to vanadium. The electrolyte was sodium chloride containing 3-6% vanadium as vanadium dichloride. Current efficiency was approximately 91%. Oxygen and nitrogen impurities were reduced by two thirds of the amount contained in the feed material. The hardness of the product was reduced from 97 Rockwell B to 35 R_B. Arc melted ingots could be given a 99% cold reduction by rolling before edge cracking appeared.

Growing interest and the industrial need for purer metals and improved alloys for application under high-temperature and high-speed conditions has demanded the elimination and/or control, as far as possible, of impurities.

As a part of this program of intensified research, the Federal Bureau of Mines Reno Metallurgy Research Center and the Boulder City Metallurgy Research Laboratory have undertaken a joint investigation to produce and evaluate high-purity vanadium.

In the past few years the Bureau of Mines has developed and proved the technical feasibility of fused salt electrorefining of metals such as titanium (1), beryllium (2), hafnium (3), zirconium, to remove impurities, such as O_2 and N_2, as well as certain other elements.

Fused salt refining of vanadium was considered because the gaseous impurities, nitrogen and ox-

[1] Present address: U. S. Bureau of Mines, Washington 25, D. C.

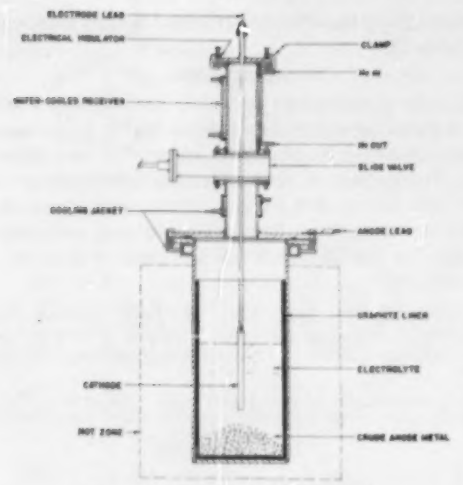

Fig. 1. Schematic drawing of cell

ygen, which can be controlled by this technique, have serious effects on vanadium's physical properties. Commercially, the production of low nitrogen-oxygen vanadium is an expensive, complicated and time-consuming process by any of the standard reduction techniques.

Since the fused salt electrorefining technique has shown the ability to control gaseous impurities in other reactive metals such as titanium and has been scaled up to a 10,000-amp cell, the technique offered a means of improving the quality of technical grade vanadium at something approaching a commercial scale.

This investigation was undertaken to ascertain the feasibility of applying the fused salt electrorefining method to the production of a metal product exceeding the purity of present commercial vanadium metal (99.5 V). The principal specific object was to improve the ductility of the final product by removing oxygen and nitrogen.

Description of Process

Input material.—The anode, or feed material, is commercially produced vanadium metal having a Rockwell B hardness of 97 and containing, according to the producer, 99.5% V, 0.30 Fe, 0.18 O_2, 0.03 N_2, 0.006 H_2, and 0.03 Cr.

Equipment.—Figure 1 is a schematic diagram of the 12-in. diameter electrolytic cell used. This cell was identical to those used for refining titanium metal, except for a graphite liner to minimize iron contamination of the bath. A receiving chamber and valve system permitted the introduction and removal of the cathode without disturbing the inert atmosphere of the cell proper.

External heat was used to maintain the electrolyte at an operation temperature of about 800°C.

Vanadium metal, crushed to $-\frac{1}{2}$ in., was charged to the bottom for the anode. On the basis of experience gained in operating similar cells on other metals, the minimum ratio of the cathode to the anode area was fixed at 1:3. Under higher anode areas, exceeding the minimum, more operative stability was obtained. The cathode used in the 12-in. diameter cell was a $\frac{3}{4}$-in. diameter iron rod.

Vanadium chloride was applied to the 60-lb sodium-chloride bath through the reaction of chlorine gas and a small amount of admixed hydrogen chloride with the granular anode metal contained in the cell bottom. The reaction of hydrogen chloride alone with the vanadium anode material was extremely slow. The hydrogen evolved from the hydrogen chloride passed from the chlorinator and through the bath assisting in the purification of the sodium chloride. The off gas was permitted to escape from the cell through an oil bubbler.

Working procedure.—The cathode, cleaned and burnished, was introduced into the cell through the receiving chamber above the bath compartment. The receiving chamber was evacuated and charged with inert gas (helium), after which the catnode was lowered into the bath through a valve. Prior to use, the cathodes were stored in a drying oven under controlled low-humidity atmosphere.

Upon completing the cathode placement, the appropriate voltage was applied for the particular test, and the refining process was conducted.

On completion of the "run," the cathode, bearing the product metal, was withdrawn into the upper cell chamber, previously evacuated and charged with inert gas, to cool before final removal from the cell.

Deposits were leached with a 2-3% HCl solution to dissolve the entrained salts and subjected to agitation in a high speed mechanical agitator to separate the metal crystals. Salt-free metal crystals were then washed with acetone to assist in the rapid removal of moisture and sized through the appropriate screens.

Testing the product.—The general quality of the product was quickly determined on the basis of hardness tests alone for preliminary "run" evaluation purposes. Individual run products shown to be similar by chemical and hardness evaluation were composited for further study. Compacts of the crystalline vanadium powders weighing 10-70 g were melted into buttons or cigar-shaped ingots in a tungsten electrode arc furnace under helium. Ingots were homogenized by remelting five times, being turned over after each melt. Samples were also taken for complete analysis or for semiquantitative analysis. Hardness was found to correlate reasonably well with the degree of purity. The relation of hardness to oxygen content is shown in Fig. 2.

Investigations

A total of 127 cycles or runs were made in the 12-in. cell before the graphite liner failed terminating the operation. The specific factors contributing to the failure of graphite were primarily the result of stresses arising from thermal cycles of the iron container and graphite liner. No evidence of corrosion or reaction with the graphite were detected as illustrated by the metal analysis of less than 0.01% carbon.

When the cell was placed in operation, the electrolyte contained 2.8% soluble vanadium. The first three cycles were made for the purpose of conditioning the electrolyte, a total of 68 amp-hr at 0.2 v. Very fine, needle-like, crystals of cathode metal were discarded because of iron contamination.

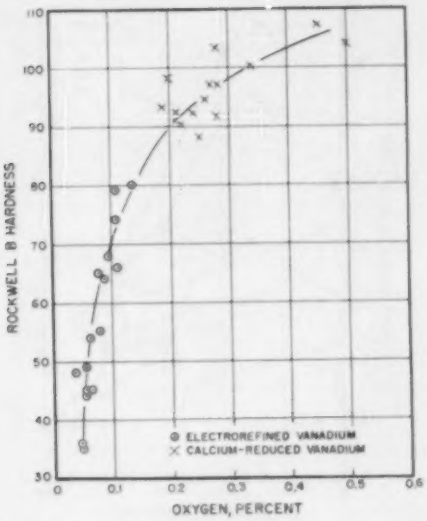

Fig. 2. Effect of oxygen on the hardness of arc-melted vanadium.

The metal product from the fourth run tested 95 R_B in hardness and there was a progressive improvement in succeeding cycles with a hardness as low as 35 on the +35 mesh fraction. Vanadium metal produced in the following 60 cycles of operation was separated into four sieve products as shown in Table I. Approximately 72% of the cathode metal produced was coarser than 80 mesh standard Tyler. The total deposited metal had a weighted average hardness of 52 R_B.

Production of soft, coarsely crystalline, cathode metal is affected by the anode area in addition to other factors. A large anode area with fresh metal surface results in a high quality product; the effect is shown in Table II. Hardness of the metal product decreases very quickly after the addition of anode material.

Table I. Typical screen and hardness distribution of vanadium deposits

	Screen size, standard Tyler mesh			
	+35	−35 +80	−80 +150	−150
Weight, %	27	45	16	12
Hardness, R_B	36	46	55	62

Table II. Effect of metal addition on product hardness

Test cycle	Hardness	Remarks
28	63	Deposit prior to 900 g addition of anode metal.
29	54	First deposit after addition.
30	60	
31	49	
32	51	
33	50	
50	84	Deposit prior to 1100 g addition of anode metal.
51	60	
52	65	
53	60	
54	59	

Fig. 3. Vanadium cathode deposit, as removed from the cell, produced 0.45 v.

Coarse crystalline metal was produced at applied voltages between 0.4 and 0.7 v. The bath contained 3.0% vanadium as the dichloride and was at a temperature of at least 800°C. Figure 3 illustrates the coarser deposits obtained at 0.45 v. Deposits produced at very low voltages (less than 0.3 v) or above 1.0 v contain much finer crystals. Voltages above 2.0 v would cause electrowinning from the bath with the evolution of chlorine gas, chemical attack on the iron of the cell, and iron contamination of the bath and the product. A typical range of analyses of the refined metal is C < 0.01%, Fe 0.003-0.05% O_2 0.04-0.10%, N_2 < 0.002%.

Current efficiencies for 100 cycles or runs were nearly all within the range of 88-94% with an average of 91%, based on the assumption that vanadium is transported at a valence of 2. At the average current efficiency, 522 amp-hr will deposit 1 lb of vanadium metal.

The first 100 runs with the 12-in. cell were made at voltages from 0.2 to 1.5 v and with initial current densities from 100 to 3500 amp/ft^2. No major importance can be given to the calculated current density because the cathode area begins to increase the instant metal deposits. The currents are kept within the limits from 2 to 68 amp by choice of immersion depth of the cathodes used.

Vanadium metal can be purified in respect to O_2 and N_2 by the fused salt electrorefining technique. Reduction of these gaseous impurities was in the order of two thirds, hardness was reduced from 97 Rockwell B to a low of 35 R_B.

Primary Fabrication

Arc-melted electrorefined vanadium is characterized by large randomly oriented grains. Within the grains are configurations (revealed by conventional etching techniques) in the form of pits and sub-boundaries similar to structures associated with dislocation sites.

After melting, the 10-g buttons were easily cold rolled to 0.005 in. sheet, a total reduction of 98%, with no intermediate anneals. Electrorefined vanadium shows a hardness increase of approximately 55 V.h.n. greater than its original annealed hardness when cold reduced 65%. Most of the hardening occurs in the 0-15% cold work range, approximately 27 V.h.n. for a reduction of 5% and about 38 V.h.n. for a reduction of 15%. Above 15% reduction range, hardening increases at a reduced rate with increasing amounts of deformation.

The large columnar grains of the larger arc-melted ingots deformed nonuniformly, and whenever annealing was preceded by heavy reductions recrystallization produced a banded structure that persisted during grain growth. After considerable experimental work with various sequences of flat rolling, swaging, square rolling, and cold pressing, a schedule of cold pressing and square rolling followed by annealing was adopted for initial large ingot breakdown of approximately 75% reduction in area. Although some banding was still present, this working sequence produced optimum grain structure and retained enough cross-sectional area for further testing.

Recrystallization

For recrystallization studies, these bars were further cold-rolled from 5 to 65% reduction in area. To protect the specimens from gaseous contamination during annealing, they were sealed in Vycor capsules, and were annealed for 1 hr at temperatures of 200° to 1000°C. The effect of temperature on the Vickers hardness for one lot of electrolytic vanadium is shown in Fig. 4.

For all reductions heated to temperatures in the range of 200° and 400°C, an increase in hardness of 3-15 V.h.n. over that of the cold worked metal is noted. As the temperature is increased above 400°C, hardness decreases rapidly for all reductions until the prior to deformation hardness is reached. The return to pre-deformation hardness occurs for annealing temperatures in the range of 900°-1000°C and corresponds to the temperature range for the beginning of grain growth. In general, for annealing temperatures between 900° and 1000°C, the 65% cold worked metal show an increase in hardness while the 5% cold work specimens show a continuing decrease in hardness. The 35% cold worked specimens exhibit both increasing and decreasing hardness in this annealing range (900°-1000°C). A similar high-temperature hardening effect was noted by Pugh (4) for 80% cold reduced vanadium annealed above 1200°C.

An anomaly occurs in the temperature range of 600° to 800°C, in the hardness *vs.* annealing temperature curve for all reductions in general; it is most pronounced for the low reductions. According to Lacy and Beck (5), this anomaly is attributed to an aging mechanism similar to strain aging in steel and titanium. Rostoker, *et al.* (6) noticed this same anomaly for high percentages of cold work rather than for the low reductions as noted in this investigation. It appears, if this anomaly is due to strain aging, that decreasing the quantity of interstitial impurities in vanadium reduces the amount of deformation necessary to promote strain aging in this temperature range.

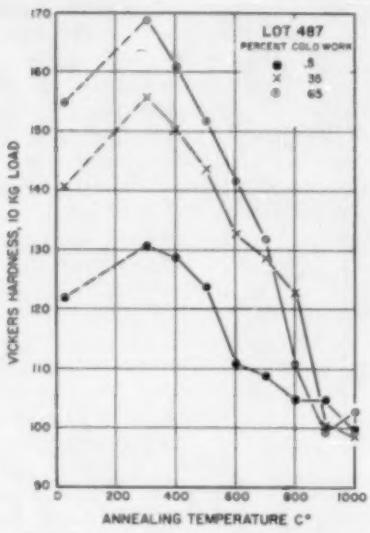

Fig. 4. Effect of temperature on the Vickers hardness of electrorefined vanadium.

The rapid decrease in hardness for the 35, 50, and 65% cold worked metal annealed in the range of 700°-800°C corresponds to the terminus of the mentioned anomaly and also to the initial microscopic evidence of recrystallization for these same reductions.

Microscopic evidence of recrystallization by nucleus growth for vanadium cold-reduced 65% is first observed for the 700°C anneal; recrystallization by nucleus growth for reductions of 35-50% is first observed for the 800°C anneal. Recrystallization is essentially complete for these three reductions after a 900°C anneal. The 35% reduction is near the minimum critical deformation necessary to promote nucleus growth rather than grain coarsening. Grain coarsening was observed for reductions of 5, 15, and 25%. Lacy and Beck (5) report metallographic recrystallization occurring in 60% extruded vanadium for annealing temperatures in excess of 750°C, while Nash, *et al.* (7) noted that metallographic evidence of recrystallization for iodide vanadium cold work 90% was present for annealing temperatures between 650° and 700°C.

Grain growth is evident in all reductions for annealing temperatures in excess of 900°C and is continuous except for the 5% cold-worked metal, which exhibits extreme discontinuous grain growth between 900° and 1000°C.

Mechanical Properties

Tensile data for vanadium cold rolled 50% and annealed at 950°C is plotted as a function of oxygen content in Fig. 5. Oxygen is used as a parameter since the authors observed it to have a greater and more consistent effect on the strength and hardness than other impurities found in high-purity vanadium.

Strength and hardness are plotted as straight line functions of oxygen content. As oxygen content increases from 0.047 to 0.109 w/o, tensile strength

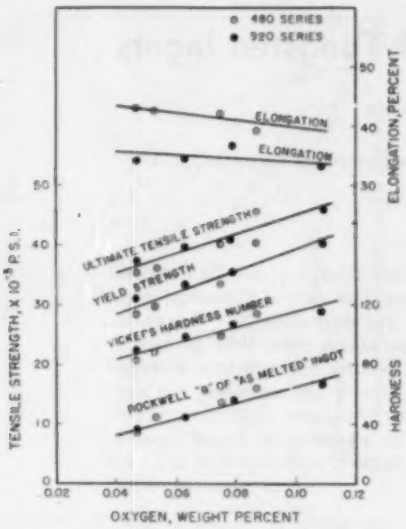

Fig. 5. Comparison of the effect of oxygen content, tensile strength, hardness and elongation of electrorefined vanadium.

increases from 35,000 to 46,000 psi while hardness increases from 83 to 116 V.h.n. Ductility as measured by tensile elongation (33-43% in 1 in.) is not appreciably influenced by oxygen content.

Approximately 60% of the tensile specimens tested exhibited a yield phenomenon similar to that noted by Lacy and Beck (5) that consists of an upper and lower yield point which differ on an average of 2,000 psi.

An indication of the significance of oxygen rather than nitrogen, which was once thought to be the major hardener and strengthener of vanadium, becomes more apparent by individual comparisons.

Lot	O_2	N_2	Y.S.	U.T.S.
A	0.093	0.016	45,600	53,000
J	0.084	0.014	41,800	48,600
B	0.055	0.014	30,000	37,200

Comparison of the above lots indicates that the tensile and yield strengths decrease progressively with decreasing oxygen content and constant nitrogen content.

Lot	O_2	N_2	Y.S.	U.T.S.
K	0.107	0.004	46,700	53,000
488	0.087	0.003	40,500	45,900
H-I	0.062	0.003	36,000	43,200

Comparison of lots K, 488, and H-I again indicates that the tensile and yield strengths decrease with lower oxygen content and constant nitrogen content of a much lower level than for lots A, J, and B.

Lot	O_2	N_2	Y.S.	U.T.S.
A	0.093	0.016	45,600	53,000
K	0.107	0.004	46,700	53,000

In this comparison, despite the very marked difference in nitrogen content, the tensile and yield strengths remain practically constant.

Lot	O_2	N_2	Y.S.	U.T.S.
486	0.053	<0.001	28,900	36,100
B	0.055	0.014	30,000	37,200
H-I	0.062	0.003	36,000	43,200

A comparison of lots 486, B and H-I shows that the tensile and yield strengths are consistent at very similar oxygen contents and very dissimilar nitrogen contents. In this case, the oxygen level is nearly one-half that of the previous comparisons of lots A and K. These comparisons indicate, within the limits of the compositions investigated, that the influence of oxygen on the mechanical properties is much more pronounced than that of nitrogen.

Further study is required to obtain more direct correlation of properties with oxygen and/or nitrogen content as these elements appear to be most potent in their specific influence.

Physical Properties

Thermal expansion properties were independent of impurity content and the derived value for the coefficient of thermal expansion at 20°C is 8.84 x 10^{-6}/°C.

Resistivity correlated well with other properties measured for the respective lots of electrolytic vanadium. Resistivity decreased with increasing purity and decreasing strength. The values obtained varied from 22.6 to 25.2 microhm-cm at 26°C, which are, in general, lower than those previously reported for vanadium: 24.8-26.0 microhm-cm.

These Bureau of Mines investigations have shown that the fused salt electrorefining technique offers a feasible means of controlling the quantity of gaseous impurities, such as O_2 and N_2, in vanadium metal to low levels consistently. The study also has shown that the properties of electrorefined vanadium are considerably different from those exhibited by commercially available vanadium because of the reduction of impurity content. The oxygen content more than any other single impurity showed the most marked affect on hardness strength and workability.

Manuscript received June 6, 1960; revised manuscript received Aug. 26, 1960. This paper was prepared for delivery before the Chicago Meeting, May 1-5, 1960.

Any discussion of this paper will appear in a Discussion Section to be published in the June 1961 JOURNAL.

REFERENCES

1. J. R. Nettle, D. H. Baker, Jr., and F. S. Wartman, Bureau of Mines Rept. of Investigations 5315, 1957, 43 pp; D. H. Baker, Jr. and J. R. Nettle, Bureau of Mines Rept. of Investigations 5481, 1959, 11 pp; O. Q. Leone, J. R. Nettle, and D. H. Baker, Jr., Bureau of Mines Rept. of Investigations 5494, 1959, 20 pp.
2. M. M. Wong, F. R. Cattoir, and D. H. Baker, Jr., Bureau of Mines Rept. of Investigations 5581, 1959, 9 pp.
3. D. D. Blue and D. H. Baker, Jr., Electrorefining of Vanadium, Chromium, Zirconium, and Hafnium, Paper presented at the Second United Nations International Conference on the Peaceful Uses of Atomic Energy, Geneva, Switzerland, June 1958, 17 pp.
4. J. W. Pugh, Discussion to Lacy and Beck, *Trans. Am. Soc. Metals*, **48**, 579 (1956).
5. C. E. Lacy and C. J. Beck, *ibid.*, **48**, 579 (1956).
6. W. Rostoker, D. J. McPherson, and M. Hansen, WADC Technical Report 52-145, Part 2, 1954.
7. J. W. Nash, H. R. Ogden, R. E. Durtschi, and I. E. Campbell, *This Journal*, **100**, 272 (1953).

On the Vacuum Sintering of Tungsten Ingots

J. W. Pugh and L. H. Amra

Refractory Metals Laboratory, General Electric Company, Cleveland, Ohio

ABSTRACT

A furnace for vacuum sintering tungsten is described, and results obtained from tungsten sintering experiments are discussed. The rate of densification at various temperatures is given special emphasis, but microstructure, hardness, fabricability, and purity are also examined. Temperatures from 1800° to 3100°C and times from 0.25 to 8.00 hr were employed. Results indicate that sintered densities at least as high as 82.5% of theoretical density are necessary for successful fabrication, and that densities as high as 97.0 have structures which are readily fabricable. High-temperature vacuum sintering is found to produce very pure tungsten, commensurate in this respect with the best arc cast tungsten.

The sintering of tungsten is not a new process. In the first decade of this century at least seven ingenious techniques were employed to consolidate tungsten so that it could be used for electric lamp filaments (1). The technique devised by Coolidge in 1909 was the most successful (2). His process which involved sintering pressed powder ingots in hydrogen and fabricating them to wire by swaging and drawing at progressively lower temperatures is essentially the one being used today. Little interest in vacuum sintered tungsten has been reported, although several advantages over hydrogen sintered metal might be expected.

Some of the most promising alloying elements for tungsten alloys are Ti, Zr, Hf, Cb, and Ta. These elements are all hydride formers, and their addition to tungsten requires consolidation in an inert atmosphere. High vacuum is perhaps the easiest and most satisfactory answer to this requirement. Moreover, vacuum offers the additional advantage of deoxidation since the vapor pressure of tungsten oxide is quite high at sintering temperatures and the vapor pressure of tungsten is relatively low. The sintering process can take effective advantage of this relatively unique situation because the vapor can be removed readily through the porous network of the compacted ingot. It is also true, of course, that the equilibrium of any purification reaction which results in gas evolution would be shifted favorably in vacuum.

In view of the foregoing, a vacuum sintering furnace was constructed, and some basic data on the vacuum sintering of tungsten were obtained.

Procedure

A schematic diagram of the furnace employed for these experiments is shown in Fig. 1. This furnace provides for heating compressed powder ingots by means of their own electrical resistance. 720 KW of powder is available between a stationary top electrode and a movable lower electrode, both of which are water cooled. Expansion and contraction of ingots during sintering is compensated for by means of a feed back device which involves a strain gauge, amplifier, and electrode drive mechanism. Vacuum of about 10^{-4} mm pressure is maintained by means of a 25 cm, (10 in.) oil diffusion pump and a Kinny 3.12 cubic meter/min, (110 ft³/min) mechanical pump. An auxiliary 0.42 cubic meter/min (15 ft³/min) mechanical pump is used for rough pumping the system.

Tungsten powders having a Fisher Sub-sieve size of 4.53 μ were compressed in a double acting hydraulic press at pressures of 1.89 metric tons/cm² (12 TSI) to form ingots having the dimensions 0.95 x 0.95 x 61.0 cm (⅜ x ⅜ x 24 in.). The green ingots were presintered 1 hr at 1200°C in hydrogen so that they had a presintered density of 11.5 g/cc. They were then placed in the vacuum sintering furnace and brought to the prescribed sintering temperature at the rate of 20°C/min. After prescribed times at temperature, each ingot was cooled rapidly to room

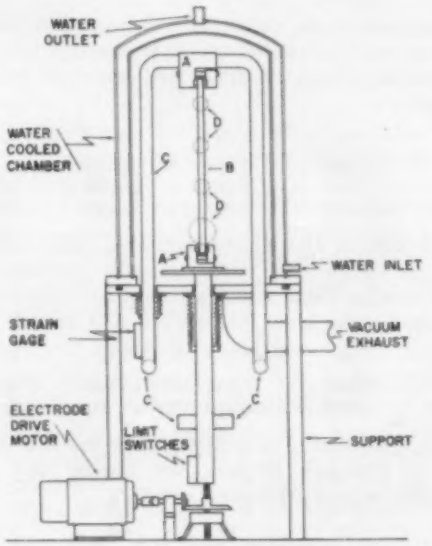

Fig. 1. Schematic representation of vacuum sintering furnace: A, electrodes; B, ingot; C, lead; D, sight port positions.

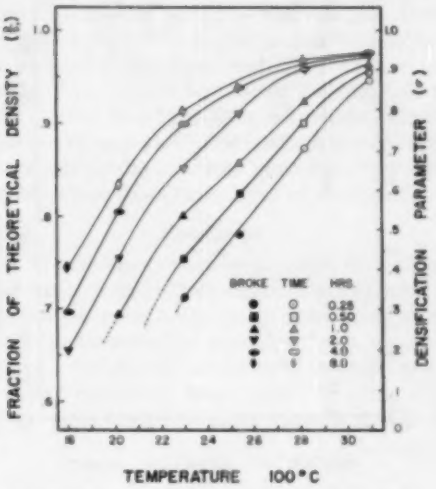

Fig. 2. Effect of temperature on the densification of tungsten ingots

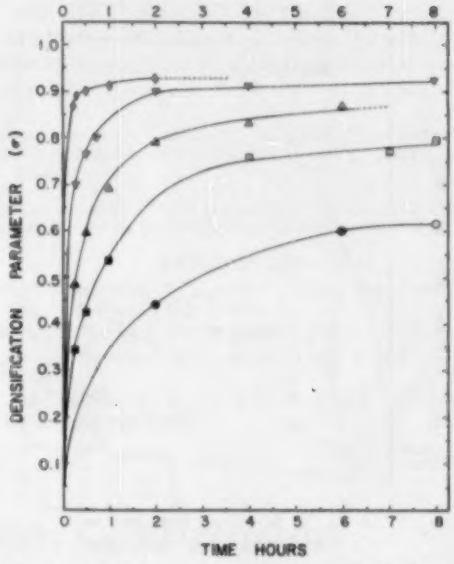

Fig. 3. Effect of time on the densification of tungsten ingots

temperature. The initial cooling rate in each case was approximately 500°C/min.

After the ingots were sintered, they were evaluated for density, microstructure, fabricability, and purity. Fabrication testing consisted of attempting to swage each ingot to 40% reduction in area after heating it to 1600°C.

Results and Discussion

Figure 2 indicates the effect of temperature on sintered density for various times at temperatures. The parameter plotted as the ordinate is the one commonly used to describe the degree of densification in sintered ingots: the density of the ingot (D) divided by the density of completely consolidated tungsten D_T. The Densification Parameter (σ) at the right is the densification achieved for the ingot divided by the maximum densification possible.

$$\sigma = \frac{D - Do}{D_T - Do}$$

where Do is the density of the ingot before sintering. The solid data point symbols in Fig. 2 represent ingots which could not be swaged satisfactorily. Apparently an ingot must attain more than 82.5% of its theoretical density before it can be fabricated in this way.

These data are plotted in another way in Fig. 3. Here the densification parameter is plotted as a function of time for each of the five temperatures employed. Figure 3 was used to plot the relationships shown in Fig. 4. Here the logarithm of sintering time is shown as a function of reciprocal absolute temperature for five different states of constant densification. These relationships are apparently straight lines and the empirical Arrhenius equation,

$$t = A \exp\left(\frac{\Delta H}{RT}\right)$$

is suggested. Here t is time, A is a constant, R is the gas constant, T is absolute temperature, and ΔH is the apparent activation energy for sintering. Note

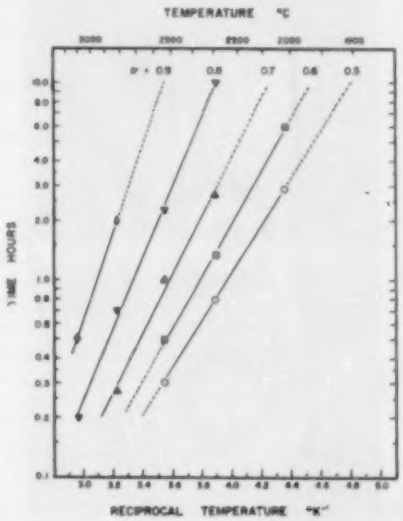

Fig. 4. Time-temperature relationships for vacuum sintered tungsten

that while these relationships are straight, they are not parallel and that the apparent activation energy changes from about 55 kcal/mole for a densification parameter of 0.5-105 kcal/mole for a parameter of 0.9. The precision of these determinations is not great, and the interpretation of these activation energies in terms of rate processes and mechanisms is not within the scope of this investigation. It does seem clear, however, that the effective or apparent activation energy as obtained from Fig. 4 increases with densification. A similar result for pre-reduced copper powder sintered in vacuum has been reported by Jordan and Duwez (3). Figure 5 shows how grain size increases as a function of time for three sintering temperature, and Fig. 6 permits a comparison of three microstructures which resulted from 2-hr treatments at the same three temperatures. The increase in pore size observed with

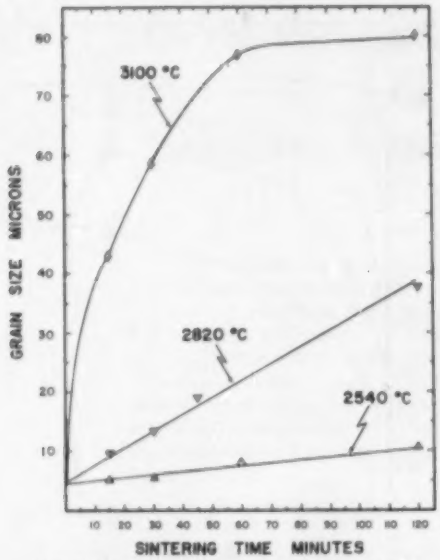

Fig. 5. Grain size for vacuum sintered ingots

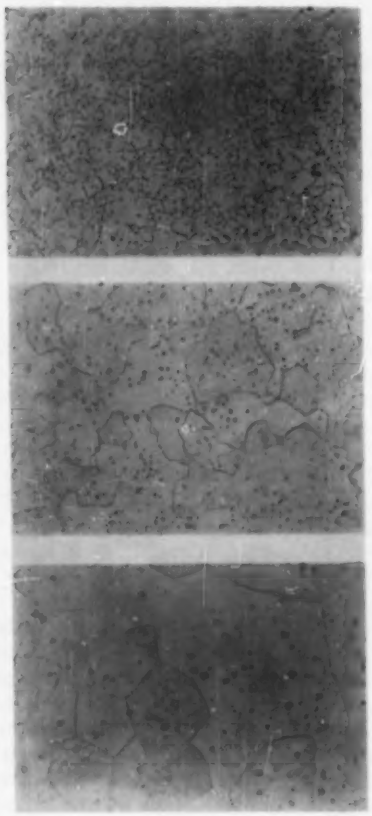

Fig. 6. Microstructures of tungsten ingots vacuum sintered 120 min. (a) (top) 2540°C; (b) (center) 2820°C; (c) (bottom) 3100°C. Magnification 250X before reduction for publication.

increasing density agrees with the findings of Rhines, Birchenall and Hughes (4). Figure 7 shows the effect of density on the hardness of the sintered ingots. Rockwell A measurements were taken first on each ingot. Diamond Pyramid Hardness was made on seven ingots to provide the relationship shown here.

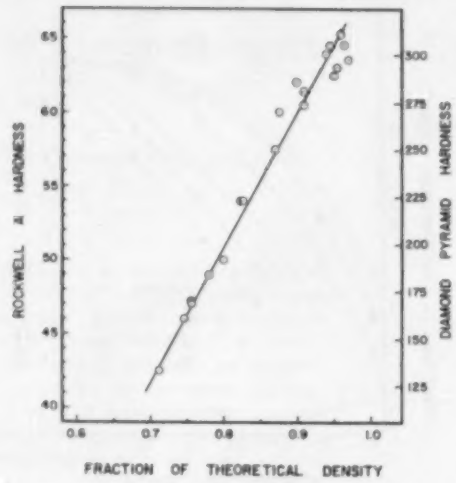

Fig. 7. Hardness of vacuum sintered tungsten

Table I. Gas analysis of sintered tungsten

No. of ingot	Conditions of sintering		Gas content, ppm*		
	temp, °C	time, min	O_2	N_2	H_2
333W17	3100	120	7	1	0
337W21	2820	122	8	2	1
315W7	2820	30	12	2	1
339W23	2540	360	1	1	0
336W20	2540	120	5	1	1
343W26	2020	120	57	5	2

* All results are ±5 ppm.

Table II. Data on sintered tungsten

Sintering conditions		Density			
Temp, °C	Time, min	g/cc	% theor.	Hardness, R "A"	Grain count, g/mm²
1800	120	Hg		25	
1800	480	14.40	74.6	46	
2020	120	14.65	75.6	47	
2020	198	14.85	77.0		
2020	360	16.00	82.6	54	
2020	480	16.10	83.4		
2300	15	13.76	71.2	42.5	
2300	30	14.57	75.4	47.2	
2300	60	15.46	80.0	50.0	
2300	240	17.34	89.8		
2300	420	17.42	90.0	62.0	
2300	480	17.65	91.3		
2540	15	15.05	78.0	49.0	
2540	30	15.95	82.5	54.3	33,500
2540	60	16.75	87.0	57.5	
2540	120	17.60	91.0	60.5	8,700
2540	240	17.94	93.7		
2540	360	18.24	94.5	64.5	
2820	15	16.85	87.3	60.0	10,600
2820	30	17.39	90.0	61.0	5,700
2820	47	17.70	91.0	61.4	
2820	120	18.49	95.7	62.4	700
2820	240	18.56	96.0	65.2	
2820	480	18.70	96.7		
3100	15	18.26	94.5	63.9	540
3100	18	18.42	95.5	63.0	
3100	30	18.44	95.5		
3100	60	18.60	96.4	64.5	
3100	120	18.75	97.0	63.5	334

Of special interest are the vacuum gas analysis results shown in Table I. The improvement in impurity content with time and temperature is remarkable. The oxygen content of the ingot sintered for 2 hr at 3100°C is perhaps comparable to the best arc-cast ingot analysis. This comparison is inexact because both products are so pure that they extend the analysis technique to its limit of resolution.

Conclusion

Table II provides a summary of the data obtained in these experiments. The information available here is sufficient to permit the programming of vacuum sintering treatments for tungsten with confidence. There are a number of unexplored avenues of practical experimentation remaining. For example, it would be most useful to know the effect of particle size and size distribution on sintering kinetics. It would also be of interest to know the effect of a variety of impurities on sintering kinetics and on gas content.

Manuscript received April 20, 1960. This paper was prepared for delivery before the Houston Meeting, Oct. 9-13, 1960.

Any discussion of this paper will appear in a Discussion Section to be published in the June 1961 JOURNAL.

REFERENCES

1. C. J. Smithells, "Tungsten," Chemical Publishing Co., Inc., New York (1953).
2. W. A. Coolidge, *J. AIEE*, p. 953 (1910).
3. C. B. Jordan and P. Duwez, *Trans. AIME*, **188**, 943 (1950).
4. F. N. Rhines, C. E. Birchenall, and L. A. Hughes, *ibid.*, **188**, 378 (1950).

Liquidus Curves for Aluminum Cell Electrolyte

III. Systems Cryolite and Cryolite-Alumina with Aluminum Fluoride and Calcium Fluoride

Anne Fenerty[1] and E. A. Hollingshead

Aluminium Laboratories Limited, Arvida, Quebec, Canada

ABSTRACT

Liquidus curves have been determined by means of cooling curves and visual examination of the cooling melt. The binary systems of cryolite with aluminum fluoride and calcium fluoride gave, respectively: peritectic point at 30% aluminum fluoride and 739°C, eutectic point at 40% aluminum fluoride and 694°C; eutectic point at 26% calcium fluoride and 945°C. In the system cryolite-alumina-calcium fluoride the ternary eutectic point was at 2.9% alumina, 21% calcium fluoride and 933°C. (Compositions are in weight per cent). Diagrams are given for the cryolite-rich part of the systems cryolite-calcium fluoride, cryolite-alumina-aluminum fluoride, cryolite-alumina-calcium fluoride, and cryolite-alumina-aluminum fluoride-calcium fluoride.

In the two preceding papers (1, 2) liquidus diagrams were reported for cryolite-alumina and for cryolite and cryolite-alumina with sodium fluoride, sodium chloride, and aluminum fluoride. The object of the present paper is to present additional data, a revised liquidus diagram for cryolite-alumina-aluminum fluoride, and liquidus diagrams for the cryolite-rich part of the systems cryolite-calcium fluoride, cryolite-alumina-calcium fluoride, and cryolite-alumina-aluminum fluoride-calcium fluoride.

Foster (3) recently reported the determination of the cryolite-alumina phase diagram by quenching methods. His results, except for pure cryolite, agree within the experimental error with those obtained in this laboratory (1) by cooling curves and visual examination of the cooling melt, the techniques used to obtain the results presented in this paper.

For the melting point of pure cryolite Foster (4) found 1004°C through quenching methods with a thermocouple calibration based in part on 992°C for the melting point of sodium fluoride. Both these are lower than the corresponding values of 1009° and 994°C found in this laboratory (2) by the cooling curve method. For comparison Grjotheim (5) found 1008.5° and 994.5°C, respectively, by the cooling curve method. Dworkin and Bredig (6) found 995°C for sodium fluoride, while Sense and others (7) found 996°C from the intercept of the vapor pressure-temperature curves of the liquid and solid. On the other hand much higher values for both cryolite and sodium fluoride, 1027° and 1012°C, respectively, were found by O'Brien and Kelley (8) from heat content measurements. It has already been noted (9) that too high a melting point was obtained in this way for nickel chloride, 1030°C *vs.* 1009° from cooling curves.

Materials

Hand-picked natural cryolite containing no visible impurities was crushed to −100 mesh or, preferably, to −20 mesh. The principal impurities in the two lots used were 0.01 and 0.02% iron and 0.01 and 0.04%

[1] Present address: Flint, Michigan.

silicon respectively. The alumina, produced experimentally, had a loss on ignition at 1000°C of 0.08% and contained 0.03% Na, 0.03% Ca, 0.03% Fe, 0.03% Si, 0.02% Ti, and 0.14% F. The aluminum fluoride was purified by vacuum distillation of Alcan dry-process aluminum fluoride. It contained 0.23% cryolite, 0.03% aluminum sulfate, 0.02% iron, 0.02% silicon, 0.01% manganese, and 98.4% aluminum fluoride (based on total fluorine content). The calcium fluoride was reagent-grade, from J. T. Baker Chemical Co. It had a loss on ignition at 110°C of 0.3-0.4% and contained 98-99% calcium fluoride (based on total fluoride content).

Method

The apparatus and methods were substantially as described in the first paper (1). The 150-g samples were made up by weight, thoroughly mixed, heated to about 100°C above the melting point, and stirred at about 100 rpm until clear and during the determination of the freezing point.

Primary freezing points were determined by the cooling-curve method when the first appearance of crystals in the melt, as observed through a telescope, corresponded to the primary break in the cooling curve. In general this was so on the cryolite side of the eutectic point. On the alumina side of the eutectic point and on most melts containing 25% or more of calcium fluoride or aluminum fluoride the primary freezing point was obtained by the visual method. In this method the temperature at which crystals first appear in the slowly cooled melt is determined. For final determinations rates of cooling of 0.1-0.15°C/min were used and the melt was observed every 5-15 min. The failure of the cooling-curve method to detect the primary crystallization of alumina is attributed to the steepness of the liquidus curve (low heat of crystallization and small percentage of crystals forming per unit decrease in temperature), and to the sluggishness with which alumina crystallizes.

The platinum, 10% rhodium-platinum thermocouples were all made from the same two spools of wire. One of them was calibrated in pure silver, in copper-silver eutectic alloy (799.0°C), and in standard samples of aluminum and copper certified by the National Bureau of Standards. Each thermocouple was checked periodically at the freezing point of reagent-grade sodium chloride, 801°C.

Accuracy

Two or more determinations were usually made for each composition and the mean or median value selected. With the cooling-curve method this value should not be in error by more than 3°C.

With the visual method duplicate values usually differed by less than 10°C. They would tend to be low because it was not possible to make a proper correction for supercooling. An upper limit for this correction was determined for one composition (cryolite—11% alumina) by cooling slowly until crystals appeared, then heating slowly with continuous stirring to determine the lowest temperature at which they would redissolve. This was found to be 10°-14°C higher than the mean temperature (972°C) at which the crystals appeared. Since some superheating must be required to redissolve, the negative bias of the visual method is probably less than 10°C.

For melts containing 25% or more aluminum fluoride results by the visual method were less reproducible than indicated above. This may be attributed in part to the greater steepness of the liquidus curve on the alumina side of the eutectic point. Changes in melt composition, as indicated by weight loss, were similar to those for cryolite-alumina melts.

Results

The liquidus diagram for cryolite-aluminum fluoride, reported in the preceding paper (2), was redetermined and slightly higher liquidus temperatures obtained. The revised values for the peritectic point are 739°C and 30% aluminum fluoride (weight per cent), for the eutectic point 694°C and 40% aluminum fluoride. It was verified by the visual method that on the aluminum fluoride side of the eutectic point the liquidus temperature rises rapidly to 860°C at 45% aluminum fluoride. This contradicts Grjotheim's finding (5) by the cooling-curve method that there is a maximum of 731°C at 45.2% aluminum fluoride corresponding to the compound $NaAlF_4$.

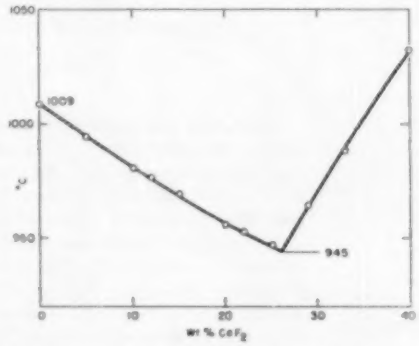

Fig. 1. Liquidus diagram for cryolite-calcium fluoride

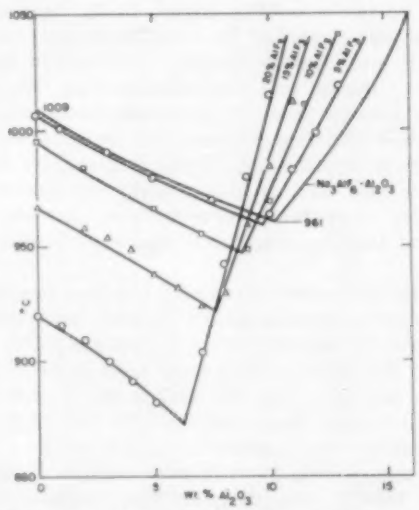

Fig. 2. Liquidus diagrams for cryolite-alumina with 5, 10, 15, and 20% aluminum fluoride.

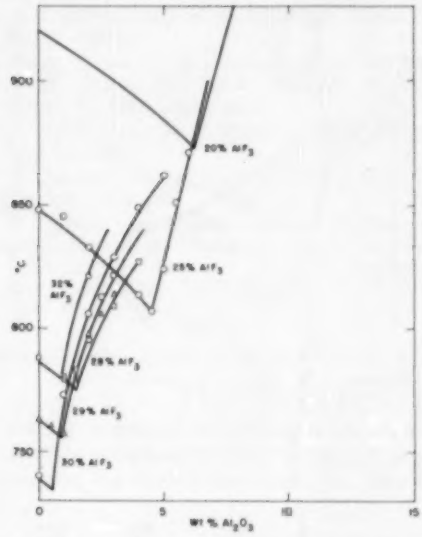

Fig. 3. Liquidus diagrams for cryolite-alumina with 25, 28, 29, 30, and 32% aluminum fluoride.

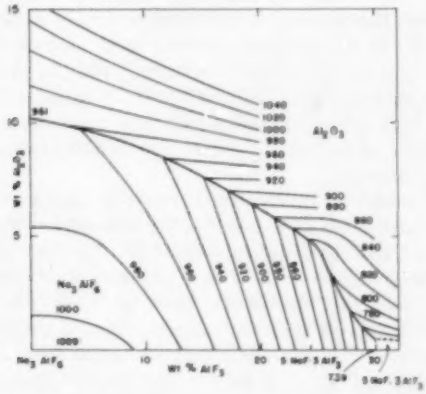

Fig. 4. Liquidus diagram for cryolite-alumina-aluminum fluoride

The liquidus diagram for cryolite-calcium fluoride (Fig. 1) was found to have a eutectic point at 26% calcium fluoride and 945°C This is in good agreement with the 25.5% calcium fluoride and 942°C obtained by Gupalo (10).

In the ternary system cryolite-alumina-aluminum fluoride sections were determined at 5, 10, 15, 20, 25, 28, 29, 30, and 32% aluminum fluoride, and the results are plotted in Fig. 2 and 3. The ternary diagram (Fig. 4) is based on these, on the revised diagram for cryolite-aluminum fluoride (see above), and on the diagram for cryolite-alumina (1) redrawn with the eutectic point at 10.2% alumina and 961°C. This ternary diagram replaces the preliminary diagram presented in the preceding paper (2). The eutectic line separating the fields of crystallization of cryolite and alumina and the isothermal contours indicating the solubility of alumina show a gradual reduction in alumina content with increasing aluminum fluoride content up to 25% of the latter. Beyond this they show a much more rapid decrease in alumina content.

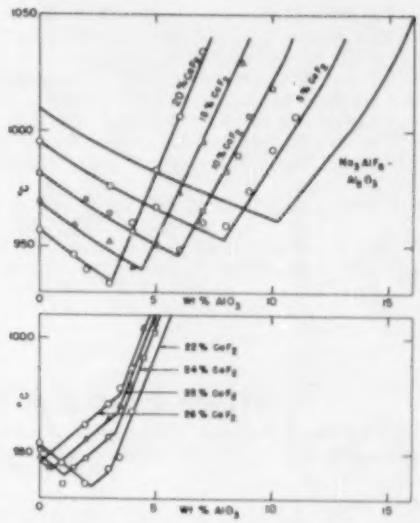

Fig. 5. Liquidus diagrams for cryolite-alumina with 0, 5, 10, 15, 20, 25, and 26% calcium fluoride.

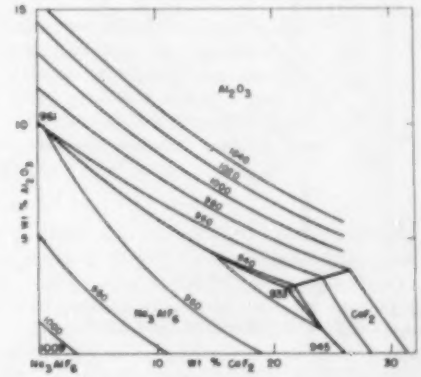

Fig. 6. Liquidus diagram for cryolite-alumina-calcium fluoride.

Kostyukov's (11) diagram for this system, based presumably on measurements by the cooling-curve method which does not adequately detect the crystallization of alumina, gives alumina solubilities which are much too high. Thus the peritectic point, at which the melt is saturated with respect to alumina, cryolite, and chiolite, is given as 5.7% alumina, 27.8% aluminum fluoride and 710°C. Also the ternary eutectic point, at which the melt would be saturated with respect to alumina, chiolite, and aluminum fluoride, is given as 3.9% alumina, 36.8% aluminum fluoride and 678°C. The more recent work of Fuseya and Takeda (12), carried out by the cooling-curve method, gave alumina contents higher than those of Kostyukov. For comparison the present work indicates that the alumina content at the ternary peritectic and eutectic points is less than 1%. It may be noted too that the results of both these laboratories for the eutectic point in the system cryolite-alumina (16 and 18% alumina, respectively) are also in error.

For the ternary system cryolite-alumina-calcium fluoride the results for sections taken at 5, 10, 15, 20,

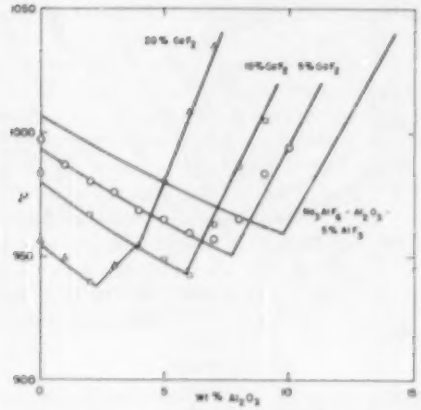

Fig. 7. Liquidus diagrams for cryolite-alumina 5% aluminum fluoride with 5, 10, and 20% calcium fluoride.

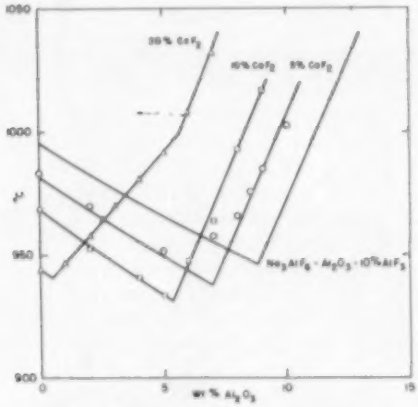

Fig. 8. Liquidus diagrams for cryolite-alumina-10% aluminum fluoride with 5, 10, and 20% calcium fluoride.

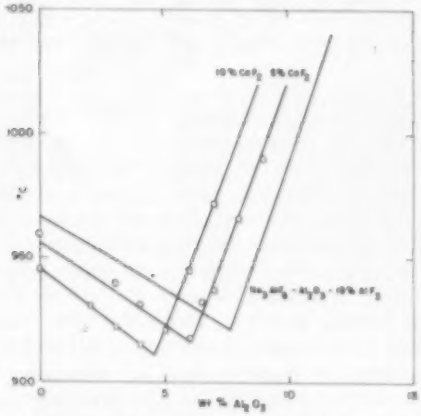

Fig. 9. Liquidus diagrams for cryolite-alumina-15% aluminum fluoride with 5 and 10% calcium fluoride.

22, 24, 25, and 26% calcium fluoride are plotted in Fig. 5. The ternary diagram, based on this and on the diagrams for cryolite-calcium fluoride and cryolite-alumina, is given in Fig. 6. It is a simple eutectic diagram with the ternary eutectic point at 2.9% alumina, 21% calcium fluoride and 933°C.

Henry and Lafky (13) determined the percentage of alumina which would dissolve in cryolite-calcium

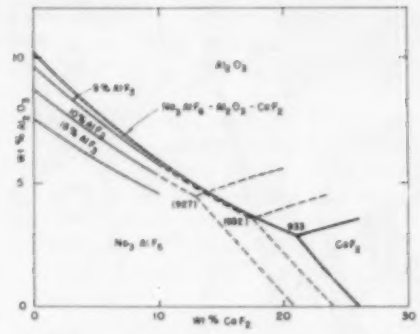

Fig. 10. Eutectic lines for cryolite-alumina-calcium fluoride with 5, 10, and 15% aluminum fluoride.

fluoride melts on prolonged stirring at a given temperature. Values at 1000°C interpolated from their results and from the present work are compared below:

	0% CaF_2	5% CaF_2	10% CaF_2	15% CaF_2
Henry and Lafky	12.0	10.3	8.5	6.8
This work	13.2	10.8	8.9	7.2

Their results are consistently slightly lower than those of the present investigation which is not unexpected in view of the methods used. Gupalo's (10) result for the ternary eutectic, 10.5% alumina, 13.6% calcium fluoride and 923°C, is quite different from that given above. Again the most likely explanation is failure to detect the initial crystallization of alumina.

The effect on the system cryolite-alumina of combined additions of 5, 10, or 15% aluminum fluoride and 5, 10, or 20% calcium fluoride was determined; results are plotted in Fig. 7, 8, and 9. Figure 10, based on these, shows the effect of 5, 10, and 15% aluminum fluoride on the eutectic lines of the system cryolite-alumina-calcium fluoride taken from Fig. 3. The field of crystallization of calcium fluoride is shifted to much lower percentages of calcium fluoride. For example, the addition of 10% aluminum fluoride shifts the ternary eutectic point from 21% calcium fluoride to approximately 13%.

In this quaternary system Abramov, Kostyukov, and Kulakov (14) have examined the pseudoternary section chiolite-alumina-calcium fluoride, which was not done by the present authors. However, in view of the method used (cooling curves and optical identification of the primary crystals) and of the discrepancy between Kostyukov's results and those reported here for the ternary system cryolite-alumina-aluminum fluoride, their alumina solubilities are most likely to be too high.

Manuscript received May 31, 1960.

Any discussion of this paper will appear in a Discussion Section to be published in the June 1961 JOURNAL.

REFERENCES

1. N. W. F. Phillips, R. H. Singleton, and E. A. Hollingshead, *This Journal*, **102**, 648 (1955).
2. N. W. F. Phillips, R. H. Singleton, and E. A. Hollingshead, *ibid.*, **102**, 690 (1955).
3. P. A. Foster, Jr., *J. Am. Ceram. Soc.*, **43**, 66 (1960).
4. P. A. Foster, Jr., *J. Phys. Chem.*, **61**, 1005 (1957).
5. Kai Grjotheim, *Kgl. Norske Videnskab. Selskabs Skrifter*, **1956**, No. 5, 1-90.

6. A. S. Dworkin and M. A. Bredig, *J. Phys. Chem.*, **64**, 269 (1960).
7. Karl A. Sense, C. A. Alexander, R. E. Bowman, R. W. Stone, and R. B. Filbert, Jr., *J. Phys. Chem.*, **61**, 384 (1957).
8. C. J. O'Brien and K. K. Kelley, *J. Am. Chem. Soc.*, **79**, 5616 (1957).
9. J. W. Johnson, Daniel Cubicciotti, and C. M. Kelley, *J. Phys. Chem.*, **62**, 1107 (1958).
10. I. P. Gupalo, Investigation of the equilibrium diagram, density and viscosity of the system cryolite-alumina-calcium fluoride, Leningrad Phys. Inst., 1952 (From A. I. Belyaev, M. B. Rapoport and L. A. Firsanova, Metallurgie des Aluminiums, Vol. 1, Berlin, VEB Verlag Technik, 1956).
11. A. A. Kostyukov, Investigation of the equilibrium diagram of the system consisting of the fluorides and oxides of aluminium and sodium. Leningrad Polytech. Inst., 1949. (Same source as ref. 10).
12. Giichiro Fuseya and Bunshichi Takeda, *J. Electrochem. Soc. Japan*, (Overseas Ed.), **27**, E 139 (1959).
13. J. L. Henry and W. M. Lafky, *Ind. Eng. Chem.*, **48**, 126 (1956).
14. G. A. Abramov, A. A. Kostyukov, and I. B. Kulakov, *Trudy Leningrad. Politekh. Inst. im M. I. Kalinina*, No. 188, 45 (1957).

The Structure of Cryolite-Alumina Melts

Perry A. Foster, Jr. and William B. Frank

Alcoa Research Laboratories, Physical Chemistry Division, Aluminum Company of America, New Kensington, Pennsylvania

ABSTRACT

The integrated cryoscopic equation, Temkin's formulation for ionic melts, and recent findings on the constitution of molten cryolite are employed to evaluate several reaction mechanisms for the solution of alumina in cryolite. The reaction mechanism that emerges as the most probable from a plot of $-\log a_s$ *vs.* $1/T$ is $3F^- + Al_2O_3 = 3/2\ AlO_3^- + 1/2\ AlF_6^{3-}$. The deviation from linearity of the plot for this reaction at high alumina contents can be attributed to some dimerization of the AlO_3^- ions to give $Al_2O_5^{2-}$ ions.

There is no method available for the direct structural evaluation of molten salts comparable to x-ray diffraction in the study of solids. A technique frequently used is to employ the integrated cryoscopic equation

$$-\ln\ a_i = (\Delta H_f/R)\,(1/T - 1/T_o) \qquad [1]$$

where a_i is the activity of the solvent, ΔH_f the cryoscopic heat of fusion of the pure solvent, T the liquidus temperature in °K, and T_o the melting point of pure solvent.

The use of this equation presupposes that ΔH_f is independently known, that ΔH_f does not vary with temperature ($\Delta C_p = 0$), that a reliable phase diagram exists from which liquidus temperatures are known over a range of compositions, and that there is no solid solubility.

Various reaction mechanisms are now hypothesized between the solvent and the solute which will permit an evaluation of the solvent activity in the liquid (a_i). For ideally behaving simple salt systems, where the solvent and solute do not dissociate, the activity of the solvent (a_i) may be equated to its weighed-in mole fraction (N_o). This criterion has been used as a test of ideality in certain molten salt systems (1). In a system such as that considered in this report, where the solvent (cryolite) dissociates on melting, knowledge of the products of dissociation and the degree of dissociation as a function of temperature is required. This information is now available for cryolite.

If the solvent activity is calculated from a reaction mechanism which properly describes the constituents present, and the system behaves ideally, a plot of $-\ln a_i$ vs. $1/T$ will be a straight line, the slope of which corresponds to the known ΔH_f.

Properties of Molten Cryolite

Dissociation of cryolite.—It is now known that cryolite dissociates partially to simpler compounds on melting. From calculations based on densities of NaF-AlF_3 melts, Frank and Foster (2) arrived at a scheme of dissociation to sodium fluoride and sodium tetrafluoaluminate, as follows:

$$Na_3AlF_6 \rightleftarrows 2NaF + NaAlF_4 \qquad [2]$$

The equilibrium constant for the reaction can be written:

$$K_D = a^2_{NaF} \cdot a_{NaAlF_4}/a_{Na_3AlF_6} \qquad [3]$$

Grjotheim (3, 4) arrived at the same scheme by an independent method, involving calculations based on a cryoscopic study of the NaF-AlF_3 system. The actual value of the dissociation constant at the melting point obtained by these two methods differs somewhat because of different approximations in the calculations. Nevertheless, this concept of molten cryolite explains so many observations of cryolite behavior that there is little doubt that the mechanism is correct.

Temperature dependence of the cryolite dissociation constant K_D.—In order to carry out the cryoscopic calculations over a range of cryolite-alumina compositions, it was necessary to know the extent of dissociation of molten cryolite as a function of temperature. The dissociation constant was determined

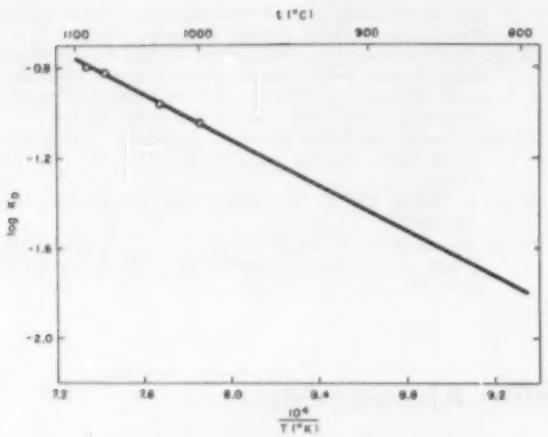

Fig. 1. Dissociation constant of cryolite as a function of temperature.

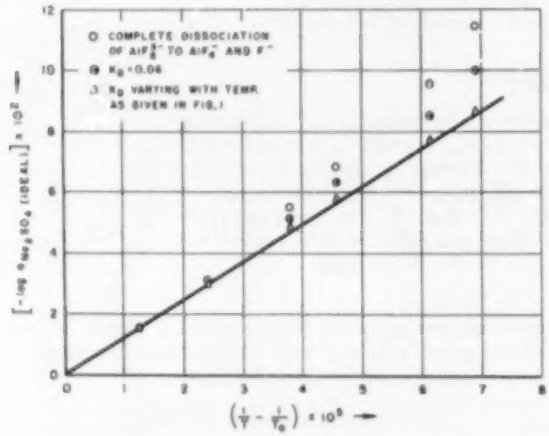
O COMPLETE DISSOCIATION OF AlF_6^{3-} TO AlF_4^- AND F^-
● K_D = 0.06
△ K_D VARYING WITH TEMP. AS GIVEN IN FIG. 1
$\left(\frac{1}{T} - \frac{1}{T_0}\right) \times 10^5$

Fig. 2. Sodium sulfate activity as a function of temperature for the system Na_2SO_4-Na_3AlF_6.

by Frank and Foster (2) at four temperatures from 1000° to 1090°C. A plot of log K_D *vs.* $1/T$ was linear and the heat of dissociation was calculated from the slope as 22.5 kcal/mole (Fig. 1).

Since the validity of calculations in the cryolite-alumina system is dependent on accurate knowledge of the cryolite dissociation, it was important to test the values of K_D in another system involving cryolite as one of the binary constituents. Grjotheim (5) reported on a cryoscopic study of the Na_2SO_4-rich side of the Na_2SO_4-Na_3AlF_6 system. The purpose of the work was to substantiate the selection of the dissociation scheme of cryolite to NaF and $NaAlF_4$ and his value of 0.06 for the dissociation constant. Results are shown in Fig. 2, where $-\log a_{Na_2SO_4}$ is plotted against $(1/T - 1/T_0)$.

The solid line represents the known calorimetric heat of fusion of sodium sulfate. The open circles give the conformity to this line when the added cryolite is considered to be completely dissociated at all concentrations. The half-filled circles show the improved conformity when Grjotheim's dissociation constant of 0.06 is used over the range of temperatures of the investigation. The triangles show the almost perfect agreement that is obtained when the variation of K_D with temperature, extrapolated from the values of Frank and Foster (2), determined in the temperature range 1000°-1090°C to the temperature of the Na_2SO_4-Na_3AlF_6 system, 800°-880°C, is used. The agreement gives confidence in the use of this information on the degree of dissociation of cryolite for further calculations in the cryolite-alumina system with liquidus temperature of 962°-1004°C.

Heat of fusion of cryolite.—Two recent calorimetric determinations of the heat of fusion of cryolite gave values of 27.91 (6) and 27.64 (7) kcal/mole. An average of 27.8 kcal is employed here. It is now recognized that this is not only the heat of fusion but also includes a heat effect due to the partial dissociation of cryolite. The true cryoscopic heat of fusion ΔH_f, for undissociated cryolite becomes

$$\Delta H_f = \Delta H_r - \alpha\,\Delta H_D \qquad [4]$$

where ΔH_r is the calorimetric heat of fusion, 27.8 kcal; α the degree of dissociation at the melting point (0.35) (from ref. 2); and ΔH_D the heat of dissociation, 22.5 kcal, for reaction [2] with reactants and products in the liquid state. A value of 19.9 kcal/mole of undissociated cryolite is obtained from Eq. [4]. This value determines the slope of the line that a given reaction scheme of cryolite and alumina must reproduce if it is to be considered valid.

The assumption that the cryoscopic heat of fusion of cryolite is independent of temperature can be shown to be valid by correcting the heat content data (6, 7) for dissociation. The four measurements of the heat content of cryolite above the melting point by O'Brien and Kelley (6) and the three measurements by Albright (7) indicate that the apparent heat capacity of the liquid is greater than the heat capacity of the solid. However, when allowance is made for the temperature dependence of dissociation and the heat of dissociation as determined by Frank and Foster (2), the heat capacities of solid and liquid cryolite are almost identical. Therefore, the assumption of a constant ΔH_f should not lead to significant error.

Activities in Cryolite-Alumina Melts

The liquidus temperatures of the cryolite-alumina system are taken from the recent work of Foster (8). These temperatures range from the melting point of cryolite (1004°) to the eutectic temperature (961°C). Only the quantity a_i, the activity of the undissociated cryolite in the melts, remains to be evaluated in Eq. [1].

Temkin ionic model for molten salts.—Temkin's formulation (9) for the activity of a component in an ionic melt is accepted. According to that model, the activity of a component M_iA_i is given by

$$a_{M_iA_i} = (n_{M_i^+}/\Sigma_i n_{M_i^+}) \cdot (n_{A_i^-}/\Sigma_j n_{A_j^-}) = X_{M_i^+} \cdot X_{A_i^-} \qquad [5]$$

where $n_{M_i^+}$ is the number of cations of species M_i, $\Sigma_i n_{M_i^+}$ the total number of cations, $n_{A_i^-}$ the number of anions of species A_i, $\Sigma_j n_{A_j^-}$ the total number of anions, $X_{M_i^+}$ the cation fraction, and $X_{A_i^-}$ the anion fraction.

The ion fractions are raised to the appropriate power indicated by the number of times a given ion

appears in the formula of the component being considered.

In mixtures of components that have a common monovalent cation, such as Na^+ in most of the cases considered in this report, the cation fraction X_{Na^+} equals unity; and it can be shown from [5] that the activities of the individual components reduce to their anion fractions $X_{A_f^-}$.[1]

Method of calculation.—From [5] it follows that the activity of cryolite a_c can be expressed as

$$a_c = X^3_{Na^+} \cdot X_{AlF_6^{3-}} \qquad [6]$$

When sodium is the only cation present in the melt, Eq. [6] can be simplified to

$$a_c = X_{AlF_6^{3-}} \qquad [7]$$

The value of the anion fraction for undissociated cryolite $X_{AlF_6^{3-}}$ is determined by the degree of dissociation α as follows. Consider the equilibrium

$$AlF_6^{3-} \rightleftarrows AlF_4^- + 2F^-$$

$$K_D = (X_{AlF_4^-}) \cdot (X_{F^-})^2/(X_{AlF_6^{3-}}) \qquad [8]$$

This expression is equivalent to Eq. [3] where K_D had been expressed in terms of activities of components rather than anion fractions.

For one mole of cryolite before dissociation, at equilibrium the number of moles of AlF_4^- is α; of F^-, 2α; of AlF_6^{3-}, $1-\alpha$; the total moles of anions, $1+2\alpha$.

The expressions for the anion fractions become:

$$\begin{aligned} X_{AlF_4^-} &= \alpha/(1+2\alpha) \\ X_{F^-} &= 2\alpha/(1+2\alpha) \\ a_c = X_{AlF_6^{3-}} &= (1-\alpha)/(1+2\alpha) \end{aligned} \qquad [9]$$

These anion fractions are substituted into Eq. [8] to give

$$K_D = 4\alpha^3/(1-\alpha)(1+2\alpha)^2 \qquad [10]$$

Since K_D is known as a function of temperature, α can be calculated, and the cryolite activity can be determined from Eq. [9].

When alumina is added to cryolite, the degree of dissociation α changes to some new value α_i that is different for different possible reaction schemes. The ion fractions, expressed as X_i, are now written in terms of both α_i and N_i, where N_i represents the weighed-in mole fractions of the starting components. The weighed-in mole fractions of cryolite and alumina are N_c and N_1, respectively ($N_c + N_1 = 1$).

For any isoplethal composition, values for T and K_D are known. An equation similar to Eq. [10] is utilized to obtain α_i. This quantity is now used in an equation similar to Eq. [9] to calculate a_c (cryolite activity). $-\text{Log } a_c$ can now be plotted against $1/T$ for each reaction mechanism. If the chosen mechanism is the proper one and the system behaves ideally, this plot should be a straight line whose slope is $\Delta H_f/(2.303R)$.

[1] The existence of a common monovalent cation permits equating the anion fraction to the simple mole fraction. This was done by Frank and Foster (*loc. cit.*) in the study of the constitution of cryolite.

Table I. Isoplethal compositions with related liquidus temperatures and cryolite dissociation constants

Wt % Al_2O_3	Weighed-in mole fraction of cryolite N_c	Weighed-in mole fraction of Al_2O_3 N_1	Liquidus temperature t °C	$10^4/T$	Cryolite dissociation constant K_D
0	1.0000	0	1004	7.830	0.0925
3.25	0.9353	0.0647	990.4	7.914	0.0845
5.16	0.8992	0.1008	981.4	7.971	0.0792
8.12	0.8459	0.1541	970.5	8.041	0.0729
10.50	0.8054	0.1946	961.6	8.099	0.0684

Possible mechanisms for the solution of alumina in cryolite.—Some of the schemes for the reaction of alumina with cryolite that have been proposed in the literature are presented below. In all but the first case, alumina is considered to be completely consumed in the formation of some new oxygen-containing species. In each case, the equilibrium between cryolite, sodium fluoride, and sodium tetrafluoaluminate is maintained. The reaction to form the oxygen-containing constituent influences this equilibrium by consuming and/or forming one of the three species, and by changing the total number of moles present.

List of Schemes

I. Simple solution, without ionization
II. $5/2AlF_6^{3-} + Al_2O_3 = 3/2AlO_2F_2^{2-} + 3AlF_4^-$
III. $AlF_6^{3-} + Al_2O_3 = 3AlOF_2^-$
IV. $AlF_6^{3-} + Al_2O_3 = 3/2Al_2O_2F_4^{2-}$
V. $Al_2O_3 = AlO^+ + AlO_2^-$
VI. $3F^- + Al_2O_3 = 3/2AlO_2^- + 1/2AlF_6^{3-}$
VII. $3F^- + Al_2O_3 = 3/4Al_2O_4^{6-} + 1/2AlF_6^{3-}$

Results

Details of the calculations for the individual schemes are given in the Appendix. The numerical values for the quantities N_c, N_1, and K_D corresponding to each liquidus temperature are listed in Table I. The values for the cryolite activity calculated for each of the seven schemes are given in Table II. The linearity of the plot of log a_c *vs.* $1/T$ and the agreement of its slope to the cryoscopic heat of fusion (19.9 ± 1.0 kcal) provide the criteria by which the schemes are evaluated. Figure 3 presents a graphical comparison of the schemes with the dashed line representing the cryoscopic heat of fusion of cryolite.

Table II. Cryolite activities for reaction schemes

Alumina content wt %	Cryolite activity a_c Scheme I	Scheme II	Scheme III	Scheme IV	Scheme V	Scheme VI	Scheme VII
0	0.3806	0.3806	0.3806	0.3806	0.3806	0.3806	0.3806
3.25	0.3670	0.3372	0.3196	0.3528	0.3429	0.3507	0.3689
5.16	0.3604	0.2986	0.2876	0.3362	0.3228	0.3314	0.3586
8.12	0.3478	0.2224	0.2399	0.3062	0.2914	0.2959	0.3345
10.50	0.3373	0.1544	0.2044	0.2800	0.2674	0.2651	0.3099

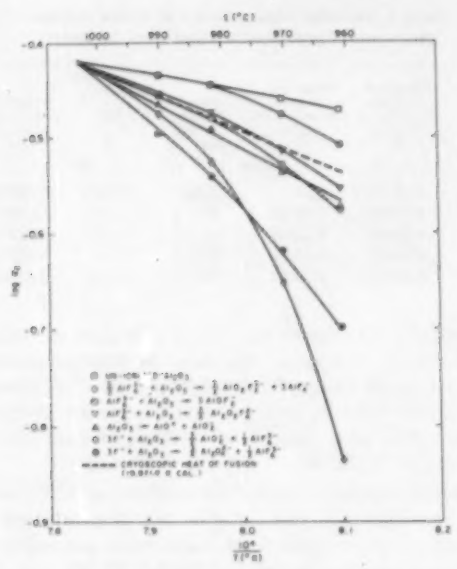

Fig. 3. Cryolite activities as a function of temperature in the system cryolite-alumina.

Scheme I, in which alumina is considered as a molecular solute, produces points falling on a line whose slope gives a low value for ΔH_f of 7.5 kcal. Schemes II, III, and V are rejected because they give high values of ΔH_f of 25 to 40 kcal in the dilute region where the curves are somewhat linear. Scheme IV ($Al_2O_3F_4^{2-}$) approximates the expected slope at low alumina concentrations. However, even the initial slope of 17.5 kcal is outside the expected error in the heat of fusion for cryolite. Scheme VII ($Al_2O_4^{2-}$) gives a low value for ΔH_f of 7.5 kcal in dilute solutions. Scheme VI (AlO_2^-) is the only scheme that reproduces the heat of fusion line in the dilute region. The points up to 5% alumina fall essentially on a line whose slope corresponds to a cryolite heat of fusion of 19.7 kcal. At higher alumina contents there is considerable deviation.

Discussion

Scheme I which produced a line whose slope gave a low value of 7.5 kcal for the heat of fusion can also be ruled out by other experimental evidence. In cryolite-alumina melts, complete exchange occurs rapidly between the aluminum of aluminum oxide and that of cryolite (10). The density of fused cryolite decreases upon the addition of the more dense aluminum oxide (11). A reaction between cryolite and alumina, rather than a physical solution of alumina in cryolite, is indicated.

Scheme VI (AlO_2^-) showed good agreement with the cryoscopic heat of fusion for alumina contents up to 5 wt %. The existence of the anion AlO_2^- in cryolite alumina melts was suggested by transport number determinations (10), viscosity and density measurements (12) in cryolite alumina melts. Sodium aluminate has been identified by x-ray powder diffraction patterns in NaF-Al_2O_3 melts quenched from above the liquidus.

It may not be unreasonable to expect that the observed deviation at higher alumina contents is due to interaction between AlO_2^- ions that gives rise to partial dimerization ($Al_2O_4^{2-}$). In the soda-alumina system, sodium aluminate ($Na_2O \cdot Al_2O_3$) is a well-established compound melting at 1650°C. The nature of its ions in the molten state is not known. Both AlO_2^- and $Al_2O_4^{2-}$ are possible anions; however, calculations of a possible equilibrium between AlO_2^- and $Al_2O_4^{2-}$ over the composition range from pure cryolite to the eutectic temperature led to an unreasonable variation in the equilibrium constant for the monomer-dimer reaction.

Although the evaluation contained in this paper cannot be interpreted as conclusive evidence of the validity of a single reaction mechanism, it is of interest to note that several proposed mechanisms can be ruled out and that the mechanism suggested by this investigation is in agreement with other experimental evidence.

Manuscript received April 22, 1960. Revised manuscript received Aug. 3, 1960.

Any discussion of this paper will appear in a Discussion Section to be published in the June 1961 JOURNAL.

REFERENCES

1. H. Flood, T. Forland, and A. Nesland, *Acta Chem. Scand.*, **5**, 1193 (1951).
2. W. B. Frank and L. M. Foster, *J. Phys. Chem.*, **64**, 95 (1960).
3. K. Grjotheim, *Kgl Norske Vidensk. Selskabs Skrifter*, **1956**, No. 5.
4. J. Brynestad, K. Grjotheim, and S. Urnes, *Z. Elektrochem.*, **63**, 707 (1959).
5. K. Grjotheim, T. Halvorsen, and S. Urnes, *Can. J. Chem.*, **37**, 1170 (July, 1959).
6. C. J. O'Brien and K. K. Kelley, *J. Am. Chem. Soc.*, **79**, 5616 (1957).
7. D. M. Albright, Thesis, Carnegie Institute of Technology (1956).
8. P. A. Foster, *J. Am. Ceram. Soc.*, **43**, 66 (1960).
9. M. Temkin, *Acta Physicochim., U.R.S.S.*, **20**, 411 (1945).
10. L. M. Foster and W. B. Frank, *J. Phys. Chem.*, **61**, 1531 (1957).
11. J. D. Edwards, C. S. Taylor, L. A. Cosgrove, and A. S. Russell, *This Journal*, **100**, 508 (1953).
12. G. A. Abramov, M. M. Vetyukov, I. P. Gupalo, A. A. Kostyukov, and L. N. Lozhkin, "Theoretical Bases of Electrometallurgy of Aluminum," Metallurgy Publishing House (1953).
13. T. Forland, H. Storegraven, and S. Urnes, *Z. anorg. u. allgem. Chem.*, **279**, 205 (1955).
14. J. F. Boner, *Helv. Chim. Acta*, **33**, 1137 (1950).
15. W. D. Treadwell, *Schweiz. Arch. angew. Wiss. u. Tech.*, **6**, 69 (1940).
16. M. Rolin, *Ann. phys.*, **6**, Series 12, 970 (1951).
17. M. Frejacques, *Bull. soc. franc. electriciens*, **9**, 684 (1949).

APPENDIX

The documentation for the complex anion product and the mathematical expressions for the cryolite activity and dissociation constant are given here.

Scheme I.—A conceivable but unlikely mechanism for the incorporation of alumina in croylite is the simple solution of un-ionized Al_2O_3 molecules. In treating this case, the Temkin model must be abandoned since there is no meaning to an "ion fraction." The cryolite activity is equated to its mole fraction, considering all components in the molecular form. At equilibrium

$$a_{Na_3AlF_6} = (N_o - N_o\alpha_i)/(2N_o\alpha_i + 1) \qquad [1]$$

The degree of dissociation α_i is calculated from the following expression for the dissociation constant

$$K_D = \left(\frac{a_i}{1-a}\right)\left(\frac{2N_o a_i}{2N_o a_i + 1}\right)^2$$

Scheme II.—Forland (13) investigated the equilibrium between carbon dioxide and molten mixtures of sodium fluoride, cryolite and aluminum oxide. The results were explained by assuming that alumina dissolves as a complex ion containing two oxygen atoms for each aluminum. Although it was difficult to determine the number of fluorine atoms in the complex, Forland suggested that two was the most probable number. The formation of this anion can be written as

$$(5/2)\,AlF_6^{3-} + Al_2O_3 \rightarrow (3/2)\,AlO_2F_2^{3-} + 3AlF_4^-$$

The anion fraction of cryolite becomes:

$$X_{AlF_6^{3-}} = (N_o - N_o a_i - (5/2)N_1)/(N_o + 2N_o a_i + 2N_1) \quad [2]$$

The value of a_i to be employed in Eq. [2] is obtained from the following expression for the dissociation constant

$$K_D = \left(\frac{2N_o a_i - 6N_o + 6}{7N_o - 2N_o a_i - 5}\right)\left(\frac{2N_o a_i}{N_o + 2N_o a_i + 2N_1}\right)^3$$

Scheme III.—Boner (14) interpreted the alumina-cryolite phase diagram and x-ray analysis of the phases in equilibrium as evidence for the existence of $AlOF_3^-$. The formation of this anion can be written as

$$AlF_6^{3-} + Al_2O_3 \rightarrow 3AlOF_3^-$$

The anion fraction for this reaction becomes

$$X_{AlF_6^{3-}} = (N_o - N_o a_i - N_1)/(N_o + 2N_o a_i + 2N_1) \quad [3]$$

The values of a_i are obtained from the following expression for the dissociation constant

$$K_D = \left(\frac{N_o a_i}{2N_o - N_o a_i - 1}\right)\left(\frac{2N_o a_i}{N_o + 2N_o a_i + 2N_1}\right)^2$$

Scheme IV.—Treadwell (15) proposed the formation of the oxyfluoride ion $Al_2O_3F_4^{2-}$ in cryolite-alumina melts. The formation of this anion can be written as

$$AlF_6^{3-} + Al_2O_3 \rightarrow (3/2)\,Al_2O_3F_4^{2-}$$

The cryolite anion fraction becomes

$$X_{AlF_6^{3-}} = (N_o - N_o a_i - N_1)/(N_o + 2N_o a_i + (1/2)N_1) \quad [4]$$

The following expression provides the values of a_i to be employed in Eq. [4].

$$K_D = \left(\frac{N_o a_i}{2N_o - N_o a_i - 1}\right)\left(\frac{2N_o a_i}{N_o + 2N_o a_i + (1/2)N_1}\right)^2$$

Scheme V.—Rolin (16) concluded, from the results of a cryoscopic study of the cryolite-alumina system, that the dissociation of alumina can be represented by the equation

$$Al_2O_3 \rightarrow AlO^+ + AlO_2^-$$

The cryolite anion fraction becomes

$$X_{AlF_6^{3-}} = (N_o - N_o a_i)/(N_o + 2N_o a_i + N_1) \quad [5]$$

The following equation is solved for a_i,

$$K = \left(\frac{a_i}{1-a_i}\right)\left(\frac{2N_o a_i}{N_o + 2N_o a_i + N_1}\right)^3$$

and $X_{AlF_6^{3-}}$ is calculated by substituting this value of a_i into Eq. [5]. However, in this case the expression does not represent the activity of the solvent, cryolite, since the cation fraction is not unity and must be evaluated also.

The cation fraction of sodium can be expressed as

$$X_{Na^+} = (3N_o)/(3N_o + N_1) \quad [6]$$

The cation-anion fraction product becomes

$$a_c = X_{Na^+}{}^3 \cdot X_{AlF_6^{3-}}$$

Substitution of expressions for anion and cation fractions, (Eq. [5] and [6]) yields

$$a_c = \left(\frac{3N_o}{3N_o + N_1}\right)^3\left(\frac{N_o - N_o a_i}{N_o + 2N_o a_i + N_1}\right)$$

Scheme VI.—Transport number determinations (10) in cryolite-alumina melts and viscosity and density measurements (12) suggest the existence of the aluminate ion. The formation of this anion can be written as

$$3F^- + Al_2O_3 \rightarrow (3/2)\,AlO_3^- + (1/2)\,AlF_6^{3-}$$

The cryolite anion fraction becomes

$$X_{AlF_6^{3-}} = (N_o - N_o a_i + (1/2)N_1)/(N_o + 2N_o a_i - N_1) \quad [7]$$

From the following expression for the dissociation constant, values for a_i are obtained

$$K_D = \left(\frac{N_o a_i}{N_o - N_o a_i + (1/2)N_1}\right)\left(\frac{2N_o a_i - 3N_1}{N_o + 2N_o a_i - N_1}\right)^2$$

Scheme VII.—Frejacques (17) postulated the existence of the compound $Na_3Al_2O_4$ in cryolite-alumina melts. The formation of the anion of this compound may be written as

$$3F^- + Al_2O_3 \rightarrow (3/4)\,Al_2O_4^{3-} + (1/2)\,AlF_6^{3-}$$

The cryolite anion fraction becomes

$$X_{AlF_6^{3-}} = (N_o - N_o a_i + (1/2)N_1)/(N_o + 2N_o a_i - (7/4)N_1) \quad [8]$$

The values of a_i to be used in Eq. [8] are obtained from the following expression of the dissociation constant

$$K_D = \left(\frac{N_o a_i}{N_o - N_o a_i + (1/2)N_1}\right)\left(\frac{2N_o a_i - 3N_1}{N_o + 2N_o a_i - (7/4)N_1}\right)^2$$

Technical Notes

On the Role of the Oxygen Concentration Cell in Crevice Corrosion and Pitting

G. J. Schafer, J. R. Gabriel,[1] and P. K. Foster

Department of Scientific and Industrial Research, Dominion Laboratory, Wellington, New Zealand

Uhlig (1) states that contact corrosion of stainless steels ". . . proceeds by a mechanism identical to that described . . . for pit growth." In the case of stainless steel others also have recognized the similarity between crevice corrosion and pitting (2), but it does not appear to have been suggested to date that the two processes are identical for any metal in any electrolyte. Possibly because of the obvious difficulties associated with measurements on pits or crevices, relatively few fundamental investigations appear to have been attempted. However, Ulanovskii and Korovin (3) showed that the solution in stainless steel crevices corroding in sea water reached pH values of about 3 while Rozenfeld and Marshakoff (4) showed that the solution pH in corroding aluminum crevices also falls below that of the bulk of the solution. (They also suggested that this low pH is more important than differential aeration after corrosion has been initiated.)

The acid nature of the solution in pits has been demonstrated for a number of metals (5, 6) and Hoar's acid theory (7-9) is at present probably the most generally accepted explanation of the pitting attack on many metals.

So it can be said that in all cases investigated, the solution pH fell at sites of local corrosion.

No oxygen concentration measurements in corroding pits and crevices have been located by the authors, but Evans and others have postulated that crevice corrosion is initiated by local exhaustion of oxygen (or inhibitor) in a crevice (10-12) while May (13) concluded that the pitting of copper in waters containing chloride was dependent on the interaction of anodically produced cuprous chloride with oxygen diffusing towards the anode, and Streicher (2) attributed stainless steel pitting to the joint action of differential acid and oxygen concentration cells.

Thus, while there is no direct evidence, it is widely held that pitting and particularly crevice corrosion are influenced by the action of differential aeration cells.

Another mechanism known as the metal ion concentration cell is well established in the literature but has been shown to be invalid (14) (see also Appendix I).

[1] Present address: Atomic Energy Research Establishment, Harwell, England.

In the present work it is suggested that pitting and crevice corrosion are identical processes, each depending on the conjoint action of the acid mechanism and differential aeration. To support this hypothesis two arguments are advanced against a differential aeration cell mechanism as the sole agent responsible for any localized corrosion.

1. Unless oxygen is used up at anodes, a self-supporting steady-state system depending solely on differential aeration is impossible. This is shown as follows: The differential aeration cell mechanism assumes that oxygen concentration on a particular anode is smaller than on adjacent cathodes. Oxygen concentration on an anode must therefore either be constant or reach a minimum value.

Consider a steady-state differential aeration system in which oxygen is transported by diffusion only, oxygen is used up only at cathode areas, no oxygen is evolved anywhere, and anodes of finite area exist.

Let C be the oxygen concentration.

At anodes no oxygen is consumed or produced, so $\text{grad}_n C = 0$ on the anode surface. It follows that C cannot be constant on the anode because if so, calculation of C and ∇C at a point close to the anode by Taylor's series would show that C and ∇C had not changed on moving off the surface. The Taylor series calculation then could be repeated for a point a little further away and so on, until it was shown that C = constant everywhere and $\nabla C = 0$ everywhere. This corresponds to the case where no corrosion action takes place and is of no interest.

Since oxygen flow is always toward cathodes, there can be no minimum of C on an anode surface, and any minima of C must be on cathodes. Since oxygen concentration is a continuous function of position, this implies that, for any anode-cathode interface in the type of system considered, there must be points on the cathode side of the interface (perhaps only very close to the interface) where the oxygen concentration is smaller than the concentration at some place on the anode side of the interface (perhaps relatively far from the interface). But this is contrary to hypothesis because it is implicit in the concept of a differential aeration cell that oxygen concentration must always be greater at cathodes than at anodes.

The only way to resolve this difficulty while retaining the requirement of steady state is to assume either that only point anodes exist, or that oxygen is consumed at anodes. The former assumption is untenable because infinite anode current densities would occur, hence oxygen must be consumed at anodes.

However, the oxygen which must be used at anodes in general represents anode corrosion due to local microcell action. Hence local microcell action at anodes is essential for the working of a self-supporting differential aeration cell and must contribute to the dissolution of metal. In other words, if the current flowing between the anodic and cathodic regions were measured, it would not be found to account for all of the observed corrosion.

2. The differential aeration mechanism itself, if considered in detail, leads to differential acid concentrations. For if a differential aeration mechanism causes localized corrosion, the pH of the solution at anodic areas must become lower than the pH of the solution at cathodic areas due to the preponderance of metal ion production and oxygen depolarization at the two respective surfaces.

It is therefore postulated that after the mechanism which determines the site of corrosion initiation has ceased to operate (*i.e.*, as soon as localized attack has begun), for any particular metal in a certain medium, exactly the same mechanism operates in the case of pitting and crevice corrosion. So in many cases of crevice corrosion it is probably an acid mechanism which chiefly accounts for the localized nature of the attack. The local exhaustion theory accounts mainly for the position at which attack is initiated.

It may be noted that the operation of an acid mechanism corrosion cell *ipso facto* produces a differential aeration effect because the microcell corrosion due to acid conditions uses up oxygen. So if, for example, a pit is initiated on a piece of stainless steel either by oxygen starvation or by acid attack (other things being equal), the final corroding systems should be identical.

Important factors such as active-passive cells (*e.g.*, stainless steels) and oxygen-absorbing anodic corrosion products (*e.g.*, copper) have not been discussed here because, while they may influence the relative importance of the differential aeration and the differential acid concentration cells, the above arguments are basically unaffected.

Conclusion

It is proposed that the crevice corrosion mechanism must, like pitting (2, 15), be divided into two stages. A differential aeration or inhibitor exhaustion mechanism is decisive in determining the locations at which crevice corrosion is initiated. After initiation, however, continued crevice corrosion depends also on the acid mechanism frequently used to explain the autocatalytic nature of pitting.

The presence of oxygen as a depolarizing agent is still essential, but not in the sense of a differential aeration mechanism. The following example illustrates this point. Copper corrodes only very slowly in oxygen-free HCl, but if oxygen is added corrosion occurs rapidly (1). Thus oxygen is necessary as a depolarizing agent for the corrosion of copper in HCl, but differential aeration plays no part.

Pitting is considered to be merely a limiting case of crevice corrosion, the difference being that macroscopic geometrical factors determine the initiation sites of crevice corrosion, while random microscopic factors usually determine the sites of initiation of pitting corrosion. For any particular metal, steady-state pitting and crevice corrosion occur by identical mechanisms involving the conjoint action of differential acid concentrations and differential oxygen (or other depolarizer) concentrations.

Acknowledgments

The authors wish to thank Mr. A. McNabb and other members of the Applied Mathematics Laboratory, Wellington, for helpful discussions, and the Director for permission to publish this work.

Manuscript received July 25, 1960.

Any discussion of this paper will appear in a Discussion Section to be published in the June 1961 JOURNAL.

REFERENCES

1. H. H. Uhlig, "Corrosion Handbook," John Wiley & Sons, Inc., New York (1948).
2. M. A. Streicher, *This Journal*, **103**, 375 (1956).
3. I. B. Ulanowskii and Iu. M. Korovin, *J. Appl. Chem. (U.S.S.R.)* (English translation), **31**, 1352 (1958).
4. I. L. Rozenfeld and I. K. Marshakoff, *J. Phys. Chem. (U.S.S.R.)*, **31**, 2328 (1957).
5. T. Hagyard and J. R. Santhiapillai, *J. Appl. Chem.*, **9**, 323 (1959).
6. W. Feitknecht, *Chem. and Ind.*, **1959**, 1102.
7. T. P. Hoar, *Trans. Faraday Soc.*, **33**, 1152 (1937).
8. T. P. Hoar, *ibid.*, **45**, 683 (1949).
9. T. P. Hoar, *Discussions Faraday Soc.*, No. 1, 299 (1947).
10. U. R. Evans, "Metallic Corrosion Passivity and Protection," p. 496 *et seq.*, Edward Arnold & Co., London (1946).
11. U. R. Evans and D. E. Davies, *J. Chem. Soc.*, **1951**, (3), 2607.
12. U. R. Evans, L. C. Bannister, and S. C. Britton, *Proc. Roy. Soc.*, **A131**, 355 (1931).
13. R. May, *J. Inst. Metals*, **82**, 65 (1953-1954).
14. G. J. Schafer and P. K. Foster, *This Journal*, **106**, 468 (1959).
15. P. M. Aziz and H. P. Godard, *Ind. Eng. Chem.*, **44**, 1791 (1952).
16. I. K. Marshakoff and I. L. Rozenfeld, *J. Phys. Chem. (U.S.S.R.)*, **33**, 219 (1959).
17. I. L. Rozenfeld and I. K. Marshakoff, *ibid.*, **30**, 2724 (1956).

APPENDIX I

The experiments of Marshakoff and Rozenfeld on copper crevice corrosion (16) call for some comment. It has been proved that the metal ion concentration cell cannot be a cause of steady-state crevice corrosion (14), (or, for that matter, any other type of localized corrosion), but Marshakoff and Rozenfeld concluded that metal ion concentration cells were in fact operative in their experiments.

We agree with their interpretation, but we consider that the experiments were designed wrongly, and while in the cases of the other metals investigated this has only quantitatively influenced the results, in the case of copper it has lead to wrong conclusions.

Our objection is that the electrolyte used in many of the experiments (and in particular the experiments on copper) was far too aggressive.

Crevice corrosion is not a serious hazard in situations where the electrolyte causes general attack of freely

Fig. 1. Section of a brazed seam from a copper water tank. Slight general attack of the copper on the inside surface has occurred. There is no special corrosion at the crevice mouth, but the copper has been attacked locally at a number of places inside the crevice. Specimens of this kind, where crevice corrosion has occurred in the absence of interfering effects are relatively rare in our experience. Magnification 9X before reduction for publication.

exposed metal (*e.g.*, copper in 2*N* NaCl solution). As shown by Marshakoff and Rosenfeld in the cases of iron (17) and copper (16) immersed in 2*N* NaCl solution, corrosion in the crevices is less severe than corrosion of the freely exposed metal surfaces, and the electrical coupling of crevices to freely exposed metal produces only small changes in this state of affairs. Thus the crevice corrosion mechanisms are inevitably masked to a greater or lesser extent by the general corrosion taking place.

Crevice corrosion is most serious and most apparent when the freely exposed metal is relatively immune to attack and metal dissolution occurs predominantly at crevices. Only under such conditions (which usually involve a much less aggressive medium than 2*N* NaCl) is it likely that mechanisms can be successfully investigated, because the interfering general corrosion is absent.

We consider the metal ion concentration effects observed by Marshakoff and Rozenfeld to be a *result* of the general corrosion caused by the aggressive electrolyte, inside and outside the copper crevice and not the *cause* of any corrosion. In the absence of the aggressive electrolyte their experimental results would have been quite different.

A further objection to the metal ion concentration cell mechanism is that it offers no explanation for the local nature of the attack at the crevice mouth referred to by Marshakoff and Rozenfeld. In a high conductivity electrolyte such as 2*N* NaCl or sea water, corrosion would be expected to spread evenly over large areas of freely exposed metal surrounding a crevice. Also crevice corrosion of copper does not always occur at the crevice mouth (Fig. 1).

Electrodeposition of Pure Copper

Sidney Barnartt

Research Laboratories, Westinghouse Electric Corporation, Pittsburgh, Pennsylvania

Electrodeposition is attractive as a method of preparing copper plates having known added impurities. Such copper test plates are useful for oxidation to cuprous oxide semiconductors in the study of rectifiers and photovoltaic cells. As a starting point, however, a method of electrodepositing high-purity copper is necessary. The present report deals with this phase. After sufficient purity is achieved, certain metallic impurities may be incorporated one at a time by addition of an appropriate salt to the electrolyte.

Smart, Smith, and Phillips (1) have described the complex purification method used by the American Smelting and Refining Company (ASR). This involved ferric hydroxide precipitation, sulfide precipitation, electrodeposition from a sulfate solution, oxidation of the molten metal, electrodeposition from a nitrate solution, and finally melting in a high-purity graphite crucible. A much simpler procedure on a smaller scale, involving one electrodeposition step and no subsequent melting, is reported here. Data on the degree of purity attained are presented.

Procedure

The electrolyte used was $CuSO_4$-0.6M, H_2SO_4-0.8M. This was prepared from $CuSO_4 \cdot 5H_2O$ (tested-purity reagent from a single manufacturer's lot number), redistilled water, and distilled H_2SO_4 obtained by fractional distillation in all-Pyrex stills. The copper sulfate was first dissolved in water, and a solution of

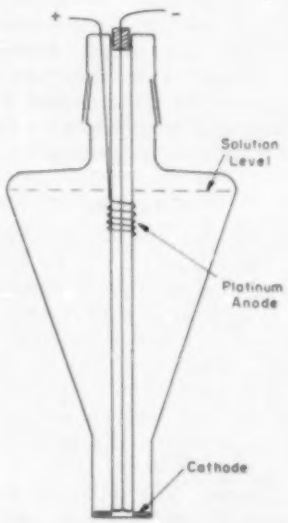

Fig. 1

reagent grade $Na_2S \cdot 9H_2O$ added to a concentration of 6×10^{-5}M. After heating to 70°C and cooling overnight, the mixture was decanted and filtered by suction through a fritted Pyrex filter ("ultrafine" porosity). The H_2SO_4 was then added and the volume adjusted.

Electrodeposition was carried out at 30°C and a cathode current density of 50 ma/cm². The Pyrex cell used is shown in Fig. 1 and was a modified inverted Erlenmeyer flask having a flat bottom. The cap of the cell held the platinum wire anode which surrounded a central vertical tube, into the bottom of which a platinum lead was sealed and protruded sufficiently to contact the cathode washer at its inner edge. The cathode diameters, 1.3 cm inner x 3.8 cm outer, closely matched the diameters of the central tube and catholyte well. The cylindrical catholyte well was 5.1 cm high and contributed to uniformity of current distribution over the cathode. All deposits were approximately 180μ in average thickness. After being stripped from the base metal and trimmed to 3.6 cm OD x 1.5 cm ID, they had a thickness variation of less than ±5%.

The cathode was a stainless steel washer having rounded edges. It was preplated with copper to a thickness of 2μ in an auxiliary acid copper bath, purified copper was deposited to the desired thickness, and then the edges of the deposit were cut to release the copper disk. The latter was treated anodically in an alkaline cyanide solution to dissolve 2.5μ of copper, thus removing the preplate layer. Final cleaning before analytical or residual resistivity measurements comprised "bright dip" in HNO_3-H_2SO_4-HCl solution followed by 10% HNO_3, redistilled water, and absolute alcohol.

Copper deposition from the acid sulfate electrolyte used resulted in a reduction of the $CuSO_4$ concentration and an increase in H_2SO_4 concentration. The solution was readjusted to the original composition after each washer was plated by removing 50 cc of the electrolyte and adding 50 cc of a purified replenishing solution having the appropriate $CuSO_4$ and H_2SO_4 concentration. By this means the solution composition was maintained constant to within ±2.5%.

Spectroscopic analysis was used for determination of metallic impurities in the copper. Arc-spectra of 50 mg samples were obtained and compared with similar spectra for high-purity copper standards.[1] Oxygen was determined on 0.7-g samples by the vacuum-fusion method, and sulfur on 1.5-g samples by a combination vacuum-fusion and mass-spectrometric procedure as described by Hickam (2, 3). Residual resistivity measurements were made on strips cut from the electrodeposit, which were vacuum annealed at 900°-940°C for 15 hr at a pressure of 10^{-4} mm Hg. On each sample resistivities measured at 4.2° and 1.9°K agreed within ±1%.

Results

The cathodic copper deposits 180 μ thick had very smooth, matte surfaces. Analyses of these deposits are given in parts per million (ppm) in Table I. Over 30 elements not listed in the table were found to be absent in the relatively sensitive arc spectra obtained. The indicated purity is 99.999+%, similar as far as is known to that of the elaborately purified ASR copper. Analytical data reported for the latter (1) are listed in the table for comparison. Actual measurements of oxygen concentration were not reported for the ASR metal, but this certainly would be less than our value of 3 ppm because ASR copper was melted in high-purity graphite as a final step.

Table I. Copper analyses, ppm

Element	Electrodeposited copper (this report)	ASR copper (1)
O	3	
S	<1	<1
Fe	<1	<0.7
As	<0.3	<2
Sn	0.2	<1
Ag	<0.1	<0.3
Pb	0.05	<1
Sb	<0.05	<1
Bi	<0.03	<0.1
Cr	Not detected	<0.5
Te		<2
Se		<1
Ni	Not detected	<1
Si	Detected*	<0.1
Mg	Detected*	
Mn	Detected*	
Zn	Detected*	

* At limit of detectability, no standards available.

Table II. Residual resistivities of polycrystalline copper

Copper used—reference	Vacuum-annealing temperature, °C	$10^{9}\rho_{4.2°}/\rho_{273.2°}$
Electrodeposited—this report	900-940	1.6-2.0
ASR—MacDonald and Pearson (4)	(as cast in graphite)	9.8
ASR—Kropschot, Garber, and Blatt (5)	950	1.85
ASR—White and Woods (6)	530	1.62
ASR—Powell, Roder, and Hall (7)	400	0.65
ASR—White and Tainsh (8)	530	0.56

Our residual resistivity measurements are compared in Table II with measurements on ASR copper, which has been studied by several authors.[2] The latter values vary over a wide range. It has been shown that the residual resistivity of high-purity copper is markedly dependent on annealing temperature and on slightly oxidizing or reducing conditions during the annealing procedure (4, 9), as well as on impurities unintentionally introduced. For annealing temperatures of 900°-950° the residual resistivities of the two types of copper are in excellent agreement, even though the ASR metal had been melted previously while the electrodeposited was not. This would indicate the same effective impurity concentration, but the agreement is probably fortuitous. Thus one can conclude only that the low value of residual resistivity found for the electrodeposited copper indicates high purity; a reliable purity rating relative to ASR copper is not possible from the data in Table II.

[1] Adam Hilger Ltd. (Johnson Matthey Ltd., England).

[2] It is assumed that the high-purity ASR copper obtained by each of these groups was metal prepared by the method of Smart, Smith, and Phillips (1).

Because of the high purity achieved, the simplified preparation described herein provides an attractive starting point for laboratory studies on copper having controlled added impurities, the impurities being added to the plating bath.

Acknowledgment

The collaboration of M. P. Garfunkel on residual resistivity measurements is gratefully acknowledged. Analytical data were contributed by Miss J. Senko, W. M. Hickam, and W. F. Harris.

Manuscript received July 1, 1960.

Any discussion of this paper will appear in a Discussion Section to be published in the June 1961 JOURNAL.

REFERENCES

1. J. S. Smart, A. A. Smith, and A. J. Phillips, *Trans. A.I.M.E.*, **143**, 272 (1941).
2. W. M. Hickam, *Anal. Chem.*, **24**, 362 (1952).
3. W. M. Hickam, ASTM Publication 149, p. 17 (1953).
4. D. K. C. MacDonald and W. B. Pearson, *Acta Met.*, **3**, 392 (1955).
5. R. H. Kropschot, M. Garber, and F. J. Blatt, *Phys. Rev. Letters*, **2**, 91 (1959).
6. G. K. White and S. B. Woods, *Phil. Trans.*, **A251**, 273 (1959).
7. R. L. Powell, H. M. Roder, and W. J. Hall, *Phys. Rev.*, **115**, 314 (1959).
8. G. K. White and R. J. Tainsh, *Phys. Rev.*, **119**, 1869 (1960).
9. S. T. Sekula, *Phys. Rev. Letters*, **3**, 416 (1959).

Some Observations on the System ZnS-AlP

Arrigo Addamiano

Lamp Research Laboratory, General Electric Company, Nela Park, Cleveland, Ohio

Zinc sulfide phosphors with phosphorus activator and chlorine coactivator have been described by McKeag and Ranby (1). More recently Apple (2) has shown that, under special conditions (presence of Cu activator), phosphorus and other group V elements can behave as coactivators in zinc sulfide. We have made some observations on the related system ZnS-AlP. Our work is in agreement with the investigations mentioned above and with the theory of charge compensation of Kröger and Dikhoff (3).

Interest in the system ZnS-AlP was motivated by the close similarity in crystal structure of the two substances, accompanied by a large difference in the band gaps (3.7 e.v. for ZnS, and 3.0 e.v. for AlP). The low-temperature modification of zinc sulfide has the cubic zinc-blende structure with a cell edge (4) of 5.4060Å. Aluminum phosphide also crystallizes with the zinc-blende structure and a lattice parameter (5) $a_o = 5.451$Å. The bonds in these compounds are at least partly covalent, and a comparison of the tetrahedral covalent radii of the atoms, as given by Pauling (6), (Zn 1.31Å; Al 1.26Å; P 1.10Å; S 1.04Å) shows relatively small differences.

For the study of the solubility of AlP in ZnS we used luminescent grade zinc sulfide (prefired in H_2S) and aluminum phosphide prepared as described in another paper (5). Intimate mixtures of fine powders of the two substances, with different molar content of AlP (0.5; 1.0; 5.0; 10; 20; 40; 60; 80%) were sealed in fused silica tubes in an argon atmosphere (measuring 200 mm at room temperature) and were fired 24 hr at 900°C. When the furnace was cool the tubes were extracted and the products obtained examined by x-ray diffraction using a GE-XRD3 diffractometer. For comparison x-ray data were collected also for pure ZnS and AlP, and for the unfired mixtures. Emission spectra under 3650Å and other optical data for the fired mixtures were obtained using a grating spectrophotometer.

The analysis of the x-ray diffraction data was delicate because most of the low-θ lines of zinc blende and aluminum phosphide overlap, while the high-θ lines are relatively weak. For a content of aluminum phosphide between 10 and 80 mole % the patterns of β-ZnS and AlP are clearly discernible, the high-θ reflections well resolved, and no other lines are present. For a content of AlP less than 10% the pattern of AlP does not show up either above the background in the fired samples or in the unfired mixtures. Yet, since no shift of the high-θ lines appears in the pattern of zinc sulfide, the conclusion is reached that the solubility of AlP in ZnS is very small, probably about 1 mole % or less. This conclusion is in agreement with the finding of McKeag and Ranby (1) who did not find "any significant deviation in structure" for their phosphorus activated zinc sulfide phosphors as compared to unactivated zinc sulfide.

To further check this point we have reacted a mixture of Zn_3P_2 and Al_2S_3 in a sealed quartz tube in an argon atmosphere at 900° for 24 hr. X-ray analysis of the products so obtained showed that an almost complete reaction had occurred, with disappearance of the patterns of Zn_3P_2 and Al_2S_3 and appearance of the patterns of AlP and ZnS.[1]

As for the emission spectra under u.v. (3650Å) irradiation, a bright yellow emission is present at liquid air temperature in all the fired mixtures for concentrations of AlP up to 80%. At room temperature, however, the yellow band appears only in the samples with small amounts of AlP added(up to about 10%), the brightness being a maximum in the interval 0.5-1.0% AlP. The maximum in the emission curve in the yellow region is at about 5750Å. A typical emission curve is shown in Fig. 1. Except for a shift of the emission peak, which may be due,

[1] A trace of zinc metal was also found. This is believed to be due to reaction between excess aluminum present in the commercial Al_2S_3 used and either Zn_3P_2 or ZnS.

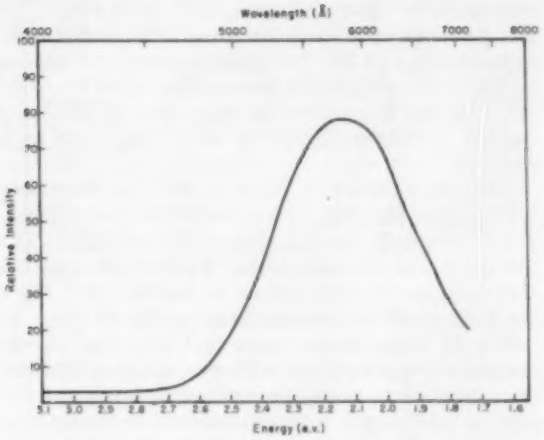

Fig. 1. Emission spectrum for ZnS:P,Al phosphors prepared with 1 mole % AlP added. Excitation by $\lambda = 3650$Å.

at least in part, to differences in experimental conditions, this emission closely resembles that observed by McKeag and Ranby in ZnS:P,Al phosphors prepared at 900°-1000°C. This similarity in the emission spectra of ZnS:P,Cl and ZnS:P,Al lends strong support to the theory of charge compensation (3) according to which a trivalent cation (Al) as coactivator should behave in the same way as a monovalent anion (Cl) coactivator.[2] It can be assumed that in ZnS:P,Al phosphorus substitutes for sulfur and aluminum substitutes for zinc.

[2] Note: It should be noted that, as mentioned by Apple (2), ZnS:P without coactivator is practically nonluminescent when prepared in H_2S at 950°.

We may summarize the results of the present investigation by saying that ZnS:P,Al phosphors with yellow emission can be prepared by diffusion of AlP in ZnS at 900°. In spite of the similarities in crystal structure and covalent atomic radii between ZnS and AlP the solubility of AlP in ZnS is very limited, probably not in excess of 1 mole %. The existence of ZnS:P,Al phosphors with emission similar to that of ZnS:P,Cl phosphors brings further support to the theory of charge compensation and shows that in ZnS:P,Al phosphors, P is the activator and Al the coactivator atom.

Acknowledgments

The author wishes to thank Dr. Eugene Apple for criticism and suggestions, Dr. Ralph M. Potter for his assistance in the measurement of the emission spectra and for critically reading the paper, and Miss Jeanette R. Cooper for the x-ray data.

Manuscript received July 13, 1960.

Any discussion of this paper will appear in a Discussion Section to be published in the June 1961 JOURNAL.

REFERENCES

1. A. H. McKeag and P. W. Ranby, *J. (and Trans.) Electrochem. Soc.*, **96**, 85 (1949).
2. E. F. Apple, *This Journal*, **106**, 271 (1959).
3. F. A. Kröger and J. Dikhoff, *Physica*, **16**, 297 (1950).
4. A.S.T.M. File Index, Card No. 5-0566.
5. A. Addamiano, *J. Am. Chem. Soc.*, **82**, 1537 (1960).
6. L. Pauling, "The Nature of the Chemical Bond," 2nd ed., p. 179, Cornell University Press, Ithaca, N. Y. (1940).

High-Temperature Base-Tab for Silicon

Leon Maissel[1]

Research Division, Philco Corporation, Philadelphia, Pennsylvania

In the course of recent work in silicon transistor development, the need arose for a base-tab that could be attached to the silicon blank early in the manufacturing process so as to serve as a holder for the silicon during subsequent steps. As temperatures in excess of 800°C occurred during one or more of these steps, it was not possible to use a conventional gold solder which fuses at approximately 360°C.

The following are the general requirements for a satisfactory base-tab solder: (i) It should readily wet the semiconductor when melted in contact with it. The existence of a eutectic reaction between solder and semiconductor guarantees this. (ii) It should be sufficiently ductile so that considerable mismatch between its coefficient of thermal expansion and that of the semiconductor can be accommodated without undue strain being introduced in the joint. Conversely, if it has a coefficient of expansion close to that of the semiconductor, it need not be so ductile. (iii) It should "dope" the region near the tab to the same type (n or p) as the rest of the semiconductor; otherwise a rectifying junction may be formed. Correct doping can be insured in practice by including a trace of suitable impurity in the solder. (iv) It should substantially reduce the minority carrier lifetime in the vicinity of the junction. Without this quality the junction, although nonrectifying, may still not be entirely ohmic. For a sufficiently potent lifetime killer, condition (iii) disappears.

Also the material of the tab itself should match the semiconductor reasonably well with regard to coefficient of expansion but, as is the case for the solder, considerable mismatch can be accommodated if the latter is sufficiently ductile.

Gold satisfies these requirements very well, but in choosing a solder having more favorable high-temperature properties than gold, platinum was considered to have the most promise. It has a eutectic reaction with silicon at 830°C (1) and possesses high ductility (2). Its effect on minority carrier lifetime in silicon was not known, but it is not one of the

[1] Present address: IBM Corp., Product Development Lab., Poughkeepsie, N. Y.

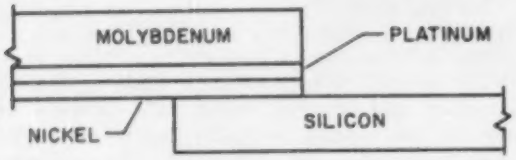

Fig. 1

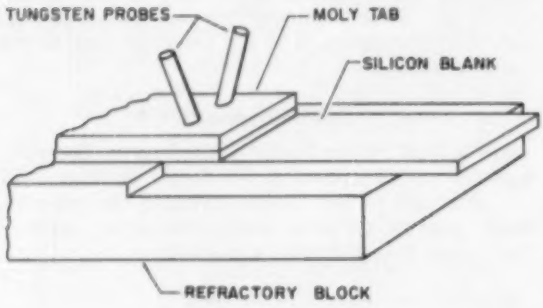

Fig. 2

recognized dopants so that it should be possible to satisfy condition (iii) for both n- and p-type silicon. Molybdenum was selected for the tab itself, having a coefficient of expansion fairly close to silicon (3) over the temperature range concerned as well as a high melting point.

Preliminary experiments showed that molybdenum could be bonded to silicon by means of platinum, but that the resulting joint had unexpectedly poor thermal properties. It was postulated that platinum ductility was being reduced by the formation of intermetallic compounds with silicon. In an attempt to reduce this effect, a number of additives to the platinum were investigated, and it was found that the introduction of a nickel layer about one third the thickness of the platinum produced a joint that was substantially strain-free and capable of temperature cycling over a wide range. This result was also somewhat unexpected since a pure Si-Ni-Mo joint was found to crack immediately on cooling. The fact that the Ni-Pt bond was much more strain-free than that using pure Pt suggested that either the Ni-Pt was more ductile than pure Pt, that the Ni-Pt matched the silicon more closely in expansion coefficient, or that Ni was suppressing the formation of Si-Pt intermetallic compounds as postulated above. Evidence against the first two mechanisms was provided by the fact that a bond formed between elements in the order Si-Pt-Ni-Mo was almost as badly strained as the straightforward Si-Pt-Mo bond, whereas the Si-Ni-Pt-Mo bond was substantially strain-free. Figure 1 shows in cross section the structure that was found best suited for joining a 5-mil molybdenum tab to a 5-mil silicon blank.

In order to prepare the tabs and bond them in a reproducible manner the following scheme was devised.

First, 5-mil Mo sheet was cleaned by scrubbing in detergent. It was then anodized in a mixture of concentrated sulfuric and phosphoric acids, dipped in a strongly alkaline solution (in this case, Lectrite N.F.) and, after rinsing, immediately given a chrome strike coat (100 to 1, CrO_3 to H_2SO_4). This was followed by a Ni strike from a standard Wood's bath after which the Pt (approximately 0.2 mils as in Fig. 1) was deposited from a solution of Platanex III.[2] The Mo was plated on both sides to protect it against oxidation during its subsequent life as a base-tab.

Following the Pt, a layer of Ni (approximately 0.1 mil thick as in Fig. 1) was deposited from a standard Watt's bath (on one side of the Mo only). The Mo sheet was cut into strips 75 mils wide and 200 mils long and bonding to the Si blanks (75 x 150 x 5 mils) was effected as illustrated in Fig. 2.

The Si blank was dipped in HF, rinsed in deionized water, dried in dry filtered air, and then laid on a refractory block, the moly-tab being pressed against it by means of two tungsten rods (or probes) as shown. Heat was produced by passing current between the probes for a pre-set period of time. For consistent results it was necessary to perform the operation in an inert atmosphere. Nitrogen does not qualify as an inert atmosphere in this instance. It was extremely important to be certain that pressure was applied uniformly by the two tungsten probes; otherwise the solder wetted only in the area of highest pressure and, in some cases, even penetrated to the other side of the Si. Optimum results were obtained by heating at approximately 1,000°C for 10-15 sec. A suitable material for the refractory block was difficult to find, the only really satisfactory one being carbon. Because of the mechanical weakness of pure carbon, in practice a block of alundum, having its surface coated with graphite, was used. The graphite coating had to be renewed frequently.

Low resistance ohmic contact could be made to p-type but not to n-type Si by this process. Spectrographic analysis of the Ni deposited from a Watt's bath showed that it contained approximately 0.05% boron. This was not surprising in view of the large quantity of boric acid in the Watt's bath. Because of the high distribution coefficient of boron, this amount was sufficient to insure ohmic contact to p-type Si and rectifying contact to n-type Si. In order to pursue this still further the 0.1-mil Ni layer was deposited from the following bath (4): $NiSO_4 \cdot 6H_2O$, 175 g/liter; $NiCl_2 \cdot 6H_2O$, 50 g/liter; H_3PO_4, 50 g/liter; H_3PO_3, 1.3 g/liter. In addition, 14 g of $NiCO_3$ were neutralized with approximately 50 g of H_3PO_3 and added to this solution.

Nickel deposited from this solution contained about 1% of phosphorus and, as expected, base-tabs prepared in this way gave low resistance contacts to n-type Si and high resistance ones to p-type Si.

Table I gives results obtained with various combinations of base-tab and silicon type. Tabs were attached as described above at opposite ends (but on the same face) of a silicon blank, and the measured resistance was compared with that calculated from the geometry of the system, the resistivity of the silicon being known from four-point probe measurements. Resistance measurements were at 3 v.

Besides satisfying the electrical requirements for base-tabs (as shown in Table I) the units were also

[2] Platinum plating solution marketed under that name by the Sel-Rex Corporation.

Table I

Silicon type	Buffer acid	Measured R ohm	Calculated R ohm	Approximate contact resistance ohm/cm²
Resistivity type				
0.2 ohm-cm p	Boric	1.2	1.1	0.001
1 ohm-cm p	Boric	45	41	0.05
5 ohm-cm p	Boric	200	180	0.25
1 ohm-cm n	Boric	20,000	50	250
1 ohm-cm n	Phosphoric	150	50	1.2
1 ohm-cm p	Phosphoric	1,500	45	18

given thermal and mechanical shock tests similar to those used for testing the conventional gold alloy base-tabs, for example, repeated plunging into liquid nitrogen from room temperature. In all cases, mechanical and thermal strength was found to be at least as good as for the conventional tabs. Silicon blanks could not be separated from their tabs until the temperature exceeded 800°C. If the pulling force was limited to the blanks' own weight they remained attached to the tabs at and above this temperature, presumably because of surface tension.

Acknowledgments

The author wishes to thank Mr. H. A. Cassel for his assistance during several phases of this work and Mr. R. Duva of Sel-Rex Corporation for valuable advice on platinum plating.

Manuscript received July 18, 1960.

Any discussion of this paper will appear in a Discussion Section to be published in the June 1961 JOURNAL.

REFERENCES

1. M. Hansen, "Constitution of Binary Alloys," 2nd ed., p. 1140, McGraw-Hill Book Co., New York (1958).
2. R. F. Vines, "The Platinum Metals and Their Alloys," p. 31, International Nickel Co., Inc., New York (1941).
3. L. Maissel, *J. Appl. Phys.*, **31**, 211 (1960).
4. A. Brenner, D. E. Couch, and E. K. Williams, *J. Research Natl. Bur. Standards*, **44**, 109 (1950).

Copper Sulfide Creep on Porous Electroplate

M. S. Frant

Research Division, AMP Inc., Harrisburg, Pennsylvania

The spread of silver sulfide from a pore site on a porous gold electroplate after exposure to sulfur vapor has been reported recently by Egan and Mendizza (1). They found that the silver sulfide creep effect was specific for gold electroplate and did not occur on rhodium or palladium plate.

This paper reports that similar creepage phenomenon has been observed on tin electroplate over copper, and that copper sulfide apparently will creep over a variety of other covering metals. Figure 1 shows samples of tin-plated copper returned from field service in a location in which sulfides were known to be present. To the naked eye the pore sites appear as small black spots. However, under magnification (Fig. 1a) the characteristic "flowery" appearance can be seen. In Fig. 1b another feature is shown: the central black area is surrounded by a thinner brown region. The outer brown region often has spots at a periphery which are black also. It has not been established whether the chemical composition of this region is different, whether the color difference can be attributed only to a difference in the film thickness, or whether it represents other pore sites.

Figure 2a shows similar black spots surrounded by the brown area on samples which had been in storage for over a year in brown kraft boxes, but which had not otherwise been exposed to an adverse environment.

Microchemical spot tests (2) were positive for copper and sulfides, negative for other likely metals and anions. To confirm, similar tin-plated copper specimens were suspended over powdered sulfur at 60°, a technique which had been used previously for evaluating antitarnish treatments on silver. Exposures of two to three days led to spots identical in appearance to the samples returned from the field, and giving the same chemical tests.

To establish that the black spots occur at pore sites, two experiments were performed. First, tin-plated specimens were deliberately scratched before exposure to sulfur vapor. Figure 2b shows such a

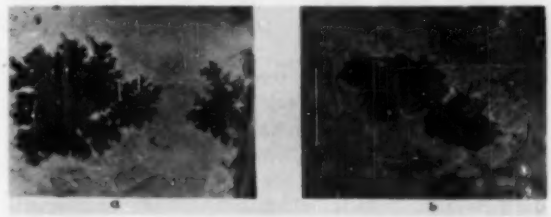

Fig. 1. Copper sulfide spots on tin-plated copper samples returned from field service. Area shown: 7.8 mm².

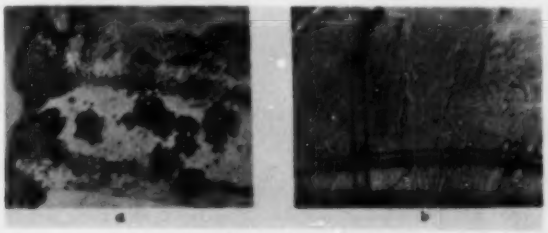

Fig. 2. a. Copper sulfide spots on tin-plated copper which had been stored in brown kraft boxes; Fig. 2b, Copper sulfide growing from scratches in tin-plated copper held 24 hr over sulfur at 60°. Areas shown: 7.8 mm².

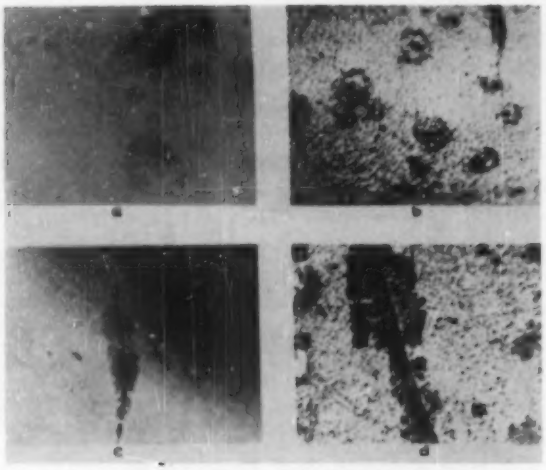

Fig. 3. Copper sulfide spots on (a) nickel-plated copper; (b) nickel-plated brass covered with palladium; (c) tin-plated silver solder; and (d) gold-plated copper. Areas shown: 7.8 mm^2, except for (c) which was 20X before reduction for publication.

Fig. 4. Copper sulfide growth from scratch in nitrocellulose lacquer on copper after 24 hr over sulfur at 60°. Area shown: 7.8 mm.

scratch after exposure. The black film can be seen spreading out from the scratch. Second, tin-plated copper samples were pressed against filter paper pads, soaked in ammonia-ammonium persulfate solution (3) which gives a blue color at pore sites. The samples were then washed, dried, and exposed to sulfur vapor. Good correlation was found.

Similar creepage phenomena have been noted on nickel-plated copper (see Fig. 3a), nickel-plated brass covered with palladium[1] (Fig. 3b), tin-plated silver solder (80% Cu, 20% Ag) (Fig. 3c), and gold-plated copper (Fig. 3d). The samples of nickel and palladium plate do not show as much of the "flowery" appearance or color differences as tin plate and gold plate. Interference colors were widely observed on gold-plated samples; spots would develop overnight on gold plate which was as much as 1 μ (40 millionths of an inch) thick.

[1] The palladium coating was approximately 2.5μ (100μ in.) thick and was applied by an electroless process using tetrammine palladous chloride through the courtesy of R. F. Vines, International Nickel Co.

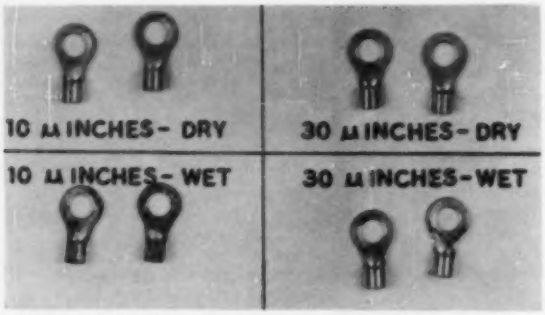

Fig. 5. Effect of moisture and gold thickness on growth on copper sulfide films. Shown are gold-plated specimens having 10 and 30 μ in. average thickness, and the results of 18 hr in a closed container with sulfur which either contained several per cent of water or had been dried overnight over P_2O_5.

To determine whether the outer metallic plating entered into a chemical reaction with the growing film, specimens of O.F.H.C. and electrolytic copper were coated with nitrocellulose or acrylic lacquers, the lacquer scratched, and the sample exposed to sulfur vapor. After several days a growth of copper sulfide (Fig. 4) could be clearly observed spreading out on top of the lacquer.

The effect of moisture on the growth rate is rather striking. After it was observed that sulfur samples and containers seemed to lose their ability to produce spots after a number of cycles, replicate tests were run on sulfur which had been dried and on sulfur containing several per cent of water. The typical result is shown in Fig. 5, in this case for gold-plated copper. The accelerating effect of moisture has been reported for H_2S attack on copper by Shklovsky (4), and for the reaction of sulfur with silver by Smith (5).

The fact that the copper sulfide films will grow on a variety of metals and on a nonmetal suggests that the surface material does not enter into the chemical reaction. Further, the spreading of a sulfide over a presumably nonconducting lacquer film must occur by a different mechanism than that proposed by Gensch and Wagner (6) for the spreading of a silver iodide film along a tantalum surface, since they attributed the spreading to the relatively easy flow of electrons through the substrate on which the spreading occurs. The differences in amount and appearance of the films on the various metals may be attributable to differences in pore size, or to the presence of an adsorbed water layer which would aid in the spread of the film.

The available literature (7) indicates that the formation of copper sulfides occurs by simultaneous diffusion of sulfur inward and copper outward, with the latter effect predominating. Such a mechanism would be consistent with the observations reported here.

The precautionary statement of Egan and Mendizza (1) on the practical importance of this phenomenon should now be extended to a much wider range of metals. Gold, nickel, and tin, on copper or copper alloy substrates are among the most widely used combinations for electrical contacts and terminations. In sulfiding atmospheres, contact failure due to sulfide formation may occur by creepage out

from pores even when "sulfide-resistant" platings are employed.

Manuscript received May 23, 1960.

Any discussion of this paper will appear in a Discussion Section to be published in the June 1961 JOURNAL.

REFERENCES

1. T. F. Egan and A. Mendizza, *This Journal*, **107**, 353 (1960).
2. F. Feigl, "Spot Tests," pp. 89, 280, Elsevier Publishing Co., Amsterdam (1954).
3. M. S. Frant, *Plating*, **45**, 157 (1958).
4. I. S. Shklovsky, *Trudy Inst. Fiz, Khim., Akad. Nauk SSSR, Issledovaniya po Korrozii Metal.*, **1**, 241 (1951).
5. J. W. Smith, *J. Chem. Soc.*, **1931**, 860; *Bull. soc. chim.* **7**, 706 (1940).
6. C. Ilschner-Gensch and C. Wagner, *This Journal*, **105**, 198 (1958).
7a, L. Czerski and S. Patzau, *Arch. Gornictwa i Hutnictwa* 2, 353 (1954); b, Y. Suge and S. Sonoike, *J. Appl. Phys. (Japan)*, **20**, 152 (1951); c, for silver, see U. Croatto, *Gazz. chim. ital.*, **79**, 458 (1949).

Brief Communication

Electronic Analysis of the Fe-Ni System

S. Yamaguchi

The Institute of Physical and Chemical Research, Tokyo, Japan

In the present study, an electron beam was applied to the crystallographic and the thermomagnetic analysis of the Fe-Ni system. Invar (Ni: 36% by weight) whose Curie point was known to be 120°C was used for the experiments described below. Invar powder was prepared by filing from an ingot. The particles of Invar were held by magnetic attraction on the sharp edge of a razor blade (5 x 5 mm) of hard steel whose remanence was known to be about 10,000 gauss. In this way the magnetic induction of the Invar particles was kept saturated. To study electron diffraction, an electron beam was allowed to graze these Invar particles as indicated in Fig. 1.

Experimental procedure.—The following process was carried out to investigate the magnetic states of the Invar particles as a function of their temperature. The diffraction pattern was first photographed with the specimen kept cool. Here care was taken not to preheat the specimen with the electron beam. Exposure to the electron beam (wave length 0.0299Å and current 0.1 ma) could be reduced to little more than the time necessary for photographing the diffraction pattern (only 0.5 sec). Second, a diffraction pattern from the specimen preheated with the electron beam for 2 min without interruption was superimposed on the first pattern from the cool specimen. In this process, the position of the photographic plate as well as the wave length and the current of the incident beam were kept constant. A double diagram obtained in this way is shown in Fig. 2.

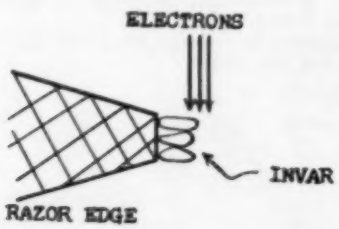

Fig. 1. Arrangement of the Invar specimen relative to the incident beam.

Analysis of the diagram.—In Fig. 2 there is evident an eccentricity between the diffraction rings corresponding to the cold and hot states of the austenitic specimen. This eccentricity means that the Lorentz effect of the cold specimen on the electron beam is distinguishable from that of the hot specimen. It is possible to calculate the difference between the magnetic induction in the two states (ΔB) from the ring eccentricity measurable in Fig. 2 (ΔZ). We have a relation between ΔB and ΔZ:

$$\Delta B = \frac{h}{eL\lambda l} \cdot \Delta Z \qquad [1]$$

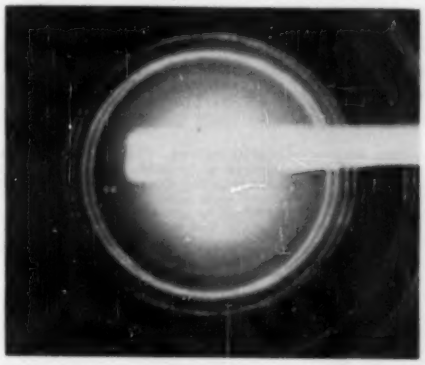

Fig. 2. Double diagram from the cold and from the hot specimen showing the difference of the Lorentz effect; wave length: 0.0299Å; camera length: 495 mm; Positive enlarged 4 times before reduction for publication.

where h is Planck's constant (6.6×10^{-27} erg. sec), e is the electron charge (1.6×10^{-20} emu), L is the camera length (495 mm), λ is the wave length of the electron beam (0.0299Å), and l is the magnetic field region traversed by the electron beam.

In Fig. 2 we measure $\Delta Z = 0.04$ cm. We obtain, therefore,

$$\Delta B \cong 4000 \text{ gauss}$$

according to Eq. [1]. Here $l \cong 3\ \mu$ was assumed.[1]

Discussion of results.—This ΔB-value is understandable as being the difference between the saturation induction of Invar and the remanence of the razor edge. It is plausible that the temperature of the specimen irradiated with the beam for 2 min was above 120°C, i.e., the Curie temperature of Invar. If this is true, then the ΔB-value here measured (4000 gauss) should equal the difference between the saturation induction of Invar at room temperature ($B_s \cong 15000$ gauss) and the remanence of the razor edge ($B_r \cong 10000$ gauss). There is indeed found to be a rough agreement between them ($B_s - B_r \cong \Delta B$).

It was observed during the present experiment that some of the Invar particles fell from the razor edge when they were irradiated with the rather strong beam. As the temperature of these particles here exceeded the Curie temperature (120°C), they followed the normal influence of gravity. In Fig. 2 there are found some weak rings corresponding to Fe_2O_3. The ferromagnetic inclusion of the high Curie point (575°C) material (2) played a rôle in holding the Invar particles on the razor edge, even after they had reached the Curie point (120°C). In fact, according to electron microscope studies it is plausible that the temperature of the object could reach 500°-600°C only with some difficulty (3).

Supporting experiments.—Figure 3 is a double diagram in which the diffraction pattern of the specimen irradiated with the electrons (0.0299Å, 0.1 ma) for 2 min and that irradiated for 4 min were superimposed by means of a double exposure technique. In this diagram there is no ring eccentricity due to the Lorentz effect, since the temperature of the specimen always exceeded the Curie point so that it behaved paramagnetically.

Figure 4 is a double diagram which consists of the diffraction pattern of the specimen irradiated with a very weak electron beam (0.0299Å, 0.03 ma) for 2 min and that irradiated for 4 min. It was possible to observe a crystalline pattern even from paraffin with this weak beam (4). Since the melting point of paraffin was about 50°C, the temperature of the Invar specimen was kept under this temperature

[1] The l-value was estimated as follows. The diffraction pattern of the specimen in its ferromagnetic state below the Curie point (*e.g.*, Fig. 3) and that of a nonferromagnetic gold foil were superimposed by means of a double exposure technique (1) The ring eccentricity here measured made it possible to calculate l in Eq [1], since ΔB in this equation was equal to the saturation induction of Invar (15000 gauss)

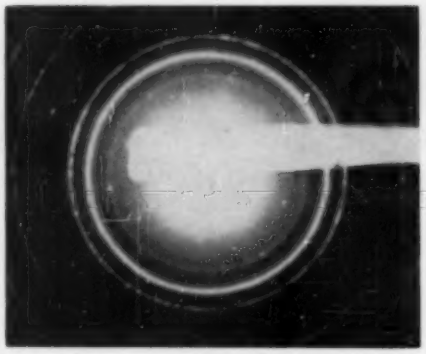

Fig. 3. Double diagram from the hot specimens heated over the Curie point (120°C). No ring eccentricity.

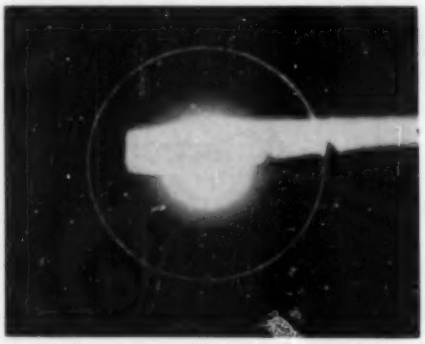

Fig. 4. Double diagram from the cold specimens kept at 50°C. No ring eccentricity.

in the case of Fig. 4. In Fig. 4 there is found no ring eccentricity. It is therefore concluded that the two magnetic states of the specimen shown in Fig. 4 are also below the Curie point.

Conclusion

In the present study, an electron beam was utilized for heating the specimen as well as for its diffraction and magneto-analysis. As the temperature of the specimen heated with the electronic irradiation can be controlled, it is possible to study the magnetic transition of the Fe-Ni system by the present process.

Manuscript received June 10, 1960.

Any discussion of this paper will appear in a Discussion Section to be published in the June 1961 JOURNAL.

REFERENCES

1. S. Yamaguchi, *This Journal*, **107**, 55 (1960).
2. R. M. Bozorth, "Ferromagnetism," p. 723, D. Van Nostrand Co., Princeton, N. J. (1956).
3. Cf. V. E. Cosslett, "Practical Electron Microscopy," p. 264, Butterworths Scientific Publications Ltd., London (1951).
4. S. Yamaguchi, *Z. angew. Phys.*, **8**, 221 (1956); *Z. Phys.*, **134**, 618 (1953).

Technical Feature

Plasma Thermionic Converters

E. W. Salmi

Los Alamos Scientific Laboratory, Los Alamos, New Mexico

Within the last year or so, a great deal of attention has been given to a method of direct conversion of heat energy to electricity which is generally termed "thermionic conversion." There are several variations on the approach to this problem. At Los Alamos, we have been concerned primarily with the cesium plasma diode, which we have also called a "plasma thermocouple." This work was initiated as part of the advanced nuclear propulsion studies under the Rover Program.

Before going into our experimental program let us examine the manner in which a plasma can be used for generating electricity. The word plasma usually is associated with the Sherwood project. While the fusion reaction requires temperatures in the millions of degrees, it is possible to generate plasmas at much lower temperatures. In fact, several gaseous elements form plasmas at temperatures around 2000°C. Of all the available elements, cesium with an ionization potential of 3.87 v is ionized the most easily. One can produce a plasma by introducing a little cesium vapor into a metal container and heating everything to about 2500°K. This is illustrated in Fig. 1. If the cesium pressure is at 0.1 mm Hg, then about 10% of the atoms will be ionized. This is strictly thermal ionization and does not depend on the nature of the container walls. The plasma will be electrically neutral so that the numbers of electrons and ions per unit volume are equal. However, in thermal equilibrium the mean velocities of the electrons and ions will not be equal. In a cesium plasma the mean velocity of the electrons is some 500 times the mean velocity of the ions and, therefore, the electron current across any arbitrary boundary will be 500 times the ion current. Under these circumstances if a small probe is introduced into the plasma as illustrated in Fig. 1, one will draw an electron current which is of the order of 500 times the ion current. The next question is, what voltage does one obtain? This is illustrated in Fig. 2. The left-hand side of the graph shows what the electrostatic potential diagram would be in the steady state (1, 2). The electrochemical potential for the electrons is constant and uniform everywhere. The electrochemical potential is the sum of the chemical potential and the electrostatic potential. Since the chemical potential of an electron in a metal is generally different from the chemical potential of an electron in a plasma there will exist an electrostatic potential difference, equal to the difference between the chemical potentials of the electrons in the metal and the plasma, as indicated in Fig. 2. On the right-hand side are shown two of the many possibilities which may arise at the probe-plasma interface. If the probe is cooled, a monolayer of cesium may form on its surface, resulting in a work function of about 1.8 v as indicated. In the upper right-hand side the case is illustrated in which the probe draws no net current. The electron current and ion current are equal. In order to reduce the electron current into the probe there must exist an

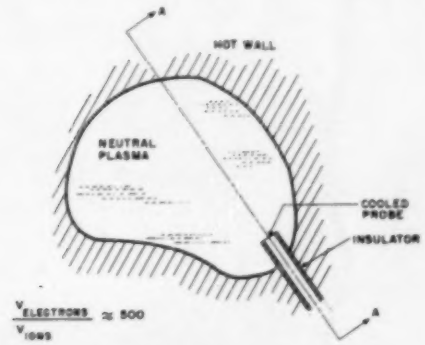

Fig. 1. Idealized model

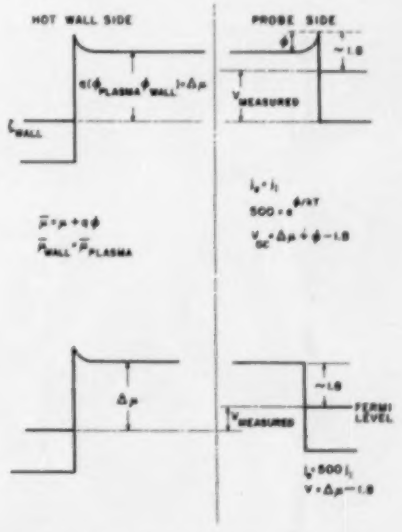

Fig. 2. Electrostatic potential diagrams

electrostatic sheath potential in the plasma at the probe-plasma interface. This potential, ϕ, must reduce the electron current by a factor of 500. Hence, we have the equation

$$500 = \exp\left(\frac{\phi}{kT}\right)$$

for the "open circuit" case (3). If a voltmeter is placed between the probe and the hot metal container one will obtain a voltage which is

$$V = \Delta\mu + \phi - 1.8$$

By lowering the voltage of the probe one begins to draw current to the probe and around the external circuit. Lowering the sheath potential ϕ increases the electron current. The particular case for which ϕ has been reduced to zero is illustrated in the lower right hand side of Fig. 2. The probe is at the same potential as the plasma and the electron current will be 500 times the ion current. These currents can be calculated from the thermodynamic equilibrium equations. The expected voltage is

$$V = \Delta\mu - 1.8$$

since in this case ϕ is zero. The power output of the device would then be the voltage V times the net current.

The above conditions are rather idealistic. However, the calculations for a cesium pressure of 0.1 mm of Hg and a temperature of 2500°K give a current of 50 amp/cm^2 and a voltage of 1.7 v. The resulting power output would be about 80 watts/cm^2. This is the type of performance one can hope for.

The experiments to date have not approached this idealistic model. In most experiments the geometry has consisted of two flat plates, so that the probe is not a small perturbation of the system but becomes one-half of the container. The cesium near the collector is, therefore, not near equilibrium with the hot walls. Also, since the hot wall is only one-half the container and must supply all the electrons which are picked up by the collector one runs into electron emission limitations from the hot wall. Despite these experimental difficulties 30 watt/cm^2 has been observed by increasing both the cesium pressure and emitter temperature (3). With this geometry the maximum short circuit current was about 60 amp/cm^2.

There have been various modifications in the experimental geometry, some of which have tended to approach the idealized model (4). In trying to interpret the data some difficulty is encountered in determining the area of the collector. Although this area is uncertain, it is believed that in several types of experiments the observed values corresponded to as much as 50 watts/cm^2. Along with this value a short circuit current of 130 amp/cm^2 was measured.

These are some of the results which have been achieved in the laboratory and most of the results have been reported in various articles. In all this work the heat source has been electrical.

About a year ago there was performed the first test in a reactor which utilized fission as a heat source. The results of this experiment also have been reported previously (5). The cell design used was complex to the point of being of little value as part of a reactor. Since the first experiment, attempts have been made to simplify the construction and to develop a cell which would be useful as a part of a reactor. In Fig. 3 is shown what is called a "triple-cell experimental rod," a device now being tested in the Omega West Reactor. The diameter across the rod is about ⅝ in. This rod consists of three cells stacked in series. Each cell consists of an emitter, or in keeping with our idealized model, a hot wall of UC:ZrC. Next comes a Cs vapor-filled gap of about 1 mm width and then a collector. Fissions in the enriched UC:ZrC keep the emitter temperature at about 2100°C. Depending on the Cs pressure and other variables, the collector runs at about 400°C. Since the Omega West Reactor is a water tank reactor, the cell will be in cool flowing water. A layer of thermal insulation is placed outside the collector which establishes the temperature gradient between the 400°C collector and the 40°C water. The water also carries away the waste heat from the cell. The emitter is held in place by a thin Nb tube which is attached to the adjacent cell so that the cells are in series. The collectors are electrically separated by small insulator spacers which are also shown in Fig. 3.

In the experimental cell there is shown a Cs bath, the temperature of which may be varied for experimental purposes. In order to establish a uniform Cs pressure in the three cells, a series of small holes are drilled into the collector at the junctions between cells. In an actual reactor the Cs pressure would be at a fixed known value and a Cs pool would be established at the bottom end of the rod and kept at a fixed temperature by the bottom cell.

Once this experimental rod has been developed one can see how to develop a reactor. Instead of stacking three cells, 10 or 20 cells can be placed in series, forming a rod about 2 ft in length. This is now a fuel element for a reactor. Several hundred of these rods can be put into a standard type of water tank reactor and it will become critical. By adding electrical connectors and putting in various control rods,

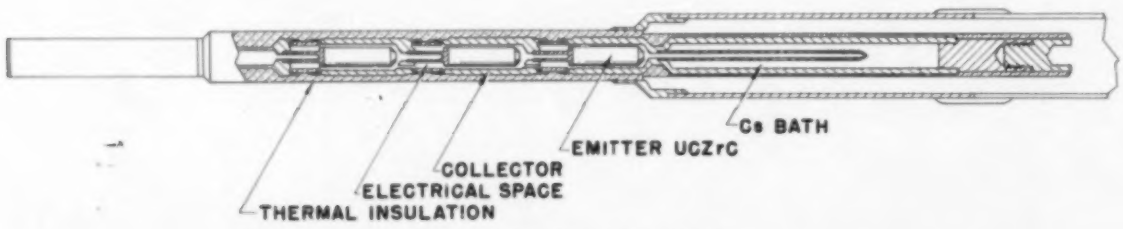

Fig. 3. Triple-cell experimental rod

one has a reactor which generates electricity directly.

Aside from the simplicity of this type of reactor there is another fundamental property of the cell which has not been mentioned. This is the temperature of the probe or collector. Normally the collector temperature is run near equilibrium with the Cs vapor pressure temperature. In some electrically heated experiments the collector temperature was increased to about 1500°K. Under these circumstances the open-circuit voltage did drop. However, the current at lower voltages remained constant, and as a result the power output also remained constant. If this remains true in further experiments, the device will be ideally suited for outer space application. A fundamental difficulty in outer space is the necessity of dumping waste heat by means of thermal radiation. If one can dump the waste heat at a high temperature, the radiator problem will be greatly reduced.

Although very attractive, outer space applications do not exhaust the potential of the thermionic converter. The reactor described earlier consisting of a bundle of rods in a tank of water may have a particular appeal in maritime propulsion and in special situations such as remote installations, if it can meet reasonable lifetime and efficiency requirements.

Present reactors fall into many different categories: fast, thermal, gas cooled, water cooled, breeders, and so forth. The same variety of direct conversion reactors is, in theory, possible using the plasma cell in one of its many forms as the fundamental building block.

Finally, a particularly interesting application of the water moderated reactor is in commercial power production. It will be recalled that the heat thrown off by the collector of the thermionic cell is still at a relatively high temperature. This heat can be used to produce steam in the usual manner and to run turbines with the further production of electrical power. This use of the plasma cell as a "topping cycle" should push up the over-all efficiency of atomic power plants to a very interesting value in the years to come.

Manuscript received April 21, 1960. This work was performed under the auspices of the Atomic Energy Commission.

Any discussion of this paper will appear in a Discussion Section to be published in the June 1961 JOURNAL.

REFERENCES

1. K. G. Hernquist, M. Kanefsky, and F. H. Norman, *RCA Review*, **19**, 244 (1958).
2. H. W. Lewis and J. R. Reitz, *J. Appl. Phys.*, **30**, 1439 (1959).
3. Pidd, G M. Grover, E. W. Salmi, Roehling, and Erickson, *J. Appl. Phys.*, **30**, 1861 (1959).
4. W. A. Ranken, G. M. Grover, and E. W. Salmi, to be published in *J. Appl. Phys.*
5 G. M. Grover, *Nucleonics*, **17**, 54 (1959).

Technical Review

Practical Neutron Activation Analysis for the Electronic Scientist

J. P. Cali and J. R. Weiner

United States Air Force Cambridge Research Laboratories, Air Research and Development Command, Bedford, Massachusetts

ABSTRACT

Neutron activation analysis is an extremely sensitive analytical method for determining trace impurities in semiconductor materials. Theoretical aspects are discussed, and procedures are outlined. Parameters which determine sensitivity are considered, as well as the techniques whereby they may be varied to increase sensitivity. Tables are included which list elements that can be determined by neutron activation analysis, their half-lives, and minimum detectable amounts. Also tabulated are elemental matrix materials of electronic interest together with naturally occurring associated impurities which are determined by neutron activation analysis and other methods. These matrices are also ranked according to extent of flux perturbations, degree of self-activation, and ease of chemical separation.

Since the advent of transistors, thermoelectric, and other semiconductor materials whose electronic properties are wholly or principally dependent on minor constituents, the importance of trace impurity analysis is apparent. With today's increased specialization, the need for communication between related fields of interest has become necessary. For this reason, it is hoped that this paper will familiarize the electronic scientist with some of the aspects of the determination of trace impurities by the relatively

new and ultra-sensitive method of neutron activation analysis.

Neutron Activation Analysis

Description of method.—Neutron activation analysis, as an important and practical analytical method, became feasible only with the advent of the nuclear reactor, because, as will be shown, a high flux of neutrons is necessary to achieve the desired detection sensitivity. Many excellent references exist which give the general principles of the method (1-3, 5). It is, in fact, the extreme sensitivity of this method which makes it valuable as an analytical tool for the determination of trace impurities in concentrations too low to be detected by more conventional methods as, for example, emission spectroscopy.

The principal nuclear reaction occurring when a stable isotope of an element is irradiated with thermal neutrons is the n, γ reaction. The resulting product nucleus is, in general, a radioactive species of the same element one mass unit higher than the original stable nucleus. Decay of the product nucleus is usually by beta or gamma emission, although other modes of decay are possible, *e.g.*, K-capture or alpha emission. Because radioactive atoms can be detected in relatively small numbers, the possibility exists for a sensitive method of detection. The subject of competing nuclear reactions to give the same product nucleus as that formed by the n, γ reaction, and the question of second order reactions, while interesting, are not covered here; the interested reader may find a full account in the cited general references.

In practice, the material of interest is irradiated in a reactor, exposing all impurities and the matrix to an intense flux of thermal neutrons. Depending on the reaction cross section, number of atoms present, time of irradiation, and other quantities covered in Eq. [1] below, the n, γ products of the impurities and matrix are formed in varying amounts. It is now necessary to separate each activity; this is usually done by employing radiochemical separations. The separated radioactivities are then counted and from a knowledge of the various parameters involved, a calculation leads to the concentration of the original impurity which gave rise to the induced, measured activity. The various parameters involved are related as follows:

$$m = \frac{AD(t)}{\phi N f \sigma (1 - e^{-\lambda t})} \qquad [1]$$

where m is the minimum detectable mass, in g, of the trace element; A is the atomic weight of the trace element in g/g at.; $D(t)$ is the minimum detectable disintegration rate, in disintegrations/sec, of the activated impurity. Also, in this term are corrections for assay (aliquoting) and losses due to incomplete recovery during the radiochemical separations (chemical yield); ϕ is the thermal neutron flux, in thermal neutrons/sec cm^2; N is Avogardo's number (6×10^{23} at./g at.); f is the fractional abundance of the target nuclide; σ is thermal neutron reaction cross section in cm^2/ target at.; and $(1 - e^{-\lambda t})$ is the saturation factor, where t is the time of irradiation, in sec, λ is the decay constant of the activity produced, in reciprocal sec.

The actual procedure which would be used in the analysis of a trace impurity in a semiconductor is now considered. Although the method is of general applicability, a specific example is used for clarity, namely, the determination of trace arsenic in silicon metal. The steps are:

1. Weigh out a gram or so of silicon. Place in a quartz needle a weighed out small amount of pure arsenic.
2. Etch (if the state of material allows) the silicon to remove surface contamination.
3. Place the silicon and the quartz needle in a suitable irradiation container.
4. Irradiate in a nuclear reactor for 5 days at highest possible flux.
5. Open the irradiation capsule. Re-etch the silicon and dissolve in suitable reagents (in this case nitric-hydrofluoric acid mixture) and add a known amount of stable arsenic (about 10 mg).
6. Use suitable radiochemical procedures to separate the arsenic (which now carries with it the induced radioactive arsenic) from all other possible induced activities (not quite so hard as it seems, since group separations, scavenging, etc., remove interfering activities in a few steps).
7. Obtain the carrier arsenic in suitable form and weigh. Mount in a suitable way and count the radioactive arsenic. Compare this count with a portion of the radioactive arsenic standard from the quartz needle. Make all corrections to the unknown count for chemical yield, assaying, weight of sample, and finally compute the mass of trace arsenic by the following:

$$M_{As} = \frac{M_{std} \times C_{As}}{C_{std}}$$

where M_{As} and M_{std} refer to the masses of the unknown arsenic and the weighed or standard arsenic, respectively, and C_{As} and C_{std} refer to the counting rate of the unknown arsenic and the known arsenic, respectively.

Theoretical sensitivity.—The sensitivity for any given element is defined as the minimum amount which can be determined under a given set of conditions. These conditions are given either directly from Eq. [1] or are implicit in it and are: 1, magnitude of the thermal neutron flux of the reactor in which the material is irradiated; 2, thermal activation cross section of the target nuclide; 3, length of time the sample is irradiated; 4, half-life of the radioisotope produced by the n, γ reaction on the target nuclide; 5, efficiency of the radiation detector in measuring the radiation produced from the decaying radionuclide; 6, amount of high cross-section material in the sample which might interfere in the separation of the desired element, or more seriously, cause flux attenuation and self-shielding; 7, loss of activity due to radiochemical separations and/or aliquoting procedures; 8, minimum amount of activity required to measure accurately the half-life, and in certain cases, the maximum beta energy of the radionuclide; 9, amount of sample available for

analysis; and 10, time required from end of irradiation to the measurement of the induced activity.

From this list, it can be seen that several of these conditions can be varied in order to attain greater sensitivity of detection should this be required. Increased sensitivity is attained by irradiation at higher neutron fluxes for longer periods of time, assuming for the latter condition, of course, that saturation has not occurred (conditions 1 and 3); by increasing the efficiency of the detection of the measured radiation, as for example, using an internal flow counter *vs.* a Geiger counter (condition 5); by increasing the amount of matrix material under irradiation (condition 9); by decreasing the loss of activity due to chemical manipulations, assaying, and aliquoting procedures (condition 7); and finally, for those induced activities having short half-lives, reducing the elapsed time from the end of irradiation to the measurement of the activity (condition 10). Conditions 2, 4, and 6 are absolutely invariant and, for a given radiation measuring system, and as a practical matter, so is item 8.

Table I. Elements determinable by N.A.A.*

Element	Nuclear reaction of interest	$t_{1/2}$	Minimum detectable amount, μg
Na	$Na^{23}(n,\gamma)Na^{24}$	14.97h	3×10^{-4}
Si	$Si^{30}(n,\gamma)Si^{31}$	2.63h	5.8×10^{-3}
P	$P^{31}(n,\gamma)P^{32}$	14.22d	5×10^{-4}
S	$S^{34}(n,\gamma)S^{35}$	87d	0.5
Cl	$Cl^{37}(n,\gamma)Cl^{38}$	37.29m	1.7×10^{-4}
K	$K^{41}(n,\gamma)K^{42}$	12.52h	3.4×10^{-3}
Ca	$Ca^{44}(n,\gamma)Ca^{45}$	164d	1
Sc	$Sc^{45}(n,\gamma)Sc^{46}$	83.9d	3.3×10^{-4}
Cr	$Cr^{50}(n,\gamma)Cr^{51}$	27.8d	6×10^{-3}
Mn	$Mn^{55}(n,\gamma)Mn^{56}$	2.576h	2.9×10^{-5}
Fe	$Fe^{58}(n,\gamma)Fe^{59}$	45.1d	1.5
Co	$Co^{59}(n,\gamma)Co^{60}$	5.24y	5×10^{-3}
Ni	$Ni^{64}(n,\gamma)Ni^{65}$	2.564h	2×10^{-2}
Cu	$Cu^{63}(n,\gamma)Cu^{64}$	12.80h	1.4×10^{-4}
Zn	$Zn^{68}(n,\gamma)Zn^{69}$	13.8h	2.4×10^{-3}
Ga	$Ga^{71}(n,\gamma)Ga^{72}$	14.3h	2.4×10^{-4}
Ge	$Ge^{76}(n,\gamma)Ge^{77}$	11.3h	7×10^{-3}
As	$As^{75}(n,\gamma)As^{76}$	26.4h	1×10^{-4}
Se	$Se^{74}(n,\gamma)Se^{75}$	121d	5×10^{-3}
Br	$Br^{81}(n,\gamma)Br^{82}$	35.87h	3.4×10^{-4}
Sr	$Sr^{88}(n,\gamma)Sr^{89}$	51d	2.4
Y	$Y^{89}(n,\gamma)Y^{90}$	64.2h	7×10^{-4}
Zr	$Zr^{96}(n,\gamma)Zr^{97}$	17.0h	0.2
Mo	$Mo^{98}(n,\gamma)Mo^{99}$	66h	1×10^{-3}
Ru	$Ru^{102}(n,\gamma)Ru^{103}$	39.8d	2×10^{-3}
Pd	$Pd^{108}(n,\gamma)Pd^{109}$	13.5h	2×10^{-4}
Ag	$Ag^{109}(n,\gamma)Ag^{110m}$	253d	1×10^{-3}
Cd	$Cd^{114}(n,\gamma)Cd^{115}$	53h	3×10^{-3}
In	$In^{115}(n,\gamma)In^{115}$	50d	6×10^{-3}
Sn	$Sn^{120}(n,\gamma)Sn^{121}$	27.5h	2×10^{-3}
Sb	$Sb^{123}(n,\gamma)Sb^{120}$	2.8d	3×10^{-4}
Te	$Te^{128}(n,\gamma)Te^{127}$	9.4h	5×10^{-3}
Cs	$Cs^{133}(n,\gamma)Cs^{134}$	2.07y	3×10^{-3}
La	$La^{139}(n,\gamma)La^{140}$	40.2h	1×10^{-4}
Hf	$Hf^{180}(n,\gamma)Hf^{181}$	44.6d	5×10^{-3}
Ta	$Ta^{181}(n,\gamma)Ta^{182}$	115d	2×10^{-3}
W	$W^{186}(n,\gamma)W^{187}$	24h	1×10^{-4}
Re	$Re^{185}(n,\gamma)Re^{186}$	89h	3×10^{-3}
Os	$Os^{192}(n,\gamma)Os^{193}$	31h	2×10^{-3}
Ir	$Ir^{193}(n,\gamma)Ir^{194}$	19h	2×10^{-3}
Pt	$Pt^{196}(n,\gamma)Pt^{197}$	18h	6×10^{-3}
Au	$Au^{197}(n,\gamma)Au^{198}$	2.70d	2×10^{-3}
Hg	$Hg^{202}(n,\gamma)Hg^{203}$	47d	1×10^{-2}
Tl	$Tl^{205}(n,\gamma)Tl^{206}$	3.56y	0.1
Pb	$Pb^{208}(n,\gamma)Pb^{209}$	3.30h	4.8
Bi	$Bi^{209}(n,\gamma)Bi^{210m}$	5.01d	0.1

* Only for the conditions set forth in this paper. Special cases are not considered.

Practical sensitivity.—In the previous section, those factors which affect the sensitivity of the neutron activation method have been considered from a theoretical viewpoint. In this section, a list of elements which can be determined by this method, giving practical minimum detectable amounts, without, however, considering the effect of the matrix, which is taken up in a later section, are shown in Table I.

The minimum detectable amounts are computed for the following conditions: 1, thermal flux: 10^{13} neutrons/sec cm^2; 2, minimum detectable activity: 10 distintegrations/sec. This is, in general, the amount of radioactivity required to confirm the half-life and maximum beta energy of the measured radionuclide. However, from practical considerations, losses of 50% each for aliquoting and chemical yield are included. This requires then, 40 disintegrations/sec before these losses yield the required 10 disintegrations/sec [$D(t) = 40$ d/s]; 3, 1-g sample size; 4, time of irradiation is until saturation occurs, or five days, whichever is first. Saturation is considered attained when the value of $e^{-\lambda t}$ is 0.05 or less; 5, no consideration in the calculations is made for loss of activity by decay after irradiation. For isotopes having a half-life greater than 12 hr this factor may be neglected; for those less than 12 hr, but greater than 2 hr, a correction lowering the sensitivity by several percent would have to be applied, but is not considered here.

Table I gives a list of those elements easily determined by this method, showing both the nuclear reaction of interest together with the half-life of the produced nuclide. In general, only elements giving induced activities with half-lives greater than 2 hr have been considered. However, for special cases, half-lives greater than a few minutes can be determined using special techniques. The rare earth elements, although extremely sensitive, have not been included, as they are not of general electronic interest, except in other rare earth matrices where the extremely high cross sections of the matrix make for a very difficult analysis.

The minimum detectable amount has been calculated from Eq. [1]. It should be noted, however, as is not the case for many similar compilations, that this calculation is extremely conservative, giving values which are readily obtainable in any laboratory, assuming of course, that the matrix material is not of high cross section, which problem is discussed next.

Matrix Problem

In order to obtain reasonable sensitivity in the use of this method, fairly large sample weights are desirable. This can, however, pose three problems, not necessarily or usually mutually exclusive: (*a*) the effect of neutron beam perturbations by materials of high absorption cross section; (*b*) the problem of handling a large amount of induced radiation of the matrix; and (*c*) the ease with which the matrix is chemically separated from the trace impurities. These criteria are discussed in order and finally tabulated for a group of matrices in Table II.

Table II. Matrices for N.A.A. ranked according to perturbation, induced activity, and ease of chemical separation effects

Group No.	Criteria of group: Total flux perturbations		Induced activity for standard irradiations given		Half-life of induced activity	Elements arranged in descending order of ease of separation
A	5% or less	and either	less than 10 mc	or	less than 12 hr	Si, C, Pb, Ba, Bi, Mg, Ti
B	5% or less	and either	10-1000 mc	or	greater than 12 hr	Ni, Te, Sn, Fe, Zn, Ge
C	5% or less	and	greater than 1000 mc	and	greater than 12 hr	As, Se, Cu, Y, La, Cr, P, Ga
D	5% to 90%	and either	10-1000 mc	or	greater than 12 hr	Mo
E	5% to 90%	and	greater than 1000 mc	and	greater than 12 hr	Hg, W, Ta
F	greater than 90%					Re, Gd

Total flux perturbation effect.—There are two simultaneous and different perturbation effects which occur when an absorbing material is placed in a neutron flux. The first is the attenuation, sometimes referred to as self-shadowing, of the neutron beam as it is absorbed progressively in its passage from the surface to the interior of the sample. Depending upon the neutron absorption and reaction cross sections, the interior of a given sample will "see" less of the unperturbed flux than will the exterior portions. When the cross sections are sufficiently high, the evaluation of this effect becomes important. The second perturbation effect is that caused by the flux gradient resulting when a neutron absorbing material is placed in an unperturbed neutron field. This effect, like the first, is directly concerned with the cross sections of the absorbing material and is similarly difficult to evaluate; in general, it will vary from reactor to reactor.

In any given situation, these perturbation effects must be determined empirically, but for the purposes of this paper, the approach given in reference (6) by Lewis of the Materials Testing Reactor, Idaho Falls, Idaho, is used. In reference to Table II, materials have been grouped according to total flux perturbations, using calculations similar to that of the cited reference. Flux perturbations of less than 5% are negligible and occur in those matrices easiest to work with, other effects being equal; perturbations between 5 and 90% give a range of materials intermediate in difficulty; and finally, those materials whose total perturbation effects are greater than 90% are not recommended for neutron activation analysis, except in very special and unusual circumstances.

Induced radiation effect.—As was explained, not only the trace impurities, but also the matrix material will become radioactive upon irradiation. The quantity of radiation induced in the trace components is negligible when considered from the handling and health safety aspects, but the radiation induced in a gram or more of high cross-section matrix material is significant. The usual radioanalytical laboratory can handle up to 10 millicuries of activity, using only general laboratory equipment and minimal lead shielding, remote handling equipment or other specialized gear. From 10 to 1000 millicuries of activity can be handled by experienced personnel, but requires a complete and well equipped "hot" or high level laboratory. Above 1000 millicuries of activity, only trained people working in the best environment should be considered. Remote handling equipment, especially designed fume hoods, proper shielding, and automatic radiation detection devices are mandatory for working at this level of radiation.

Concurrently with the radiation intensity, the half-life of the induced activity must be considered. For short-lived activities, the intensity of the induced radiation will fall off rapidly and it is then possible to wait for a short period before starting the radiochemical separation process. Materials whose activities have half-lives less than 12 hr are considered to be in this category.

Ease of chemical separation effect.—A very unfavorable matrix element, considering the first two effects only, may under certain conditions be reconsidered should its chemical properties be such that it is easily, rapidly, and specifically removed by chemical manipulations from the induced trace activities. In Table II the elements in each group have been arranged in descending order according to this effect.

Table II has taken all these considerations into account and lists a group of elements of present or possible future electronic interest, according to the criteria given.

In general, should the element of interest fall into Groups A, B or C then no great problems should arise and activation analysis can be successfully done. Sensitivities generally will be as in Table I since 1-g samples are usually feasible within this class. Elements falling into Groups D and E will require considerable attention and complete "hot" facilities. The difficulty of working with these classes is great but not insurmountable, and the sensitivities for the trace impurities will probably decrease by a factor of approximately 10, since smaller samples will undoubtedly have to be used.

Elements classified in Group F present great difficulty and, because very small sample sizes must be used, it is probable that other methods of analysis will yield more sensitive results.

Summary

In Table III, a group of elements of present or potential electronic interest have been listed. The trace impurities tabulated are those found, usually in the part per million range, upon careful spectrographic analysis of the highest purity materials available at present.

An illustration shows how the information contained in this paper could be used by the electronic scientist.

Table III. Matrices of electronic interest and naturally occurring associated impurities

Matrix element	Associated impurities: Determination by N.A.A.	Associated impurities: Determination by other methods*
Carbon	Si, Na, Fe	Mg
Magnesium	Zn, Fe, Mn, Pb, Si, Ca, K, Na, Cu, Ni, Ag, Sn	Al
Silicon	Ga, In, P, As, Sb, Fe, Cu, Zn	B, Al
Phosphorus	Ca, Fe	
Titanium	Sn, Si, Fe, Ca, Na, Cu	Al, Mg
Chromium	Fe, Ca, Cu, Si, Ni	Al, Mg, Ti
Iron	Si, Mn, Ni, Cu, Ag, Na, Cr, Mo	Al, Mg, Ti
Nickel	Fe, Si, Na, Ca, Cu, Ag, Mo, Cr	Al, Mg
Copper	Si, Ca, Pb, Ag, Ni	Mg
Zinc	Pb, Ca, Cu, Fe, Na, Si, Ag, K	Al, Mg, Ti
Gallium	Sn, Pb, Tl, Cu, Ag, Na, Ca	Mg
Germanium	Ca, Cu, Ag	Mg
Arsenic	K, Na, Fe, Si, Ag	
Selenium	Si, Na, Fe, Ni, Ag, Ca, Cu, Mn, Te	Al, Mg, Ti
Yttrium	Fe, Si, Na, Cu, Ag	Al, Mg, Tb, Dy
Molybdenum	Si, Fe, Na, Ca, Cu	Mg
Tin	In, Ge, K, Ag, Ca, Fe, Pb, Si, Na, Bi, Cu, Zn, As	Al, Mg
Tellurium	Ag, Mn, Ca, Si, Na, Cu, Fe, Pb, Se	Mg
Barium	Ca, Fe, Si, Cu, Mn, Na, Sr	Al, Mg, Ti
Lanthanum	Ca, Si, Sn, Fe, Pb, Cu, Na	Mg, Pr, Nd
Gadolinium†	Pb, Ca, Si, Fe, Na, Cu	Mg, Tb, Sm, Eu
Tantalum	Cu, Na, Si	Al, Nb
Tungsten	Mo, Fe, Ca, Si, Cu, Na	Mg
Rhenium†	Fe, Si, Ca, Na, Cu	Mg
Mercury	Cu, Ag, Ca, Na	Mg
Lead	Cu, Ca, Fe, Si, Ag	Al, Mg
Bismuth	Fe, K, Si, Ca, Cu, Pb, Ag, Na	Al, Mg

* Magnesium, aluminum, titanium, and certain rare earths can be done using special techniques under carefully controlled conditions.
† These elements are not recommended for N.A.A.; they fall into Group VI.

PROBLEM; Determine in the part per million range (or lower) the Periodic Group III impurities in silicon carbide.

1. Consider first the matrix. Use Table II to determine the ease with which an analysis could be performed. (Note: when considering compounds, treat each element separately.) In reference to Table II, both silicon and carbon are in Group A, presenting no problem for activation analysis. A compound such as bismuth telluride, where the bismuth falls into Group A, but the tellurium falls into Group B, would be considered to be a Group B classification.

2. Consider the sensitivities of the trace impurities to be analyzed. Table I shows boron and aluminum absent; therefore, other methods would have to be considered for those two elements. However, gallium, indium, and thallium all fall within the sensitivities required.

3. In normal high-purity material (before further purification) what is the expectation of finding these elements? Consider Table III. Here they are absent in carbon, but both gallium and indium are found in silicon. It should be realized, however, that this Table III considers impurities at the spectroscopic level, generally about 1 ppm.

A whole group of materials of electronic interest has been covered. Most of the II-IV compounds are represented, *e.g.*, magnesium silicide, magnesium stannide, and magnesium plumbide. Many of III-V compounds, such as gallium arsenide and indium antimonide, are represented. The semiconductor metallics, germanium, silicon, and silicon carbide, are given. The thermoelectrics are represented by bismuth telluride and bismuth selenide.

In a general survey of this type, it is impossible, practically, to cover every possible permutation of trace and matrix element. However, it is hoped enough general and specific information has been imparted to the electronic scientist so that he may better understand the problems encountered in the important area of electronic materials.

For those interested in obtaining more details, the following extensive bibliographies by Meinke (7, 8), are cited.

An excellent handbook on activation analysis has been prepared by Koch and is invaluable for workers in this field (4).

Manuscript received Feb. 2, 1960; revised manuscript received Aug. 10, 1960.

Any discussion of this paper will appear in a Discussion Section to be published in the June 1961 JOURNAL.

REFERENCES

1. G. E. Boyd, *Anal Chem.*, **21**, 335 (1949).
2. H. Brown, *et al.*, *Science*, **109**, 347 (1949).
3. D. J. Hughes, "Pile Neutron Research," Addison-Wesley Publishing Co., New York (1953).
4. R. C. Koch, "Activation Analysis Handbook," Nuclear Science and Engineering Corp., Pittsburgh, Pa. (1958).
5. G. W. Leddicote, *et al.*, *Nucleonics*, **8**, 62 (1951).
6. W. B. Lewis, *ibid.*, **13**, 82 (1955).
7. W. W. Meinke, *Anal. Chem.*, **28**, 736 (1956).
8. W. W. Meinke, *ibid.*, **30**, 686 (1958).

Discussion Section

This Discussion Section includes discussion of papers appearing in the JOURNAL of the Electrochemical Society, Vol. 106, No. 6 (June 1959), and Vol. 107, No. 1, 2, and 6 (January, March, and June 1960). Discussion not available for this issue will appear in the Discussion Section of the June 1961 JOURNAL.

Chemical Etching of Silicon, I. The System HF, HNO_3, and H_2O

Harry Robbins and Bertram Schwartz (pp. 505-508, Vol. 106, No. 6)

B. A. Irving[1]: The authors present measurements of the etch rate of silicon in mixtures of nitric-hydrofluoric acids of various concentration and interpret these in terms of a two-stage diffusion-controlled reaction involving thermal and chemical autocatalysis. However, the chemical kinetic basis of this interpretation seems misleading. This discussion seeks to clarify some points in this and to show how an empirical rate expression may be deduced in accord with all the experimental observations.

Chemical autocatalysis takes place when one of the products of a chemical reaction is able to catalyze the reaction itself. Cretella and Gatos,[2] in a paper published after Robbins and Schwartz's paper had been submitted, report investigations of an analogous autocatalytic process, the oxidation of germanium by nitric acid. Nitrous acid produced by the oxidation acts as an intermediate catalyst. Similar reaction schemes, based on the results of Vetter,[3] can be written for the oxidation of silicon. The initial slow reaction is with HNO_3 or NO_3^- to produce nitrous acid.

$$2\epsilon^- \text{ (from Si)} + 3H^+ + NO_3^- \rightarrow H_2O + HNO_2 \quad [1]$$

The nitrous acid reacts with more nitric acid to give N_2O_4 which rapidly can oxidize silicon and eventually produce a double quantity of nitrous acid.

$$HNO_2 + HNO_3 \rightarrow N_2O_4 + H_2O \text{ slow} \quad [2]$$

$$N_2O_4 \rightarrow 2NO_2 \quad [3]$$

$$2\epsilon^- \text{ (from Si)} + 2NO_2 \rightarrow 2NO_2^- \quad [4]$$

$$2NO_2^- + 2H^+ \rightarrow 2HNO_2 \quad [5]$$

The initial reaction [1] soon becomes swamped and the rate of oxidation then is determined by the availability of HNO_2 and, hence, by the amount of reaction already taken place. It is, therefore, an exponential function of time. When the rate has reached a certain value, however, there is adequate HNO_2 and the availability of HNO_3 becomes a limiting factor. The rate then becomes constant in time with HNO_3 (or equally H^+ and NO_3^-) diffusing to the surface at a steady rate and the surface concentration of HNO_3 is maintained constant, the balance between the net rate of production by the reaction and the rate of loss by out-diffusion.

The difference between the etch rate of ground and polished surfaces lies in the time required for the steady-state etch rate to be reached. The activation energy for the reaction [1] and [4] on ground surfaces (containing many dislocations) is expected to be less than for a more perfect etched or carefully polished surface,[4] and, therefore, the catalyzed reaction gets started more readily. Adding nitrous acid (nitrite or nitrogen oxides) similarly helps initiate the catalyzed reaction.

The way the steady-state etch rate varies with concentration (the measured etch rate-concentration function) reflects the availability of nitric acid (HNO_3) at the surface since reported etch rates are "steady-state" values. The diffusion gradient of HNO_3 (or H^+ and NO_3^-) will be affected by increases in the bulk nitric acid concentration, tending to increase the concentration at the surface. The increase in rate expected from this also increases the concentration of HNO_2 at the surface which increases the rate still more. Similarly, the heat of reaction increases the rate, as a higher etch rate is equivalent to higher rate of liberation of heat and, hence, an increased surface temperature. This, in turn, affects the diffusion rates to and from the surface in the way outlined by Robbins and Schwartz. The diffusion gradient, the surface concentration of nitrous acid, and surface temperature are all power functions of the bulk concentrations. The etch rate will, therefore, be some power function of the nitric acid concentration. The index is expected to be greater than 1 but not necessarily integral. A plot of log (etch rate) against log (nitric acid concentration) at 80% hydrofluoric acid concentration, taken from Robbins and Schwartz's Fig. 2, is shown in Fig. 1 published here. This has a slope about 2 and indicates an etch rate approximately proportional to the square of the nitric acid concentration.

The second stage of the dissolution process is the reaction of the oxidized silicon with hydrofluoric acid to give soluble silicofluoride ions or silicon tetrafluoride.

$$Si - 4\epsilon^- + 6F^- \rightarrow SiF_6^{--} \quad [6a]$$

$$Si - 4\epsilon^- + 4F^- \rightarrow SiF_4 \quad [6b]$$

The reaction may be written with either F^-, or HF, or HF_2^-, all of which exist in hydrofluoric acid solutions.[5] This reaction is not chemically catalyzed but is, of course, hastened by a rise of temperature. The reaction is not expected to be kinetically of sixth or fourth order as the numerous addition steps will not necessarily have equal rates and the slowest step will be rate determining. A plot of log (etch rate at 60% nitric acid concentration) against log

[1] Research Lab., Associated Electrical Industries, Aldermaston Court, Aldermaston, Berkshire, England.
[2] M. C. Cretella and H. C. Gatos, *This Journal*, 105, 487 (1958).
[3] K. J. Vetter, *Z. physik. Chem.*, 194, 199 (1950).
[4] N. Cabrera, "Semiconductor Surface Physics," p. 342, University of Pennsylvania Press, Philadelphia (1957).
[5] See, for instance, review by H. R. Leech, Supplement to Mellors' "Treatise on Inorganic Chemistry," pp. 111-119, Longmans Green & Co., New York (1956).

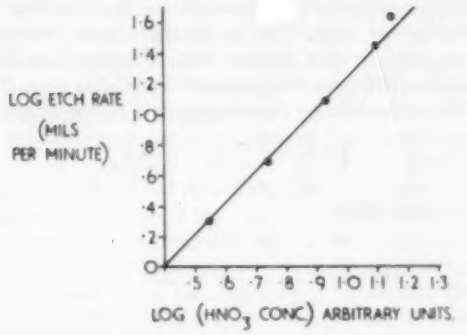

Fig. 1

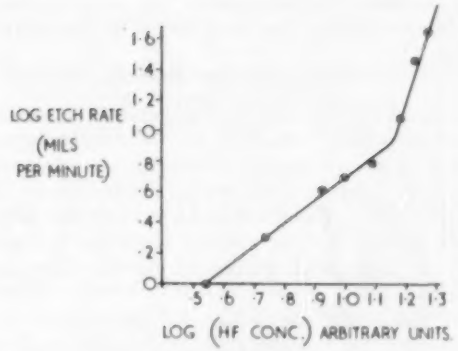

Fig. 2

(hydrofluoric acid concentration), taken from Fig. 2 of Robbins and Schwartz's paper, is shown in Fig. 2 published here. The slope is about 3/2 on the left and rises to about 6 at the right, though the latter figure is doubtful. The rate is approximately proportional to the 1.5 up to 6 power of the nominal hydrofluoric acid concentration.

Combining the two partial rate expressions gives: Rate $\propto$ (nitric acid concentration)^n (hydrofluoric acid concentration)^n, $n = 1.5 \rightarrow 6$ [7]

The approximate linear plots of Robbins and Schwartz's Fig. 3 can be explained using the above rate expression. If the fraction of nitric acid is x, then the fraction of hydrofluoric acid is $(1 - x)$ and rate $\propto x^n (1 - x)^n$, $n = 1.5 \rightarrow 6$; therefore: log (rate) $= 2 \log x + n \log (1 - x) +$ const.

Plots of $2 \log x + n \log (1 - x)$ against x for x between 0.1 and 0.9 give curves of the general form shown in Robbins and Schwartz's Fig. 3. The position of the maximum etch rate depends on the value of n and can be estimated by differentiating the rate expression, equating to zero and solving for x. A value of $n = 4.5$ gives a maximum at $x = 0.3$ in agreement with the "no added water" curve of Robbins and Schwartz's Fig. 3. This value for n is reasonable because the acid strengths correspond to the portion of Fig. 2 where the slope is about 4.5. A value of about 6 would be applicable in the strongest acid mixtures and 1.5 for the diluted etchants (etch rate 1-2 ml/min). The position of the maximum varies accordingly from $x = 0.25$ for the most concentrated acids ($n = 6$) to $x = 0.56$ for the diluted etchants ($n = 1.5$). This is in accord with Robbins and Schwartz's results for various levels of added water.

It is seen, therefore, that, although the reaction is diffusion controlled, an empirical rate expression [7] can be deduced which is in satisfactory agreement with all the experimental results and which is to be preferred to the exponential function indicated by Robbins and Schwartz. This expression should not be interpreted stoichiometrically, but the reactions taking place may be inferred by comparison with other data on the reduction of nitric acid and the composition of acidic fluoride and silicofluoride solutions.

Harry Robbins and Bertram Schwartz: In our discussions of the chemical etching of silicon[6,7] in work subsequent to that being discussed by Mr. Irving, we have considered several alterative mechanisms for the oxidation process. One of these is similar to the mechanism discussed by Mr. Irving. We feel that the situation is considerably more complex than that outlined by him, and are inclined to consider that the mechanism of Abel and Schmid[8] makes a substantial contribution to the over-all reaction. This mechanism involves the oxidation of silicon by HNO_2 as the oxidant. The HNO_2 is formed autocatalytically in a two-step reaction as follows:

$$HNO_2 + HNO_3 \rightleftarrows N_2O_4 + H_2O \quad [1]$$

$$N_2O_4 + 2NO + 2H_2O \rightleftarrows 4HNO_2 \quad [2]$$

The NO for the reaction is available, since it is the reduction product of HNO_2. We also feel that the direct reaction of HNO_3 with silicon is also possible under certain conditions, so that there exist several parallel paths for the oxidation step. In our study of the temperature dependence of the reaction, we have found at least two "activation energies" that we have associated with the oxidation step, and which lend support to the possibility that more than one oxidation mechanism may be important in the over-all reaction.

The steady-state reaction via HNO_2 need not involve the diffusion of HNO_2 to the silicon surface as implied by Mr. Irving. Reactions [1] and [2] may well take place within the boundary layer, since the HNO_2 at the silicon surface may be depleted by reaction with the silicon, so that the concentration of HNO_2 will be a maximum within the boundary layer. Under this condition, the situation becomes exceedingly complex, involving concentration gradients of NO, HNO_3, N_2O_4, and HNO_2 within the boundary layer, and complicated interactions between these species, as suggested by Spahn and Schmid.[9]

The situation is complicated still further by the oxide removal process, and by the probability that the reaction is not strictly diffusion controlled over the entire range of compositions of etching solution we have considered. Under the latter condition, as we have discussed elsewhere,[7] the practice of using bulk solution concentration values in a rate equation cannot be justified, but it becomes necessary to take

[6] H. Robbins and B. Schwartz, *This Journal*, **107**, 108 (1960).
[7] H. Robbins and B. Schwartz, *This Journal*, Manuscript submitted for consideration for publication.
[8] E. Abel and H. Schmid, *Z. physik. Chem.*, **132**, 55 (1928).
[9] G. Schmid and H. Spahn, *Z. Metallk.*, **45**, 138 (1955).

cognizance of the actual concentrations existing at the surface of the semiconductor, and the nature of the surface itself may then also influence the kinetics. These and other problems have made exceedingly difficult the derivation of a kinetic expression that would be valid over even a very limited range of compositions.

With respect to the kinetic expression derived by Mr. Irving, we wish to note first that the expression will be valid only on the no-added water line, and cannot be used in the form presented where the sum of the weight fraction of HF and HNO_3 does not equal 1. We have also plotted the expression

$$\log R = 2 \log X + n \log (1-x)$$

as a function of x, for values of $n = 6$ and $n = 4.5$, and it was seen that the curves were only a very crude approximation to the data published. Furthermore, if one takes the empirical rate expression

$$\log R = 2 \log x + n \log (1-x) + \log A$$

where A is the constant of proportionality in the expression

$$R = A\, x^2\, (1-x)^n$$

and calculates A by inserting the values of the measured etch rates on the no added-water line, the values of A so obtained vary by as much as three orders of magnitude. We are, thus, not inclined to agree with Mr. Irving that the empirical expression is in satisfactory agreement with the experimental data.

Electrolytic Reduction of Thorium Oxide

L. H. Meyer, (pp. 43-47, Vol. 107, No. 1)

J. R. Chalkley[10]: It would seem necessary to refer to the problem of oxyhalide formation in the systems Dr. Meyer has been considering.

In the fused chloride system, it has been shown that thorium oxychloride plays a vital role in the electrolysis.[11] Thorium oxide does not dissolve in the NaCl-KCl eutectic melt, but the oxychloride is soluble. (It is also soluble in water.) It decomposes at low Th^{4+} concentrations into the oxide and tetrachloride, and it has a low decomposition potential, depositing a finely divided mixture of metal and oxide. The oxychloride is formed by dissolving thoria in melts containing higher concentrations of thorium tetrachloride, and it is necessary that these higher concentrations should be avoided in any chloride cell used for the electrolytic reduction of thoria. But, even at the lower concentrations, it has been shown conclusively that $ThOCl_2$ is formed as a direct product of the anode reaction (anodic chlorination), and that its rate of decomposition (to ThO_2 and $ThCl_4$) is not sufficiently rapid to prevent its appearance in the catholyte and the deposition of a fine, low-grade deposit.

It is misleading to draw direct conclusions from the anode gas analysis; theoretically, chlorine would be expected to be evolved if an inert anode could be used. As evidence for this, it is easily demonstrated that oxygen will displace chlorine from a thorium tetrachloride melt. The graphite anode, however, plays an important part in the electrolysis as illustrated by the following equations, which also show that chlorine is the primary product in the anode:

$$ThOCl_2 \rightleftharpoons ThO^{++} + 2Cl^-$$

$$ThCl_4 \rightleftharpoons Th^{++} + 4Cl^-$$

At the anode:

$$Cl^- \rightarrow Cl$$

$$ThO_2 + 2Cl + C \rightarrow ThOCl_2 + CO_2$$

$$ThO_2 + 4Cl + C \rightarrow ThCl_4 + CO_2$$

It is interesting to note that chlorination with molecular chlorine under similar conditions forms only the tetrachloride directly, the oxychloride being formed during the later stages by the back-reaction:

$$ThO_2 + ThCl_4 \rightleftharpoons 2ThOCl_2$$

It would not be justifiable to extend this behavior to cover similar reactions in the fluoride system, since it is known that many oxides are appreciably soluble in fused fluoride melts. On thermodynamic evidence, oxygen would then be the primary product at the anode, but, on present evidence, the possibility of oxyfluoride formation in the melt cannot be discounted.

The fused chloride system has been shown to be unfavorable for the operation of a direct oxide electrolytic process. Nevertheless, the two-stage process in which thoria is directly and completely chlorinated in situ in the melt and then electrolyzed[12,13] is, over-all, equivalent to the oxide electrolytic process. Very high efficiencies are obtained by this process, and, as with most fused chloride systems, the following advantages over the corresponding fluoride systems are shown:

(*A*) Lower operating temperatures.

(*B*) Easier leaching conditions due to higher chloride solubilities. 'Stripping' of thorium from the melt is advocated, but thorium in leach liquors is effectively recovered by oxalate precipitation.

(*C*) Less corrosive conditions, giving a wider choice of refractory and insulator materials.

Influence of Electrode Surface Conditions on the Electrical Strength of Liquefied Gases

D. W. Swan and T. J. Lewis (pp. 180-185, Vol. 107, No. 3)

A. H. Sharbaugh[14]: It is gratifying to note the general agreement of Dr. Lewis' values for the electric strength of *liquid* nitrogen and our measurements on *gaseous* nitrogen at high pressures. We observed values of the order 1.8 mv/cm at densities which are about one-quarter of the liquid density.[15] Thus, it would appear that there is no marked discontinuity in electric strength in passing from the gaseous to liquid phase.

[10] Impregnated Diamond Products Ltd., Tuffley Crescent, Gloucester, England.

[11] J. R. Chalkley and W. H. Cleaver, "Examination of an Anodic Chlorination Process for the Preparation of Thorium from Thoria," *Atomic Energy Research Estab.*, Report X/M 165, 1959.

[12] A. R. Gibson, J. H. Buddery, J. R. Chalkley, and R. P. Marshall, "Thorium Metal Production by a Chlorination Process," *Proc. 2nd. Intern. Conf. Peaceful Uses Atomic Energy, Geneva 1958*, 4, pp. 237-242.

[13] A. R. Gibson and J. R. Chalkley, "Production of Thorium Metal," *Bull. Inst. Mining Met.*, 69 (Part 6), 281 (1960).

[14] Research Lab., General Electric Co., P. O. Box 1088, Schenectady, N. Y.

[15] 1957 *Ann. Rep., Conf. on Elec. Ins.*, p. 32.

I should like to call attention to two earlier examples of the influence of the anode properties on the measured values of electric strength of hydrocarbon liquids. The first was observed in n-hexane where we measured a decrease of about 10% in the electric strength when a smooth flat stainless steel anode was roughened by grit blasting.[16] The "hill-to-valley" depth of the roughened surface was of the order of 10% of the 70μ gap separation. A second example was reported for some measurements in benzene where solutions with different concentrations of electrolyte were employed as anodes. In this case, the effect was interpreted as being due to the space-charge enhancement of the applied field by positive ions emitted from the anode.[17]

Molecular Structure and the Electrical Strength of Liquid Hydrocarbons

T. J. Lewis (pp. 185-191, Vol. 107, No. 3)

P. K. Watson[18]: The model which has been proposed appears to have at least two notable defects: It indicates that the mechanism of breakdown in liquids takes place by means of an electron multiplication process, and it implies that the breakdown strength of a liquid should be virtually independent of an applied hydrostatic pressure.

Now, on the basis of our recent experiments on high-field conduction currents in hexane in the microsecond region, we have concluded that there is no significant multiplication process in hexane even at fields of 1.3 mv/cm.[19]

Moreover, recent experiments have indicated that the breakdown strengths of liquids are strongly pressure dependent, even for pulses as short as 1 μ sec.[20]

Obviously, there is a correlation between electrical breakdown strength and some parameter associated with molecular structure, but the relationship must be more indirect than Dr. Lewis has indicated.

A. H. Sharbaugh[21]: By analogy with Townsend-type breakdown in gases, a theory of liquid breakdown which involves an electron multiplication (α-process) predicts that the value of the product $\alpha\delta$ will be approximately constant for wide ranges of gap width δ and ionization coefficient α. At *constant* δ, we have observed a 50% decrease in the electric strength E, of liquid hexane when the electrode area is increased from $\sim$ 0.2 to 3 cm^2.[22] Since α, if it exists, would be expected to be a strong function of E, it is difficult to reconcile this experimental observation with the hypothesis of a multiplication process for breakdown in liquid hexane.

[16] *1955 Ann. Rep., Conf. on Elec. Ins.*, p. 16.
[17] *J. Appl. Phys.*, 25, 382 (1954).
[18] Research Lab., General Electric Co., P. O. Box 1088, Schenectady, N. Y.
[19] A. H. Sharbaugh and P. K. Watson, "High-Field Conduction Currents in Liquid Hexane under Pulse Conditions," Abstract No. 20, ECS Meeting, Philadelphia, Pa., May 1959.
[20] K. C. Kao and J. B. Higham, "Effects of Hydrostatic Pressure, Temperature, and Voltage Duration on the Electric Strengths of Hydrocarbon Liquids," Abstract No. 11, ECS Meeting, Philadelphia, Pa., May 1959.
[21] Research Lab., General Electric Co., P. O. Box 1088, Schenectady, N. Y.
[22] *1955 Ann. Rep., Conf. on Elec. Ins.*, p. 16.

T. J. Lewis: The statement by Dr. Watson, that the model implies that breakdown occurs by an electron multiplication process and should be independent of an applied hydrostatic pressure, is not really correct. The criterion set up is one for the necessary field to overcome various loss processes and so provide some electrons of sufficient energy to contribute effectively to the next stage in the breakdown sequence.

Only when all the succeeding stages of the breakdown (some of which may be pressure dependent) are maintained in a reasonably constant manner, i.e., C constant, will comparison between experiments be possible in terms of this criterion. Such a situation should arise for a series of similar hydrocarbons.

One should not proceed too far by analogy with gas discharges in expecting clearly measurable values of α since the actual value might be small or only significant when breakdown is imminent or even masked by the other processes embodied in C. Even when α is small, however, the liquid still can exert a marked influence through the loss process envisaged.

The results mentioned by Dr. Sharbaugh, in which a decrease in strength of n-hexane is observed when the electrode area is increased at constant gap width, provide evidence, I believe, not for liquid mechanisms but for quite a different aspect of the subject. It should be recalled that these measurements were made using the microsecond pulse technique. Under these conditions, an analysis of the variation of strength with area according to the concepts outlined in Abstract 13[23] will indicate that the observations are exactly in agreement with a statistical model of the breakdown process and do not, therefore, shed any light on the possibility of a multiplication process.

A New Statistical Theory for the Breakdown of Liquid Hydrocarbons

B. W. Ward and T. J. Lewis (pp. 191-195, Vol. 107, No. 3)

Oliver H. LeBlanc, Jr.[24]: It has been shown experimentally by Goodwin and Macfadyen and by Crowe that the time lags observed with application of short pulses are directly proportional to the electrode spacing. This seems to me to be clear evidence that the time lag must be formative and not statistical.

P. K. Watson[25]: For a time lag to be ascribed to a statistical process, similar to the well-known effect in gases, it is necessary to postulate the nature of the event for which one is waiting. In the gaseous case, this event is the arrival of an initiating electron, and Dr. Lewis has suggested that, by invoking a similar phenomenon for liquids, one can explain the dependence of breakdown strength upon pulse width in the microsecond region.

[23] "A New Statistical Theory of the Breakdown Process and the Reinterpretation of Pulse Breakdown Measurements in Liquid Hydrocarbons" by T. J. Lewis, ECS Meeting, Philadelphia, Pa., May 1959.
[24] Research Lab., General Electric Co., P. O. Box 1088, Schenectady, N. Y.
[25] Research Lab., General Electric Co., P. O. Box 1088, Schenectady, N. Y.

This hypothesis is not, in fact, consistent with the experimental facts:

(*A*) The currents which are observed in liquids, under microsecond pulses of voltage, at fields in the range 1 to 1.5 mv/cm, are of the order of milliamp per cm².[29] Assuming a value for electron mobility of the order of 10^{-3} cm/sec/v/cm,[27] this gives an electron emission rate of 10^{15} electrons/sec/cm² from the cathode. It is difficult to see how such a copious emission can be consistent with statistical time lags in the microsecond region.

(*B*) If, however, one supposes that the probability of an electron initiating a breakdown is very small (say 1 in 10^6 or so), then it might be argued that the experimental evidence is still consistent with a statistical time lag, in that one is awaiting the emission of a very large number of electrons from the cathode. This again, however, is at variance with the observed facts: If, as has been suggested, the electron emission from the cathode is a field-assisted thermionic process (Schottky emission), then one would expect any statistical time lags to be strongly temperature dependent. In fact, the experiments of Kao and Higham indicate that the time lags are independent of temperature.[28]

Finally, it may be thought that the electrons are field emitted: In this case, however, one would expect a marked reduction in time lag if, by some means or other, one were able to increase the field needed to cause breakdown. This can be done by changing the hydrostatic pressure applied to the liquid, and Kao and Higham find that in hexane, for example, there is no change in the critical time lag, in going from atmospheric pressure, up to 25 atm, despite a very marked increase in the breakdown strength.

Thus, one is forced to conclude that the observed time lags in liquids are not consistent with a statistical model.

T. J. Lewis: The present theory does not preclude the existence of a formative time lag. In fact, it states that both statistical and formative times exist and that the latter is expected to be dependent on the electrode spacing, thus leading to the results obtained by Goodwin and Macfadyen and by Crowe. The important result, which may not have been adequately presented in the paper but which can be properly developed in a full treatment, is that the formative time is not that associated with the "knee" of the electric stress-pulse duration curve, but is a much smaller quantity.

Dr. Watson's concluding comment is that the observed time lags in liquids are not consistent with a statistical model. I submit that the experimental evidence obtained by many different workers employing short-duration pulses is overwhelmingly to the contrary. The reasons are:

(*A*) When a proper statistical analysis is made both of the method used and the results obtained for the electric strength as a function of pulse duration, the existence of a statistical process becomes very evident. Failure to take account of the nature of the experimental method has led to erroneous conclusions in the past.

(*B*) If a step-function voltage pulse is employed instead of microsecond pulses, the breakdown time lag can be measured directly and has obvious random fluctuations.

We have made measurements on n-hexane under both categories (*A*) and (*B*) above to confirm this, and it is important to note that it is *not* necessary to postulate the nature of the random process in order to establish these experimental facts.

However, it is profitable to proceed further by enquiring into the nature of the random events which give rise to the effects noted. In the paper, I have attempted to do this by postulating a random process of rate *IW* which is partly cathode and partly liquid dependent. It would be wrong to assume at this stage more than the property that *IW* increases with field, provided all other conditions remain constant. It is certainly not justifiable to dismiss the evidence for a statistical time lag as Dr. Watson does, simply because *I* in the presence of hydrocarbon does not conform to vacuum emission laws.

If *I* is identical with the electron emission rate from the cathode and that is, in the worst case, 10^{13} electrons/sec and concentrated on a single emission site, then it is true than *W* would need to be $< 10^{-6}$ to give time lags of the right order. Further consideration indicates that this is not at all unlikely. In fact, values of *W* very much less than this are probable, if only the most energetic electrons in the liquid are capable of initiating a breakdown. Even when *W* is of this order of smallness, one is not awaiting the emission of a large number of electrons since any electron, even the first, may lead to breakdown.

The form of *IW* chosen in the paper to illustrate the theory was unfortunate in that it did not indicate that large changes in *I* and *W* can be tolerated provided *IW* remains of the right order of magnitude.

[27] A. H. Sharbaugh and P. K. Watson, "High-Field Conduction Currents in Liquid Hexane under Pulse Conditions," Abstract No. 20, ECS Meeting, Philadelphia, Pa., May 1959.
[27] O. H. LeBlanc, *J. Chem. Phys.*, In press; "Electron Drift Mobility in Liquid n-Hexane," Abstract No. 22, ECS Meeting, Philadelphia, Pa., May 1959.
[28] K. C. Kao and J. B. Higham, "Effects of Hydrostatic Pressure, Temperature, and Voltage Duration on the Electric Strengths of Hydrocarbon Liquids," Abstract No. 11, ECS Meeting, Philadelphia, Pa., May 1959.

The System BaO-TiO_2-P_2O_5: Phase Relations, Fluorescence, and Phosphor Preparation

D. E. Harrison (pp. 217-221, Vol. 107, No. 3)

Mary V. Hoffman[29]**:** The x-ray data presented in this paper for the compound 2BaO: TiO_2: P_2O_5 differ considerably from those obtained by Ranby, Mash, and Henderson[30] and more recently in this laboratory (Table I). The pattern as presented apparently was obtained on material recrystallized from the melt. This method results in considerable crystal growth, and, with this compound, in severe orientation. A more representative pattern is ob-

[29] Luminescent Materials Lab., Lamp Metals and Components Dept., General Electric Co., Cleveland, Ohio.
[30] P. W. Ranby, D. H. Mash, and S. T. Henderson, *Brit. J. Appl. Phys.*, Supplement No. 4.

Table I. X-ray diffraction pattern: $2BaO \cdot 1TiO_2 \cdot 1P_2O_5$

From paper		From low-temperature firing	
d	I/I	d	I/I
8.34	30	8.40	16
		4.70	20
		4.51	22
		4.29	3
4.17	80	4.17	27
3.90	25	3.90	75
		3.75	8
3.59	10	3.60	100
		3.50	7
		3.36	22
		3.23	31
2.84	5	2.84	18
2.78	100	2.79	47
2.73	10	2.72	33
2.65	3	2.65	29
2.39	3	2.39	27
		2.35	9
		2.33	15
2.28	3	2.28	10
2.25	3	2.25	14
		2.20	17
2.19	3	2.19	14
2.14	5	2.14	31
		2.08	8
		1.99	13
		1.96	7
1.94	3	1.94	10
		1.90	5
		1.87	11
		1.79	8
1.75	10	1.75	20
		1.72	7
		1.69	5

tained by firing at low temperatures, preferably at or below 1000°C. Noticeable orientation will occur in material fired at 1090°C. The differences in the patterns are large enough to obscure positive identification, since the orientation tends to suppress those lines which distinguish 2:1:1 from the similar pattern of $Ba_2P_2O_7$. The x-ray data were obtained on a General Electric diffractometer, XRD-5, using CuK radiation, nickel filter.

An Investigation of the Reaction between Aluminum and Water

W. J. Bernard and J. J. Randall, Jr. (pp. 483-487, Vol. 107, No. 6)

F. J. Burger and D. M. Cheseldine[m]: This paper confirms a number of results which we obtained in the course of work carried out under Canadian Government Contract DRB 700129, "Development of Aluminum Electrolytic Capacitor, ECRDC Project C44." These were summarized in the First and Second Quarterly Reports of November 1958 and February 1959, respectively.

In our investigation, two methods were used to determine the degree of hydration of the product of the reaction of hot deionized water on aluminum.

In one method, the volume of hydrogen evolved during the reaction was measured directly and correlated with the weight increase of the aluminum specimen. The ratio of these two quantities varies according to the degree of hydration of the oxide formed, as illustrated, e.g., by equations [1] and [2], which represent the formation of mono- and trihydrates, respectively.

$$2Al + 4H_2O = Al_2O_3 \cdot H_2O + 3H_2 \quad [1]$$

$$2Al + 6H_2O = Al_2O_3 \cdot 3H_2O + 3H_2 \quad [2]$$

Calculations show that for a weight increase of 1 mg the volume of hydrogen at NPT is 1.02 cc in the case of monohydrate formation, and 0.66 cc in the case of trihydrate.

In a typical experiment, a specimen of 99.99% pure, etched aluminum foil (measuring 2 in. x 2 in. x 0.0035 in., and having attached to one of its sides a tag 2 in. long by ¼ in. wide) was immersed in deionized water ($\rho_{m\text{-}c} > 10^6$ ohm-cm) at 90°C, as follows.

The weighed specimen was placed under an inverted short-stemmed glass funnel and secured by leading the tag out through the stem of the funnel and turning its end over. Funnel and foil then were completely immersed in the hot water and an inverted burette filled with water placed over the stem of the funnel to collect the evolved hydrogen. After a suitable reaction time (say 1 hr), the foil was quickly removed from the water, dried either at 110°C or *in vacuo* at room temperature, and reweighed.

The volume of hydrogen, measured at room temperature and atmospheric pressure and corrected for 0°C, was found to be 32 cc.

Corrections for barometric pressure, water vapor pressure, and losses due to solubility of hydrogen in water were not applied. The corresponding weight increase of the foil specimen after drying under vacuum at room temperature was 43.5 mg, i.e., a weight increase of 1 mg was accompanied by evolution of approximately 0.74 cc of hydrogen (NPT). The hydration calculated from these figures is 2.4 moles H_2O and 1 mole of Al_2O_3. The mean value obtained by this method from 7 separate experiments was 2.8 moles of water.

In our second series of experiments, applying the method of Lewis and Plumb[n] in which the oxide is stripped in an aqueous solution containing 2% CrO_3 and 5% H_3PO_4 at 85°C, we found a somewhat lower figure for the hydration. In these experiments, too, the same type of etched, 99.99% pure Al foil was used. Foil specimens were immersed in boiling deionized water for 5, 30, and 60 min. The times required for stripping these layers were about 10, 30, and 40 min, respectively. The weight changes observed, namely, first, after boiling and, second, after stripping the aluminum foil, are shown in Table I published here. In each of these cases, the foil was

[m] The Telegraph Condenser Co., (Canada) Ltd., 50 Bertal Rd., Toronto 15, Ont., Canada.

[n] J. E. Lewis and L. C. Plumb, *This Journal*, 105, 499 (1958).

Table I. Weight changes on, first, boiling and, second, stripping 4-sq.-in. etched aluminum foil

Reaction time (min)	5	30	60
(A) Weight increase after boiling (mg)	60.8	98.2	119.2
(B) Weight loss after stripping (mg)	98.3	159.8	193.6
Ratio $\frac{(A)}{(B)}$	0.62	0.63	0.63

dried in vacuo at room temperature for ½ hr before weighing.

The composition of the reaction product is shown to be independent of reaction time in the range covered by reference to the bottom line of the table which lists the ratio of combined oxygen and hydrogen (weight increase) to hydrated alumina (weight loss). The mean of this ratio, being 0.63, corresponds to 2.1 moles H_2O per mole of alumina, the values for mono- and tri-hydrate being, respectively, 0.55 and 0.665.

Both methods, therefore, support the view that the hydrate formed is not mono-hydrate as has been commonly assumed hitherto, but is of a higher order.

Growth of Single Crystal Silicon Overgrowths on Silicon Substrates

Albert Mark (pp. 568-569, Vol. 107, No. 6)

R. C. Sangster[m]: Very similar work was reported by Sangster, Maverick, and Croutch.[n] The lead paragraph reads as follows: "A study has been made of the feasibility of growing Si crystals by the reaction of gaseous $SiBr_4$ with H_2 at the surfaces of hot Si seed filaments. The immediate objective has been to produce deposits of a purity and a crystal perfection sufficient for semiconductor device purposes. An ultimate objective has been the deposition of arbitrary, complex, p-n junction structures by control of the types and amounts of impurities deliberately introduced into the process gas stream. This is a partial report covering the more interesting observations and results." Included were descriptions of the apparatus used, an analysis of the deposition process with respect to both the fundamental phenomena involved and the effects of process variables, microphotographs of epitaxial single crystal silicon deposits, description of the optimum experimental conditions, and some preliminary electrical results on epitaxially grown p-n junction structures. The authors feel that the current interest in techniques of this sort is quite justified and long overdue. We hope that Mr. Mark's contribution will help stimulate further activity in this field.

[m] Central Research Labs., Texas Instruments Inc., P. O. Box 1079, Dallas 21, Texas.

[n] R. C. Sangster, E. F. Maverick, and M. L. Croutch, *This Journal*, 104, 317 (1957).

June 1961 Discussion Section

A Discussion Section, covering papers published in the July–December 1960 JOURNALS, is scheduled for publication in the June 1961 issue. Any discussion which did not reach the Editor in time for inclusion in the December 1960 Discussion Section will be included in the June 1961 issue.

Those who plan to contribute remarks for this Discussion Section should submit their comments or questions in triplicate to the Managing Editor of the JOURNAL, 1860 Broadway, New York 23, N. Y., *not later than March 1, 1960*. All discussion will be forwarded to the author(s) for reply before being printed in the JOURNAL.

FUTURE MEETINGS OF
The Electrochemical Society

Indianapolis, Ind., April 30, May 1, 2, 3, and 4, 1961
Headquarters at the Claypool Hotel
Sessions probably will be scheduled on
Electric Insulation, Electronics (including Luminescence and Semiconductors), Electrothermics and Metallurgy, Industrial Electrolytics (including a Symposium on Fuel Cells), and Theoretical Electrochemistry (including a Symposium on Instrumentation)

★ ★ ★

Detroit, Mich., October 1, 2, 3, 4, and 5, 1961
Headquarters at the Statler Hotel

★ ★ ★

Los Angeles, Calif., May 6, 7, 8, 9, and 10, 1962
Headquarters at the Statler Hilton Hotel

★ ★ ★

Boston, Mass., September 16, 17, 18, 19, and 20, 1962
Headquarters at the Statler Hilton Hotel

Papers are now being solicited for the meeting to be held in Indianapolis, Ind., April 30-May 4, 1961. Triplicate copies of each abstract *(not exceeding 75 words in length)* are due at Society Headquarters, 1860 Broadway, New York 23, N. Y., *not later than January 2, 1961* in order to be included in the program. *Please indicate on abstract for which Division's symposium the paper is to be scheduled, and underline the name of the author who will present the paper.* No paper will be placed on the program unless one of the authors, or a qualified person designated by the authors, has agreed to present it in person. Complete manuscripts should be sent in triplicate to the Managing Editor of the JOURNAL at 1860 Broadway, New York 23, N.Y.

Presentation of a paper at a technical meeting of the Society does not guarantee publication in the JOURNAL. However, all papers so presented become the property of The Electrochemical Society, and may not be published elsewhere, either in whole or in part, unless permission for release is requested of and granted by the Editor. Papers already published elsewhere, or submitted for publication elsewhere, are not acceptable for oral presentation except on invitation by a Divisional program Chairman.

Abstracts of "Recent News" Papers

Presented at Electronics Division Semiconductor Symposia

Houston Meeting
October 10-12, 1960

The Shape of Melt-Crystal Interfaces During Float Zoning of Silicon

J. H. Braun and R. A. Pellin, Pigments Dept., E. I. du Pont de Nemours & Co., Inc., Wilmington, Del.

The thermal environment of the interface of growth of a silicon crystal during float zoning is described. Depending on operating conditions, the interface between the melt and the growing crystal can be convex, near flat, or concave. The shape of the interface was made visible by slot doping of n-type silicon with an excess of boron dope to give a p-n junction between n-type crystal and p-type melt. This junction, delineating an interface, was decorated with a staining etchant.

Growth of Large Crystals by Grain Growth

L. R. Shiozawa and Allan Carlson, Electronic Research Div., Clevite Corp., Cleveland, Ohio

Monocrystals of CdS-type compounds have been grown up to a half pound by "grain-growth" recrystallization. As in growth and destruction of froth bubbles, molecules diffuse across cell walls in response to curvature-induced differences in vapor pressure, resulting in reduction of interfacial boundary area ultimately to zero. A temperature gradient is used to form and maintain maximum density. The method appears useful for any solid having a reasonable sublimation pressure.

Device and Material Considerations for Germanium Tunnel Diodes

T. R. Selig and R. C. Thomas, Semiconductor Products Dept., General Electric Co., Syracuse, N. Y.

The process for low peak current, low capacitance, germanium tunnel diodes, with high peak to valley current ratios, is described. The doping and crystal growing techniques employed yield homogeneous wafers. Material is selected by four-point probe resistivity measurements based on Hall carrier concentration. Device capacitance and the peak to valley current ratio have been correlated with carrier concentration. Junction formation is accomplished by alloying an appropriately doped metal to the germanium pellet in a reducing atmosphere. The peak current is tailored with an electrolytic etch. Tunnel diodes with the following characteristics are being obtained. I_p, 1 ma ± 10%; I_p/I_v, 10:1; C, 4 $\mu\mu f$; $-g$, 0.008 mho.

Inhomogeneous Impurity Distributions in InSb Crystals

A. J. Strauss and T. C. Harman, Lincoln Lab., Massachusetts Institute of Technology, Lexington, Mass.

Four-point resistivity measurements and differential chemical etching have been used to investigate transverse and longitudinal inhomogeneities in the distribution of various impurities in pulled crystals of InSb. The data indicate that in the case of Zn, at least, the increase in impurity concentration due to the presence of a <111> facet at the growth interface is associated with impurity "adsorption" at the interface. The mechanism of facet growth is discussed.

A Modified RF Coil to Facilitate Floating Zone Techniques

S. J. Silverman (present address: Research Lab., General Electric Co., Schenectady, N. Y.), Bell Telephone Laboratories, Allentown, Pa.

In conjunction with the floating zone technique, a modified rf work coil has been designed and used to create stable molten zones with length to diameter ratios less than unity. It is believed that these results are achieved because the coil concentrates the rf power in a limited region rather than because of enhanced electromagnetic levitation forces. The concentration of power promotes the formation of a flatter liquid-solid interface, and in practice permits the growth of crystals of larger diameter than we have otherwise been able to obtain by a floating zone procedure using Ge or GaAs.

Preparation and Properties of Some Peritectic Semiconducting Compounds

D. R. Mason and D. F. O'Kane, Dept. of Chemical and Metallurgical Engineering, University of Michigan, Ann Arbor, Mich.

Preliminary results on the preparation and properties of ternary semiconducting compounds in the homologous series $I^bInVI_2^b$ and $II^bIn_2VI_4^b$ are available where the group I^b elements are copper and silver, the group II^b elements are zinc, cadmium, and mercury, and the group VI^b elements are selenium and tellurium. All these compounds are semiconductors, as predicted from structure studies made by Hahn, *et al.*, and rules delineated by Mooser and Pearson.

Some knowledge of the ternary phase diagrams in which these compounds appear is desirable in order to aid in the preparation of homogeneous samples for evaluation. These ternary compounds represent a linear combination of two binary constituents, each of which has semiconducting properties. One constituent can be represented by the chemical formula $III_2^bVI_3^b$ and the other constituent either as $I_2^bVI^b$ or as II^bVI^b. Since each of the binary constituents is a pure chemical component, adequate equilibrium relationships can be obtained by investigating only the pseudobinary plane which joins them in the ternary system.

A redetermination of the melting points and phase diagrams of some of the binary constituents has been undertaken in order to correct several serious inaccuracies in the literature. The determination of the phase diagrams for the various pseudobinary systems is in progress, using differential thermal analysis, and microscopic and x-ray examinations.

It has been found that $HgIn_2Te_4$ is the only compound in either series that is definitely known to be congruently melting; the remaining nine compounds appear to be peritectics. The system CdTe-In_2Te_3 has been characterized quite completely, and homogeneous samples of the peritectic compounds in this system have been prepared using zone refining techniques. Preliminary electrical measurements are available.

Preparation and Structure of Compounds in the Samarium-Sulfur System

M. D. Houston, Ceramics Section, Materials Labs., Westinghouse Electric Corp., 7325 Penn Ave., Pittsburgh, Pa.

The preparation of samarium sulfides is discussed on the basis of the chemistry of the reactants and the reaction. X-ray diffraction data for compound and structure identification are presented. Physical properties of polycrystalline compacts are given.

Epitaxial Films of Silicon and Germanium by Halide Reduction

H. C. Theurer and H. Christensen, Bell Telephone Laboratories, Inc., Murray Hill, N. J.

Epitaxial films of silicon and germanium on low-resistivity substrates are required for the new high-fre-

quency mesa transistors and other semiconductor devices. These films are conveniently prepared with controlled thickness and conductivity type by the hydrogen reduction of either $SiCl_4$ or $GeCl_4$.

The reduction apparatus utilized for film preparation consists essentially of a source of pure hydrogen, a halide saturator, and a water-cooled quartz reaction vessel. The substrate wafer to be coated rests in a silicon or graphite heating pedestal within the reactor and is heated externally by a radio frequency generator. In the case of silicon, the substrate is first heated at 1295°C for ½ hr in dry hydrogen to remove surface oxygen. For film deposition, treatment in hydrogen containing 2 mole % $SiCl_4$ at a flow of 1 l/min for 5 min at 1270°C results in an epitaxial layer 6-8 μ thick. For germanium, the hydrogen pretreatment is carried out at 830°C for 10 min. Subsequent treatment in hydrogen containing 0.2 mole % $GeCl_4$ with a hydrogen flow of 1 l/min for 10 min at 830°C results in a film approximately 5 μ thick.

The kinetics of the two reduction processes are quite similar, and, in this presentation, the chemistry of the silicon process is discussed in some detail. Doping of $SiCl_4$ with BBr_3 and PCl_3 for p- and n-type films of controlled resistivity is included. Films prepared by the halide reduction method are good single crystals with the orientation of the substrate as determined from electron diffraction patterns which show Kukuchi lines.

Moisture Gettering with Porous Vycor

M. J. Rand, Bell Telephone Laboratories, Inc., Allentown, Pa.

Extensive aging experiments on alloy transistors at Bell Telephone Laboratories have established that device reliability is much improved by including a porous Vycor moisture getter in the enclosure. An apparatus to study the adsorptive capacity of the Vycor at relative humidities below 5% is described. Results to date on the adsorption isotherms at various temperatures and the rate of attainment of equilibrium are presented. The activation of the Vycor by heating and pumping also has been investigated.

Influence of Hydrofluoric Acid on the Mechanism of Dissolution of Germanium

Wolfgang Mehl, Radio Corp. of America, RCA Labs., David Sarnoff Research Center, Princeton, N. J.

Hydrofluoric acid lowers the activation energy for both the electrolytic and the chemical dissolution of germanium. For the anodic dissolution of p-type germanium, the Tafel slope changes from 130 mv in the absence of HF to a limiting value of 60 mv after the addition of sufficient HF. The anodic limiting current for the dissolution of n-type germanium increases when HF is added to the electrolyte. The implications of these measurements for the theory of the germanium electrode are presented.

Solid Solutions of InTe and CdTe in PbTe and SnTe

A. J. Rosenberg (present address: TYCO Inc., Boston, Mass.), Lincoln Lab., Massachusetts Institute of Technology, Lexington, Mass.

Single crystals of the compositions $Pb_{.97}In_{.03}Te$, $Pb_{.97}Cd_{.03}Te$, $Sn_{.97}In_{.03}Te$, and $Sn_{.97}Cd_{.03}Te$ have been prepared. The crystals have the rock-salt structure type characteristic of PbTe and SnTe, but with smaller lattice parameters than the pure compounds. The macroscopic densities agree with the values calculated on the assumption that Cd and In replace Pb and Sn. Despite the fact that the concentrations of valence electrons in PbTe and SnTe are reduced by as much as 3×10^{20}/cm^3 by these substitutions, the magnitude of the free charge carrier concentration remains unaffected in every case. The general significance of these results is discussed.

Voltage Breakdown of Silicon Rectifiers as Influenced by Surface Angle

O. M. Clark, Semiconductor Products Div., Motorola Inc., Phoenix, Ariz.

In high-voltage silicon rectifiers, the angle at which the space charge region of a reverse biased junction intersects the die edge can influence surface breakdown. Reversed biased junctions having shallow angles at the die edge have been observed to have higher surface breakdown voltages. Since the breakdown voltage of a given junction can be increased by spreading the space charge at the die surface over a greater area, a new method of producing single junction multikilovolt rectifiers is feasible. Single junction devices have been produced which can be reverse biased as high as 3500 v with less than 10 μa of leakage current.

Silicon Carbide Transistors

L. F. Wallace and H. C. Chang, Westinghouse Electric Corp., Pittsburgh, Pa.

High-temperature unipolar transistors exhibiting power gain have been made using n-type α-SiC for the channel material. The p-type gates were formed by the aluminum-diffusion process. The high-purity material was prepared in a Lely-type furnace and has a minimum resistivity of about 500 ohm-cm at room temperature. Control of the channel geometry was achieved by diffusion and electrolytic etching techniques. The design principles and electrical characteristics are presented.

Base-Layer Design for High-Frequency Transistors

H. S. Veloric, D. Rauscher, and C. R. Fuselier, Semiconductor and Materials Div., Radio Corp. of America, Somerville, N. J.

Total base impurity concentrations have been determined for the complementary error function (erfc) distribution, an outdiffused impurity distribution, and the Gaussian distribution. Base-width control and "reach-through" voltage is considered for the three cases. The "reach-through" voltage is calculated from the solution of Poissons equation for each type of distribution. For the distributions considered, control of base width in the range of 0.02-0.03 mil is shown to be difficult. Experimental results are presented for the "box method" of boron deposition and for diffusion.

Section News

New York Metropolitan Section

The first meeting of the new season was held at Swartz's restaurant in New York City on October 5. Speaker was Dr. Herbert H. Uhlig, professor in charge of the Corrosion Laboratory, M.I.T.

Dr. Uhlig discussed developments in the electrochemical theory of corrosion which are leading to practical applications. He mentioned that stable passivity can be obtained by suitable alloy additions to the base metal. For example, the addition of 0.2% palladium to commercial titanium reduced the corrosion rate in hydrochloric acid from 10,000 to 0.1 mils/yr.

Dr. Uhlig pointed out that high-temperature oxidation is an electrochemical phenomenon. As an example, he cited the castatrophic corrosion in boilers resulting from the use of fuel oils containing vanadium. If the V_2O_5, formed as a product of combustion, unites with other elements to form low-melting compounds, corrosion is severe. Rates can be reduced by lowering the operating temperature below the melting point of the compounds, which may not be practical, or by adding materials such as calcium compounds to raise the melting point of the mixture.

San Francisco Section

The first meeting of the 1960-1961 season was held on September 28 at the University of California, Men's Faculty Club. After transaction of some Local Section business, the group enjoyed a discussion of "Image Furnaces" by Robert De La Rue of Stanford Research Institute.

A historical survey pointing out different structures and optics for image furnaces led to the contrast of energy sources: solar or arc image. Such furnaces are used for the creation of high temperatures in a controllable ambient and in the absence of an electric field. With pulse shutter control, they can be used for

ECS Assistance Award

Dr. Charles L. Faust, Chairman of the Honors and Awards Committee of the Society, announces that, in accordance with approval by the Board of Directors of the Society, Assistance Awards will be made to fellows or teaching assistants pursuing work between the degrees of B.S. and Ph.D. on a subject in a field of interest to the Electrochemical Society.

The Assistance Award will amount to $800 for one year only. Three such awards are available for the period June-September 1961. It is intended that an award shall be made to the possessor of a nine-month grant for the academic year 1961-1962 and who shall have been the holder of a similar grant for the academic year 1960-1961. The Assistance Award is intended to cover a period during which the recipient has no financial support for the continuance of his work.

Interested students should write to Dr. H. A. Laitinen, Dept. of Chemistry and Chemical Engineering, University of Illinois, Urbana, Ill. Dr. Laitinen is Chairman of the Subcommittee of the Honors and Awards Committee to consider recipients.

---

studying the biological effects of intense radiation such as atomic blasts as well as for high-temperature inorganic fusions.

The next meeting, on "Micro Circuit Components," will be in November.

Worden Waring, *Vice-Chairman*

Personals

M. J. Allen is leaving Ciba Pharmaceutical Products, Inc., Summit, N. J., early in December to take up his new duties as director of chemical research, Electro-Optical Systems, Inc., 125 N. Vinedo Ave., Pasadena, Calif., on January 1, 1961.

G. M. Bestler has joined the manufacturing department of the Remington Rand Univac Military division in St. Paul, Minn., with responsibility for the development of techniques for the manufacture of film memories for Univac computers. Formerly he was employed by Minneapolis-Honeywell Regulator Co., most recently as manager of the new product development section, semiconductor division, at West Palm Beach, Fla.

J. J. Harwood has been named manager of the metallurgy department of Ford Motor Co.'s Scientific Lab. in Dearborn, Mich. In his new position, Mr. Harwood will direct extensive fundamental research programs in the physics of metals and alloy systems, physical metallurgy, and ceramic science. Previously, he was head of the Metallurgy Branch of the Office of Naval Research, Washington, D. C.

R. W. Hull, of Basking Ridge, N. J., has been appointed vice-president in charge of reliability of the recently expanded Semiconductor Division of the General Instrument Corp. Dr. Hull will head up a special Reliability Dept. to analyze and evaluate process techniques, materials, test, and rating procedures at the division's three major plants in Newark, N. J., Jamaica, N. Y., and Woonsocket, R. I. He formerly was the division's director of research.

Manuel Shaw has been named to head electrochemical research for the Electric Autolite Co., Toledo, Ohio. In his new post, Dr. Shaw will have under his direction the company's fuel cell program. He also will direct a greatly expanded research effort on various types of electrical energy conversion systems. Previously, Dr. Shaw was affiliated with the Chrysler Corp. in Detroit, Mich., and the Ovitron Corp. in Long Island City, N. Y.

News Items

1960 Annual Index

The Annual Index for Vol. 107 (1960) of the JOURNAL will appear in the February 1961 issue. Reprints of the Index can be obtained about the middle of March by writing to The Electrochemical Society, 1860 Broadway, New York 23, N. Y.

Second Seminar in Electrochemistry

The Second Seminar in Electrochemistry will be held at the Central Electrochemical Research Institute, Karaikudi-3, Madras State, India, from December 17 to 20, 1960.

Abstracts will be printed and copies supplied in advance of the meeting. The proceedings will not be published.

Meetings of the International Committee of Electrochemical Thermodynamics and Kinetics (CITCE)

Meeting in Belgium.—The 12th Meeting of CITCE will take place in Brussels, April 24-29, 1961. Sessions of the following Commissions are scheduled: 1. Tension-pH diagrams; 3. Experimental Methods in Electrochemistry; 4. Batteries; 5. Corrosion; 6. Kinetics. The general theme of the meeting will be Corrosion. The session on Batteries will have two themes: (*a*) Fuel Cells, (*b*) Methods of Determination of Particle Size, Porosity, Surface Area, and Activity of Electrode Materials.

Meeting in Canada.—A meeting of CITCE will take place August 7-9, 1961, in Montreal, within the frame of the IUPAC Congress. The general theme will be Electrochemistry of Fused Salts. A session of Commission 6 of CITCE (Electrochemical Kinetics) also is scheduled.

Correspondence regarding attendance or presentation of papers at these meetings can be addressed to N. Ibl, Secretary General of CITCE, Lab. for Physical Chemistry, Swiss Federal Institute of Technology, Universitätstr. 6, Zurich, Switzerland.

Correspondence regarding the 12th Meeting's general theme on Corrosion should be addressed to M. Pourbaix, Université Libre de Bruxelles, 50 Ave. F. D. Roosevelt, Bruxelles, Belgium.

Conference on Ultrapurification of Semiconductor Materials

The Electronics Research Directorate of Air Force Cambridge Research Laboratories will sponsor an unclassified Conference on the Ultrapurification of Semiconductor Materials, to be held at New England Mutual Hall in Boston, Mass., April 11-13, 1961. It is hoped that the Conference will provide a focal point for scientific work carried out in the field of ultrapurification of semiconductor materials. Leading workers on ultrapurification in this country and abroad will be invited to attend.

Papers, limited to approximately 30 minutes, including discussion period, have been invited on the following topics: 1. Synthesis—Methods and techniques for the preparation of elemental and compound semiconductor materials; 2. Purification—Employment of conventional or novel techniques for

obtaining high-purity semiconductors; 3. Analysis—Including activation, spectroscopy, resonance phenomena, and other techniques for the analysis of trace impurities; 4. Physical Chemistry—Embracing the classical physical chemical studies of thermochemistry and kinetics and the chemistry of the defect solid state.

High-Temperature Materials Conference

The Cleveland Section of the American Institute of Mining, Metallurgical, and Petroleum Engineers will sponsor a High-Temperature Materials Conference in the Hotel Pick-Carter, Cleveland, Ohio, April 26 and 27, 1961, in cooperation with the High-Temperature Alloys Committee and the Refractory Metals Committee of the Institute of Metals Division of The Metallurgical Society. The society is a constituent organization of the institute.

Subjects will cover materials suitable for use above 1600°F and will include: "Requirements for High-Temperature Alloys," "Cobalt and Nickel Alloys," "Molybdenum and Columbium Alloys," "Tungsten and Tantalum Alloys," "Graphite and Refractory Compounds," "Coatings on Refractory Metals," and "Processing and Fabrication of Refractory Metals."

Expansion of Niagara Falls, Ont., Plant of Strategic Materials

Strategic Materials Corp. and Universal-Cyclops Steel Corp. have signed an agreement for the joint development of the use of the Strategic-Udy processes in the production of materials for use in stainless steels and/or heat-resisting alloys.

Under the agreement, Strategic Materials will build a $1,500,000 addition to its plant at Niagara Falls, Ont., expected to be in operation by the end of this year. This represents a large-scale increase in the pilot plant facility that has been in operation for nearly three years exploring the use of low-grade ores previously considered unusable.

Frank W. Chambers, president of Strategic Materials Corp., explained that the Strategic-Udy processes for the first time may permit the economical utilization of low-grade lateritic and chromite ores in the commercial production of high-quality stainless steels and/or heat-resisting alloys. Such low-grade ores are available in abundance in many areas of the world and this development would provide markets for such deposits.

Strategic will build the new plant addition and be responsible for its operation while Universal-Cyclops will furnish technical assistance arising from its more than 75 years' experience in producing specialty steels. The plant addition will include an electric furnace and a kiln as well as auxiliary facilities, using the already available personnel and laboratories in Niagara Falls.

World Adopts New Standard of Length

At 6:00 P.M. Paris time on October 14, the world adopted a new international standard of length—a wave length of light—replacing the meter bar which has served as the standard for over 70 years. The announcement was made from Paris by Dr. Allen V. Astin, director of the National Bureau of Standards, U. S. Dept. of Commerce, Washington, D. C. The action was taken by the 11th General Conference on Weights and Measures, which met in Paris the week of October 10.

The new definition of the meter as 1,650,763.73 wave lengths of the orange-red line of krypton 86 will replace the platinum-iridium meter bar which has been kept at Paris as an international standard for length since 1889 under the Treaty of the Meter.

Enthone Appoints French Licensee

Enthone, Inc., of New Haven, Conn., subsidiary of the American Smelting and Refining Co., has announced the licensing of Pernix Grauer & Weil of Paris to manufacture, sell, and service Enthone products in France, Belgium, Spain, Portugal, and French Overseas Territories.

New Fuel Cell Research Activities

A long-term research program to advance fuel-cell technology, described as "a major research effort being underwritten by some 25 companies," has begun at Battelle Memorial Institute, Columbus, Ohio.

The program, at present on a five-year schedule, "will be fundamental in nature and is designed to complement existing government, industrial, and academic studies on fuel cell technology," according to Dr. John McCallum, project director. "Before the fuel cell's full potential can be realized as a source of power for automobiles, domestic heating and cooling, and industrial processes," he said, "there will have to be a number of inventions, innovations, and breakthroughs. Battelle, with its diversity of scientific disciplines,

Manuscripts and Abstracts for Spring 1961 Meeting

Papers are now being solicited for the Spring Meeting of the Society, to be held at the Claypool Hotel in Indianapolis, Ind., April 30, May 1, 2, 3, and 4, 1961. Technical sessions probably will be scheduled on Electric Insulation, Electronics (including Luminescence and Semiconductors), Electrothermics and Metallurgy, Industrial Electrolytics (including a Symposium on Fuel Cells), and Theoretical Electrochemistry (including a Symposium on Instrumentation).

To be considered for this meeting, triplicate copies of abstracts (*not exceeding 75 words in length*) must be received at Society Headquarters, 1860 Broadway, New York 23, N. Y., *not later than January 2, 1961. Please indicate on abstract for which Division's symposium the paper is to be scheduled and underline the name of the author who will present the paper.* No paper will be placed on the program unless one of the authors, or a qualified person designated by the authors, has agreed to present it in person. Complete manuscripts should be sent in triplicate to the Managing Editor of the JOURNAL at the same address.

Presentation of a paper at a technical meeting of the Society does not guarantee publication in the JOURNAL. However, all papers so presented become the property of The Electrochemical Society, and may not be published elsewhere, either in whole or in part, unless permission for release is requested of and granted by the Editor. Papers already published elsewhere, or submitted for publication elsewhere, are not acceptable for oral presentation except on invitation by a Divisional program Chairman.

hopes to contribute to this process of discovery."

Much of Battelle's research on the cell will be aimed at obtaining a better understanding of the properties of materials required in a cell.

One approach to improved materials for the fuel cell that Battelle will use is to study the internal electronic structure of alloys. From this study, scientists hope that they will be able to develop an alloy composition with unique electrical and electrochemical properties for cell electrodes.

Another approach to be employed in the Battelle program is the study of thin films of metals.

Other phases of the research program will include study of active carbon electrodes with metal-chelate surfaces and the use of unusual plating techniques to apply porous metal surfaces to electroformed electrodes for the cell. Concurrent with the experimental work, Battelle will collect and interpret new data on fuel cells for the use of participating companies.

McGraw-Edison Co. and Standard Oil Co. (Indiana) also recently announced an agreement for joint research and development on fuel cells.

The initial two-year agreement for the project, subject to renewal, calls for combining know-how in their respective fields of the Thomas A. Edison Research Laboratory division of McGraw-Edison at West Orange, N. J., and Standard Oil's research and development department at Chicago and Whiting, Ind.

The project was disclosed by Dr. Donald W. Collier, president of the Thomas A. Edison Research Laboratory, and Dr. Philip C. White, general manager of research and development for Standard Oil.

The Edison Laboratory specializes in electrochemistry, electrolytes, cell reactions, electrode construction and activation, and electrochemical cell construction. Standard Oil researchers will contribute their knowledge of catalysis, combustion oxidation, and hydrocarbon or petroleum fuel characteristics.

New RCA Plant at Mountaintop, Pa., Gears for Full-Scale Operation

With pilot production of transistors already under way, the Radio Corp. of America's new plant at Mountaintop, Pa., is being geared for full-scale operation at a level of several million transistors and other semiconductors a month.

The new manufacturing unit will provide RCA with facilities to meet the current heavy demand for semiconductors and permit still further expansion as the market continues to grow.

The plant, which is scheduled for full-scale production by spring 1961, will be one of the world's largest facilities devoted exclusively to the design, development, and manufacture of industrial and military semiconductor products.

Its product line will include both germanium and silicon devices in the low, medium, and high power ranges for use in navigational equipment, industrial controls, mobile communications, space satellite and ballistic missile instrumentation, and electronic power supplies, among others.

Polytechnic Institute of Brooklyn to Build Graduate Center on Long Island

Ground was broken in September at Farmingdale, N. Y., for Polytechnic Institute of Brooklyn's new Graduate Center, Long Island's first graduate school of engineering.

The facility, with attendant research laboratories, is being established at a cost of $1,600,000 on 25 acres of land located on Route 110, a half mile east of the Nassau-Suffolk border. Donated to Polytechnic by Republic Aviation Corp., the site formerly was part of Republic's Farmingdale property.

The main building will be a combination one- and two-story structure, providing nine classrooms with seating capacities ranging from 30 to 200, a science library for 20,000 volumes, administrative offices, dining area, lounge, and meeting room. The dining area, lounge, and meeting room are of a flexible design, capable in combination of seating up to 500 persons.

Included in the main building will be 12 laboratories for research in aero-space engineering, electrical engineering, physics, and electrophysics. The main building will contain 53,000 square feet of floor space.

The second building will be a steel frame structure of 12,000 square feet, housing three laboratories for basic research in aerodynamics and high-power electronics. It will be covered with aluminum and expandable in all four directions.

Study will be restricted to graduate work leading toward the master's and doctor's degrees in full-time and part-time, day and evening sessions. Courses will be offered by the departments of aero-space engineering, electrical engineering, mechanical engineering, mathematics, and physics.

Notice to Members

Re Voting Ballot

By now you have received your official voting ballot from Society Headquarters. If you have not already done so, please return the ballot *by December 15* so that your vote can be included in the final election count.

Ford Grant Awarded to Western Reserve University for New Science Center

A grant of $100,000 over a three-year period has been awarded to Western Reserve University for its new Science Center by the Ford Motor Co. Fund, it has been announced by president John S. Millis.

Of the $6,270,000 goal needed to build and maintain the Center, $5,495,876 has been pledged. With the Ford grant, $674,124 still has to be raised.

The first part of the building, which will be named for Dr. Millis, is expected to be completed by the fall of 1961 and will be used by the chemistry department. The remainder will be ready for occupancy by spring 1962. Construction began in August 1960.

The structure represents the first phase in the development of a new basic science building. It will provide laboratories, a library, auditorium, and teaching and research facilities for the departments of biology, chemistry, physics, geology, astronomy, and mathematics.

Pfizer Dedicates New Medical Research Laboratories

The newest and largest scientific research center of Chas. Pfizer & Co., Inc., was dedicated on October 6, 1960 in Groton, Conn.

Nearly 1000 physicians, research scientists, educators, government officials, community leaders, and drug industry executives looked on as Dr. Irvine H. Page, director of research at the Cleveland Clinic Foundation, unveiled a bronze plaque dedicating the new Pfizer Medical Research Laboratories. The day-long dedication program featured tours of the laboratories and the company's nearby production plant. The laboratories house some 400 scientists, technicians, and supporting personnel.

Macrobiological, chemical, and biochemical research units, formerly housed chiefly in the company's Brooklyn, N. Y., laboratories, have

been consolidated in the modern, 177,000-square-foot structure on a 19-acre landscaped site overlooking the Thames River.

The new laboratories make possible a fully integrated research program against a variety of medical problems, including heart and blood vessel ailments, mental illness, infectious diseases, and metabolic disorders.

The major objective of the new laboratories is a coordinated attack on current therapeutic and pharmaceutical problems by physicians and scientists skilled in such fields as synthetic and analytical chemistry, pharmacology, biochemistry, bacteriology, and many other scientific disciplines.

Book Reviews

Handbook of Electrochemical Constants, by Roger Parsons. Published by Academic Press, Inc., New York, 1960. vii + 113 pages; $6.00.

Professor Parsons has crammed an amazing amount of information into this pocket-size book, partly by an excellent organization of his tables and partly through the use of fine, though readable, print. The topics covered range from equilibrium constants and thermodynamic functions through viscosity and diffusion, to conductivity and kinetic properties. Molten salts, organic, and some inorganic systems are covered, in addition to the usually aqueous systems. Inevitably, some topics have been treated sketchily and others omitted altogether. The orientation is that of the theoretical physical chemist and theoretical electrochemist rather than that of the applied electrochemist. Although, to facilitate use of the data, the equations are given from which the calculations have been made and in some cases the experimental methods are indicated, there is no bibliography and only a few references are mentioned. Thus, either corroborating or supplementing these data from the literature would be very difficult. In spite of this, the book is highly recommended. It should prove to be very convenient and helpful, especially in the laboratory.

H. W. Salzberg

3rd Colloque de Métallurgie Sur la Corrosion. Published by North-Holland Publishing Co., Amsterdam, The Netherlands, 1959. 239 pages; $10.00

This volume contains 20 papers on the corrosion of a fairly wide range of materials, with particular emphasis on those materials of interest to nuclear technologists. Also included in the text is a transcript of discussions by participating members of the symposium. The papers can be classified as approximately 25% review articles, with the balance either material evaluation studies or work of a more fundamental nature on the mechanism of specific corrosion reactions.

High-temperature oxidation is considered in seven papers with carbon dioxide or air as the oxidizing gas. The materials studied in this high-temperature work include magnesium, carbon, uranium, some ferrous alloys, and miscellaneous transition metals. One paper in this group presents data on the ignition temperatures of magnesium and uranium in carbon dioxide.

Corrosion of zirconium alloys, nickel-base alloys, and stainless steels in high-temperature water is the subject of three separate papers. Also in the aqueous corrosion field, some new data is given on the precipitation of chromium carbides in stainless steel and subsequent sensitization to intergranular corrosion. Further papers include work on the corrosion of steel by hydrogen sulfide saturated aqueous solutions, and a radiochemical investigation of the effect of adsorbed sulfur on the corrosion of iron in hydrochloric acid.

On the whole, the symposium is an interesting "potpourri," and most workers in the field of corrosion should find something of value in the published proceedings.

B. E. Hopkinson

Extractive Metallurgy, by Joseph Newton. Published by John Wiley & Sons, Inc., New York, 1959. 532 pages; $9.75.

Professor Newton's book has been written to fill a great need in teaching—a descriptive text in extractive metallurgy for students taking no other courses in the subject. The book is arranged from a unit-operations viewpoint with chapters on ore dressing, pyrometallurgy, hydrometallurgy, and electrometallurgy, along with chapters on sources of metals, chemical principles, fuels and refractories, ingots, and a rather lengthy chapter on the structure of metals and alloys.

The author has handled the problem of jargon quite well, keeping it to a minimum, and introducing it in a free-flowing style by the use of italics. Thus, the index may be used instead of a separate glossary to find rapidly the definitions of the terminology. The use of worked examples in the text and the problem lists at the end of the chapters will prove to be a help to the student and remove some of the burden from the teacher.

There are aspects of the book, however, which seem somewhat less desirable. The author devotes 43 pages to chemical principles and 88 pages to the structure of metals and alloys. This emphasis on structure of metals instead of chemical and thermodynamic principles seems unfortunate in a treatment of extractive metallurgy, where thermodynamic and chemical principles could be so fruitfully used. In other respects, too, the balance in treatment of the subject may be disappointing to some. Of the 514 pages of text, only slightly over 200 pages are devoted to the actual operations used in extracting metals from their ores. Also, after devoting a liberal amount of space to an explanation of phase diagrams, he hardly uses them in the discussion of the extraction processes. Instructors who emphasize iron and steelmaking will undoubtedly find insufficient the single page devoted to coke production.

The author has a tendency to introduce new material in the summaries, possibly resulting in some confusion to the student.

In summation, it may be said that the author has achieved his stated objective by writing a clear exposition of the material he has chosen to present. As in any subject, the exact

Notice to Subscribers

Your subscription to the JOURNAL of The Electrochemical Society will expire on *December 31, 1960.* Avoid missing any issue. Send us your remittance now in the amount of $24.00 for your 1961 subscription. (Subscribers located outside the United States must add $1.00 to the subscription price for postage, and payment must be made by Money Order or New York draft, not local check.) A final expiration notice has been mailed to all subscribers.

A bound volume of the 1961 JOURNALS may be obtained for $18.00, subject to prior acceptance. Bound volumes are *not* offered independently of your JOURNAL subscription.

topics and their order of presentation is a matter of individual preference. However, this text is sure to appeal to many teachers.

Marvin Metzger

Announcements from Publishers

"Photochemistry in the Liquid and Solid States." Edited by L. J. Heidt, R. S. Livingston, Eugene Rabinowitch, and Farrington Daniels. Published by John Wiley & Sons, Inc., New York, 1960. 174 pages; $6.00.

This volume contains some of the papers presented at a symposium held in September 1957 and therefore probably already is outdated. The purpose was to exchange ideas and to decide which lines of basic research should be followed in investigating energy-storing photoreactions not requiring living plants. The discussions were concerned primarily with the absorption of energy but there was brief mention of photogalvanic cells as one obvious method of using the stored energy.

"Technology of Non-Metallic Coating," by A. Ya. Drinberg, E. S. Gurevich, and A. V. Tikhomirov. Published by Pergamon Press, Inc., New York, 1960. 547 pages; $15.00.

"Boron—Synthesis, Structure, and Properties," the technical papers comprising the proceedings of the Conference on Boron, sponsored by the Institute for Exploratory Research, U. S. Army Signal Research and Development Lab., Fort Monmouth, N. J., held at Asbury Park, N. J., during September 1959. Published by Plenum Press, Inc., New York, 1960. 208 pages; $8.50.

"Electrical Noise," by W. R. Bennett. Published by McGraw-Hill Book Co., New York, 1960. 288 pages; $10.00.

"Nuclear Metallurgy, Vol. VII." Published by The Metallurgical Society of the American Institute of Mining, Metallurgical, and Petroleum Engineers, New York, 1960. The 10th in a Special Report Series of the society's Institute of Metals Division, the volume includes technical papers prepared for presentation at the Fall Meeting of the society in Philadelphia, Pa., October 17-20, 1960. 29 pages; $7.00.

"The McGraw-Hill Encyclopedia of Science and Technology," a 15-volume compendium of today's scientific and technological knowledge. Published by McGraw-Hill Book Co., New York, 1960. $175.00.

"The Structure of Glass, Vol. 2," American edition, the Proceedings of the Third All-Union Conference on the Glassy State held in Leningrad, November 16-20, 1959. Published by Consultants Bureau Enterprises, Inc., New York, 1960. 525 pages; $25.00.

"Development of Protective Coatings for Refractory Metals," C. G. Goetzel and others, New York University, for Wright Air Development Div., U. S. Air Force, Feb. 1960. Report PB 161736,* 57 pages; $1.50.

"Protective Coatings for Refractory Metals," C. G. Bergeron and others, University of Illinois, for Wright Air Development Div., U. S. Air Force, Jan. 1960. Report PB 161739,* 50 pages; $1.25.

"Further Investigation of the Effects of Molten Boron Oxide on High Temperature Materials," J. W. Rosenbery, University of Dayton Research Institute, for Wright Air Development Div., U. S. Air Force, Jan. 1960. Report PB 161703,* 102 pages; $2.50.

"Oxidation of Tungsten and Tungsten Based Alloys," E. A. Gulbransen and others, Westinghouse Electric Corp., for Wright Air Development Div., U. S. Air Force, Feb. 1960. Report PB 161718,* 86 pages; $2.25.

"Beryllium Research for Development in the Area of Casting," F. A. Crossley and others, Armour Research Foundation of Illinois Institute of Technology, for Wright Air Development Div., U. S. Air Force, Feb. 1960. Report PB 161754,* 102 pages; $2.50.

"Investigation of the Properties of Tantalum and Its Alloys," F. F. Schmidt and others, Battelle Memorial Institute, for Wright Air Development Div., U. S. Air Force, March 1960. Report PB 161758,* 112 pages; $2.50.

* Order from Office of Technical Services, U. S. Dept. of Commerce, Washington 25, D. C.

ELECTROCHEMICAL RESEARCH CHEMISTS

Expanded fuel cell research and development program presents new opportunities with The Electric Autolite Company in the Toledo Ohio laboratories. Present requirements include the following:

Physical Chemist with post-graduate or equivalent experience in catalysis and chemical kinetics. Practical experience in adsorption and rate study measurements.

Organic Chemist with post-graduate experience or equivalent in organic synthesis, especially high polymers.

Electrochemist with post-graduate work in electro-chemistry (Ph.D.) including knowledge of latest laboratory techniques. Experience in use of electronic instrumentation and construction of measuring circuitry.

Mail complete résumé and salary requirements to: W. B. Richardson, Personnel Manager, P. O. Box 931, The Electric Autolite Company, Toledo 1, Ohio.

Literature from Industry

Short Form Semiconductor Catalog. An up-to-date, 24-page catalog published by International Rectifier Corp. covers over 800 semiconductor devices, including ratings, characteristics, and descriptive data on silicon glass diodes; silicon small-power, medium-power, and high-power, rectifier cells; high-voltage cartridge rectifiers; zener diodes and reference elements; silicon controlled rectifiers; silicon and selenium rectifier stacks; silicon solar cells; and selenium contact protectors. Also included is a comprehensive listing of JEDEC rectifier types, with cross reference to device classification, rating, and page number.

For a free copy, write on company letterhead for Short Form Catalog, International Rectifier Corp., El Segundo, Calif.

Hoffman Semiconductor Catalog. A new 20-page catalog details the complete and current product line of the Semiconductor Division of Hoffman Electronics Corp. It contains electrical and physical parameters of Hoffman's silicon solar devices, silicon transistors, silicon diodes, silicon controlled rectifiers, zener regulators, and zener reference devices.

Copies are available from Publications Section, Semiconductor Division, Hoffman Electronics Corp., 1001 N. Arden Dr., El Monte, Calif.

H-VW-M New Products and Processes Bulletin. Hanson-Van Winkle-Munning Co. has announced the availability of a four-page, color bulletin listing and describing all company products and processes, including the three new nickel processes, Levelume 220, the improved Levelume; Permalume, the latest semibright processes that can be continuously carbon treated; and Superlume, the premium superbright, superhigh-leveling bright nickel bath.

Write for Bulletin No. PP-103 to Hanson-Van Winkle-Munning Co., Church St., Matawan, N. J.

TVA Chemical Engineering Bulletin No. 4, entitled "Evaluation of Reducing Carbons for Use in Electric Phosphorus Furnaces," compiled by J. C. Barber, E. C. Marks, and G. H. Megar, reports studies of the partial substitution of various types of coal for coke in the electrical smelting of phosphate rock.

Single copies of the bulletin can be obtained without charge from Tennessee Valley Authority, Division of Chemical Development, Wilson Dam, Ala.

Paper Electrophoresis Brochure, eight pages, describes application of a high-resolution buffer to the LKB paper electrophoresis equipment, which is designed for complete electrophoretic procedure, from controlled application of sample to paper, to the final steps of staining and washing. A horizontal-type strip housing with tightly fitting lid allows complete saturation in a short time, and more reproducible results.

The brochure, No. 3276-04, can be obtained from LKB Instruments, Inc., 4840 Rugby Ave., Washington 14, D. C.

New Products

Exide Nickel-Cadmium Batteries. Exide Industrial Division of the Electric Storage Battery Co. has added pocket-type nickel-cadmium batteries to its broad line of industrial storage batteries. The new line

CHEMIST
ELECTRO
PH. D.

Exceptional position now available in research & development division of large precious metals concern located in Newark, New Jersey, for electro chemist with doctorate degree.

Previous experience preferred but not essential. Excellent potential for advancement and liberal employee benefits program.

Submit resume with full particulars

Box A-286,
c/o Electrochemical Society,
1860 Broadway, New York 23, N. Y.

PHOSPHOR DEVELOPMENT CHEMIST

General Electric's electronic phosphor engineering group has an opening for a chemist or chemical-physicist for solid state development work on cathode ray tube and electroluminescent phosphors.

This position offers the opportunity to participate in the continuing expansion of challenging products and a challenging science. The work is in fully equipped laboratories in Cleveland. Salary commensurate with education and experience.

Write informally or send résumé to W. N. Halbedel, Employee & Community Relations Supervisor, General Electric Company, 1099 Ivanhoe Road, Cleveland 10, Ohio.

is available in 22 electrical sizes, with 8-hr capacity ratings ranging from 10 to 450 amp-hr, and in other special types and sizes.

Further information can be obtained from Exide Industrial Division, Electric Storage Battery Co., Rising Sun and Adams Aves., Philadelphia 20, Pa.

Dow Single-Crystal Silicon. Single-crystal, high purity silicon is now being produced by Dow Corning Corp., Midland, Mich.

Resistivity and lifetime profiles indicate uniform characteristics over the entire length of each crystal, and from crystal to crystal. This uniformity is expected to result in increased yield of quality semiconductor devices, especially power rectifiers, diodes, and pnpn switches.

Single-crystal silicon is produced at Dow Corning by processing polycrystalline rod of their own manufacture in vacuum zone refiners of the type internationally recognized as the world's finest—zoners that have produced the highest purity silicon ever refined.

Available in various diameters to 26 mm (approx. 1 in.) and lengths to 350 mm (13¾ in.), undoped P-type single crystals have less than 0.15 ppb of boron; greater than 1000 ohm-cm; minority carrier lifetime, greater than 400 μ sec.

Employment Situations

Positions Available

Glass-Ceramics—Ph.D. or perhaps M.S. for advanced work with glasses and ceramics for special applications in semiconductor devices. Professional level in Research and Development Department. Basic research is desired as well as some applications to particular devices. Please send detailed résumé including salary requirements to Mr. Don Palmer, Fairchild Semiconductor Corporation, 545 Whisman Road, Mountain View, California. Interviews for qualified applicants will be arranged from anywhere in the United States. All inquiries strictly confidential and acknowledged.

Surface Physics—Ph.D. or possibly M.S. for research on surface physics of semiconductors. Some experience is advantageous but not essential. Professional level in Research and Development Department. Well equipped laboratory near major universities. Please send detailed résumé including salary requirements to Mr. Don Palmer, Fairchild Semiconductor Corporation, 545 Whisman Road, Mountain View, California. Interviews for qualified applicants will be arranged from anywhere in the United States. All inquiries strictly confidential and acknowledged.

Four challenging research positions for experienced surface chemists, in fully-equipped laboratory devoted to research and development on aluminum and copper alloys, involving: A. Electrochemical kinetics, adsorption, and oxide film structure investigations related to finishing processes. B. Studies of interfacial surface reactions between polymeric resins and metal oxide surfaces relating to strength and permanence of joints in the adhesive bonding of metals. C. Mechanisms relating to surface phenomena, associated with liquid metal-solid metal inter-action as applied to soldering and brazing. D. Surface and electrochemical reactions effecting the kinetics of general, localized, and stress corrosion processes. Pleasant living, with access to major university. Send reply to R. H. Endriss, Personnel Manager, Olin Mathieson Chemical Corp., 125 Munson St., New Haven, Conn.

Position Wanted

Chemical Engineer, B.S.—Thirteen years of electrolytic background in development and production work. Supervisory experience. Desires responsible position in either process engineering or production. *Reply to Box No. 370, c/o The Electrochemical Society, 1860 Broadway, New York 23, N. Y.*

Advertiser's Index

American Brass Company	266C
Electric Autolite Company	274C
General Electric Company	275C
Great Lakes Carbon Corp., Electrode Division	Cover 2
Pratt & Whitney Aircraft	276C
E. H. Sargent & Company	262C
Stackpole Carbon Company	263C
Sylvania Electric Products Inc.	265C

ELECTROCHEMIST

Doctor's Degree—5 to 10 Years' Experience

To head a newly organized group of electrochemists and physical chemists devoted to research on fuel cells.

This is a challenging position in a new field. It requires considerable theoretical background, experimental skill and inventive talent.

Work is strongly supported by the Corporation and directed at commercial exploitation. The position has excellent potential for growth.

A new laboratory building has been erected in our plant at East Hartford, Connecticut.

Send resume and minimum salary requirements to Mr. P. R. Smith, Office 61,

PRATT & WHITNEY AIRCRAFT
Division of United Aircraft Corporation
East Hartford 8, Connecticut

Monographs of The Electrochemical Society

ECS Series

The following are books developed and sponsored by The Electrochemical Society and published by John Wiley & Sons, Inc., 440 Fourth Ave., New York 16, N. Y. Members of The Electrochemical Society can receive a 33 1/3% discount by ordering volumes from Society Headquarters, 1860 Broadway, New York 23, N. Y. Book and invoice will be mailed by John Wiley & Sons. Nonmembers (including subscribers) should order direct from Wiley.

Corrosion Handbook. Edited by Herbert H. Uhlig. Published 1948, 1188 pages, **$16.00**

Modern Electroplating. Edited by Allen G. Gray. Published 1953, 563 pages, **$8.50**

Abstracts of the Literature on Semiconducting and Luminescent Materials and Their Applications. Compiled by Battelle Memorial Institute.

Vol. I, 1953 Issue—published 1955, 169 pages, **$5.00** (soft cover)

Vol. II, 1954 Issue—published 1955, 200 pages, **$5.00** (soft cover)

Vol. III, 1955 Issue—Edited by E. Paskell; published 1957, 322 pages, **$10.00** (hard cover)

Vol. IV, 1956 Issue—Edited by E. Paskell; published 1959, 456 pages, **$12.00** (hard cover)

Vol. V, 1957 Issue—Edited by C. S. Peet; published 1960, 449 pages, **$12.00** (hard cover)

Electrochemistry in Biology and Medicine. Edited by Theodore Shedlovsky. Published 1955, 369 pages, **$11.50**

Vapor Plating (The Formation of Metallic and Refractory Coatings by Vapor Deposition), by C. F. Powell, I. E. Campbell, and B. W. Gonser. Published 1955, 158 pages, **$5.50**

High-Temperature Technology (Materials, Methods, and Measurements). Edited by I. E. Campbell. Published 1956, 526 pages, **$15.00**

Stress Corrosion Cracking and Embrittlement. Edited by W. D. Robertson. Published 1956, 202 pages, **$7.50**

Arcs in Inert Atmospheres and Vacuum. Edited by W. E. Kuhn. Published 1956, 188 pages, **$7.50**
(Papers Presented at the Symposium on Arcs in Inert Atmospheres and Vacuum of the Electrothermics and Metallurgy Division of The Electrochemical Society, April 30 and May 1, 1956, San Francisco, Calif.)

Technology of Columbium (Niobium). Edited by B. W. Gonser and E. M. Sherwood. Published 1958, 120 pages, **$7.00**
(Papers Presented at the Symposium on Columbium—Niobium of the Electrothermics and Metallurgy Division of The Electrochemical Society, May 15 and 16, 1958, Washington, D. C.)

The Structure of Electrolytic Solutions. Edited by Walter J. Hamer. Published 1959, 441 pages, **$18.50**
(Based on a Symposium held in Washington, D. C., in May 1957, sponsored by The Electrochemical Society, New York, and The National Science Foundation, Washington, D. C.)

Mechanical Properties of Intermetallic Compounds. Edited by J. H. Westbrook. Published 1959, 435 pages, **$9.50**
(A Symposium, Sponsored by the Electrothermics and Metallurgy Division of The Electrochemical Society, May 4, 5, and 6, 1959, Philadelphia, Pa.)

The Surface Chemistry of Metals and Semiconductors. Edited by Harry C. Gatos, with the assistance of J. W. Faust, Jr., and W. J. La Fleur Published 1960, 526 pages, **$12.50**

[Proceedings of an International Symposium Sponsored Jointly by the Office of Naval Research and The Electrochemical Society, Inc. (Corrosion and Electronics Divisions), October 19, 20, and 21, 1959, Columbus, Ohio]

Vacuum Metallurgy

Vacuum Metallurgy, third printing, 1958. Edited by J. M. Blocher, Jr.; 216 pages; **$5.00,** less a 20% discount to ECS members only. Available from Electrochemical Society Headquarters, 1860 Broadway, New York 23, N. Y.

(Papers Presented at the Vacuum Metallurgy Symposium of the Electrothermics and Metallurgy Division of The Electrochemical Society held in Boston, Mass., October 6 and 7, 1954)

THE ELECTROCHEMICAL SOCIETY, INC.

The Electrochemical Society is an international organization of individuals and companies concerned with or interested in Electrochemistry and allied subjects.

The Society is dedicated to the advancement of the theory and practice of Electrochemistry and related subjects, as shown in the following divisions:

Battery
Corrosion
Electric Insulation
Electrodeposition
Electronics
Electro-Organic
Electrothermics and Metallurgy
Industrial Electrolytic
Theoretical Electrochemistry

Among the means to this end are the holding of meetings for the reading and discussion of professional and scientific papers on these subjects, the publication of such papers, discussions, and communications as may seem appropriate, and cooperation with chemical, electrical, and other scientific and technical societies.

It is an incorporated society without capital stock. The affairs of the Society are managed by a Board of Directors under a Constitution and Bylaws. Officers are nominated by a nominating committee appointed by the Board of Directors and elected by the members.

Direct all general correspondence and inquiries regarding membership to Society headquarters at 1860 Broadway, New York 23, N. Y.

Officers of the Society

President	R. A. SCHAEFER
Past President	W. C. GARDINER
Vice-President	H. B. LINFORD
Vice-President	F. L. LAQUE
Vice-President	W. J. HAMER
Treasurer	L. I. GILBERTSON
Secretary	I. E. CAMPBELL

The Electrochemical Society

Patron Members

Aluminum Co. of Canada, Ltd., Montreal, Que., Canada

International Nickel Co., Inc., New York, N. Y.

Olin Mathieson Chemical Corp., Niagara Falls, N. Y.
Industrial Chemicals Div., Research and Development Dept.

Union Carbide Corp.
Divisions:
Union Carbide Metals Co., New York, N. Y.
National Carbon Co., New York, N. Y.

Westinghouse Electric Corp., Pittsburgh, Pa.

Sustaining Members

Air Reduction Co., Inc., New York, N. Y.

Ajax Electro Metallurgical Corp., Philadelphia, Pa.

Allen-Bradley Co., Milwaukee, Wis.

Allied Chemical & Dye Corp.
General Chemical Div., Morristown, N. J.
Solvay Process Div., Syracuse, N. Y. (3 memberships)

Allied Research Products, Inc., Detroit, Mich.

Alloy Steel Products Co., Inc., Linden, N. J.

Aluminum Co. of America, New Kensington, Pa.

American Metal Climax, Inc., New York, N. Y.

American Potash & Chemical Corp., Los Angeles, Calif. (2 memberships)

American Smelting and Refining Co., South Plainfield, N. J.

American Zinc Co. of Illinois, East St. Louis, Ill.

American Zinc, Lead & Smelting Co., St. Louis, Mo.

American Zinc Oxide Co., Columbus, Ohio

M. Ames Chemical Works, Inc., Glens Falls, N. Y.

Basic Inc., Maple Grove, Ohio

Bell Telephone Laboratories, Inc., New York, N. Y. (2 memberships)

Bethlehem Steel Co., Bethlehem, Pa. (2 memberships)

Boeing Airplane Co., Seattle, Wash.

Burgess Battery Co., Freeport, Ill. (4 memberships)

Canadian Industries Ltd., Montreal, Que., Canada

Carborundum Co., Niagara Falls, N. Y.

Catalyst Research Corp., Baltimore, Md.

Ciba Pharmaceutical Products, Inc., Summit, N. J.

Columbian Carbon Co., New York, N. Y.

Columbia-Southern Chemical Corp., Pittsburgh, Pa.

Consolidated Mining & Smelting Co. of Canada, Ltd., Trail, B. C., Canada (2 memberships)

Continental Can Co., Inc., Chicago, Ill.

Cooper Metallurgical Associates, Cleveland, Ohio

Corning Glass Works, Corning, N. Y.

Diamond Alkali Co., Painesville, Ohio (2 memberships)

Dow Chemical Co., Midland, Mich.

Wilbur B. Driver Co., Newark, N. J. (2 memberships)

E. I. du Pont de Nemours & Co., Inc., Wilmington, Del.

Eagle-Picher Co., Chemical Div., Joplin, Mo.

Eastman Kodak Co., Rochester, N. Y.

Thomas A. Edison Research Laboratory, Div. of McGraw-Edison Co., West Orange, N. J.

Electric Auto-Lite Co., Toledo, Ohio
C & D Division, Conshohocken, Pa.

Electric Storage Battery Co., Yardley, Pa.

Englehard Industries, Inc., Newark, N. J. (2 memberships)

The Eppley Laboratory, Inc., Newport, R. I. (2 memberships)

Erie Resistor Corp., Erie, Pa.

Exmet Corp., Tuckahoe, N. Y.

Fairchild Semiconductor Corp., Palo Alto, Calif.

Food Machinery & Chemical Corp.
Becco Chemical Div., Buffalo, N. Y.
Westvaco Chlor-Alkali Div., South Charleston, W. Va.

Foote Mineral Co., Paoli, Pa.

Ford Motor Co., Dearborn, Mich.

General Electric Co., Schenectady, N. Y.
Chemistry & Chemical Engineering Component, General Engineering Laboratory
Chemistry Research Dept.
General Physics Research Dept.
Metallurgy & Ceramics Research Dept.
Aircraft Accessory Turbine Dept., West Lynn, Mass.

General Instrument Corp., Newark, N. J.

(Sustaining Members cont'd)

General Motors Corp.
Delco-Remy Div., Anderson, Ind.
Guide Lamp Div., Anderson, Ind.
Research Laboratories Div., Detroit, Mich.
General Transistor Corp., Jamaica, N. Y.
Gillette Safety Razor Co., Boston, Mass.
Globe-Union, Inc., Milwaukee, Wis.
Gould-National Batteries, Inc.,
Minneapolis, Minn.
Grace Electronic Chemicals, Inc.,
Baltimore, Md.
Great Lakes Carbon Corp., New York, N. Y.
Hanson-Van Winkle-Munning Co.,
Matawan, N. J. (2 memberships)
Harshaw Chemical Co., Cleveland, Ohio
(2 memberships)
Hercules Powder Co., Wilmington, Del.
Hill Cross Co., Inc., New York, N. Y.
Hoffman Electronics Corp., El Monte, Calif.
Hooker Chemical Corp., Niagara
Falls, N. Y. (3 memberships)
Hughes Aircraft Co., Culver City, Calif.
Industro Transistor Corp.,
Long Island City, N. Y.
International Business Machines Corp.,
Poughkeepsie, N. Y.
International Minerals & Chemical
Corp., Skokie, Ill.
ITT Laboratories, Nutley, N. J.
Jones & Laughlin Steel Corp.,
Pittsburgh, Pa.
K. W. Battery Co., Skokie, Ill.
Kaiser Aluminum & Chemical Corp.
Div. of Chemical Research,
Permanente, Calif.
Div. of Metallurgical Research,
Spokane, Wash.
Kennecott Copper Corp., New York, N. Y.
Keokuk Electro-Metals Co., Keokuk, Iowa
Libbey-Owens-Ford Glass Co., Toledo, Ohio
M. & C. Nuclear, Inc., Attleboro, Mass.
Mallinckrodt Chemical Works, St. Louis, Mo.
P. R. Mallory & Co., Indianapolis, Ind.
McGean Chemical Co., Cleveland, Ohio
Merck & Co., Inc., Rahway, N. J.
Metal & Thermit Corp., Detroit, Mich.
Minnesota Mining & Manufacturing Co.,
St. Paul, Minn.
Monsanto Chemical Co., St. Louis, Mo.
Motorola, Inc., Chicago, Ill.
National Cash Register Co., Dayton, Ohio
National Lead Co., New York, N. Y.
National Research Corp., Cambridge, Mass.
National Steel Corp., Weirton, W. Va.
New York Air Brake Co., Kinney Vacuum
Div., Boston, Mass.
Northern Electric Co., Montreal, Que.,
Canada
Norton Co., Worcester, Mass.
Olin Mathieson Chemical Corp.,
Research & Engineering Operations,
Energy Div., New Haven, Conn.
Ovitron Corp., Long Island City, N. Y.
Peerless Roll Leaf Co., Inc., Union City, N. J.
Pennsalt Chemicals Corp.,
Philadelphia, Pa.
Phelps Dodge Refining Corp., Maspeth, N. Y.
Philco Corp., Philadelphia, Pa.
Philips Laboratories, Inc., Irvington-on-
Hudson, N. Y.
Pittsburgh Metallurgical Co., Inc.,
Niagara Falls, N. Y.
Poor & Co., Promat Div., Waukegan, Ill.
Potash Co. of America,
Carlsbad, N. Mex.
Radio Corp. of America
Tube Div., Harrison, N. J.
RCA Victor Record Div., Indianapolis,
Ind.
Ray-O-Vac Co., Madison, Wis.
Raytheon Manufacturing Co.,
Waltham, Mass.
Reynolds Metals Co., Richmond, Va.
(2 memberships)
Rheem Semiconductor Corp.,
Mountain View, Calif.
Schering Corporation, Bloomfield, N. J.
Shawinigan Chemicals Ltd., Montreal, Que.,
Canada
Speer Carbon Co.
International Graphite & Electrode
Div., St. Marys, Pa. (2 memberships)
Sprague Electric Co., North Adams, Mass.
Stackpole Carbon Co., St. Marys, Pa.
Stauffer Chemical Co., New York, N. Y.
Sumner Chemical Co., Div. of
Miles Laboratories, Inc., Elkhart, Ind.
Sylvania Electric Products Inc., Bayside,
N. Y. (2 memberships)
Tennessee Products & Chemical Corp.,
Nashville, Tenn.
Texas Instruments, Inc., Dallas, Texas
Three Point Four Corp., Yonkers, N. Y.
Titanium Metals Corp. of America,
Henderson, Nev.
Tung-Sol Electric Inc.,
Newark, N. J.
Udylite Corp., Detroit, Mich.
(4 memberships)
Universal-Cyclops Steel Corp.,
Bridgeville, Pa.
Upjohn Co., Kalamazoo, Mich.
Victor Chemical Works, Chicago, Ill.
Western Electric Co., Inc., Chicago, Ill.
Wyandotte Chemicals Corp.,
Wyandotte, Mich.
Yardney Electric Corp., New York, N. Y.